

Ventilator associated pneumonia: the development of an antimicrobial endotracheal tube and clinical study to understand the infection.

Georgia S.K. Fleet

Supervisors Prof. Ivan P. Parkin & Dr. Elaine Allan

University College London

Degree: Doctor of Engineering

I, Georgia Fleet, confirm that the work presented in my thesis is my own.

Where information has been derived from other sources, I confirm that this has been indicated in the thesis.

ABSTRACT

This thesis describes the development of light activated antimicrobial materials for use in medical devices, as a way to reduce the need for antibiotics in hospitals and consequently slow down the progression of the antimicrobial resistance crisis. As well, to help combat common hospital acquired infections such as ventilator associated pneumonia (VAP), which is the largest cause of death in critical care units (Prof D. Walker, University College Hospital London, 2019). An antimicrobial endotracheal tube was developed to reduce the mortality caused by VAP, as VAP is caused by bacterial biofilms growing on the endotracheal tube. An antimicrobial endotracheal tube was developed here both by using swell encapsulation methods and alternatively by a photocured 3D printing method. Both endotracheal tubes utilise a mix of photosensitizer dye combined with nanoparticles (gold nanoclusters for the swell encapsulated or zinc oxide nanoparticles for the 3D printed) which are then incorporated into polymers by the chosen method. The antimicrobial activity was tested against clinically relevant isolates of *P. aeruginosa*, *E. coli* and MRSA cultured directly from extubated endotracheal tubes. The antimicrobial activity was tested in the dark as well as with laser light and white light activation. Within 15 minutes of laser light exposure and 3 hours of white light exposure all isolates were eliminated for both swell encapsulated and 3D printed endotracheal tubes. As well, both antimicrobial endotracheal tubes were able to inactivate infectivity of SARS-CoV-2 within 15 minutes in the dark with no light activation required. To our knowledge this is the most active broad-spectrum material of this kind developed to date; and has a wide range of potential applications due to its powerful antimicrobial properties. An ongoing clinical study has supported this

work by analysing extubated endotracheal tubes from patients who were intubated for 5 or more days and provides insights into the types of organisms growing on endotracheal tubes as well as a potential rapid diagnostic technique by using NMR analysis.

IMPACT STATEMENT

My research has purposely been designed to be downstream from the beginning, and therefore to have real-world impact by design. An initial literature review performed in my first year highlighted a gap in research regarding endotracheal tubes and ventilator associated pneumonia (VAP) where it was causing the highest number of unnecessary deaths in hospitals, yet most of the research was aimed towards catheter associated infections, which although is highest in numbers doesn't tend to result in high mortality rates like VAP.

The immediate benefits of the development of an antimicrobial endotracheal tube, presented by two different methods of synthesis in my thesis, is that this would aim to reduce or eradicate VAP and as a result unnecessary deaths in hospitals. In turn, this should lead to decreased bed days resulting in lowering costs for the NHS, in turn freeing up more space for other patients, and also reduce widespread use of antibiotics in critical care specifically which will reduce the spread of antimicrobial resistance.

The aim is that this technology could also spread out into developing countries where it's been shown endotracheal tubes are reused between patients. An antimicrobial endotracheal tube of comparable cost could help reduce rates of infections in these countries, where antibiotics and other treatments are also scarce, and therefore improve patient care overall and reduce mortality rates.

As well, the clinical study conducted to support this research provides future researchers insight into causative pathogens for VAP, any patterns presenting between incidence of VAP and antibiotics administered, and effects of co-

infection of Covid-19 and VAP. The NMR study aims to provide insight into the makeup of the biofilms particularly the chemical structure of the extracellular polymeric substances holding biofilms together, aligned with SEM images to create a visual full picture of biofilms present on endotracheal tubes.

Lastly, the novel 3D printing method developed (patent filed 16th December 2022) has the potential to be applied in many different settings, healthcare included. This technology utilises two compounds well known and already used throughout healthcare settings, which are commercially available at a low cost. This therefore improves the commercialisation prospects and ease of scale up. However, what this technology is proposed to be used in should be carefully considered in the wider context of antimicrobial resistance, and the materials use closely monitored over time to determine any potential resistance developing.

ACKNOWLEDGEMENTS

Firstly, I would like to thank my supervisors Ivan Parkin and Elaine Allan for their support throughout what has been quite an interesting and chaotic time, who supported me through all my (crazy) ideas I wanted to explore... like renting my own lab and starting a clinical study during a pandemic.

I would also like to thank all the colleagues who have helped me along the way, including Ingrid Green for giving me the quickest crash course in microbiology after Elaine retired, as well as Haitham Hussain and Anna Tymon for helping me arrange the move of my equipment to the Royal Free. Also, to all those involved in helping me through the funding application process and to Sri Srimurugananthan who helped me ferry huge equipment like centrifuges in the back of my mini convertible across London during a pandemic. Likewise, to those who helped get this clinical study started, a huge thank you to David Brealey, David Walker and the critical care team at UCLH who eventually helped push the paperwork over the finish line in 2022.

Lastly, I would like to thank my incredible partner and friends. Thank you to Sri Srimurugananthan, Seema Doll, Carla Southworth, Kade Flowers, Amy Rollinson, Tom Hamilton, Alice Hagan and Robyn Denney-Foster for checking in on me and making sure I'm still sane these past 4-5 years. And thank you to Christopher Clatworthy for bringing me endless soda water, and Pickles for bringing me endless cuddles.

Thank you also to those who conducted analysis included in this thesis:

Michela Mazzon - Coronavirus NL63 testing

Maximillian Woodall - SARS-CoV-2 testing

Kristopher Page - Water droplet analysis

Cesar Reyes - Infrared and UV-Vis analysis

M. Emre Sener & Oliver Hagger - Initial 3D printing

CONTENTS

Αk	ostra	ct		3
lm	pact	tsta	tement	5
Ac	kno	wled	lgements	7
Co	ontei	nts		1
Fi	gure	s		4
Та	bles	·		10
1	Ch	apte	er 1 – Introduction to Ventilator Associated Pneumonia	1
	1.1 in De		Overview of Antimicrobial Endotracheal Tubes on the Market pment	
2		•	er 2 - The Development of Light Activated Antimicrobial	
			eal Tubes	
	2.1		oduction	
-	2.2		thods	
	2.2		Gold Nanocluster Synthesis	
	2.2		Zinc Nanoparticle Synthesis	
	2.2		Synthesis of the Antimicrobial Endotracheal Tube	
	2.2		Materials Analysis of Raw Endotracheal Tube Material	
	2.2		Safety & Stability Analysis	
	2.2		Stress Strain Analysis	
	2.2		Microbiological Assay	
	2.2	_	Biofilm Development Protocol	
2	2.3		sults & Discussion	
	2.3		Stress Strain Analysis - Tensile Stress	
	2.3		Safety & Stability Leaching Outcomes	
	2.3	_	Optimisation for Microbiological Activity	
	2.3 Da		Incorporating Zinc Nanoparticles for Antimicrobial Activity in 51	1 the
	2.3	3.5	Antimicrobial Endotracheal Tube Activity	55
	2.3	3.6	Antimicrobial Activity against Biofilms	63
3		•	er 3 – The Effect of Covid-19 on Ventilator Associated	
			a	
,	3.1	Intr	oduction	70

3	.2	Met	thods	72
	3.2	.1	Coronavirus NL-63 Assay	72
	3.2	.2	SARS-CoV-2 Assay	73
3	.3	Res	sults & Discussions	76
	3.3	.1	Activity Against Coronavirus NL-63	76
	3.3	.2	Activity Against SARS-CoV-2	78
4 app		-	r 4 – 3D Printing Antimicrobial Materials for other	81
4	.1	Intr	oduction	81
4	.2	Met	thod	84
	4.2	.1	Printing Medical Devices	84
	4.2	.2	Materials Characterisation	85
	4.2	.3	Screening Study of Photosensitiser Nanoparticle Mixes	86
	4.2	.4	Microbiological Assay	90
	4.2	.5	SARS-CoV-2 Assay	91
4	.3	Res	sults & Discussion	92
	4.3	.1	Printed Medical Devices Microbiological Activity	92
	4.3	.2	Materials Characterisation	97
	4.3	.3	Screening Study Microbiological Activity	104
	4.3	.4	Activity against SARS-CoV-2	107
	4.3	.5	Broader Applications of 3D Printing	111
5	Cha	apte	r 5 – Clinical Study	111
5	.1	Intr	oduction	111
5	.2	Me	thods	114
	5.2	.1	Study Outline	114
	5.2	.2	Study Design	115
	5.2	.3	Study Schedule	115
	5.2	.4	Microbial Culture	117
	5.2	.5	SEM Analysis	119
	5.2	.6	NMR Analysis	120
5	.3	Res	sults & Discussion	121
	5.3	.1	Microbial Culture	121
	5.3	.2	Patient data	127

	5.3	.3 SEM Analysis of Biofilm	129
	5.3	.4 NMR Analysis of Biofilm	140
	5.3	.5 Conclusions	157
6	Fin	al Remarks	160
7	Ref	ferences	163
8	Apı	pendix	175
	8.1	Spiral Plater and the Automatic Colony Counter	175
	8.2	Colony Morphology Analysis for Clinical Study	177
		NMR Spectra and Chemical Structure for Suggested Compou	
	8.4	Setting Up a New Laboratory during Covid-19 pandemic	183

FIGURES

Figure 1. Illustration of intubated patient, with endotracheal tube highlighted in blue and relevant organism examples to show the pathway from tube to open airways and lungs3
Figure 2. Diagram illustrating the mechanism of action of the photosensitizer dye and nanocluster acting in synergy to produce reactive oxygen species9
Figure 3. The microfluidics synthesis set up for the Au25(Cys)18 cluster synthesis from gold precursor solution, a) carbon monoxide alarm and inlet system b) pressure regulator valve c) pressure sensor d) gold precursor solution e) hot plate and oil bath f) tube
Figure 4. Chemical structure of zinc di(octyl) phosphinic acid (DOPA)25
Figure 5. Chemical structure of methylene blue26
Figure 6. The simple synthesis set up in parallel for swell encapsulation of the endotracheal tubes to make them antimicrobial27
Figure 7. Image of the tensiometer machine used for tensile stress testing, as well as a dumbbell shaped test sample in the top righthand corner
Figure 8. Image showing the humidity chamber described with x3 samples being tested32
Figure 9. An image to compare the manual plating method to the spiral plating method, where on the left-hand side (manual) colonies are manually spread using an L-shaped spreader, and each individual dilution will have a different plate similar to this. Which was then counted and recorded manually. Here for comparisons sake this is shown on the automatic colony counter. On the righthand side (spiral) are the rings which represent dilutions going from N (in the centre) to -5 (the outer ring). Therefore, having all dilutions on one plate, easily read by the automatic colony counter as illustrated here. An example of the exported PDF results can be found in the appendix.
Figure 10. Image of the samples used in biofilm experiments cut to 1.5cm length35
Figure 11. Removal of the sample for analysis of biofilm, this image shows the sample with biofilm being lifted upwards until 'snapping'
Figure 12. A graph summarising the results of the tensile stress testing, where the red bar and red line across the graph show where the untreated endotracheal tube material lies. The graph is colour coded to table 2. Paired two tailed T test for 3 h P = 0.44

Figure 13. Leaching profile of methylene blue over 10 days from swell encapsulated antimicrobial endotracheal tube
Figure 14. 5-Point calibration curve for methylene blue concentration leaching analysis
Figure 15. Graph showing the first repeat of antimicrobial optimisation experiments where blue represents dark control conditions and the orange representing the light conditions, of which samples were exposed for 3 h at 10,000 lux. Paired two tailed T test for L2 significance $P < 0.0001$. Paired two tailed T test for L3, L5 $P = 0.04$
Figure 16. Antimicrobial activity using the new white light source (SAD lamp) of antimicrobial endotracheal tube samples
Figure 17. Antimicrobial activity using the old white light source of antimicrobial endotracheal tube samples (some dark controls not performed due to issues sourcing sterile saline during Covid-19 pandemic). * = below detection level (1E+02)48
Figure 18. Light spectrum for the new white light source (SAD lamp)49
Figure 19. Light spectrum for the old white light source (fluorescent bulb)50
Figure 20. Results from antimicrobial endotracheal tube with additional Zn(DOPA) embedded in white light against two different isolates of <i>E. coli.</i> Two biological replicates
Figure 21. Results from antimicrobial endotracheal tube with additional Zn(DOPA) embedded after laser light exposure for 10 minutes against a clinical isolate of <i>E. coli</i> . Two biological replicates
Figure 22. Graph showing antimicrobial testing of endotracheal tube pieces against laboratory strains of <i>S. aureus</i> and <i>E. coli</i> when exposed to 10,000 lux white light for 3 hours compared to that in the dark. Two biological replicates performed. * = below detection level (1E+02)56
Figure 23. Graph showing antimicrobial testing of endotracheal tube pieces against the clinical isolate of <i>E. coli</i> when exposed to 10,000 lux white light for 6 hours compared to that in the dark. Three biological replicates performed
Figure 24. Image to show the set up for the early laser experiments measured output 150mW in a direct beam down onto the sample59
Figure 25. Graphs showing antimicrobial results against clinical isolate of <i>E. coli</i> when exposed to 150 mW laser light for 5 and 15 minutes. Three biological replicates performed. * = below detection level (1E+02)60
Figure 26. Image to show the new laser set up of experiments using diffuser tip measuring intensity of 14 mW/cm ² 61

Figure 27. Graph showing preliminary results (one biolgical replicate) of the antimicrobial endotracheal tube against the clinical isolate of <i>E. coli</i> using laser light for 4 minutes, 10 minutes and 14 minutes at 14 mW/cm ² 63
Figure 28. Comparison of the initial experiment testing MRSA only, P. aeruginosa only, 1:2 and 1:5 mixed biofilms at the beginning and end of the 2-week biofilm formation.
Figure 29. Biofilm growth of <i>P. aeruginosa</i> on the antimicrobial endotracheal tube compared to blank controls grown over 14 days, which were exposed to either complete darkness or exposed to white light for x3 hours (10,000 lux) once on day 0 and 7. Two biological replicates
Figure 30. Biofilm formed after two weeks of growth on control sample. The same is not seen for the antimicrobial samples also left for two weeks in the same inoculum
Figure 31. Repeat 1 - Graph by Virology Research Services on the outcome of the activity of the antimicorbial endotracheal tubes against coronavirus NL63 when exposed to white light at 10,000 lux for 3 h. One biololgical replicate. * = below detection limit (25 PFU)
Figure 32. Repeat 2 - Graph by Virology Research Services on the outcome of the activity of the antimicorbial endotracheal tubes against coronavirus NL63 when exposed to white light at 10,000 lux for 15 mins. One biological replicate. * = below detection limit (25 PFU)77
Figure 33. Image of plaque assay results from testing MB and Au(25)Cys18 swell encapsulated samples against SARS-CoV-2. Thee biological replicates.
Figure 34. Graph showing the reduction levels achieved within 15 minutes in the dark and in white light (10,000 lux) using swell encapsulated antimicrobial endotracheal tube samples, * = below detection level reduction (detection level = 25 PFU). Three biological replicates
Figure 35. On the left-hand side a 3D computer aided design (CAD) from GrabCAD of a tracheostomy tube and on the right-hand side the subsequent print using the antimicrobial mix
Figure 36. Chemical structure of rose Bengal
Figure 37. Image of the methylene blue, rose Bengal, ZnO and Au ₂₅ (Cys) ₁₈ resin mixtures before 3D printing
Figure 38. The curing process after 3D printing and isopropyl washes for sample squares produced for antimicrobial testing

Figure 39. 3D prints for the screening of different mixes including ZnO only, Au ₂₅ (Cys) ₁₈ only, MB only, RB only, MB + ZnO, RB + ZnO, and MB + Au ₂₅ (Cys) ₁₈ 90
Figure 40. Graph showing the activity of 3D printed methylene blue and zinc oxide materials against drug resistant isolates of gram-positive and -negative bacteria (MRSA US137 and <i>P. aeruginosa</i> RS080) within 15 minutes of laser activation. Two biological replicates
Figure 41. Side by side image of pieces of endotracheal tube broken off for testing, the left-hand side is before laser activation and the right-hand side is after laser activation95
Figure 42. Graph showing the activity of 3D printed methylene blue and zinc oxide materials against drug resistant isolates of gram-positive and -negative bacteria (MRSA US137 and <i>P. aeruginosa</i> RS080) within 3 hours of white light exposure. Two biological replicates96
Figure 43. Scanning electron microscope image of the blank 3D printed control square
Figure 44. Scanning electron microscope image of the methylene blue 3D printed control square99
Figure 45. Scanning electron microscope image of the zinc oxide 3D printed control square99
Figure 46. Scanning electron microscope image of the antimicrobial 3D printed sample containing methylene blue and zinc oxide. Hole illustrated by arrow and note
Figure 47. Infrared spectrum of 3D printed antimicrobial sample containing methylene blue and zinc oxide (green), methylene blue control (blue), zinc oxide control (red), and blank control (black)
Figure 48. Chemical structure of methylene blue with IR assignments102
Figure 49. Antimicrobial activity of 3D printed materials using mixes of rose Bengal, methylene blue with zinc oxide or gold nanoclusters, against clinical isolate of <i>E. coli</i> using white light exposure (3h at 10,000 lux). Two biological replicates
Figure 50. Results showing the activity of 3D printed antimicrobial material using MB and ZnO mixes against SARS-CoV-2 within just 10 minutes in the dark and exposed to white light. Three biological replicates. * = below detection level (25 PFU)
Figure 51. Images of the endotracheal tube after it has been removed from its sealed bag, intact. Below this is a comparative image of the prepared sections (top, middle, bottom = T, M, B) for analysis

Figure 52. Image showing three Mannitol Salt agar plates which illustrate the difference in concentration of certain bacteria throughout the tube. In this case suspected <i>S. aureus</i> is in high concentration at the top of the tube and low concentration at the bottom of the tube
Figure 53. SEM image of the surface of a sterile unused Portex endotracheal tube (inner lumen)
Figure 54. SEM images of ET001, suspected <i>S. epidermis</i> due to cocci shaped bacteria of the right size (0.5-1.5µm)
Figure 55. SEM images of ET001, suspected <i>P. aeruginosa</i> or <i>C. difficile</i> , due to rod-shaped bacteria of the right size for both (1-5µm)132
Figure 56. SEM images of ET002, either <i>S. aureus</i> and/or <i>S. pneumoniae</i> due to both having cocci shaped bacteria of the right size (0.5-1.25µm)133
Figure 57. SEM images of ET002 at lower magnifications to see overarching biofilm extracellular polymeric substance architecture
Figure 58. SEM image of ET003, suspected <i>S. pneumoniae</i> due to the smaller cocci shaped bacteria in singular chains
Figure 59. SEM images of ET003, suspected <i>S. aureus</i> due to cocci shaped bacteria of the right size slightly larger than the above (0.5-1.5µm)
Figure 60. SEM image of ET004, either <i>S. aureus</i> and/or <i>S. pneumoniae</i> due to both having cocci shaped bacteria of the right size $(0.5-1.25\mu m)$
Figure 61. SEM image of ET004, either <i>S. aureus</i> and/or <i>S. pneumoniae</i> due to both having cocci shaped bacteria of the right size $(0.5-1.25\mu m)$
Figure 62. SEM image of ET005. Top image suspected <i>C. glabrata</i> due to the singular spherical shapes. Bottom image suspected <i>S. agalactiae</i> due to appearance of a chain, though size is slightly too large
Figure 63. NMR spectra of D2O used to dissolve the powdered biofilm after drying. 1H NMR (700 MHz, D2O) δ 4.79 (s, 1H)
Figure 64. NMR spectra of clean tube material exposed to the pure water used in step 1 of biofilm processing. 1H NMR (700 MHz, D ₂ O) δ 4.73 (s, 6H), 3.57 (s, 3H), 1.22 (s, 0H)
Figure 65. NMR spectra of clean tube material exposed to the NaOH used in step 2 of biofilm processing. 1H NMR (700 MHz, D ₂ O) δ 8.21 (s, 3H), 1.67 (s, 1H), 1.62 (s, 2H), 1.10 – 1.05 (m, 2H), 0.99 (s, 1H)
Figure 66. NMR spectra of the water-soluble parts of ET001145
Figure 67. NMR spectra of the NaOH-soluble parts of ET001146
Figure 68. NMR spectra of the water-soluble parts of ET002147

Figure 69. NMR spectra of the NaOH-soluble parts of ET002	148
Figure 70. NMR spectra of the water-soluble parts of ET003	149
Figure 71. NMR spectra of the NaOH-soluble parts of ET003	150
Figure 72. NMR spectra of the water-soluble parts of ET004	152
Figure 73. NMR spectra of the NaOH-soluble parts of ET004	154
Figure 74. NMR spectra of the NaOH-soluble parts of ET005	155
Figure 75. NMR spectra of the water-soluble parts of ET005	155
Figure 76. An example of one of the pages from the PDF export from the automatic spiral plate colony counter	175
Figure 77. Summary table of the observations from cultures on blood, MacConkey and Mannitol Salt plates and gram staining	177
Figure 78. ¹ H NMR spectrum and chemical structure for proline available of the Human Metabolome Database	
Figure 79. ¹ H NMR spectrum for acetoin available on the Human Metabolome Database	179
Figure 80. ¹ H NMR spectrum for succinate available on the Human Metabolome Database	180
Figure 81. ¹ H NMR spectrum for arabinitol available on the Human Metabolome Database	181
Figure 82. ¹ H NMR spectrum for acetate available on the Human Metabolome Database	182
Figure 83. Image of the shipping container turned lab, everything was set by me and the help of a 'bubble' friend during the Covid-19 pandemic	•
Figure 84. Alternative view of the shipping container lab	185
Figure 85. Image of the shipping container lab from the outside	186

TABLES

Table 1. World Health Organization statistics from 2017 publication on Prioritisation of Pathogens Guide ²⁷
Table 2. Table summarising the swell encapsulation parameters for the tensile stress optimisation experiment
Table 3. Table summarising the amounts of antimicrobial components added into optimisation experiment samples for antimicrobial testing
Table 4. Table summarising the amounts of antimicrobial components added into round 2 of optimisation experiments samples for antimicrobial testing. 47
Table 5. Summarising the results for the initial biofilm experiment on blank commercially available endotracheal tubes, exploring 1:2 and 1:5 ratios for mixed biofilms with recovery and colony counting on Mannitol Salt and MacConkey agar
Table 6. Table summarising assignments for peaks of IR spectra between 3D printed antimicrobial samples
Table 7. Summary of the mean contact angle (CA) measurements of water and diiodo-methane in air and total surface free energy (SFE)
Table 8. Summary of the suspected organisms growing on the endotracheal tubes from samples 1-5 based off colony morphology, gram stain and selective agar plate growth.
Table 9. Table summarising the primary anonymised data collected from patients from tubes ET001-ET005

1 CHAPTER 1 – INTRODUCTION TO VENTILATOR ASSOCIATED PNEUMONIA

Hospital acquired infections have long been a problem in hospital settings worldwide. Just in NHS England hospitals in 2016/2017, hospital stays were increased (7.1 million occupied hospital beds, equivalent to 21% of the annual number of all bed days across NHS England), there has been absenteeism amongst staff (79,700 days), and a huge cost associated (£2.7 billion) ¹. Most importantly, there was a recorded 28,500 patient deaths in the year as a result of hospital acquired infections, just in England¹. Deaths which potentially could have been avoided. The culprit responsible for the highest percentage of these is as a result of ventilator associated pneumonia (VAP) at ~22.8% ^{2, 3}, which occurs as a result of bacteria growing on the endotracheal tube and costs the NHS between £10-20,000 per VAP case⁴. The endotracheal tube is a perfect open airway passage through to the lungs, forcibly stopping reflexes such as coughing which might help protect against infection, and as a result the patient gets ill and their chance of mortality increases by 30% ⁴.

VAP itself is a term used to describe patients that develop pneumonia (lung infection) after being on mechanical ventilation for more than 48 hours.⁵ In general, infections developing in under four days are classed as early onset, whereas after four days this is classed as late onset. Multi-drug resistant pathogens occur more often in late onset VAP.⁶ Risk factors include patient characteristics such as age and gender (older people and men tend to develop VAP more often), as well as ventilation time, co-morbidities, prior antibiotic therapy and burns, as a few examples.⁷ Lacking definition of symptoms and similarities of symptoms to other conditions like sepsis leads to both under and

overdiagnosis, and a suspicion of pneumonia is advised to prompt the immediate administration of broad spectrum antibiotics – accounting for around half of all antibiotics given in critical care units.⁵

The level of reduction in both bacterial and viral counts for European Standards to be classed as virucidal must reach at least 4-log reductions⁸ and in the case of bactericidal must reach at least 5-log reductions.⁹ Though some of the materials and activity described are below these defined log reductions, it's important to note the tests performed here were against clinically relevant, multi-drug resistant isolates, cultured directly from endotracheal tubes. These isolates are more representative of the types of bacteria found in the environment and therefore the level of reductions achieved in the real-world. To determine if these materials pass the European Standards further tests would be required against the standard types of organisms named.

This research aimed to develop a highly active antimicrobial endotracheal tube which could be commercialised and implemented relatively easily to prevent VAP occurrence and as such the related mortality and antibiotic use with these cases. As well, to find an alternative method for making antimicrobial materials to swell encapsulation. Lastly, to conduct a clinical study which helps answer the big questions like what the causative pathogens of VAP are, if any, and where are these bacteria coming from e.g., the environment or the body.

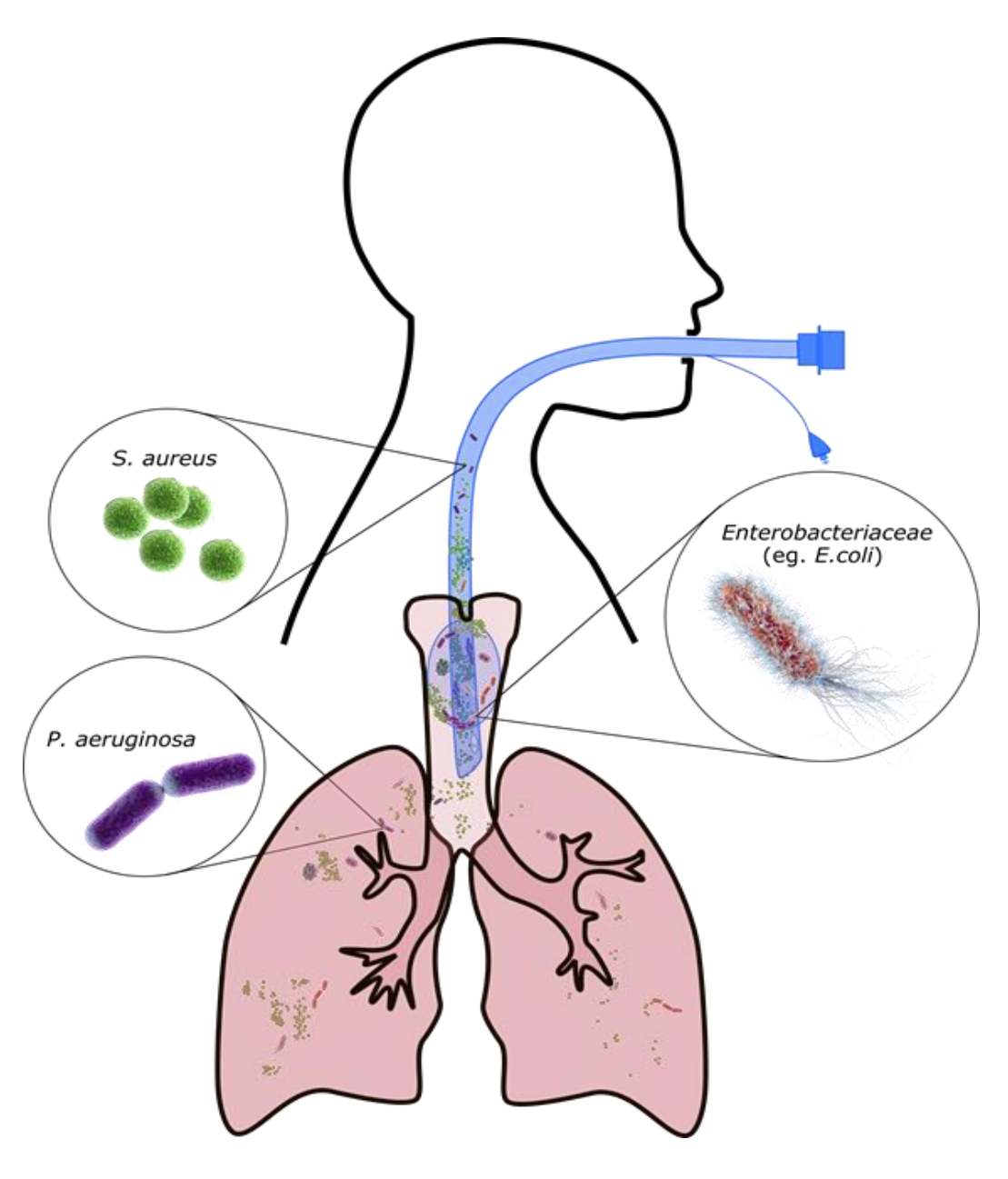


Figure 1. Illustration of intubated patient, with endotracheal tube highlighted in blue and relevant organism examples to show the pathway from tube to open airways and lungs.

Before the SARS-CoV-2 pandemic, VAP was the largest cause of death in critical care (Prof D. Walker, Critical Care consultant at UCLH), which was not only unnecessary and potentially avoidable with the right diagnostic tools, treatment, or prevention; but of course, when the pandemic began in 2019 and more patients found themselves needing ventilation. Therefore, this pattern of secondary infections leading to deaths was assumed continued throughout the pandemic, but a lack of continuity and standardisation in reporting data like this UK wide and worldwide has meant it's hard to make any meaningful conclusions. Though the pandemic in itself did shine a light on the issue of VAP, and so progress and research in this area has accelerated since 2020 dramatically.

An interesting area of research has been focused on the co-infection of viral and bacterial infection, and how these interact with each other, for example does co-infection affect the species of bacteria seen colonising endotracheal tubes if there is competition between pathogens. One paper shows Covid-19 patients were significantly more likely to develop VAP than patients without Covid-19 (p = 0.0015), with an increase incidence density of over twice that of non-Covid patients (p = 0.009). Potentially this could be due to the nature of Covid-19 already being a respiratory disease, and so is particularly weakened in this area and unable to defend against VAP as well as someone who has been intubated as a result of say a head injury/coma/other non-respiratory disease reason. As well, researchers have investigated how SARS-CoV-2 may actually induce secondary bacterial infections. This is thought to be due to the damage caused to the respiratory epithelium by viruses, which encourages

subsequent bacterial colonization and adherence ^{11, 12}. Another study noted increased levels of infection related biomarkers and inflammatory cytokines in patients with SARS-CoV-2, which provides evidence that viral infections like SARS-CoV-2 induce secondary bacterial infections by dysregulating the immune system ¹³.

So, it would be interesting to see data on immune compromised patients (aka Covid-19 patients) versus others, and see if the pattern is the same, and therefore not related to Covid-19 specifically but rather a compromised immune or respiratory system. Though a potential reason for an increase in VAP occurrence in Covid-19 patients could be down to factors such as staffing levels during this time and the use of staff with only brief training in the area of critical care leading to VAP. The only notable difference between colonisers in Covid-19 patients versus non-Covid patients were 3 cases of invasive aspergillosis seen in the Covid-19 patients (an infection caused by a type of fungus), out of a total 94 Covid-19 patients and 144 non-Covid patients. At the lung microbiome level, no difference in the composition of organisms was observed between Covid-19 and non-Covid patients.

Though recording of data during the pandemic was not standardised and therefore impossible to say for certain, but it's reasonable to postulate should VAP had not occurred in these critically ill patients with Covid-19, mortality rates may have been significantly reduced. This assumption is strengthened by the confirmation that patients with hospital or community acquired infections overall had worse outcomes than those without.¹⁴

Though the pathogenesis of VAP and risk factors are still being debated, 15 the general consensus is that due to the nature of intubation, natural protective mechanisms like coughing is prevented, allowing the oropharynx to easily become colonised with pathogenic bacteria. The colonisers then form a biofilm on the endotracheal tube, which serves as a reservoir for infection. As a result of ventilator cycling and micro-aspirations, pathogenic bacteria are able to travel into the lower respiratory system, subsequently causing VAP. 16, 17 Recent research (2020) has shown the most common pathogens involved in VAP were Enterococcus faecium, E. faecalis, Staphylococcus aureus, Klebsiella spp., and Acinetobacter spp,18 though this was a relatively small analysis of 12 patients who developed VAP. The most common widely accepted causative pathogens of VAP are primarily Gram-negative including Pseudomonas aeruginosa, Escherichia coli, Klebsiella pneumoniae, and Acinetobacter. As well as Gram-positive Staphylococcus aureus. 19 20

It is important to find cost-effective, easily implementable and sustainable approaches to combat hospital acquired infections like VAP, particularly in developing countries, where the frequency is much higher. Though data is limited, a 2011 review by the World Health Organization on healthcare associated infections in Africa highlighted the prevalence of VAP in ventilated patients in Senegal was 50%.²¹ Though not ideal, where endotracheal tubes are being reused (which was shown to be the case in 40% of critical care units in Ethiopia),²² then a comparably priced antimicrobial endotracheal tube may help reduce mortality in these countries from VAP. This may even help lower

overall costs of patient stays, as a preventative strategy to reduce VAP may then reduce need for further treatment and the resulting cost after the fact.

Strengthening the argument for a more preventative strategy regarding VAP is the lack of early detection and risk prediction, ²³ despite it being so prevalent in critical care, more often than not once VAP is diagnosed, the infection has already set in, and is very difficult to treat thereafter. Additionally, a knock-on effect of VAP is the indirect promotion of antimicrobial resistance (AMR) by over-prescription of antibiotics. For example, VAP exhibits similar symptoms to other serious life-threatening infections such as sepsis. As a result, healthcare professionals (HCPs) often prescribe multiple antibiotic medications to cover all the bases until the microbiology culture results come back (2-3 days). If for example it is then found to be a viral infection or caused by a bacterium resistant to the antibiotics administered, this further proliferates the progression of AMR. AMR is thought to soon become the world's largest cause of death, currently causing 700,000 deaths each year worldwide and expected to cause at least 10 million a year by 2050 ²⁴.

The first antimicrobial endotracheal tube made it to market in 2008, so this idea to reduce VAP in this way is not new. It was based on silver technology (Agento™), but due to the mode of action of silver (release of Ag+ ions) it was not effective enough and was found to yield no significant difference to standard endotracheal tubes in trials regarding intubation duration, length of stay, or mortality ²⁵. In addition to this, resistance to silver ions (Ag+) has been recognised for many years and it's recently been discovered that resistance to silver nanoparticles may also be developing as a result of indiscriminate use

in healthcare products.²⁶ It's important to keep in mind for any potential antimicrobial material moving where this is used should be combined with regulatory practices that restrict widespread use to save active materials for where they are most needed. The below statistics on the prevalence of antimicrobial resistance in healthcare associated infections specifically are taken from 2017 World Health Organization (WHO) publication on the Prioritisation of Pathogens to Guide Discovery, Research and Development of new Antibiotics for Drug-Resistant Bacterial Infections, including tuberculosis, which highlights the high levels of resistance and therefore importance of slowing down the progression of AMR, and finding alternatives.²⁷

Table 1. World Health Organization statistics from 2017 publication on Prioritisation of Pathogens Guide²⁷.

Bacteria species	Resistance level
S. aureus	> 50% methicillin
E. faecium	80-85% vancomycin
K. pneumoniae	10% carbapenem
E. coli	16-36% third-generation
	cephalosporin
P. aeruginosa	25% carbapenem
A. baumannii	45-65% carbapenem, 40-70%
	multidrug

This research discusses the development of two antimicrobial endotracheal tube materials based off light-activated technology. One involving novel gold nanoclusters capped by cysteine (Au₂₅(Cys)₁₈) and photosensitizer dye such as methylene blue (MB), the other involving commercially available ZnO nanopowder and either MB or rose Bengal (RB), whereby the dye and nanoparticle work in synergy to deliver an enhanced antimicrobial effect.

The mechanism of action for the photosensitizer-nanocluster synergy involves firstly light absorption by the photosensitizer dye, resulting in an excited singlet state, of which then either returns to the ground state or crosses over into to an excited triplet state.²⁸ Two types of photochemical reaction are undergone by molecules in the excited triplet state known as type 1 and 2 to produce reactive oxygen species (ROS) ²⁹. Through internal unreported ROS scavenger/quencher assays in the group, it was thought the MB/ Au₂₅(Cys)₁₈ mix released primarily hydrogen peroxide (H₂O₂).

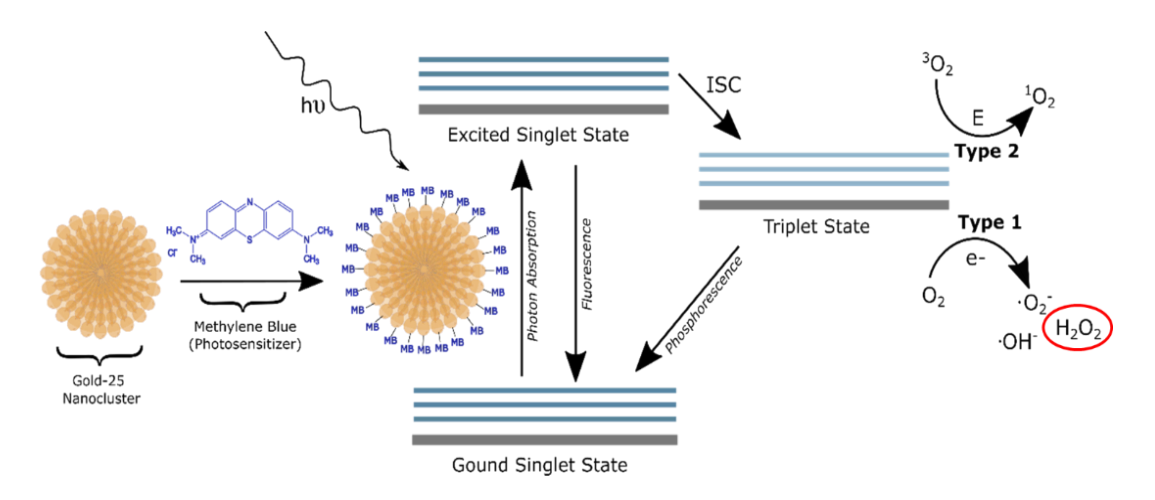


Figure 2. Diagram illustrating the mechanism of action of the photosensitizer dye and nanocluster acting in synergy to produce reactive oxygen species.

Lastly, although this thesis details a successful proof-of-concept antimicrobial endotracheal tube, this has been developed based on buying in commercially available tubes, and swell encapsulating the active components into the polymer. This process is hugely wasteful and is also hard to control with regard to the amount of each component being encapsulated. This could give rise to manufacturing issues later down the line when batch size is increased, thus a new method to incorporate the clusters and dye was investigated. Extrusion techniques were chosen primarily so that components could be added in directly in the tube manufacturing process, as well as looking into 3D printing using both extrusion and resin-curing printers. Ultimately due to no access to a small-scale extrusion printer, resin-cured 3D prints were investigated as an alternative to swell encapsulation methods.

A successful 3D printed prototype of a tracheostomy tube using MB and ZnO is described in this thesis. This was developed as an alternative to using swell encapsulation methods which are wasteful, hard to quantify and not easily scalable. But also, as an alternative to using Au₂₅(Cys)₁₈ nanoclusters which are highly unstable in liquid form (required for swell encapsulation process). It was originally thought that MB and ZnO would undergo the same mechanism as the MB and Au₂₅(Cys)₁₈ mix to produce antimicrobial activity as per previous studies³⁰ and research in the group,³¹ by enhanced photosensitiser action producing ROS to kill bacteria. However, a 2018 study demonstrates that ROS and toxic ion dissolution in ZnO do not fully explain the levels of antimicrobial activity seen in an example where MRSA was tested, and that alterations in ZnO causes changes in carbohydrate metabolism and bioenergetics

(specifically uridine monophosphate (UMP) synthesis) are more largely responsible, though not solely.³² In fact, they debate whether the presence of ROS may actually lead to an increase in biofilm development, as many studies show bacterium are able to combat and survive exposure to ROS by incorporating ROS into metabolic and respiratory pathways.^{33, 34, 35, 36, 34, 37}

Initially, ROS were thought to be favourable over antibiotics, as antibiotics kill bacteria through specific intracellular targets, whereas ROS do not, and therefore are less likely to promote AMR. However, if bacteria evolve to use ROS or inactive through metabolic and respiratory pathways, then materials causing high levels of oxidative stress may be inadvertently creating a new type of resistance to materials not yet seen in levels such as with antibiotics. One paper describes two different bacteria, Pseudoalteromonas sp. SM9913 and Pseudoalteromonas haloplanktis TAC125, the former lives at very low oxygen concentration in deep-sea sediment, compared to the latter, a closely related but surface seawater bacterium. Pseudoalteromonas sp. SM9913, though living at lower oxygen levels than Pseudoalteromonas haloplanktis TAC125, was sensitive to ROS however had an increased ability to form biofilm once exposed to oxygen.³⁸ There is a danger that ROS production may be equally as harmful to AMR if as overused as antibiotics over time, however it is thought to be highly unlikely given the current data on this. Photodynamic therapies which produce ROS as their mode of action using for example MB solution have shown after repeated light cycles no resistance is seen against either bacteria or viruses 39-41.

Therefore, when developing antimicrobial materials such as described in this work, caution must be taken during development to ensure appropriate log levels of kill is achievable to reduce the likelihood of AMR developing further. As well, due to the described mechanisms above surrounding ROS production and the potential ability for bacteria to evolve to use ROS, it may be beneficial if ZnO does not rely solely on ROS as its primary mechanism of action of kill.

Toxicity to mammalian cells is not seen with this material, but know ROS to be damaging to mammalian cells.⁴² Therefore more mechanism work should be done on both materials using both ZnO and Au₂₅(Cys)₁₈ to fully determine the primary mechanism of action of the nanocluster/nanoparticle and dye mix, to ensure this doesn't potentially promote AMR.

Regulatory concerns for the swell encapsulated endotracheal tubes primarily pertain to the use of acetone in the swell encapsulation process and any potential leaching of nanoparticles. Acetone is highly irritating and also highly flammable. Washings would have to be sufficient enough to satisfy regulatory bodies that no acetone would be in contact with the skin post swell encapsulation and that the exposure to acetone did not negatively effect the mechanical properties of the endotracheal tube. In conditions replicating a ventilated patient leaching studies would also have to show no nanoparticles leach out. For 3D printed materials the regulatory pathway may be trickier as these products are more novel, however 3D printing is being increasingly used in healthcare and with every new 3D product entry to the market there sets a precedence for other 3D printed materials to enter more easily. Similarly with the swell encapsulated product this would have to show the original function

of the product is not disturbed by the additive 3D printing approach, and that no nanoparticles in particular leach out.

1.1 AN OVERVIEW OF ANTIMICROBIAL ENDOTRACHEAL TUBES ON THE MARKET AND IN DEVELOPMENT

There are only two antimicrobial endotracheal tubes currently available on the market (Agento[™] and Bactiguard®). Due to the pandemic, there has however been an increased interest in the area, and therefore there are companies now with emergency use approval or seeking health agency approvals for such products. Below describes an overview of products either on the market or in development.

Agento[™] – The first commercially available antimicrobial endotracheal tube on the market, which received food and drug administration (FDA) approval in 2008. It is coated with silver, and the release of silver ions disrupts cell functions to prevent bacterial growth ^{25, 43, 44}.

A randomized trial, designed to be a prospective, single-blind controlled study across multiple centres in North America, on 1509 patients expected to require mechanical ventilation > 24h. It was found that microbiologically confirmed rates of VAP fell from 7.5% to 4.8% with the use of the AgentoTM endotracheal tube (p = 0.03), and that it was associated with a delayed occurrence of VAP (p = 0.005). However, there were no statistical differences between controls and the AgentoTM when it came to intubation duration, length of stay, or mortality 25 .

A potential reason for the significant reduction in VAP incidence, yet not in mortality rates, is that this trial only accounts for early onset VAP. The average duration of intubation of patients was not given, so it is suspected this may have been around or below 5 days, where after late onset VAP sets in and has

a much higher risk of mortality. Therefore, silver-based technology may fall short of providing the best antimicrobial protection to emerging companies who offer more long-term solutions. Other aspects that could contribute to the short-term efficacy is that the coating is only on the outer surface (and biofilms form on all surfaces), as well as the growing presence of silver-resistance genes in the environment. There is also a lack of selectivity of silver ions to target bacterial cells over mammalian cells⁴⁵, which for the application of ETTs where long-term intubation is often necessary, could potentially be causing serious damage of which the consequences have not been fully investigated.

Bactiguard® - This technology utilizes a silver-palladium-gold alloy coating, which is reported to induce a galvanic effect that reduces cell attachment. Having previously been used in urinary tract and central venous catheters (FDA market approval 1994 and 1996 respectively), they utilized the same technology for endotracheal tubes and received market approval in 2011.⁴⁶

The Bactiguard® website quotes reduced incidence rates of VAP by 67% (p = 0.14), a 'significant' drop in antibiotic use (p = 0.05) and an average reduction in hospital stay of 2 days, when using their antimicrobial endotracheal tube as opposed to standard ones.⁴⁶ However, these values were only representative of VAP incidence at 5 days, therefore can only be classed as data on early-onset VAP (similar to Agento[™] tests). Thus, no data is available on VAP primarily as a result from multi-drug resistant (MDR) bacteria (late onset VAP) – which is the most pertinent and challenging to treat of all VAP cases. The clinical study does not appear to be published to the public, with the website referencing 'data on file'. So, it is difficult to conclude if this product protects

against the primary bacteria known to cause VAP or if any information on VAP incidence ≥ 5 days was even investigated.

A post-market clinical trial has been published, included 19 patients who were intubated with the antimicrobial endotracheal tube for a median time of 5 h.⁴⁷ With such a small study size and short intubation duration, there was not enough data to draw conclusions on potential protection against late-onset VAP from this study either.

However, more recently a study which started in 2018 and was published in January 2022, conducted in Belgium, Bactiguard Infection Protect (BIP) (gold, silver and palladium coated endotracheal tubes) were once again tested in their efficacy against VAP.⁴⁸ It was a multi-centre, randomised, controlled double-blind prospective study of ventilated patients who were randomly intubated with either noble metal coated endotracheal tubes or non-coated as a control group. A total of 323 patients were enrolled with 168 in the study group and 155 in the control group. Overall, they found less antibiotics were used in the noble metal coated endotracheal tube group (number of antibiotic days decreased by 6.6%) and a decrease in VAP incidence of 5.1%. Therefore, though numbers are only marginally decreased, it does provide evidence which supports coated endotracheal tubes can reduce rates of VAP and as a result the need for antibiotic intervention. It is also noted that the funding for the study nurses for two years to conduct this study was provided by Bactiguard®.

N8 Medical CeraShield™ - This endotracheal tube design has a ceragenineluting coating, which has not yet been granted FDA market approval. Ceragenin is a synthetic mimic of antimicrobial peptides (AMPs), which are key components of our natural defence system against antimicrobial colonization. The coating presents as a broad-spectrum antibacterial and antifungal material, which attempts to prevent microbial growth.⁴⁹ The elution of ceragenin from the coating is controlled by both the polyurethane coating structure as well as ion exchange. To better illustrate the polymicrobial aspects of real-world biofilms,⁵⁰ mixed species of *P. aeruginosa* with either methicillinresistant *S. aureus* (MRSA) or *Candida auris* were used in their microbial testing, which saw a delayed onset of biofilm formation on endotracheal tube segments by 2-3 days compared to controls. By day 3-4 however, there was little difference between biofilm formation of CeraShield™ coated and control segments.⁴⁹

These endotracheal tubes were granted emergency use by Health Canada on April 2nd 2020⁵¹.

Sharklet® - This design doesn't require the release of an antimicrobial agent from the surface, but instead optimises a micro-patterned surface inspired by the topography of shark scales, to prevent initial cell attachment and biofilm growth. It is thought that the pattern on the surface increases overall surface energy, which is able to interrupt the quorum sensing between bacteria (the process by how bacterial cells communicate with each other). ^{52, 53} The use of surface manipulation over the release of an antimicrobial agent is highly desirable when considering the safety of medical devices, and was undergoing an accelerated device pathway for FDA approval (2016), however there appears to be no news since and thus the conclusion is this wasn't successful.

To compare this to the previous silver-based technology of Agento[™], an *in-vitro* drip-flow biofilm model was used to compare the Sharklet® against Agento[™] using a lab strain of *P. aeruginosa*. This saw reductions in biofilm by 71% (p = 0.016) and 65% (p = 0.064) respectively, compared to standard untreated endotracheal tubes. This showed a potential 6% increase in protection over Agento[™],⁵² however considering trials eventually concluded there was no significant difference when using Agento[™] over standard tubes, a 6% on this increase may not be enough to translate into real world differences.

Commonwealth Scientific and Industrial Research Organisation (CSIRO)/Boulous & Cooper Pharmaceuticals Pty. Ltd. – Published in April 2020 was a novel styrylbenzene-based antimicrobial (BCP3) whereby similarly to the swell encapsulated work described in this thesis, BCP3 mixed with poly(lactic-co-glygolic acid (PLGA) was applied to endotracheal tube segments (polyvinyl chloride (PVC) based) through a 'facile dip-coating' which is effectively the same process as swell encapsulation. Their process involved using tetrahydrofuran (THF) as a solvent and 'dip coating' twice. The highest concentrations of BCP3 and PLGA yielded their best results, whereby 91% and >95% kill was achieved for methicillin-resistant *S. aureus* (MRSA) and methicillin-sensitive *S. aureus* (MSSA) respectively, and a maximum of 63% kill for *P. aeruginosa*. Also, bacterial strains used were laboratory based ATCC 29213 (MSSA), ATCC 43300 (MRSA) and ATCC 27853 (*P. aeruginosa*), which does not include what is thought to be one of the most prevalent causes for VAP which is primarily gram negative bacteria such as *E.* coli⁵⁴. However,

benefits include that PLGA is already FDA approved for medical devices and there was no cytotoxicity observed.

Ondine Biomedical Ltd. – The technology Ondine use is based around photodynamic therapy (PDT). It is non-invasive and uses medical grade methylene blue to kill bacterial cells upon laser light activation. It does this by inducing fatal photo-oxidation on cells that have absorbed the photosensitizer This technique was approved in 2013 by Health Canada, and is regularly used in products such as MRSAid™, which prevents post-surgical MRSA infections⁵⁵, and has been used throughout the pandemic in care homes to stop spread of the disease⁵⁶. The treatment in its entirety is 6 minutes and includes swabbing the nose with methylene blue, followed by laser light treatment, and this process repeated once more (MRSAid laser manual). It is this laser meant for the MRSAid™ technology which has been used in the most recent experiments detailed in 3.3.1.

Ondine have deployed this technique in ventilated patients to understand how to deliver transbronchial therapy⁵⁷, and have demonstrated by an *in-vitro* study on the reduction of endotracheal tube biofilms using antimicrobial PDT (published 2011) explores this treatment⁵⁸.

An intubation model was used to represent a real-life clinical setting, which involved replicating the airway path of an intubated patient. This included not only the ETT, but a mechanical ventilator, humidifier, and ventilator airway circuitry tubing, so that conditions were as realistic as possible. Also, the ETT was positioned at an angle to simulate a patient following the advised elevated head position in the VAP bundle.⁵⁹ Clinical isolates of *P. aeruginosa* and

MRSA were used to grow mixed biofilms on the inside of standard ETTs, which were then used in the PDT procedure. The procedure involved spraying photosensitizer solution (in this case MB) into the lumen of the ETT, then placing a fibre optic catheter through the lumen of the ETT, activating the MB through laser light at 664 nm (MBs maximum absorbance). There were two treatments with the laser lasting 12 minutes each, with a break of 5 minutes in-between. It was reported that using this method of light treatment gave a 3 log₁₀ reduction (equating to 99.9%) (p < 0.005) of the mixed biofilm,⁵⁹ which considering are clinical and relevant strains to VAP, is the most successful bactericidal method without risk of promoting AMR investigated so far.

Though promising, this technology is not without its drawbacks. This study carefully recognised that this method was intraluminal, and that alone neither the MB nor laser was harmful to human tissue. 60, 61 However, any cell that has absorbed MB, will be affected if subsequently exposed to the light treatment. MB is known to be absorbed by mammalian cells as well as bacterial, thus could prove problematic if the initial MB spray is not confined to just the bacterial cells on the endotracheal tube.

As well, it is known that biofilm develops on both the inside and outside of the endotracheal tube (D. Walker, Consultant Anaesthetist, personal communication), so the risk of further biofilm growth is not completely eliminated with each treatment. Hence, unless a photosensitizer selective to pathogenic bacterial cells is developed, or a way to keep the outer surface separate from surrounding tissue, it may be difficult to completely eradicate biofilm using this technology alone. Lastly, though highly effective in that

moment of fatal photo-oxidation, once completed the antimicrobial activity halts and biofilm is free to build up again. The study proposes a recommendation that this treatment is provided every 8h, however without clinical trial information it is unknown whether this may do more harm than good in potentially dislodging surrounding bacterial biofilm in the process of reswabbing with dye.

In addition to this, through personal communication Ondine have been told by Health Canada that an alternative solution must be found to replace the swabbing with MB. A suitable alternative may be development of an antimicrobial endotracheal tube (as described in this thesis) combined with Ondine's laser technologies to enhance its action.

2 CHAPTER 2 - THE DEVELOPMENT OF LIGHT ACTIVATED ANTIMICROBIAL ENDOTRACHEAL TUBES

2.1 INTRODUCTION

This chapter describes the development of an antimicrobial endotracheal tube by using swell encapsulation techniques, tested against multiple multi-drug resistant bacteria all cultured directly from endotracheal tubes. As well, testing against biofilms which were grown over the span of 2 weeks.

2.2 METHODS

2.2.1 GOLD NANOCLUSTER SYNTHESIS

The MB was purchased (Acros Organics, pure certified, code: 414240250) and the Au₂₅(Cys)₁₈ made by microfluidic synthesis in UCL Department of Engineering (L. Panariello and S. Pal) as per⁶². Below is a schematic of the system.

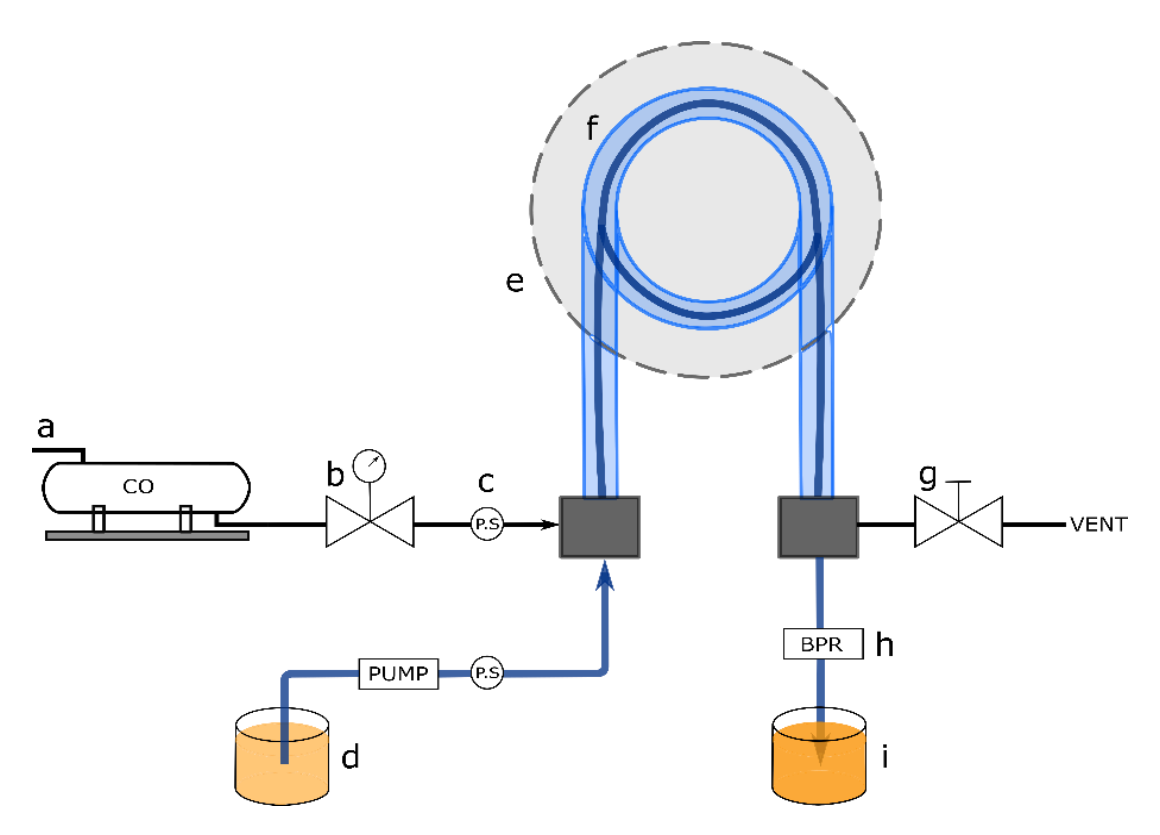


Figure 3. The microfluidics synthesis set up for the Au25(Cys)18 cluster synthesis from gold precursor solution, a) carbon monoxide alarm and inlet system b) pressure regulator valve c) pressure sensor d) gold precursor solution e) hot plate and oil bath f) tube.

50 mL of precursor solution was made by dissolving L-cysteine in a minimum amount of DIW in a 50 mL volumetric flask, then by adding 20 mL of gold (III) chloride trihydrate, followed by 1.66 mL of sodium hydroxide (NaOH) 2 M solution. Upon addition of the NaOH, the solution should change from cloudy to clear, and the remainder of the volumetric flask made up to 50 mL using

DIW. The precursor solution was then placed at (d) for the synthesis to start. Stirring speed was 800 rpm and liquid flow rate at 0.33 mL/min. 6 mL is let pass through the system before collection of Au₂₅(Cys)₁₈ starts. After this, once ~1-2 mL has passed through the system and collected at (i), this was tested by UV-Vis spectroscopy to check the Au₂₅(Cys)₁₈ concentration. 200 uL was diluted into 800 uL of DIW and absorbances should show at ~0.35 at 670nm and ~0.18 at 610nm for a resulting 10 mM Au₂₅(Cys)₁₈ solution. The synthesis, full materials characterisation and use of Au₂₅(Cys)₁₈ as part of an antimicrobial mix used together with crystal violet was published in 2020.²⁸

2.2.2 ZINC NANOPARTICLE SYNTHESIS

Zinc (II) dioctylphosphinate (C₃₂H₆₈O₄P₂Zn / Zn(DOPA) for short use in figures) was synthesized according to a method in literature.3 Di(octyl) phosphinic acid (0.55 mL, 1.72 mmol) was dried under vacuum for 1h. Anhydrous toluene (57.5 mL) and diethyl zinc (ZnEt2) (0.86 mL, 8.61 mmol) were added and left stirring overnight ~18 h. A solution of water (0.31 mL, 17.22 mmol) and acetone (29 mL, 400 mmol) was slowly added over 15 minutes and stirred for a further 2 h. The solution was transferred to a centrifuge tube and acetone added to precipitate. This was then separated by centrifugation (20 minutes, 4000 rpm) and washed x2 with toluene and acetone (10 mL). Waste solvent was removed

after final centrifugation and air-dried overnight ~ 18 h. The product was then transferred to a mortar and pestle to yield a white powder. Yield 0.61 g (52 %).

Figure 4. Chemical structure of zinc di(octyl) phosphinic acid (DOPA).

2.2.3 SYNTHESIS OF THE ANTIMICROBIAL ENDOTRACHEAL TUBE

To prepare the antimicrobial endotracheal tubes, endotracheal tubes already commercially available on the market (TimescoTM) were bought in and antimicrobial components MB and $Au_{25}(Cys)_{18}$ were swell encapsulated into the polymer. The endotracheal tubes were cut to ~ 1x1cm pieces using a scalpel in sterile conditions. These pieces were then separated into beakers containing the relevant solution, whether that be a blank control or a sample mix. Sample mix solutions contained varying amounts of MB and $Au_{25}(Cys)_{18}$ [or swapping the $Au_{25}(Cys)_{18}$ for Zinc (II) dioctylphosphinate] in a 1:1 ratio of acetone to deionised water (DIW). 10 mL of solution was used per x1 sample piece, e.g., 10 samples = 100 mL.

$$\begin{array}{c|c} & & & \\ & & \\ & & & \\ & & & \\ & & & \\ & & \\ & & & \\ & & & \\ & & & \\ & & & \\ & & & \\ & & & \\ &$$

Figure 5. Chemical structure of methylene blue.

The samples were then mixed in dark conditions at 450 rpm for 4h at 30 °C, and subsequently washed x5 times for 5 mins at 40 °C in sterile phosphate buffered solution (PBS), and a further x5 times for 5 mins at room temperature

(RT) in DIW. Samples were patted dry and left to airdry overnight between two filter paper sheets to absorb any remaining moisture before microbial testing.

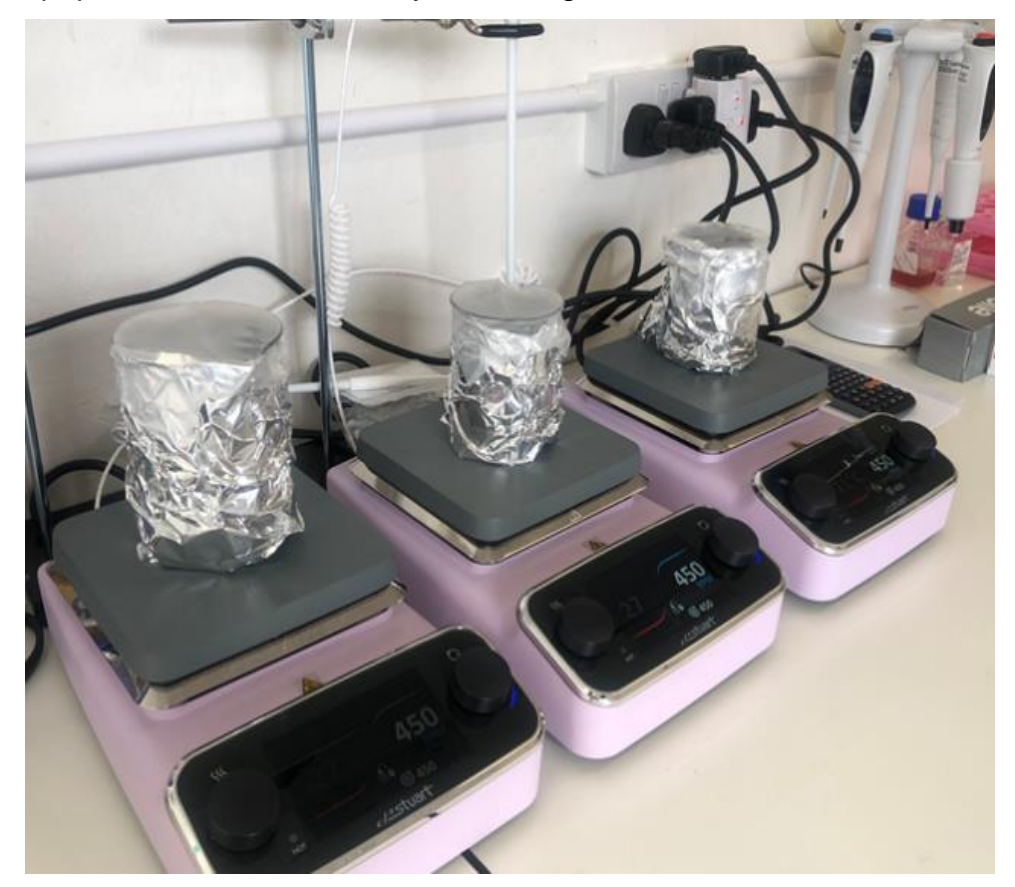


Figure 6. The simple synthesis set up in parallel for swell encapsulation of the endotracheal tubes to make them antimicrobial.

2.2.4 MATERIALS ANALYSIS OF RAW ENDOTRACHEAL TUBE MATERIAL

X-ray Photoelectron Spectroscopy (XPS)

XPS (Thermo Scientific, K-Alpha Surface Analysis) was used to determine commercial ETT composition, as well as the effect of using silicone-coated syringes in the swell encapsulation process. Survey scans as well as point analysis at two depth profiles was carried out and interpreted using casaXPS software.

Scanning Electron Microscopy (SEM)

Samples were gold sputtered (Agar Scientific, Sputter Coater) for 10 seconds at 0.08 mbar, and analysed via scanning electron microscopy (SEM) (JOEL JSM-7601F field emission microscope) to investigate surface morphology of the ETTs (plain commercial, controls and samples).

Water Contact Angle

For detecting changes in surface hydrophobicity before and after swell encapsulation of antimicrobial agents, a water contact analyser (FTA 1000 Drop Shape Instrument) was used using a gauge 27 needle. Prior to analysis, as a flat sample surface was required, ETT segments were all placed under compression for 1h. Drops used in analysis were 6.5 µL DIW using FTA32 software for subsequent analysis. Three repeats were performed.

2.2.5 SAFETY & STABILITY ANALYSIS

A leaching investigation was conducted where a sample was placed in a 50 mL centrifuge tube with 10 mL sterile PBS. This was left at 37 °C h over 10 day and the resulting solution measured by UV-Vis spectroscopy to determine dye leaching and X-Ray fluorescence (XRF) for presence of nanoclusters. For the UV-Vis a 5-point calibration curve was used to determine the concentration of leaching methylene blue. Cytotoxicity was conducted externally by Virology Research Services using ISO21702.

2.2.6 STRESS STRAIN ANALYSIS

Standard ASTM D638 – 14, Standard Test Method for Tensile Properties of Plastics was followed as closely as possible, changes made are described below. Before swell encapsulation of endotracheal tube pieces, the tube was cut into sections which were 6cm long, cut by scalpel. Pieces were then swell encapsulated with varying amounts of MB and Au₂₅(Cys)₁₈ and were swell encapsulated at varying temperatures and times (detailed in section 3.3) before drying as per 3.2.1.

Samples were then taken to Boston Scientific (previously BTG Biocompatibles) for tensile testing. A template for the British standard dumbbell shape was created and using a scalpel the rectangle endotracheal tube pieces were cut into the standard dumbbell shape for testing.

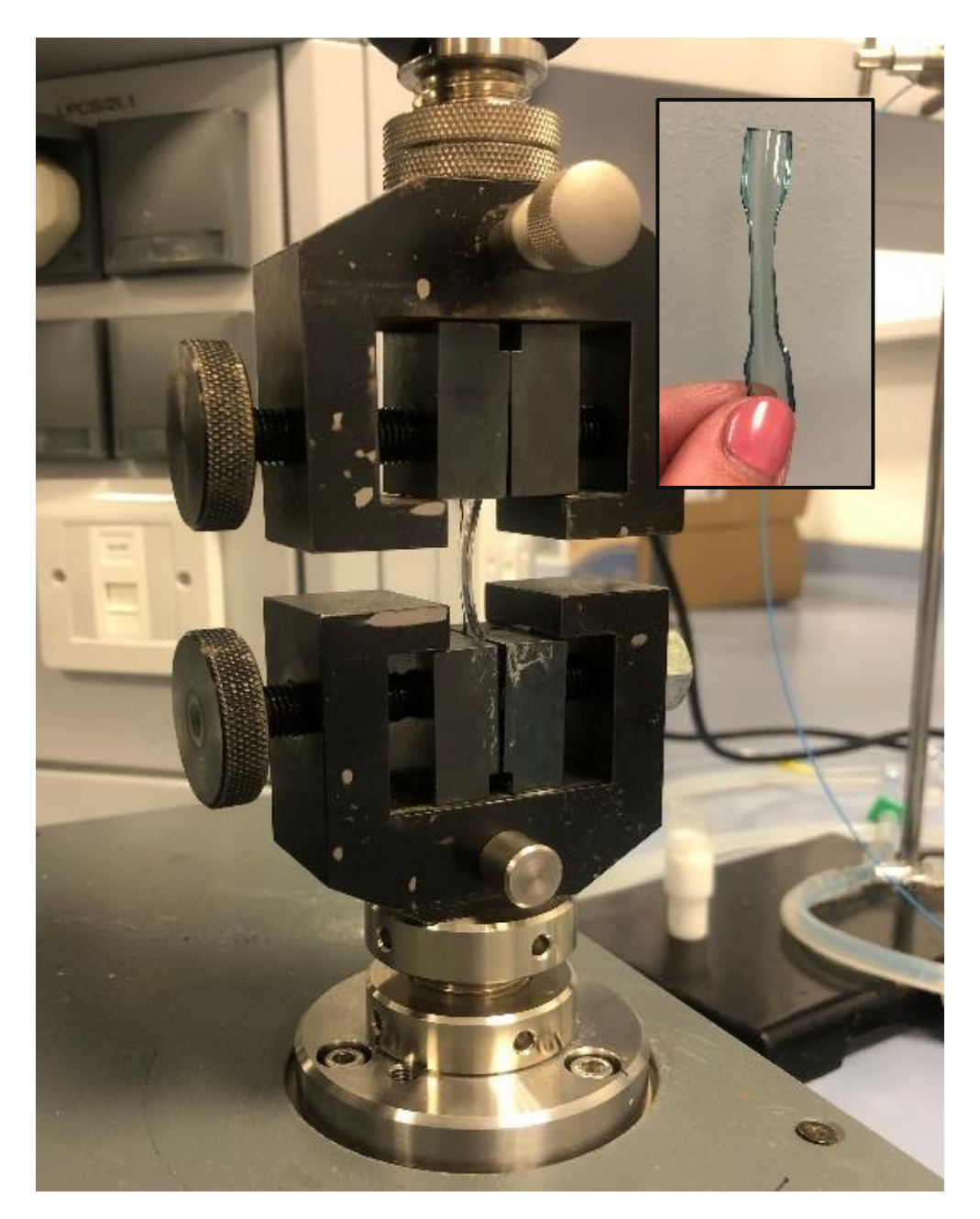


Figure 7. Image of the tensiometer machine used for tensile stress testing, as well as a dumbbell shaped test sample in the top righthand corner.

A benchtop Lloyd tensiometer machine was used to carry out the tensile tests. Direction speed used was 100 mm/min and both load at break and machine extension recorded. Each sample test was repeated three times to get an average result for each sample type.

2.2.7 MICROBIOLOGICAL ASSAY

This testing assay is one developed and used by UCL Microbiology to enable comparisons within the group. The only deviation is 1) no coverslip used to press down the bacteria, the bacteria remains as a droplet on the material surface for testing and 2) the addition of the spiral plater for serial dilutions, where a validation experiment was conducted to ensure continuity between manual and automated methods.

A total of 10 mL BHI was placed into a 50 mL centrifuge tube. Using a sterile loop, one bacterial colony (strains used: *E. coli* ATCC 25922, *S. aureus* 8325-4 or clinical strain *E. coli* cultured from an ETT) was placed into the BHI and cultured at 37 °C at 200 rpm for 18h. This was then centrifuged at 21 °C at 5000 rpm for 5 mins. The waste supernatant BHI was removed and replaced with 10 mL PBS. The solution was vortexed until the bacterial pellet was resuspended. This was then centrifuged again, and the process repeated in order to wash the cells. From this inoculum, 10 uL was placed in 990 uL PBS to gain a final inoculum (x) of roughly 10⁵ colony forming units (CFU/mL).

To prepare the sample chambers a filter paper was placed inside a petri dish, which was wetted with 2 mL PBS. Then two toothpicks were placed parallel to each other on top of the wetted filter paper, of which a microscope slide was placed on top of perpendicular to the toothpicks. This creates a sterile humidity chamber to keep the bacteria from drying out, particularly in biosafety cabinet settings where the flow of air is constant.

Endotracheal tube sample pieces are placed with the inner lumen facing up on the microscope slides, and 25* uL of inoculum (x) is placed on top of each sample in a droplet. These petri dishes are then either placed in a dark box or in light conditions (set to 10,000 lux, confirmed by light meter (Onecall, mini light meter, resolution 0.1 lux) for a determined amount of time (detailed in section 3.3 with corresponding results). *(50 uL for new spiral plated method)

Manual method (experiments pre-May 2021) – 450 uL PBS was placed into a 50 mL centrifuge tube. Upon completion of light/dark exposure time, the sample was carefully lifted into the centrifuge tube and vortexed. This was repeated for each individual sample. From this 200 uL from each sample tube was taken and placed into 96 well plates, which becomes the neat (N)

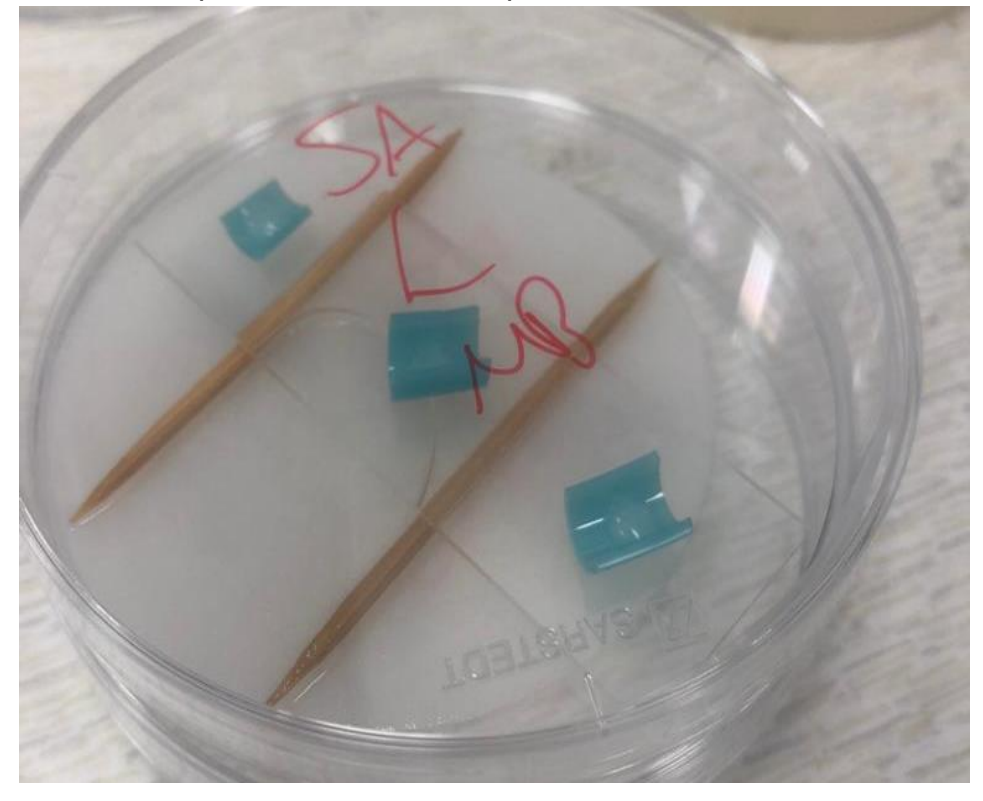


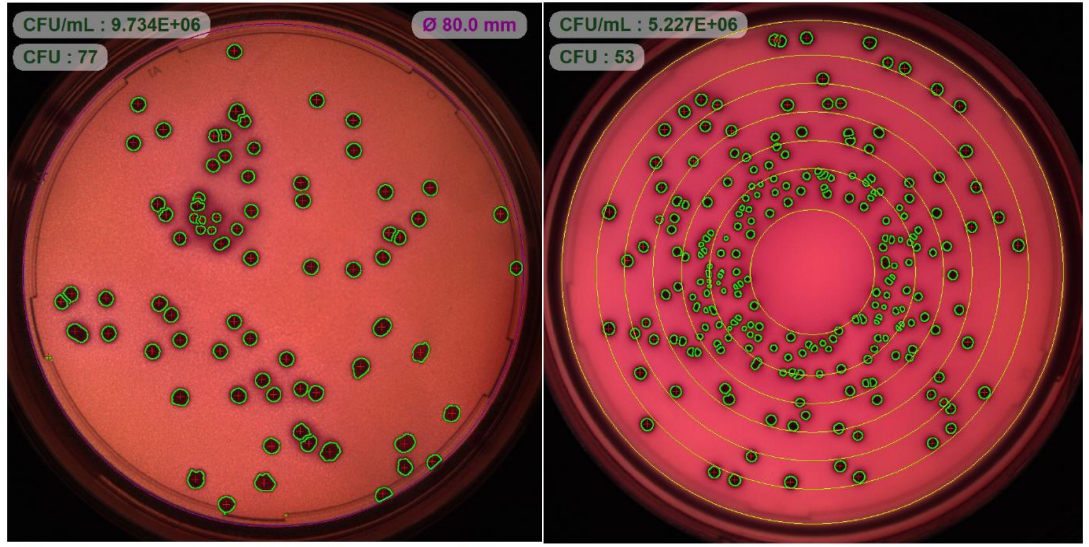
Figure 8. Image showing the humidity chamber described with x3 samples being tested.

suspension. Serial dilutions were performed by diluting 20 uL of N into 180 uL, continuing this for a further 5 times to get a 100,000-fold dilution. N \rightarrow -1 (10-fold) \rightarrow -2 (100-fold) \rightarrow -3 (1,000-fold) \rightarrow -4 (10,000-fold) \rightarrow -5 (100,000-fold). Each dilution was then plated by taking 100 uL from the well and spreading onto agar plate (MacConkey agar for *E. coli*, mannitol salt agar for *S. aureus*). The plates were incubated at 37 °C for 24 h. The plates were read by manual counting method with a >300 colony limit exclusion.

Automated spiral method (experiments post-May 2021) – 900 uL PBS was placed into a 50 mL centrifuge tube. Upon completion of light/dark exposure time, the sample was carefully lifted into the centrifuge tube and vortexed. This was repeated for each sample. From this 600 uL was taken and placed into a 0.5 mL Eppendorf tube. The Eppendorf tube is then placed into the holder on the automatic spiral plater (Intersciece, EasySpiral Dilute, ref: 414 000), and the desired dilution selected, and 'plate' pressed, to plate in a spiral dilution from N to -5.

The settings selected were 50 uL total volume plated, on 90 mm petri dishes, on exponential plating mode. If this was still too concentrated, the N sample was diluted first to either -1, -2, or -3, and then spiral plated further. An average over two dilutions was taken by the plate counter and CFU/mL calculated automatically. For the samples which have undergone an extra dilution step (50 uL inoculum in 900 uL PBS) compared to inoculum in which 600 uL was taken directly from the suspension and into the Eppendorf tube, the CFU/mL results for the samples were multiplied by 19 to account for the extra dilution step (dilution factor 950 / 50 = 19).

The new spiral plated method was validated by repeating experiments three times using both the manual and spiral plated method, where when three consistent results within the same log as each other were achieved the method



Sample analysed with SCAN 500®, version 8.6.5.0

Sample analysed with SCAN 500®, version 8.6.5.0

Figure 9. An image to compare the manual plating method to the spiral plating method, where on the left-hand side (manual) colonies are manually spread using an L-shaped spreader, and each individual dilution will have a different plate similar to this. Which was then counted and recorded manually. Here for comparisons sake this is shown on the automatic colony counter. On the righthand side (spiral) are the rings which represent dilutions going from N (in the centre) to 5 (the outer ring). Therefore, having all dilutions on one plate, easily read by the automatic colony counter as illustrated here. An example of the exported PDF results can be found in the appendix.

was considered ready for use. It is thought the manual method was less accurate due to the manual dilution stage and potential for ease of contamination during these steps, and therefore slight variation in result consistency was accepted as normal.

2.2.8 BIOFILM DEVELOPMENT PROTOCOL

This protocol was developed by me using two isolates cultured directly from an endotracheal tube were used in this biofilm protocol (UCLH). MRSA US137 and P. aeruginosa RS080 with VEB (Vietnamese extended-spectrum β -lactamase) ESBL (extended-spectrum β -lactamase) from the Royal Free Hospital. In particular, ESBL producing pathogens are a major cause of resistance to existing antibiotics, and in this case treatment options are limited.

A total of 10 mL BHI was placed into a 50 mL centrifuge tube. Using a sterile loop, one bacterial colony was placed into the BHI and cultured at 37 °C at 200 rpm for 18h. Optical density measurement taken by 4-fold dilution in BHI (0.25 mL inoculum into 1.25 mL BHI).

The inoculum was then centrifuged at 21 °C at 5000 rpm for 5 mins. The waste supernatant BHI was removed and replaced with 10 mL PBS. The solution was vortexed until the bacterial pellet was resuspended. This was



Figure 10. Image of the samples used in biofilm experiments cut to 1.5cm length.

then centrifuged again, and the process repeated. *P. aeruginosa* was diluted further by placing 25 uL inoculum into 9900 uL fresh PBS.

Two sterile 12 well plates were used, one to be exposed to light and one as a dark control, and 1.5cm long pieces of endotracheal tube were placed in well (both blank controls and antimicrobial samples) with the lumen facing up. The mixed co-culture biofilms of *P. aeruginosa* and MRSA were inoculated in the following ratios (mL): 1:1, 1:2, 1:3, 1:4, 1:5 to a total of 2mL fill. For the antimicrobial results reported on with *P. aeruginosa* only biofilms a 2mL fill was used with only *P. aeruginosa* inoculum.

For the light exposed samples, the 12 well plate was placed under white light for 3h at 10,000 lux (the same light intensity as planktonic bacteria experiments detailed previously), and the dark placed in a dark box for 3h. Following the exposure, the 12 well plates are placed into a Tupperware box, with sterile water just covering the bottom to ensure humidity is kept. This box was placed in an incubator at 37 °C and left for a week.

At one week, the solution in each well was carefully removed by pipetting slowly from the side of the well, careful not to disturb any growing biofilm.

This is replaced with a fresh 2 mL of BHI and put back into the Tupperware box in the incubator at 37 °C and left for a further week.

To collect biofilm, prepare 50 mL centrifuge tubes with 900 uL sterile PBS, one tube per sample. Using sterile tweezers, the endotracheal tube slice is pulled upwards until the biofilm 'snaps' (see figure 9). The sample with biofilm

was then placed into the 50 mL centrifuge tube with sterile PBS. Vortex each sample until biofilm is visibly mixed with the PBS (~30 seconds each). From this, the protocol as per the microbiological assay above is performed using the spiral plater. 600 uL is taken from each tube and transferred to a 0.5 mL Eppendorf tube, which is then spiral plate diluted to the desired dilution. For MRSA only biofilms Mannitol Salt agar plates (PO1169A) were used. For *P. aeruginosa* MacConkey agar without salt (PP0470). For mixed biofilms, both MacConkey and Mannitol Salt agar plates are used, as well as Nutrient agar plates (PO0155A).

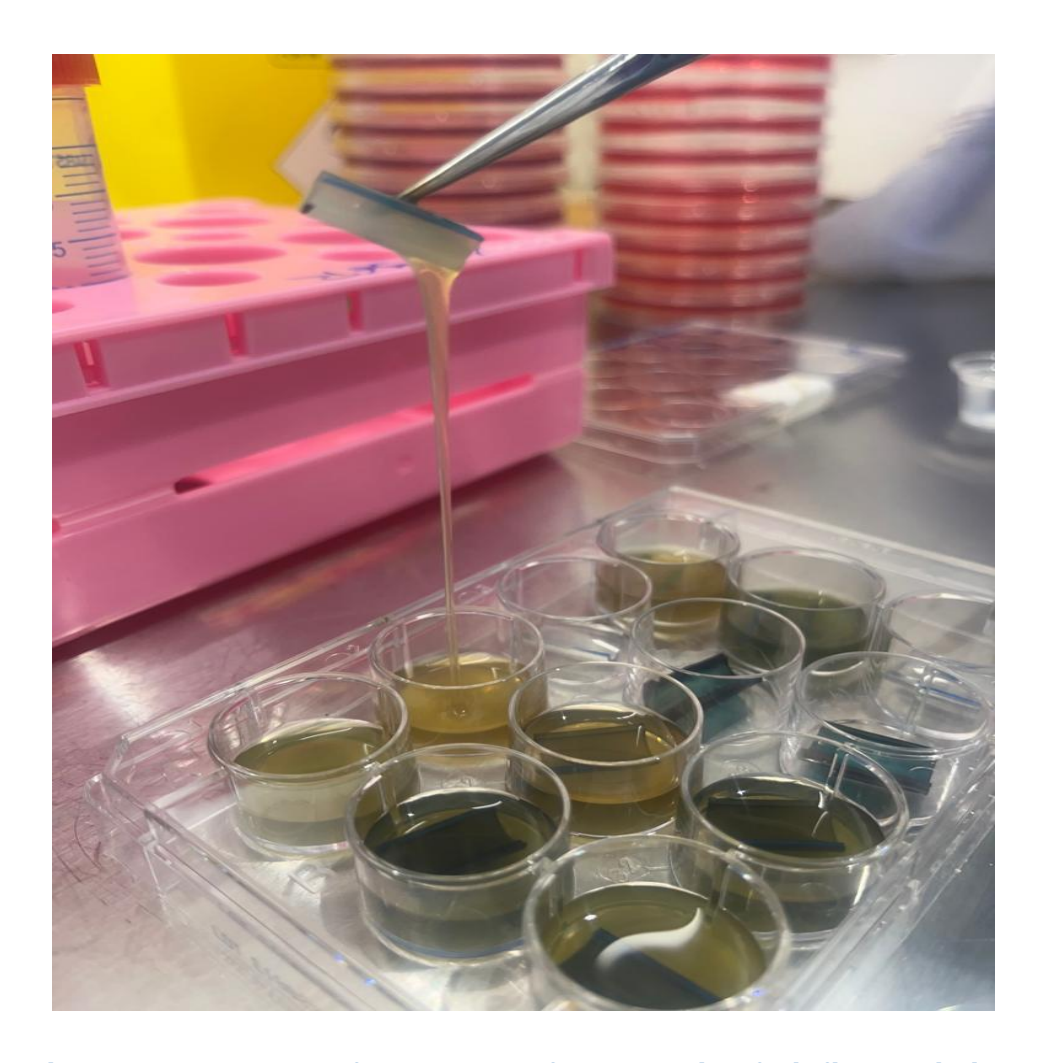


Figure 11. Removal of the sample for analysis of biofilm, this image shows the sample with biofilm being lifted upwards until 'snapping'.

2.3 RESULTS & DISCUSSION

2.3.1 STRESS STRAIN ANALYSIS - TENSILE STRESS

Tensile stress testing was carried out to determine the effects of the swell encapsulation process on the functionality of the endotracheal tube. The tube must not become brittle and must still be elastic enough to mould to the shape of the patients' airways when intubated. Therefore, it is important the polymer's properties post-swell encapsulation do not change significantly.

Table 2. Table summarising the swell encapsulation parameters for the tensile stress optimisation

parameters for the tensile stress optimisation			
1st experiment			
MB added (g)	Conc. (ppm)		
0.048	800		
0.024	400		
0.006	100		
2nd experiment			
Au25(cys)18 added (mL)	Conc. (% v/v)		
1	1		
3	5		
6	10		
3rd experiment			
Time (h)			
3			
6			
18			
4th experiment			
Temp (°C)			
20			
30			
40			

In table 2 are the details of the experiments and the changes made in each. Other parameters not detailed in each experiment were kept as per the original protocol: 800 ppm MB, 10% v/v Au₂₅(Cys)₁₈, room temperate (20 °C), and for 18h overnight. The table is colour coded to match the graph, to focus on the changing parameter in each section.

Below are the results from a range of changes made to the swell encapsulation process including amount of MB, amount of Au₂₅(Cys)₁₈, time and temperature – colours relating to table 2 above. This was then compared to an original sample of endotracheal tube, illustrated in red and by a red line running across the graph for easy reading.



Figure 12. A graph summarising the results of the tensile stress testing, where the red bar and red line across the graph show where the untreated endotracheal tube material lies. The graph is colour coded to table 2. Paired two tailed T test for 3 h P = 0.44.

The graph shows a slight increase in the average load at break when the MB is increased above 400 ppm, therefore it was determined 400 ppm would be

optimal. When increasing the amount of Au₂₅(Cys)₁₈ from 1% to 10%, the average load at break decreased. Therefore, taking into consideration the costs of gold with the load at break properties, it was determined that 5% Au₂₅(Cys)₁₈ would be optimal. Regarding the time of the swell encapsulation, increasing the time did increase the average load at break, however the increase in time does not directly correlate with an increase in average load at break, and the shortest swell encapsulation time at 3h decreases the load at break by an average of 13N. However, this is still not a statistically significant decrease (P > 0.05). An increase in temperature decreased the load at break raising from 20 °C to 40 °C, with the closest result to the original sample coming out as 30 °C. Therefore, it was decided that the overall new parameters for testing for optimal tensile stress properties, remaining as unchanged as possible compared to the original untreated endotracheal tube sample, would be 400 ppm, 5% Au₂₅(Cys)₁₈, 4h encapsulation time, at 30 °C. It was using this new protocol of a 4h encapsulation time at 30 °C that the antimicrobial optimisation samples were made. Overall, none of the parameter changes were enough to be statistically significant, though it is desirable to keep as unchanged as possible.

There was an issue using the die cutter to cut the exact dumbbell shape due to the strength of the polymer material, and so a scalpel was used to cut the dumbbell shape from a template. Therefore, there may have been small discrepancies in tensile stress results due to this. Preferably this experiment would be repeated with a laser cutter to ensure accuracy and repeatability between samples. A design of experiment was planned for this optimisation

work regarding both the antimicrobial activity and functional tensile stress testing; however, it was decided what is required for the microbiology and the repeats required for a design of experiment, it would be too lengthy and would require a dedicated team and much more resource than what was available.

2.3.2 SAFETY & STABILITY LEACHING OUTCOMES

Methylene blue has a widely known and understood toxicology profile, ⁶³ and is currently used as medication in a safe dose of <2 mg/kg (1% methylene blue solution) for methemoglobinemia, and also already used in the cuff of the endotracheal tube mixed with saline to immediately detect damage to the cuff during certain surgeries. ⁶⁴ However, it has been shown to precipitate serotonin toxicity at >5 mg/kg, ⁶⁵ and patients also taking drugs with serotonergic activity (such as widely used antidepressants) may have increased risk of this. ⁶⁶ Therefore, it's important to know if any how much methylene blue is leaching out over time, even if risk overall is low.

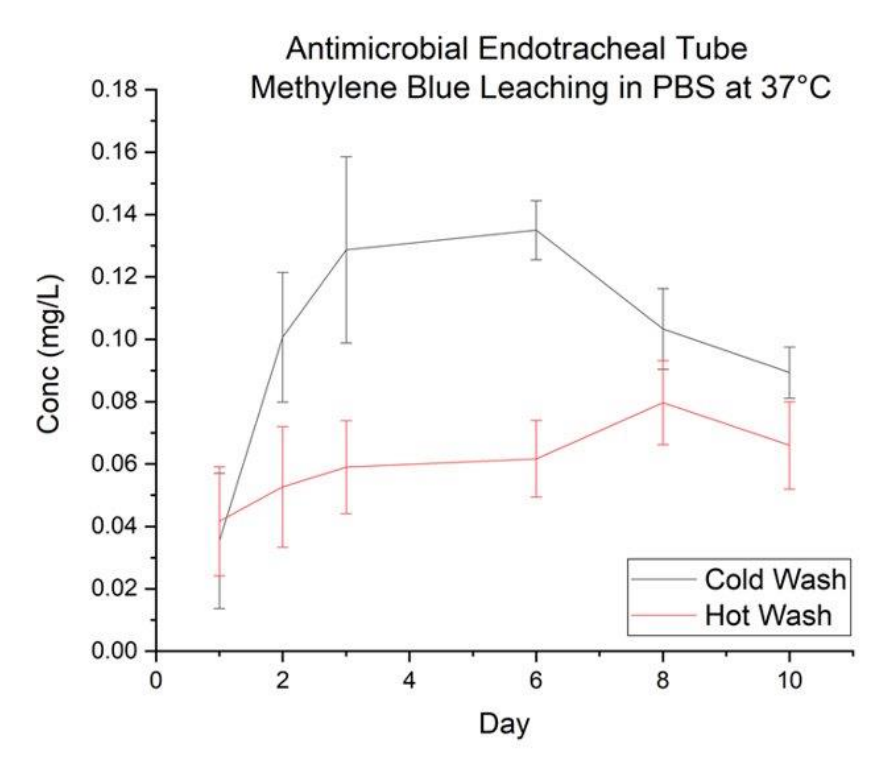


Figure 13. Leaching profile of methylene blue over 10 days from swell encapsulated antimicrobial endotracheal tube.

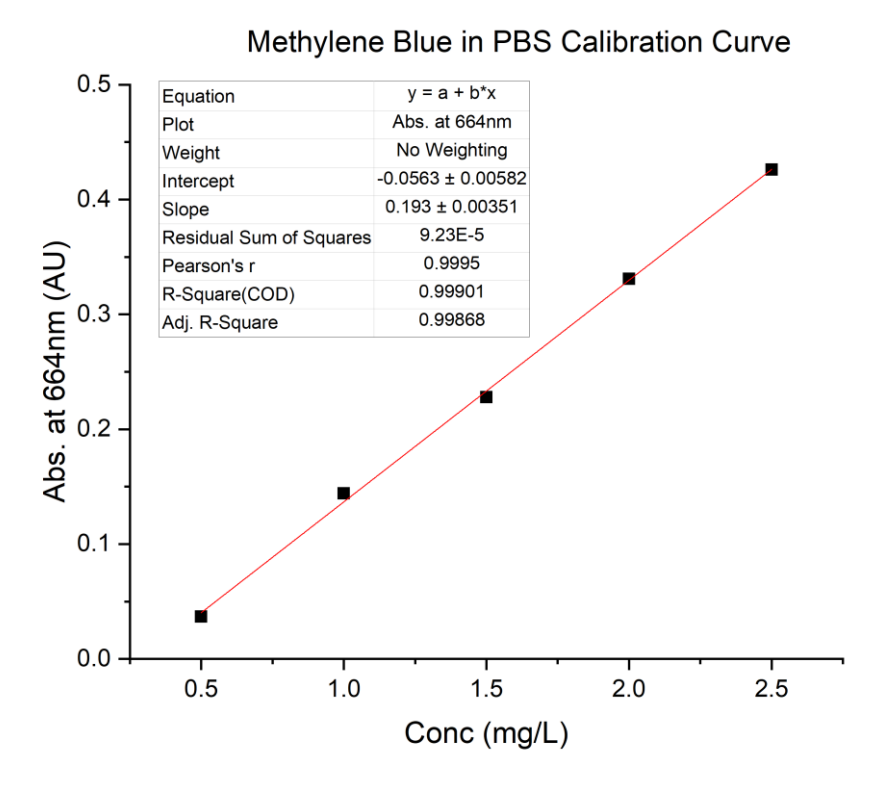


Figure 14. 5-Point calibration curve for methylene blue concentration leaching analysis.

What this shows is that even without the addition of a hot wash after the swell encapsulation step, the leaching over 10 days is still well below toxic levels at ~0.07 mg/L and ~0.09 mg/L for hot and cold wash processes respectively.

2.3.3 OPTIMISATION FOR MICROBIOLOGICAL ACTIVITY

Experiments until this point had been carried out at what was thought to be a maximum amount of MB and Au₂₅(Cys)₁₈ for proof of concept. The next set of experiments were planned to determine the minimum effective concentration of each MB and Au₂₅(Cys)₁₈ in the antimicrobial solution for swell encapsulation, and how changing the amounts of each affected the antimicrobial activity both in the dark and light. Currently only one repeat of the white light has been carried out, with plans to continue to x3 repeats of both white light and laser light before deciding on an optimal amount of MB and Au₂₅(Cys)₁₈ to continue development with.

The table below describes the six different mixes used, based on low, medium, and high amounts of each MB and Au₂₅(Cys)₁₈. Note so far experiments have been using 800 ppm for MB and 10% v/v for Au₂₅(Cys)₁₈.

Table 3. Table summarising the amounts of antimicrobial components added into optimisation experiment samples for antimicrobial testing.

Experiment No.	МВ	Au ₂₅ (Cys) ₁₈
(D/L = dark/light)	(ppm)	(% v/v)
0	0	0
1	100	5
2	400	5
3	800	5
4	400	2.5
5	400	5
6	400	10

White light exposure (3h, 10k lux) ETT Optimisation Summary - x2 biological repeats

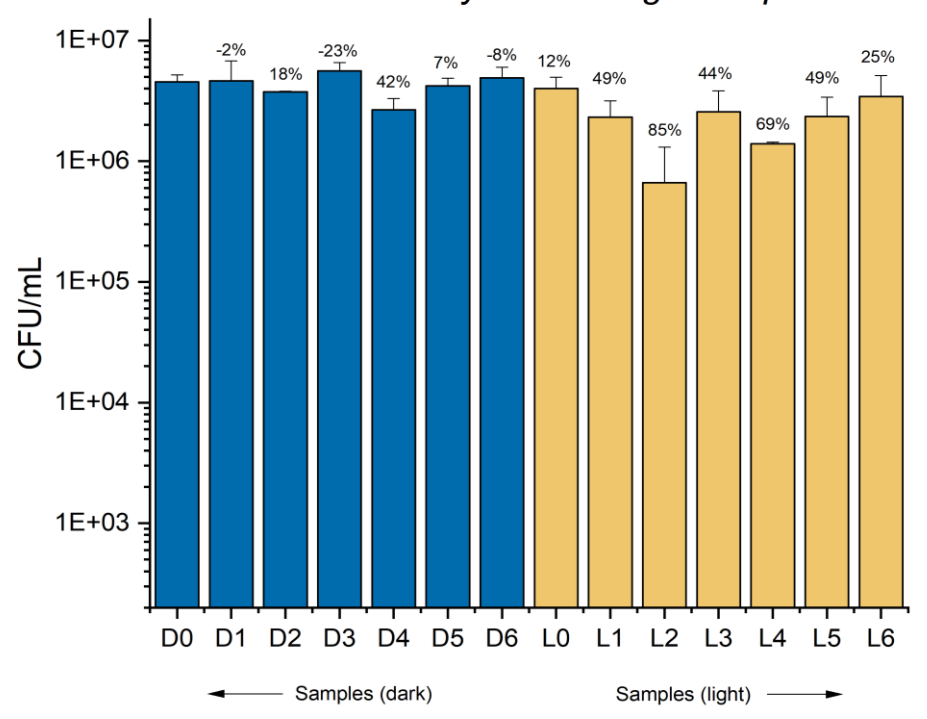


Figure 15. Graph showing the first repeat of antimicrobial optimisation experiments where blue represents dark control conditions and the orange representing the light conditions, of which samples were exposed for 3 h at 10,000 lux. Paired two tailed T test for L2 significance P < 0.0001. Paired two tailed T test for L3, L5 P = 0.04.

Originally lower levels (detailed in table 2) than what had been tested previously were explored for optimisation as it was assumed an extremely high amount was used for proof-of-concept experiments. However, these results show the maximum kill reached in the same setting was 85%, which is significantly lower than previously seen below detection level kills (> 3 log reductions). Therefore, optimisation experiments were repeated at higher levels, as well, both using 3h swell encapsulation time as well as 18h swell encapsulation time to see if the experiment time could be bought down.

Table 4. Table summarising the amounts of antimicrobial components added into round 2 of optimisation experiments samples for antimicrobial testing.

Experiment No.	МВ	Au ₂₅ (Cys) ₁₈
(D/L = dark/light)	(ppm)	(% v/v)
0	0	0
1	100	2.5
2	400	5
3	800	10

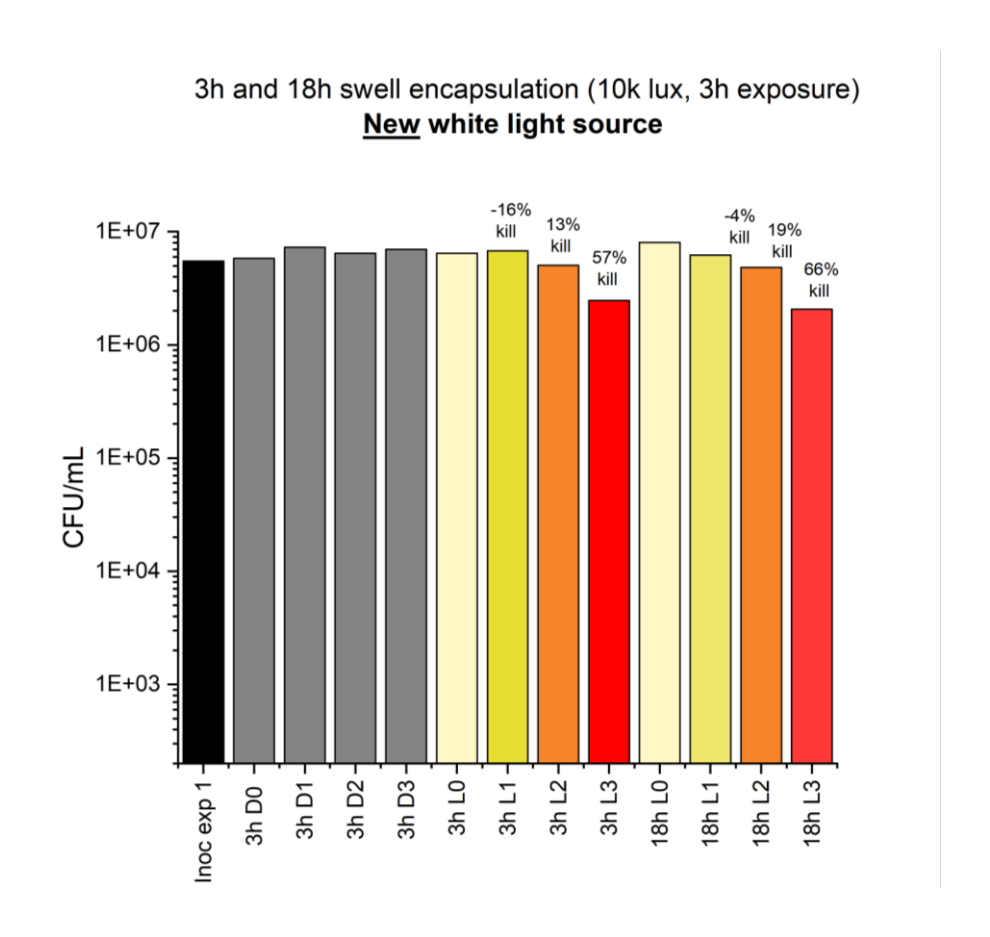


Figure 16. Antimicrobial activity using the new white light source (SAD lamp) of antimicrobial endotracheal tube samples.

It is important to note here between previous experiments and these optimisation experiments a laboratory move had occurred and as a result a different white light source was being used. This new white light source was a SAD lamp (Amazon, brand OKEEY). As seen from the second round of optimisation experiments includes the higher level used previously (D3/L3) yet the same level of kill wasn't reached, and again a maximum of 66% kill was reached. The lamp change was then considered as a factor and the same samples and experiment repeated with the old white light source.

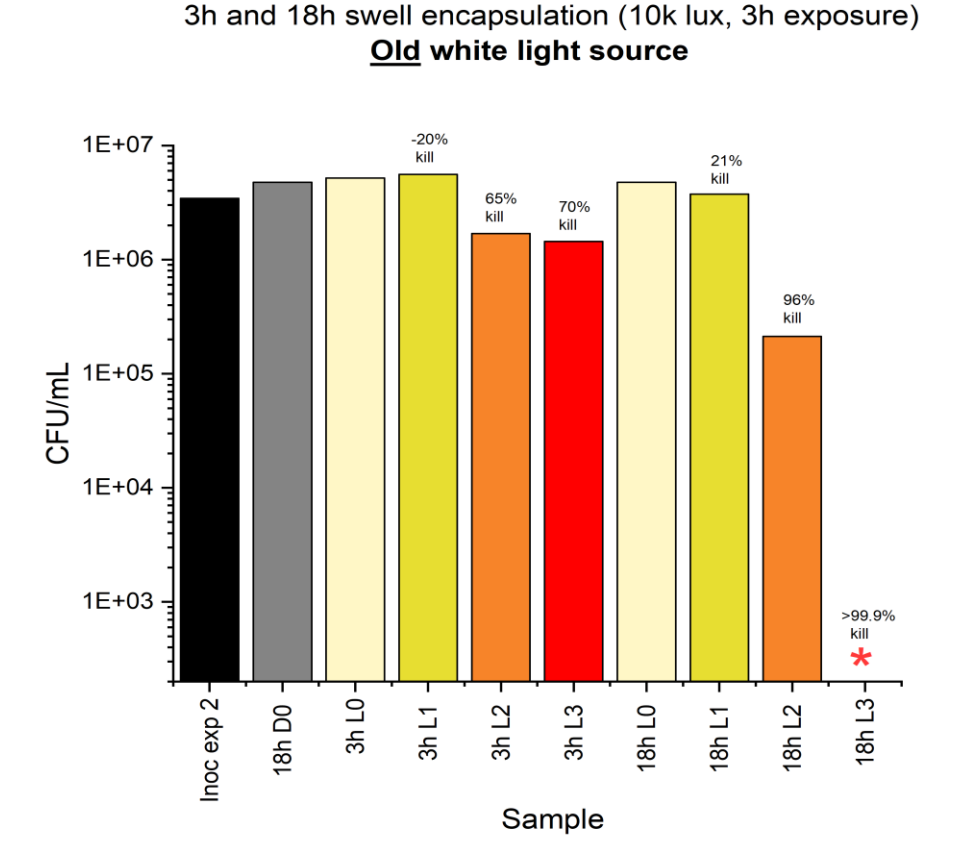


Figure 17. Antimicrobial activity using the old white light source of antimicrobial endotracheal tube samples (some dark controls not performed due to issues sourcing sterile saline during Covid-19 pandemic). * = below detection level (1E+02).

From these results it was clear the light source is important in determining the level of kill achievable. Therefore, light spectra for each white light source were measured. The new light source (SAD lamp) has two major peaks, a sharp one at approximately 450nm (indigo/blue) and another wider peak ranging 500-700nm (green to red).

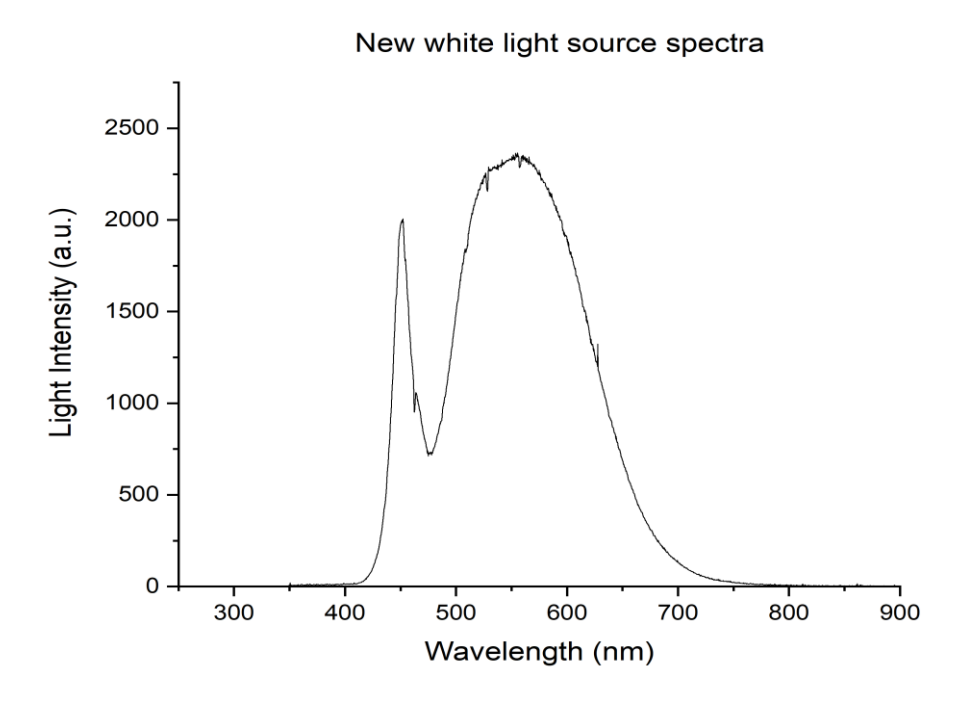


Figure 18. Light spectrum for the new white light source (SAD lamp).

Whereas the old white light (fluorescent lamp) has 3 notable sharper peaks at approximately 430nm (violet/indigo), 550nm (green) and 625nm (red). MB

absorbs at 668nm, primarily covered by the wide peak of the new white light source.

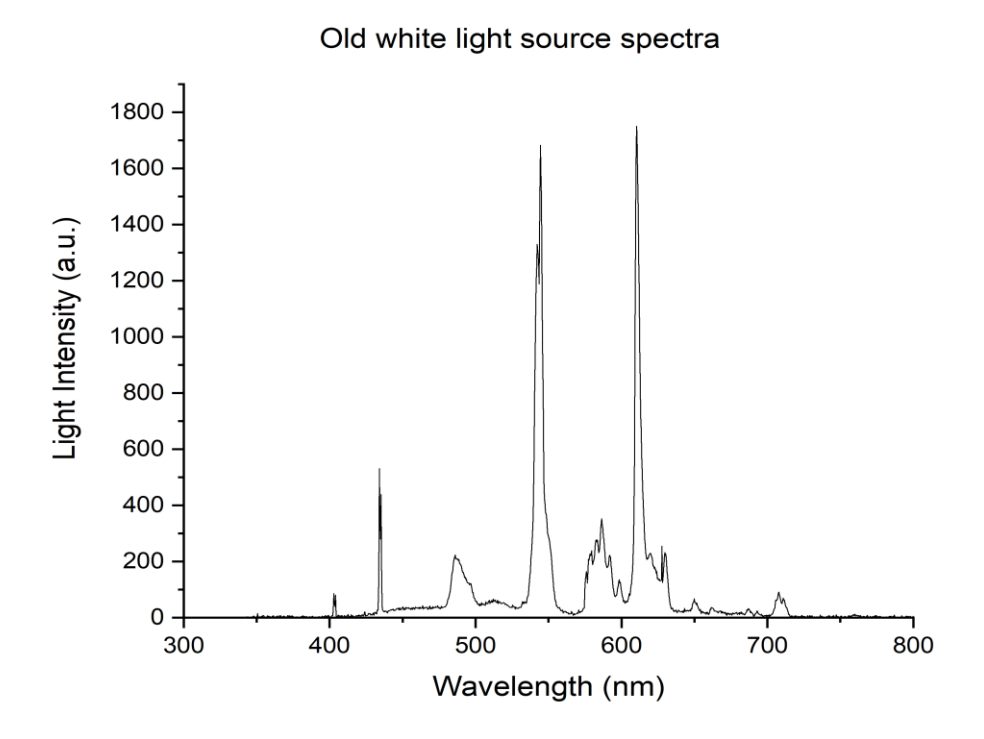


Figure 19. Light spectrum for the old white light source (fluorescent bulb).

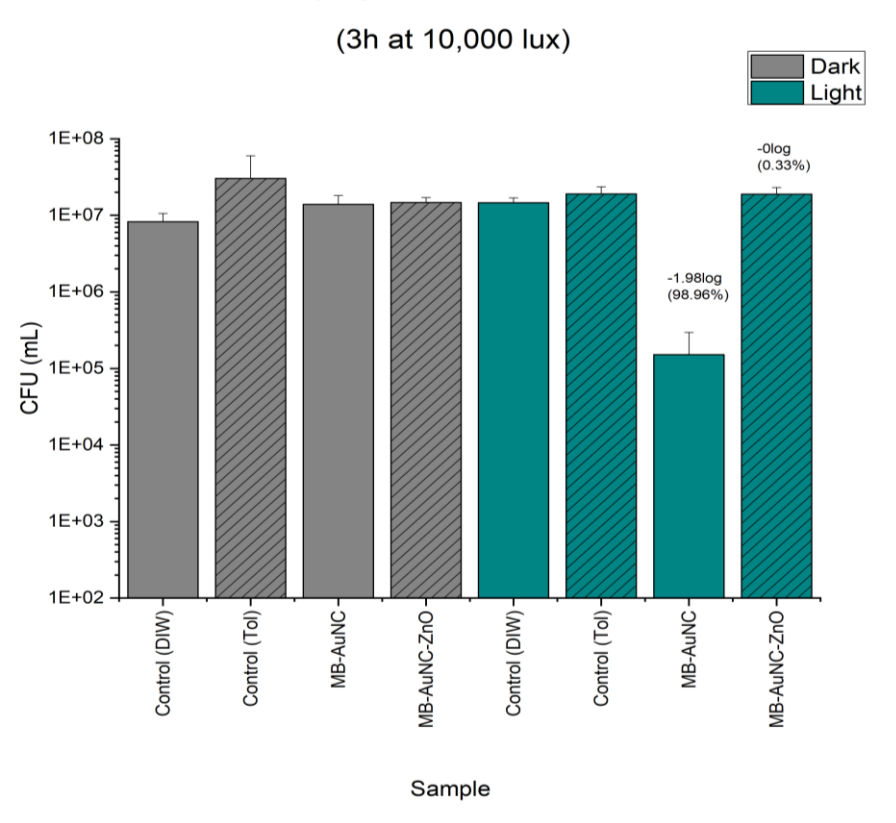
A reason for the improved results using the old white light source, despite both being white light and measuring the same 10,000 lux light level, could be because it was a fluorescent lamp which emit low levels of UV which is known to kill organisms.

2.3.4 INCORPORATING ZINC NANOPARTICLES FOR ANTIMICROBIAL ACTIVITY IN THE DARK

As the material only showed antimicrobial activity in the dark in the case of *S. aureus*, Zinc (II) dioctylphosphinate was synthesized by the colleague's materials research centre to test, as the group had seen previous success against gram negative bacteria such as *E. coli* with zinc compounds in dark conditions. This nanoparticle had to be capped with an organic ligand however, so it could be used in the swell encapsulation process alongside the Au₂₅(Cys)₁₈ and MB for even incorporation as it was not water soluble. It was preferable to have all swell encapsulating at one time so that the material did not have layers of active material and for example a Zinc (II) dioctylphosphinate layer covering the Au₂₅(Cys)₁₈ layer and dampening its effect. However, ZnO was found to dissolve best in toluene, so added an additional swell encapsulation step where Zinc (II) dioctylphosphinate dispersed in toluene were incorporated into the endotracheal tubes after the MB mix.

Below are the results of the new double-swell encapsulated MB/Au₂₅(Cys)₁₈ /ZnO(DOPA) mixes against *E. coli* ATCC 25922 and the clinical isolate of *E. coli* in white light, as well as the clinical isolate of *E. coli* using laser light.

Activity against E. Coli ATCC 25922





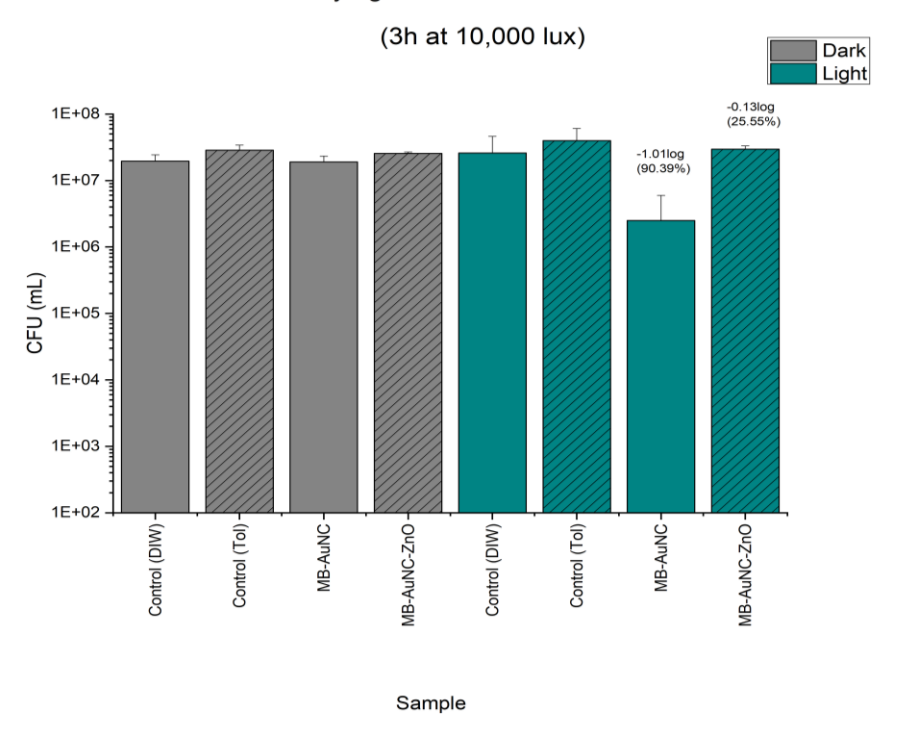


Figure 20. Results from antimicrobial endotracheal tube with additional Zn(DOPA) embedded in white light against two different isolates of *E. coli.* Two biological replicates.

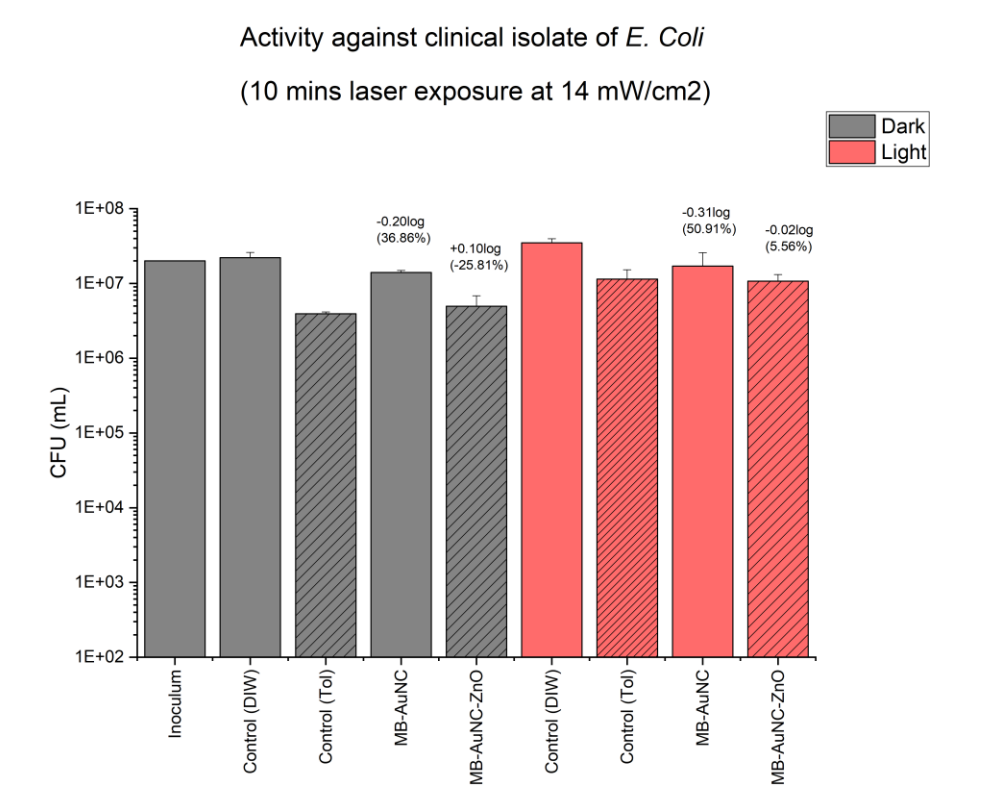


Figure 21. Results from antimicrobial endotracheal tube with additional Zn(DOPA) embedded after laser light exposure for 10 minutes against a clinical isolate of *E. coli*. Two biological replicates.

Sample

The MB/Au₂₅(Cys)₁₈ mixture still gave the highest kill, and the addition of Zinc (II) dioctylphosphinate didn't yield any significant difference (figure 25) (P > 0.05) in kill in the dark. The addition of Zinc (II) dioctylphosphinate actually appeared to block the action of the MB/ Au₂₅(Cys)₁₈ so that in light the material was not as effective as previously seen. The double swell encapsulation could be cause for this, either creating a layer of ZnO over the MB/Au₂₅(Cys)₁₈ rather than having an even surface containing all three components, or during the secondary toluene based swell encapsulation the MB/Au₂₅(Cys)₁₈ mix was displaced by Zinc (II) dioctylphosphinate.

In the case of white light against both laboratory strains and clinical strains of *E. coli*, the addition of Zinc (II) dioctylphosphinate actually hindered its antimicrobial effect. The combination showed no improvement in antimicrobial activity in the dark and reversed the previously seen excellent antimicrobial activity seen in the light. Therefore, the Zinc (II) dioctylphosphinate may have displaced or be interfering negatively with the synergy between Au₂₅(Cys)₁₈ and MB regarding the enhanced triplet state formation that is providing its enhanced antimicrobial activity.

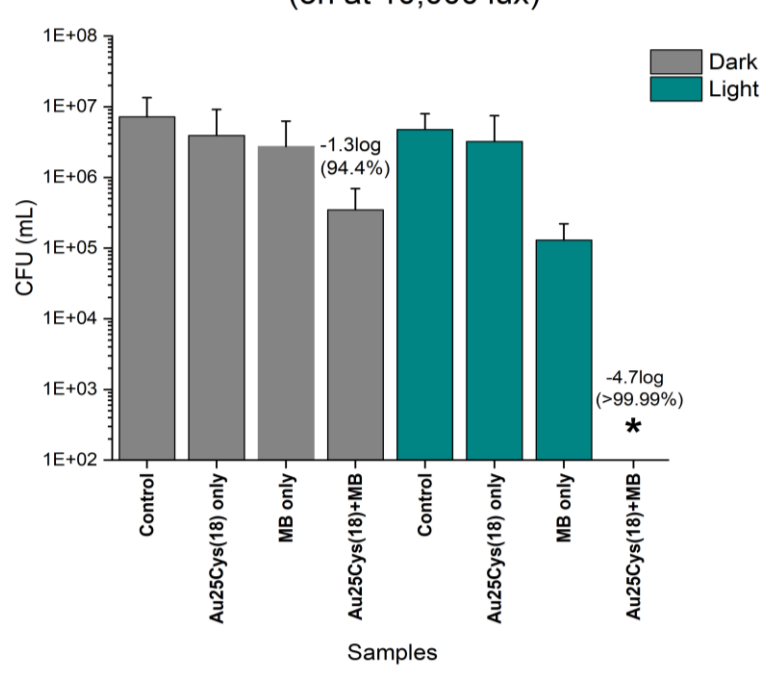
In the case of laser light against the clinical isolate of *E. coli*, though there initially appears to have been a reduction, it's thought this could have been due to insufficient washing off the toluene during swell encapsulation, as the toluene control also shows a reduction in the dark. As well, the antimicrobial activity in the light is dampened, showing no activity.

Though these results have not been successful in combining the MB-Au₂₅(Cys)₁₈ technology with a ZnO compound, other routes of adding another compound to give antimicrobial activity in the dark should be explored. As the limitations of this incorporation were due primarily to the swell encapsulation technique, alternatives to incorporating compounds into polymers was investigated. Eventually, MB and ZnO nanoparticles were successfully 3D printed (Chapter 4) based off these early ideas of finding a way of incorporating an antimicrobial substance active in the dark, as well as the need to find an alternative to wasteful and costly swell encapsulation techniques.

2.3.5 ANTIMICROBIAL ENDOTRACHEAL TUBE ACTIVITY

Below is a summary of the activity of the antimicrobial endotracheal tube developed using Au₂₅Cys(₁₈) and MB against *S. aureus* 8325-4 and *E. coli* ATCC25922 as well as an *E. coli* coliform cultured directly from an endotracheal tube. Samples were exposed to white light for 3h at 10,000 lux. Samples were active against all bacteria to >99% when exposed to light. As well, *S. aureus* was also susceptible in the dark, where a kill of 94% was achieved. All experiments were performed with a minimum of two biological replicates.

Antimicrobial activity against *S. aureus* 8325-4 (3h at 10,000 lux)



Antimicrobial activity against *E. coli* ATCC25922 (3h at 10,000 lux)

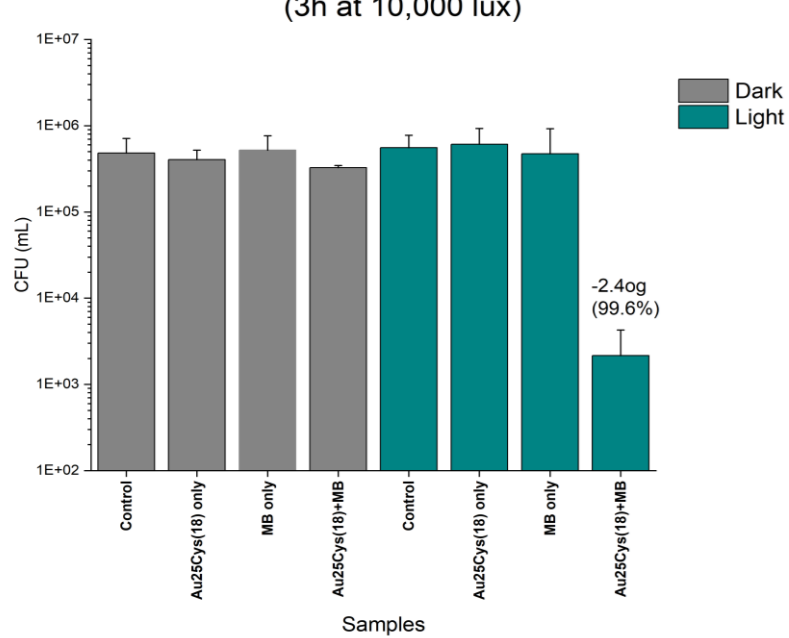


Figure 22. Graph showing antimicrobial testing of endotracheal tube pieces against laboratory strains of *S. aureus* and *E. coli* when exposed to 10,000 lux white light for 3 hours compared to that in the dark. Two biological replicates performed. * = below detection level (1E+02).

A patients' extubated endotracheal tube was provided from Prof D. Walker (UCLH Critical Care Consultant) and cultured a pure culture of *E. coli* from the biofilm on the surface of the tube. Below is the activity of the antimicrobial endotracheal tubes against this *E. coli* isolate. This was important to compare as although laboratory strains are good for comparisons to other researchers within the team and in the microbiological community as a whole, these behave differently to clinical strains as they are domesticated, and thus testing with clinical strains gives a better overall picture of how well these materials may work in practice.

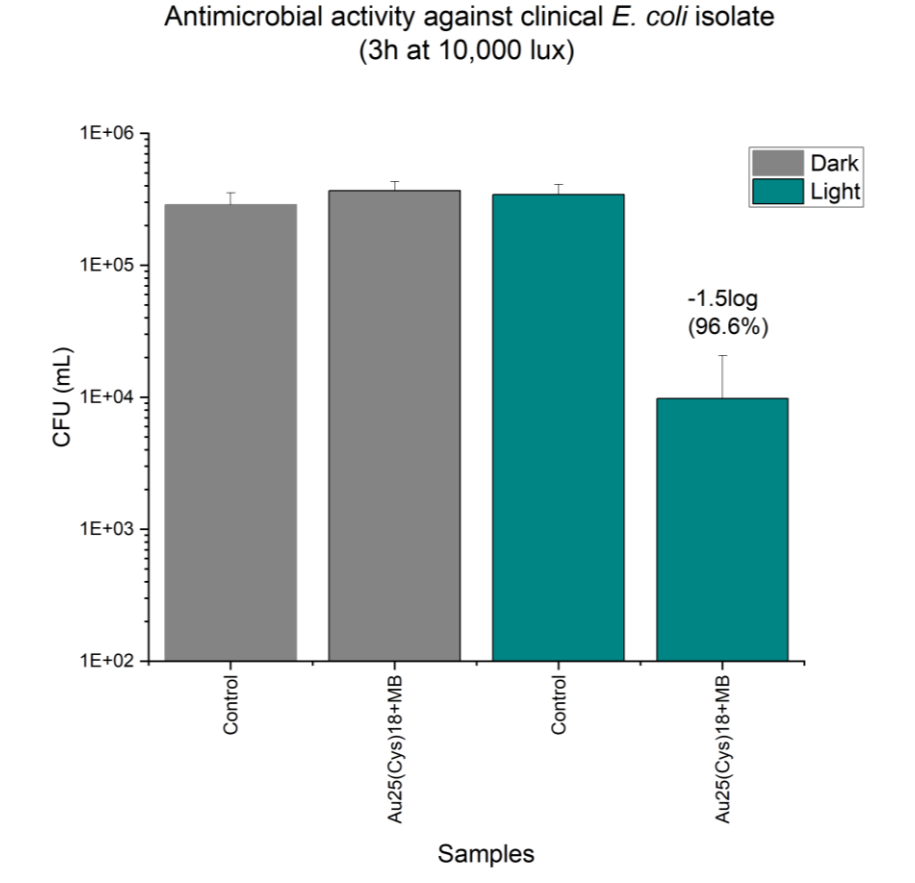


Figure 23. Graph showing antimicrobial testing of endotracheal tube pieces against the clinical isolate of *E. coli* when exposed to 10,000 lux white light for 6 hours compared to that in the dark. Three biological replicates performed.

The level of bacterial reduction was reduced in this case and only a 96.6% kill was achieved. As a result, further endotracheal tube samples were made to a 'maximum' concentration to enhance the amount of antimicrobial kill in experiments going forward.

There were questions surrounding how entire endotracheal tubes, once intubated, may be exposed to white light without taking them out and disturbing the patient. So, to combat this problem a laser strategy could be applied. Ondine Biomedical Ltd. are currently treating VAP patients with laser irradiation, by spraying MB solution down the lumen of the endotracheal tube and following it down with a fibre optic laser, where laser treatments are then given in 2-minute bursts to remove biofilm growing on the tube. Ondine have reported in personal communications that this is messy for the patients and there is a risk if MB drips onto tissue, that if irradiated, the cells would also be destroyed. Thus, using Ondine lasers the antimicrobial endotracheal tubes were tested again using this new light source, with the idea the laser could be used in the same way, but negating the need for medical grade MB solution (which is also very costly at £100 per mL).

Three biological replicates were carried out with laser light with exposure times of 5 and 15 minutes at 150 mW. At just 5 mins the material was found to kill 99.9% (P = 0.05) of the clinical strain of *E. coli*, and within 15 mins the kill was to below the detection level limit (P < 0.05). It is important to note here the laser irradiation in this case was concentrated on one spot from above the material as seen in figure 20 and the measured power output was 150 mW.

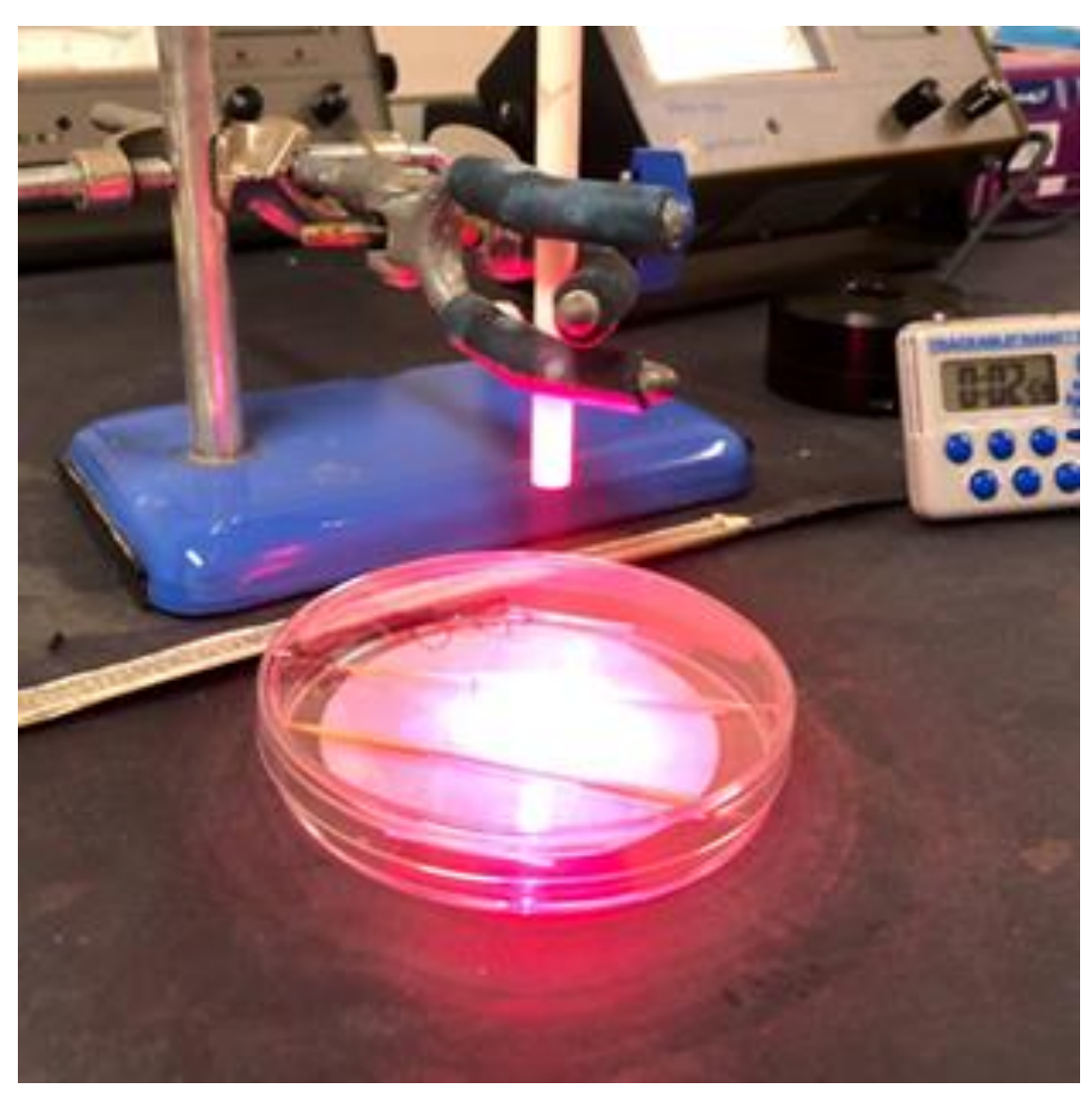
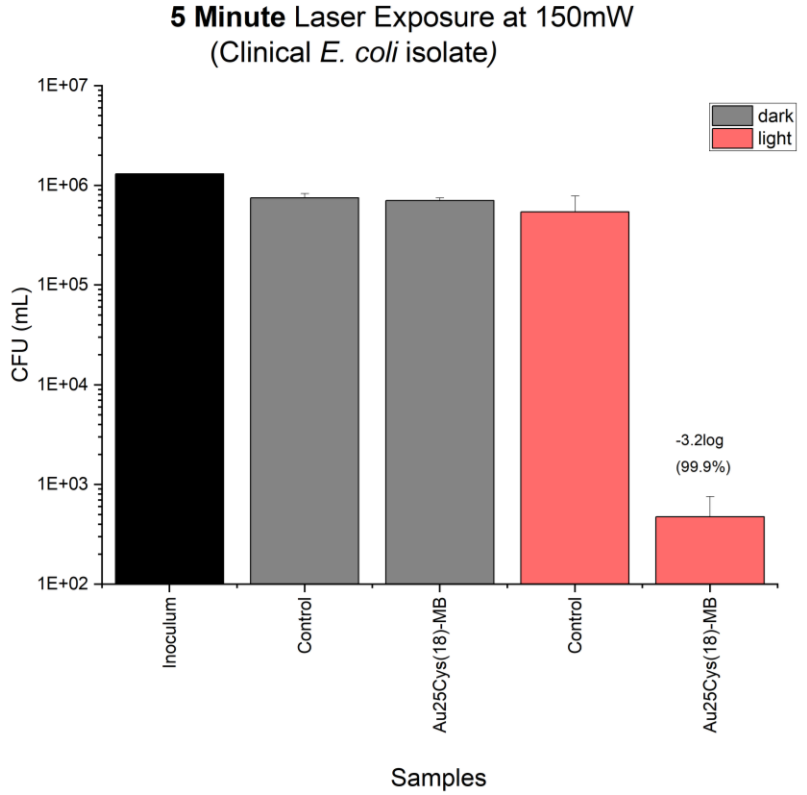


Figure 24. Image to show the set up for the early laser experiments measured output 150mW in a direct beam down onto the sample.



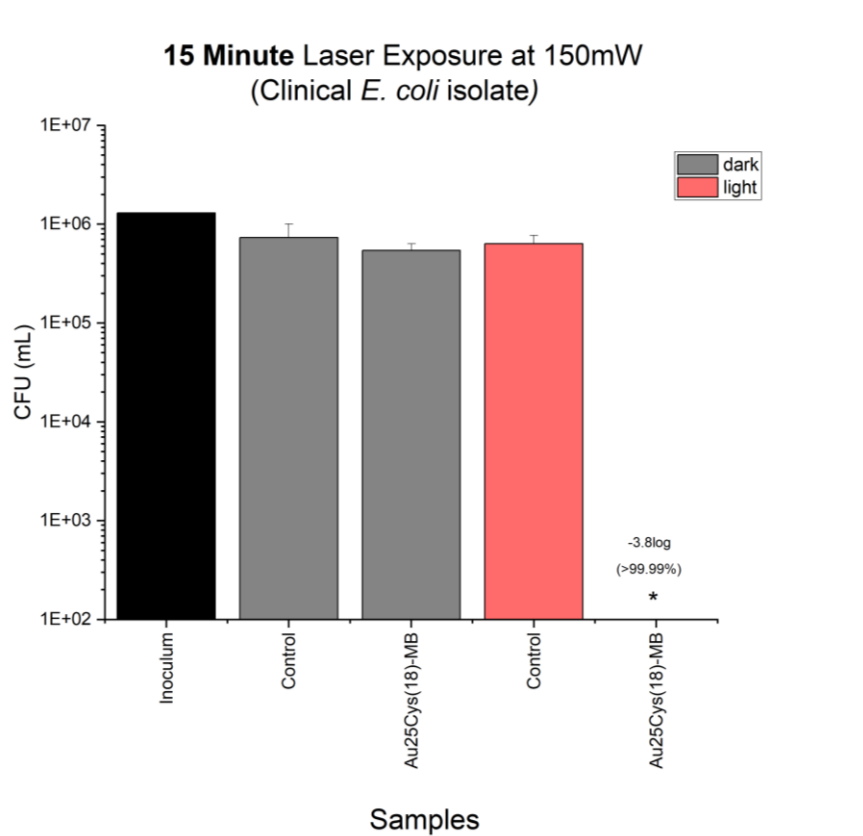


Figure 25. Graphs showing antimicrobial results against clinical isolate of *E. coli* when exposed to 150 mW laser light for 5 and 15 minutes.

Three biological replicates performed. * = below detection level (1E+02).

Since the results from these early laser experiments, Ondine offered in-kind support on a funding application to accelerate the development of the antimicrobial endotracheal tube as a result of the pandemic and the potential increased need for such a product. The funding was awarded and as in-kind support to the project new lasers were provided. These lasers are the ones currently being used by Ondine in their 'MRSAid' product, which treats methicillin-resistant *S. aureus* (MRSA) by MB administration to the nostril and x2 2-minute treatments of laser light exposure. The laser is set to 70 mW and has a diffuser tip which gives an intensity of 14 mW/cm², meaning the beam was not concentrated as the laser before (figure 26).



Figure 26. Image to show the new laser set up of experiments using diffuser tip measuring intensity of 14 mW/cm².

To imitate a situation where a laser is passed through an endotracheal tube in a patient, the laser was held directly above the endotracheal tube square sample, ~1-2 cm in height away (resting on the side of the petri dish). In this case, as the new laser automatically runs in set 2 min treatment times, three experiments were ran complied of a total of 4, 10 and 14 mins. This new laser (wavelength 655-675 nm) at a 70 mW setting described in the graphs below, at 2cm distance from the sample gives an intensity of 14 mW/cm².

Below shows the outcome of preliminary data with the new laser set up, using the clinical isolate of *E. coli* to test the antimicrobial endotracheal tube. In 4 minutes only 26% kill was achieved, so the experiment was extended to 10-and 14-min exposure times, which gave 85% and 98% kills respectively (figure 27). Only one biological repeat was conducted at this stage as this experiment was used as an indicator to appropriate exposure times for further experiments.

All of the results so far show great activity in the light, but not in the dark. Therefore, the following section experiments with the addition of zinc oxide nanoparticles (ZnO), in the hope that it might offer better antimicrobial activity in the dark.

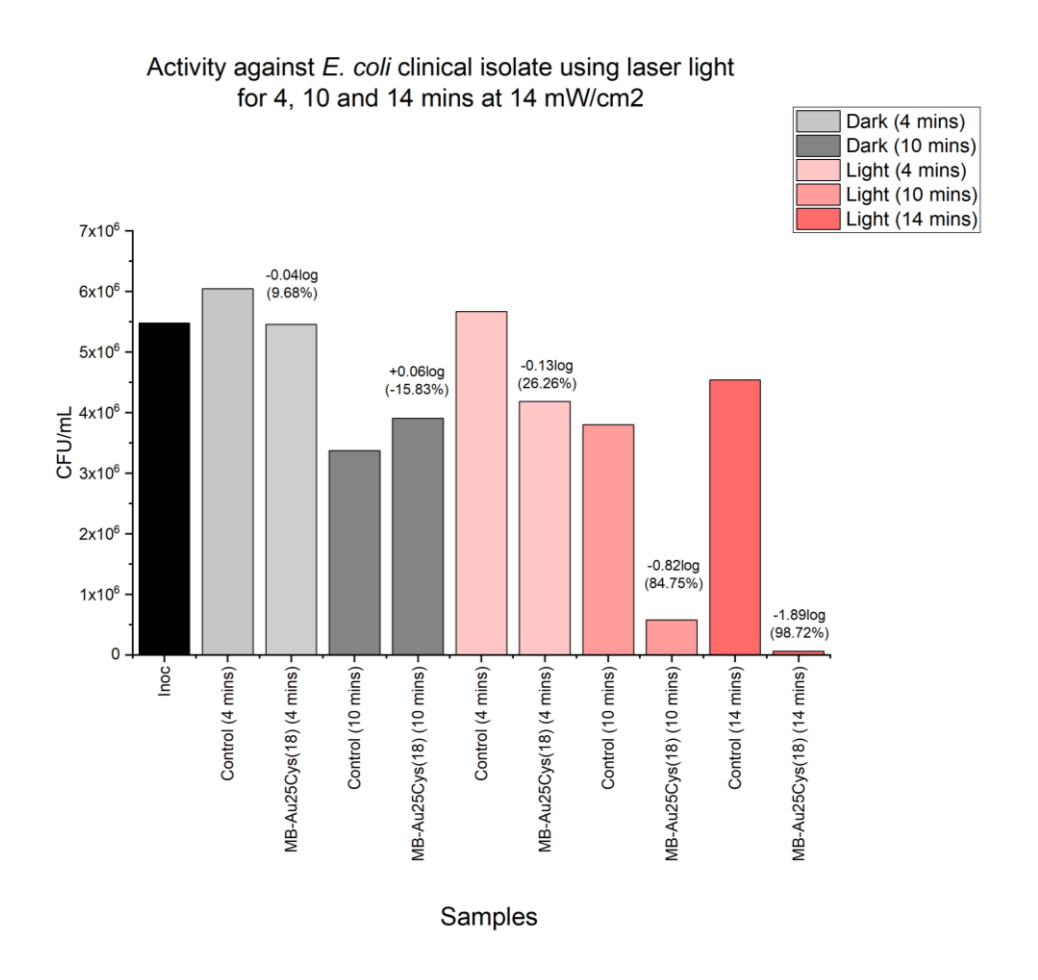


Figure 27. Graph showing preliminary results (one biolgical replicate) of the antimicrobial endotracheal tube against the clinical isolate of *E. coli* using laser light for 4 minutes, 10 minutes and 14 minutes at 14 mW/cm².

2.3.6 ANTIMICROBIAL ACTIVITY AGAINST BIOFILMS

Infections also most often occur in a polymicrobial settings, particularly regarding biofilms causing VAP.^{67,68} Therefore, it is important to try and replicate this in-vitro in the laboratory, to determine 1) if this antimicrobial endotracheal tube is active against biofilms and 2) active against polymicrobial biofilms such as those seen in nature.

P. aeruginosa in previous studies has shown to have been the most common pathogen associated with development of VAP, also associated with high mortality rates.⁶⁹ However, the predominant and competitive nature of *P. aeruginosa* means it often outcompetes other organisms,^{70, 71} hence the 1:5 ratio to give MRSA the best chance at successfully colonising in our biofilm model. One article describes that *P. aeruginosa* and MRSA coexist due to the overproduction of *P. aeruginosa* alginate in real world examples, however in the lab compete.⁷² So, successful co-culture biofilm of *P. aeruginosa* and MRSA together would suggest as close to a real-world scenario as possible was reached within the laboratory.

As the most common causes of VAP are thought to be *P. aeruginosa* followed by MRSA,⁶⁹ these were chosen to develop our biofilm model. Both were cultured directly from an endotracheal tube, *P. aeruginosa* RS080 was from the Royal Free Hospital with VEB and EBSL, and MRSA US137 was from University College London Hospital, both strains had limited treatment options due to multi-drug resistance.

The initial trial experimented with ratios including 1:1, 1:2, 1:3, 1:4 and 1:5, and all formed visible biofilms. Light exposure was not used in this experiment. This was repeated using 1:2 and 1:5 as well as *P. aeruginosa* only and MRSA only controls as seen below.



Figure 28. Comparison of the initial experiment testing MRSA only, P. aeruginosa only, 1:2 and 1:5 mixed biofilms at the beginning and end of the 2-week biofilm formation.

Table 5. Summarising the results for the initial biofilm experiment on blank commercially available endotracheal tubes, exploring 1:2 and 1:5 ratios for mixed biofilms with recovery and colony counting on Mannitol Salt and MacConkey agar.

Sample name	Count	Dilution used (spiral plater)	CFU/mL
MRSA only	68	1.00E-05	1.27E+10
PA only	34	1.00E-05	1.29E+09
1:2 (MRSA)	32	1.00E-03	1.22E+07
1:2 (PA)	42	1.00E-05	1.60E+09
1:5 (MRSA)	46	1.00E-03	1.75E+07
1:5 (PA)	46	1.00E-05	1.75E+09

From this it was concluded growing mixed biofilms with these isolates was possible using ratios of 1:2 (*P. aeruginosa*: MRSA). The CFU/mL value for MRSA in the 1:5 ratio is slightly higher (1.75E+07 compared to 1.22E+07), suggesting the higher proportion of MRSA to *P. aeruginosa* helps in allowing the two to co-exist in more equal respects (one biological replicate). Therefore, the ratio of 1:5 was chosen for further planned experiments to give MRSA the best chance at co-existing with *P. aeruginosa* in a laboratory biofilm environment.

This mixed biofilm grew an observable amount of biofilm, first time round, with no issues. This is potentially due to the fact the isolates were cultured directly from an endotracheal tube, and isolates may have adapted to enhance their chance of co-existence, in particular MRSA adapting to co-exist with the usually dominant *P. aeruginosa*. However, due to time constraints (please refer to Covid impact statement) two biological replicates of a *P. aeruginosa* only biofilm was performed and reported on.

Activity of swell encapsulated antimicrobial endotracheal tubes against *P. aeruginosa* RS080 with VEB ESBL biofilm growth over 14 days

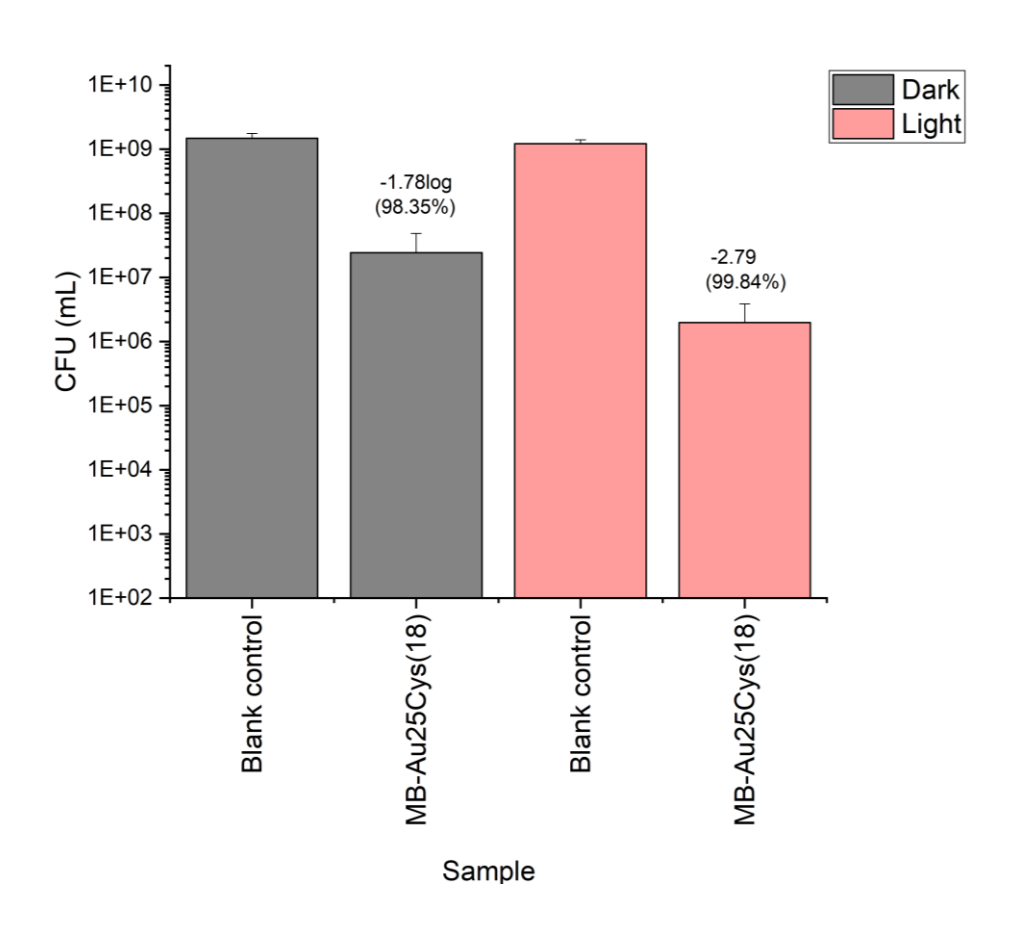


Figure 29. Biofilm growth of *P. aeruginosa* on the antimicrobial endotracheal tube compared to blank controls grown over 14 days, which were exposed to either complete darkness or exposed to white light for x3 hours (10,000 lux) once on day 0 and 7. Two biological replicates.

The biofilm does not appear to develop even in antimicrobial endotracheal tubes kept in the dark, which was first noted by the absence of the sticky EPS substance when pulling up the tube from the well plate. In the dark a 1.78-log reduction (98.35%) was observed compared to the control samples also kept in the dark. For the samples exposed to light once on day 0 at the beginning of the experiment and once on day 7 (both for 3h at 10,000 lux) a 2.79-log reduction (99.84%) was observed. This is extremely promising that the antimicrobial endotracheal tube developed is active against biofilms of a multidrug resistant *P. aeruginosa* isolated directly from an endotracheal tube to such a high level. It was also noted that the observed sticky biofilm (figure 9) was absent the test wells containing antimicrobial samples. provides insight into how the antimicrobial endotracheal tube works and suggests the action of the MB/ Au₂₅(Cys)₁₈ mix prevents the initial biofilm from growing in the first place.



Figure 30. Biofilm formed after two weeks of growth on control sample.

The same is not seen for the antimicrobial samples also left for two weeks in the same inoculum.

3 CHAPTER 3 – THE EFFECT OF COVID-19 ON VENTILATOR ASSOCIATED PNEUMONIA

3.1 INTRODUCTION

Due to the pandemic a new stream of work was developed to test against coronaviruses and determine whether these materials could also be useful in stopping transmission in hospitals between patients and staff. This work originally began during the pandemic, where the first work testing the material against coronavirus NL63 was sought to get proof of concept to fund additional work. The testing against NL63 then allowed for a successful IAA funding application, which the purpose was to accelerate the development of the swell encapsulated endotracheal tube to commercialisation, including outsourced testing of SARS-CoV-2.

VAP has been a problem since before the days of Covid-19, and hence this research began. However, the pandemic has shone a light on the problem due to the disease leading to respiratory failure and ventilation often required. Thus, a larger question has evolved on how these co-infections between viral and bacterial organisms behave, and ultimately whether a reduction or eradication of unnecessary bacterial infections acquired as a result of being in hospital would have any significant effect on mortality rates, particularly in Covid times. This is highlighted by an alert article written in 2020, raising the concerns around the risks of VAP and the importance of early diagnosis, as coinfection has the potential to worsen clinical condition and increase mortality rates ⁷³.

There are few retrospective studies on the incidence of VAP in Covid-19 patients, however data must be considered in the fact that VAP is difficult to diagnose at the best of times, let alone during a pandemic. For this reason, it is expected that figures were vastly underreported.

One study Investigated the incidence of VAP and secondary infections using microbial culture and TaqMan multi-pathogen array, to determine the lung microbiome composition using 16S RNA analysis ¹⁰. The study comprised of 81 Covid-19 patients and 144 non-Covid-19 patients, all receiving ventilation between March 15th 2020 – August 30th 2020. They found Covid-19 patients were significantly more likely to develop VAP than patients not presenting with Covid-19 with an incidence x2.15 times the rate of those without (p = 0.009) ¹⁰. The conclusion was there appears to be an increased risk of VAP in Covid-19 patients, which was not explained by the prolonged duration of ventilation ¹⁰. This suggests there are other factors such as the interaction between the bacterium responsible for the development of VAP and viral infection from Covid-19 such as tissue damage caused by the virus, that could be increasing the susceptibility of those patients to acquiring VAP.

Another study found that amongst 197 Covid-19 patients in critical care, that nearly half (44.7%) experienced at least one secondary bacterial infection, with pneumonia (39.1%) being the most common ⁷⁴. The researchers also monitored episodes and origin. 6.5% were found to have been community acquired, 9.1% were non-ventilated hospital acquired pneumonia, and 84.4% were VAP. Frequent bacteria involved in these cases were found to be *S. aureus* (26.2%), *P. aeruginosa* (16.9%), *K. pneumoniae* (13.8) and *E. coli*

(12.3%).⁷⁴ This interestingly contradicts the information available so far on causative pathogens, and therefore begs the question whether this potentially could be related to the co-infection of patients already infected with Covid-19. Length of hospitalization was also longer for patients presenting with VAP, by 23 days vs 8 days (p < 0.001) ⁷⁴

3.2 METHODS

3.2.1 CORONAVIRUS NL-63 ASSAY

This initial antiviral work was outsourced to Virology Research Services (Michela Mazzon, PhD) in May 2020. The method used for the testing was as per ISO 21702:2019. Measurement of antiviral activity on plastics and other non-porous surfaces. Light exposure was kept at 10,000 lux and 3 h for the initial test at repeat 1. For repeat 2, as the light exposure was too powerful and killed off the control sample as well as the antimicrobial sample, the second repeat involved light exposure for just 15 mins of white light at 10,000 lux.

The new round of funding awarded to accelerate the development of the antimicrobial endotracheal tubes includes testing against novel strains of coronavirus including SARS-CoV-2, available to the Institute of Child Health carried out with collaborators Dr Claire Smith and Dr Maximillian Woodall. Based off earlier results on NL63 conducted by Virology Research Services, it was planned to test for 15 minutes under white light exposure at 10,000 lux as a direct comparison to the NL63 tests and adjustments made from there. The

conditions of the experiment were the same as in the bacterial experiments with a humidity chamber set up to allow for comparisons.

3.2.2 SARS-COV-2 ASSAY

This work was performed by Dr Maximillian Woodall at the Clinical Centre for Microbiology, as this requires biosafety level 3 training to test against SARS-CoV-2. The assay followed was a group assay within the Institute of Child Health, where we ensured the experimental set up followed the same conditions as the bacteriology testing to ensure continuity e.g. same light source used etc.

Microbiology: SARS-CoV-2 Plaque Assay standard operating procedure MM12 Version - A, derived from Public Health England methods was used.

Class 2 preparations:

VeroE6 cells (Crick) were grown in flasks until confluence. Following detachment of VeroE6 cells from flask using trypsin (0.05%)/ ethylenediaminetetraacetic acid (EDTA) (ThermoFisher, 25050014), the number of cells/mL counted using a haemocytometer. 1.15-1.5 x 10⁵ cells seeded in 0.5mL media (Dulbecco's Modified Eagle Medium (DMEM) (Gibco 21090-022), with 10% foetal calf serum (FCS) (Sigma Aldrich, F0804), 1% Penicillin-Streptomycin (Pen-Strep) (ThermoFisher, 15140122) per well of 24 well plate Incubate plates overnight at 37 °C in incubators with 5% CO². Cells transferred to class 3 laboratory.

A sterile microcrystalline cellulose suspension (2.4% [w/v] in water) was prepared. 2.4 g of microcrystalline cellulose powder dispersed in 100 mL of distilled water, using a standard magnetic stirrer, until complete dissolution of the powder. The suspension was autoclaved at 121 °C for 20 min and stored at room temperature before use. Two Temin's modification (MEM) (Gibco, 12037549) media was prepared by diluting commercial MEM with sterile water and add 4% FCS, 1x L-glutamine (Gibco, A2916801), 1,000 units/mL penicillin, and 1 mg/mL streptomycin. The pH of the 2x MEM was adjusted to around 7.35 with a sterile sodium bicarbonate solution (Gibco, 25080092) at 7.5%, following the colour indicator. Media was filtered and stored at 4 °C.

Plates were sealed with parafilm and transported in a Tupperware container to the class 3 laboratory.

Class 3:

Frozen aliquots of SARS-CoV-2 were thawed immediately prior to infection. Virus was diluted serially using five rounds of 10-fold dilution (50 uL in 450 uL using reduced serum media (OptiMEM)). Media was aspirated off from the 24 well plates and to each well 200 uL of viral inoculum was added. Plates were processed one at a time to avoid desiccation of the monolayer. Control wells received media alone. The 24-well plates were wiped with tissue paper soaked in tristel and placed in a 37 °C CO² incubator for 1h (with gentle rock once after 30 mins). During the 1h virus absorption, the microcrystalline cellulose overlay was prepared by mixing 1:1 of 2.4% microcrystalline cellulose suspension with the 2x MEM (+4% FCS, L-Glutamine, Pen-Strep, pH 7.35) according to the desired volume and mixed vigorously. The virus was aspirated off and 0.35-

0.5 mL of Avicell (Sigma Aldrich, 435244) overlay added to each well. This was placed in the 37 °C CO² incubator for 2 days.

After 2 days, the Avicell overlay was aspirated off. 0.2 mL of fixative [2% paraformaldehyde + 2% glutaraldehyde (PolySciences)] was added to each well and left for 20 minutes at RT. The fixature was aspirated off and 0.2 mL of crystal violet solution (8% crystal violet + 20% ethanol made in water) was added to each well and left for 10 mins, then removed. The wells were washed over the sink with tap water and left to dry. The plaques were counted and PFU calculated.

3.3 RESULTS & DISCUSSIONS

3.3.1 ACTIVITY AGAINST CORONAVIRUS NL-63

As illustrated in figure 31, the initial repeat at 3 h white light exposure time killed off both the reference and treatment light. However, a >99% kill was still seen in the 'treated dark' condition (the antimicrobial endotracheal tube sample placed in the dark for 3 h.

Antimicrobial Endotracheal Tube Activity Against Coronavirus NL63 - Repeat 1

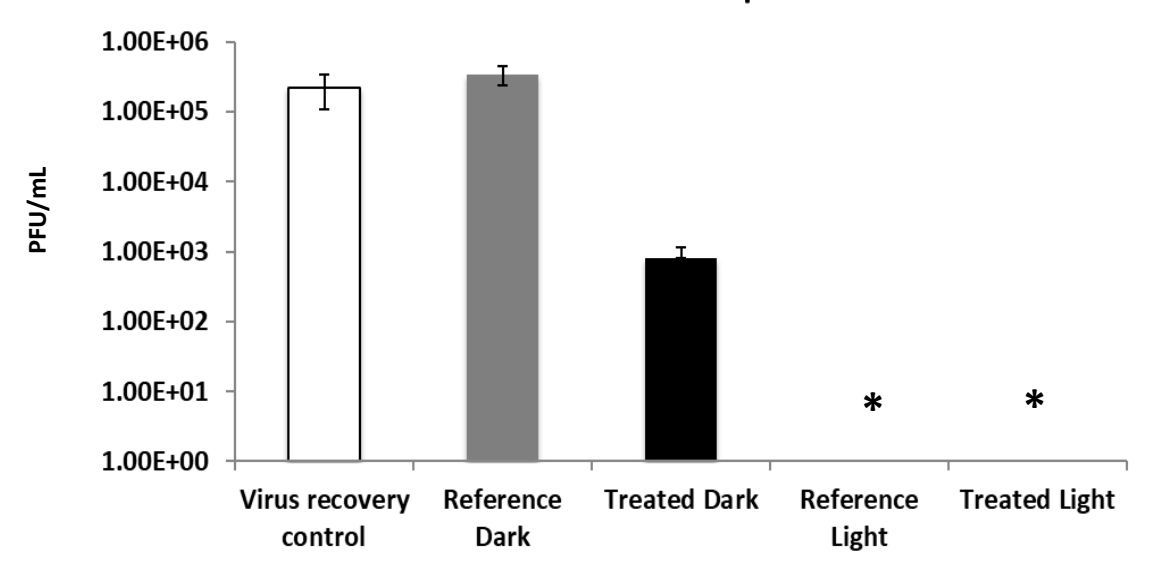


Figure 31. Repeat 1 - Graph by Virology Research Services on the outcome of the activity of the antimicorbial endotracheal tubes against coronavirus NL63 when exposed to white light at 10,000 lux for 3 h.

One biololgical replicate. * = below detection limit (25 PFU).

Therefore, the experiment was repeated again (figure 32) this time having the light condition set to 10,000 lux white light exposure for only 15 mins. The dark kill (still kept at 3 h for repeatability) was reported as >90%, and the light kill

for the antimicrobial sample at 15 minutes light exposure was reported as below detection levels (>99.99%). This was considered promising since infectious virus was reduced to below detection levels in only 15 minutes compared to 3 h for bacteria (Chapter 1).

Antimicrobial Endotracheal Tube Activity Against Coronavirus NL63 - Repeat 2

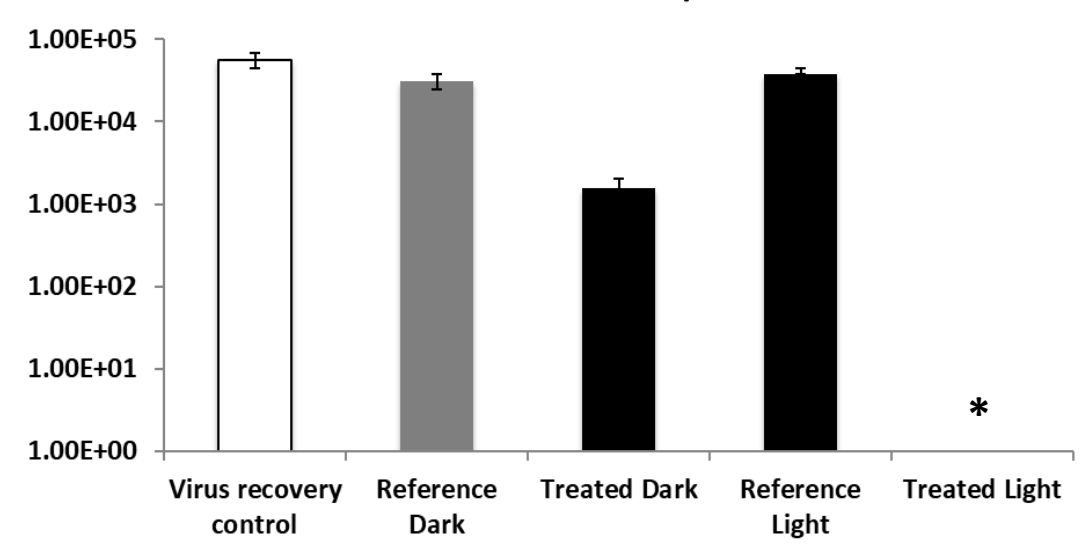


Figure 32. Repeat 2 - Graph by Virology Research Services on the outcome of the activity of the antimicorbial endotracheal tubes against coronavirus NL63 when exposed to white light at 10,000 lux for 15 mins. One biological replicate. * = below detection limit (25 PFU).

Though only one biological replicate was performed, this gave us the proof to go further and gain funding to test these materials against SARS-CoV-2.

3.3.2 ACTIVITY AGAINST SARS-COV-2

This plaque assay included x2 technical repeats to n=3. Swell encapsulated antimicrobial endotracheal tubes using MB and Au(25)Cys18 mixes were tested in the dark and white light for 15 minutes, with blank and dark controls. The results showed complete kill to below detection level, including those in the dark. The plaque assay image below shows there are plaque forming units for each repeat in all cases for the blank control samples, but not for the samples in either the dark or light, clearly illustrating the level of reduction.

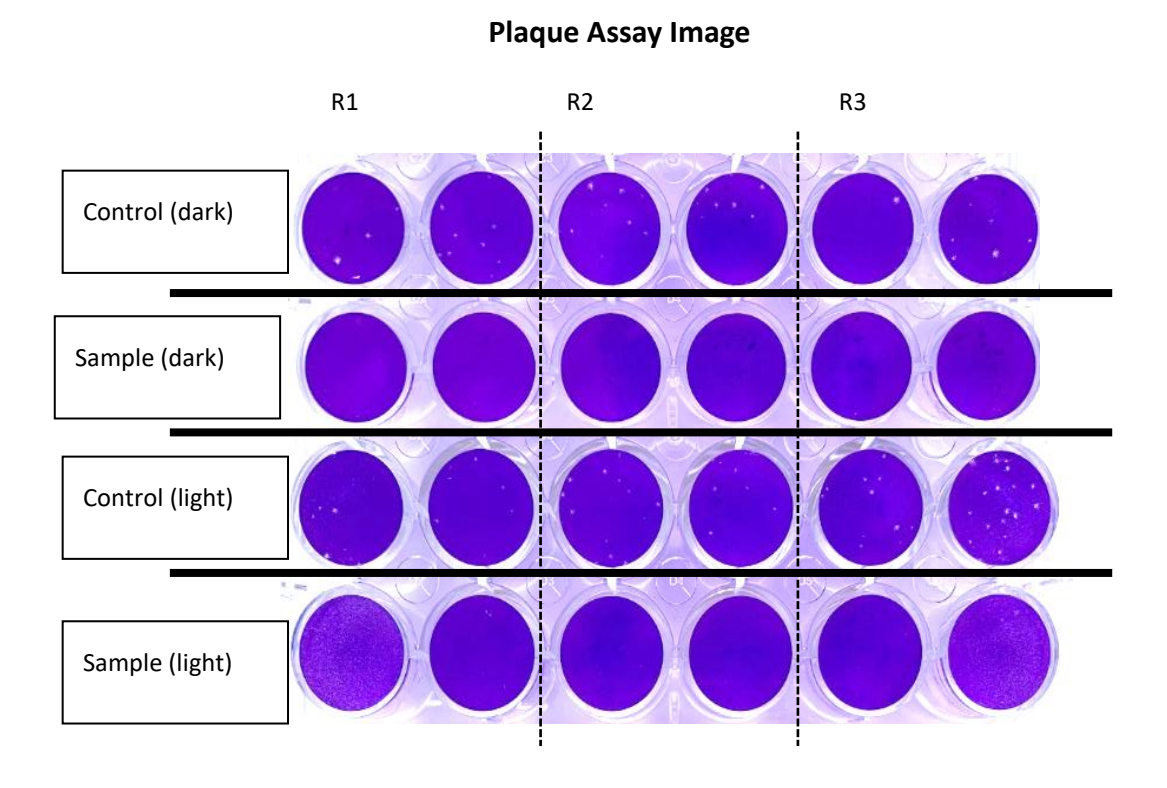


Figure 33. Image of plaque assay results from testing MB and Au(25)Cys18 swell encapsulated samples against SARS-CoV-2. Thee biological replicates.

This illustrates complete reduction to below the detection level (25 PFU/mL) for each repeat for the antimicrobial endotracheal tube in both the dark and light within 15 minutes.

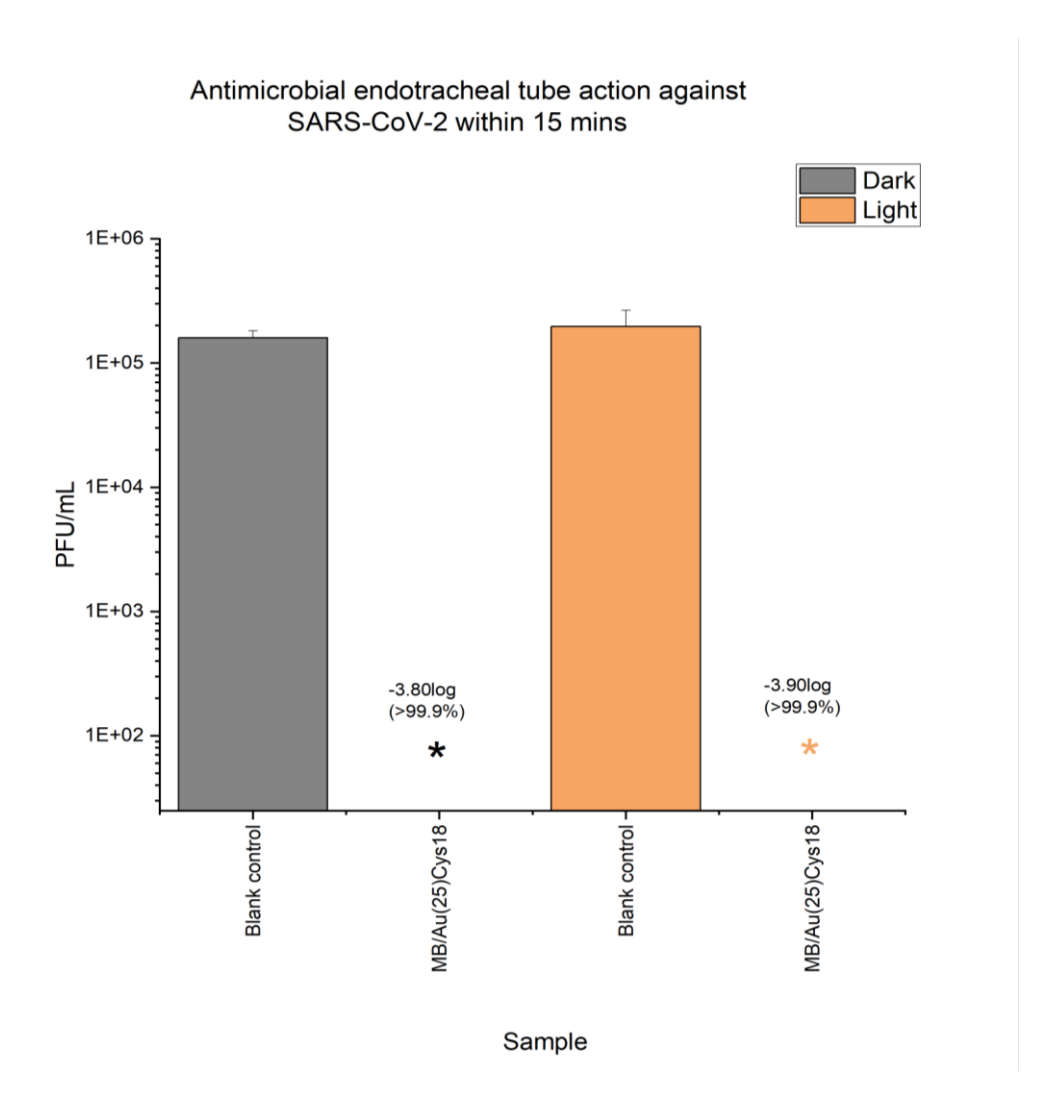


Figure 34. Graph showing the reduction levels achieved within 15 minutes in the dark and in white light (10,000 lux) using swell encapsulated antimicrobial endotracheal tube samples, * = below detection level reduction (detection level = 25 PFU). Three biological replicates.

Similarly, to the test against coronavirus NL-63, within 15 minutes below detection level reduction in SARS-CoV-2 was seen when exposed to light.

Below detection level reduction in the dark for SARS-CoV-2 was also seen, but not with NL-63. There is a difference in the methods used to work up the analysis which could account for the difference in results from coronavirus NL-63 and SARS-CoV-2, as it was expected SARS-CoV-2 would be harder to kill, or it could be that SARS-CoV-2 genuinely is more susceptible to these types of photosensitiser-based materials. It is important to note these experiments were performed in different laboratories, by different people, and therefore there may be differences in the way the experiment was set up too, though both were given the same instructions and equipment to follow with images of the set up to ensure continuity. As well, only one biological repeat was performed in the case of NL-63 so more repeats would be required before making any definitive conclusions about its susceptibility to these materials compared to SARS-CoV-2.

4 CHAPTER 4 – 3D PRINTING ANTIMICROBIAL MATERIALS FOR OTHER APPLICATIONS

4.1 INTRODUCTION

This research into 3D printed materials came about when trying to find an alternative for swell encapsulating materials. Though easy, the use of acetone may cause issues in getting regulatory approval, as well, the process is messy and wasteful. I originally wanted to try extrusion so that the antimicrobial mix could be added directly into the extrusion during the endotracheal tube manufacturing process. However, when printing a part for another piece of equipment I came up with the idea to try adding the antimicrobial mix to the resin and directly try and print using a photocuring printer as opposed to extrusion. This, to everyone's surprise, worked well and yielded a very highly active antimicrobial material, which is cheap and easy to produce and print into any shape.

This thesis describes the first time 3D printing has been used to create antimicrobial coatings using photosensitiser dyes and nanoparticles which have survived the printing process. However, 3D printing is not new to the world of healthcare, currently most often used in the application of "medical phantoms" in the medical field, where artificial models are made for specific human subjects. An example of this being the pioneering surgery that took place at Great Ormond Street Hospital (GOSH), which successfully separated twins joint at the top of the head. The HCPs involved said 3D printed plastic models of their brains, skulls and blood vessels helped to practice the procedures and build cutting guides prior to the actual surgery ⁷⁵. The same

technique was used less than 12 months later to repeat a similar surgery on another set of conjoined twins ⁷⁶. Not only this, but 3D printing is being explored as a solution to prosthetics, implants, surgical instruments, and even human organs and tissues ⁷⁷.

So, 3D printing will not be novel to HCPs and recently the healthcare industry as a whole have been calling upon 3D printing to ease shortages of vital medical equipment such as personal protective equipment (PPE) and ventilators during the pandemic ⁷⁵. This chapter describes how 3D printing was used to incorporate the antimicrobial mix into resins which can then be printed into any desirable shape. Not only is this beneficial to the aim of this research surrounding endotracheal tubes and ventilator parts as an alternative method of incorporation to swell encapsulation methods previously described, but also in the other areas listed above such as prosthetics, implants and surgical equipment.

There are some doing this already with polylactic acid (PLA) (XYZ Printing) and copper-based technologies (Copper 3D Antimicrobial Innovations), which are advertised for primary use in household surfaces and prostheses, respectively. The use of copper is widely researched ⁷⁸⁻⁸⁰ and has been known since ancient times for its antimicrobial properties ⁸¹. However, copper antimicrobial action relies primarily on the release of Cu2+ ions particularly when referring to copper surfaces ⁸²⁻⁸⁴, which is finite and as a result long term activity is limited. As well, this toxicity to bacterial cells is not cell specific, and the Cu2+ ion release is also toxic to mammalian cells leading to DNA damage ^{85,86}. So, this would not be the best application for materials which come into

contact with cells such as the mucus lining which are very delicate and easily irritated. Therefore, 3D printing an antimicrobial material based off light-activated technologies as previously described in this thesis, which are selectively toxic to bacterial cells [MB/RB and ZnO/Au₂₅(Cys)₁₈ mixes] could be beneficial for those industries where materials will be in contact with cells where irritation would cause discomfort.

This research details the development of an antimicrobial endotracheal tube at proof-of-concept stage, made by inexpensive and simple 3D printing techniques. In this research, well known light activated technology which utilises the synergy between photosensitiser dyes and nanoparticles to enhance its antimicrobial effect has been used ^{28,87-91}. UV photocurable resin is mixed with methylene blue (MB) or rose Bengal (RB), as well as commercially available zinc oxide nanoparticles (ZnO), and 3D printed. Though this is at an early stage of development, it provides an insight into a new strategy for making antimicrobial surfaces and shows that they are effective against a wide range of pathogenic microorganisms. 3D printing allows formation of virtually any shaped object and the surprising outcome was that the relatively sensitive dyes and nanoparticles were well dispersed within the plastic and generated potent antimicrobial surfaces. This provides hope for the future of reducing hospital acquired infections and the progression of the global AMR crisis.

4.2 METHOD

4.2.1 PRINTING MEDICAL DEVICES

As MB has the most widely known toxicology profile in healthcare it was decided to trial this and the ZnO mix to print an endotracheal tube as reducing incidence of VAP is the focus of this research. Though a hard curing resin was used in this design for proof of concept, this would in the future be designed with a biocompatible flexible resin. The same printing settings were used to print this medical device, simply using a downloaded 3D computer design from GrabCAD model library.



Figure 35. On the left-hand side a 3D computer aided design (CAD) from GrabCAD of a tracheostomy tube and on the right-hand side the subsequent print using the antimicrobial mix.

4.2.2 MATERIALS CHARACTERISATION

UV-Vis Spectroscopy

UV-Vis absorbance spectra were obtained using a Shimadzu UV-2600 UV-Vis spectrophotometer with a wavelength range of 1000 to 200 nm in standard transmission mode.

Scanning Electron Microscopy

Samples were then gold sputtered (Agar Scientific, sputter coater) for 10 secs at 0.08 mbar, and analysed using the Zeiss Field Emission Scanning Electron Microscope, FESEM Sigma 300VP.

Infrared Spectroscopy

Infrared (IR) spectra were obtained using a Bruker Alpha FTIR spectrometer with a Platinum ATR attachment. The set wavenumber range was 400-4000 cm-1, with 15 scans taken per measurement.

Contact Angle and Surface Free Energy

Contact angle and surface free energy data was obtained using a Krüss DSA 25E drop shape analyser and Advance software (Krüss GmbH, Hamburg, Germany). Multiple regions of interest were examined, and the mean values calculated in Advance. Samples were tested using a double dosing unit liquid

needle system, simultaneously dispensing both water and diiodomethane test liquids. Static contact angles in air were recorded with 5 uL droplets of both test liquids and the surface free energy was calculated automatically in Advance according to the OWRK model.

4.2.3 SCREENING STUDY OF PHOTOSENSITISER NANOPARTICLE MIXES

Methylene blue (MB / C₁₆H₁₈CIN₃S) and rose Bengal (RB / C₂₀H₂Cl₄I₄K₂O₅) were purchased (Acros Organics, pure certified, code: 414240250 and code: 10730891 respectively). As well, ZnO used was purchased from Sigma Aldrich (6% Al doped, <50 nm nanopowder, CAS: 1314-13-2). Au₂₅(Cys)₁₈ was dried down from liquid form by splitting 50mL solution into 10mL glass vials. The vials were covered in aluminium foil and holes poked through the top using a needle stick. The vials were freeze dried and put under vacuum

for a week. The remaining powder was ground using a mortar and pestle ready for use.

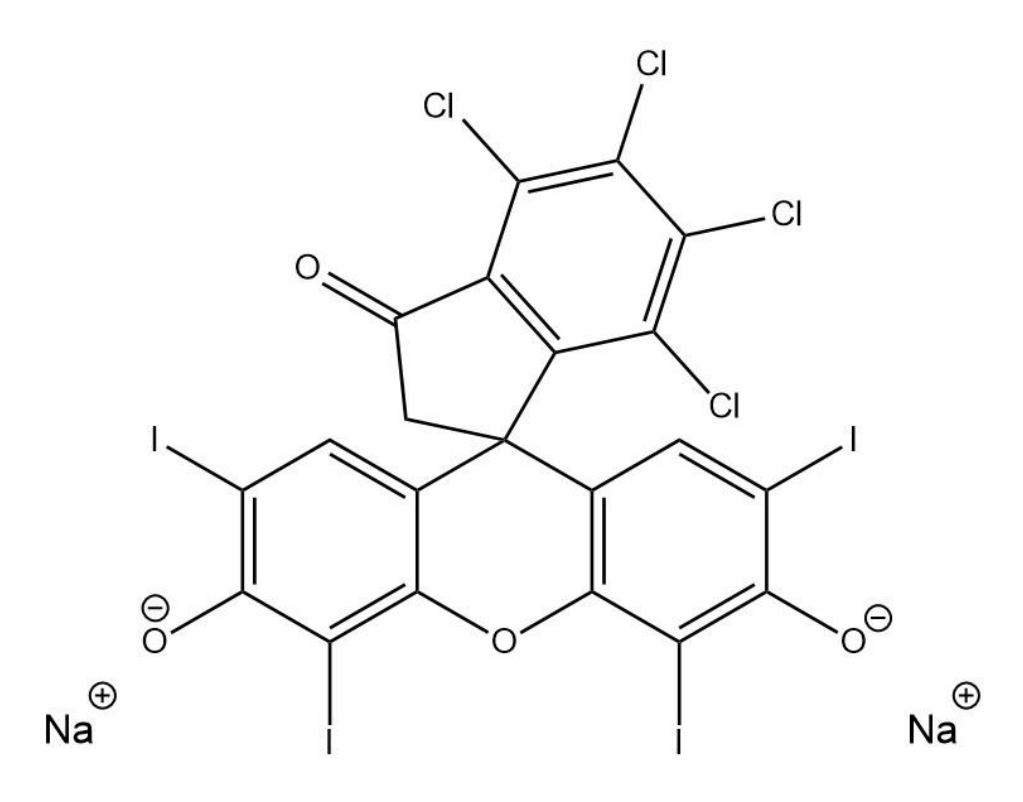


Figure 36. Chemical structure of rose Bengal.

Resin (Formfutura, clear LCD resin, methacrylate oligomer-based photopolymer) (~1 mL per printed square sample) was placed in centrifuge tubes. The relevant antimicrobial component (MB or RB and ZnO) was weighed and added. Dyes were made to 800 ppm, the ZnO was made to a 0.1 M solution in resin and $Au_{25}(Cys)_{18}$ a 0.01 M solution in resin. The centrifuge tubes were then vortexed for 3 mins each to sufficiently mix the solution.



Figure 37. Image of the methylene blue, rose Bengal, ZnO and $Au_{25}(Cys)_{18}$ resin mixtures before 3D printing.

The original 3D printing was carried out by Mustafa Sener in UCL Chemistry. The printer used was Mars 2 Pro 3D Printer, print details as follows: layer thickness (100 um), exposure per layer (3.6 s). Post printing the samples were washed in 99% isopropyl alcohol (IPA) for 5 mins and then fully cured for 3 mins under UV lamp (Elegoo Mercury Plus 2). Samples were then washed in sterile PBS (x3 washes for 5 minutes each at 40 °C) and DIW (x3 washes for 5 minutes each at 40 °C, or until water runs clear).



Figure 38. The curing process after 3D printing and isopropyl washes for sample squares produced for antimicrobial testing.

Samples were made into 1x1cm squares for proof-of-concept testing as seen below, before moving onto printing other shapes such as endotracheal tubes.

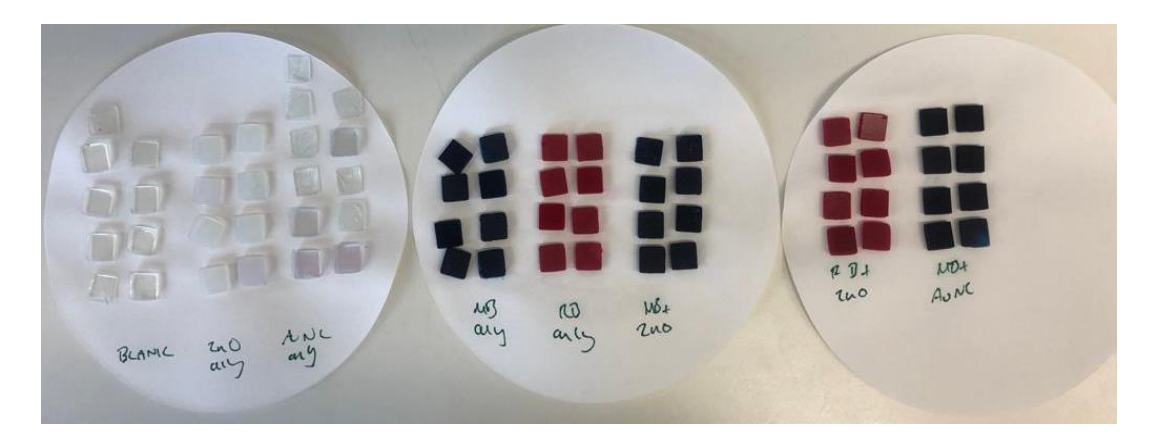


Figure 39. 3D prints for the screening of different mixes including ZnO only, Au₂₅(Cys)₁₈ only, MB only, RB only, MB + ZnO, RB + ZnO, and MB + Au₂₅(Cys)₁₈.

4.2.4 MICROBIOLOGICAL ASSAY

10 mL brain heart infusion (BHI) (Oxoid, Thermo Scientific CM1135) was placed into a 50 mL centrifuge tube. Using a sterile loop, one bacterial colony (strains used P. aeruginosa RS080, MRSA US137, E. coli coliform ET496) was placed into the BHI and cultured at 37 °C at 200 rpm for 18h. This was then centrifuged at 21 °C at 5000 rpm for 5 mins. The waste supernatant BHI was removed and replaced with 10 mL sterile Dulbecco's Phosphate Buffered Saline (PBS, Sigma Aldrich, D8537). The solution was vortexed until the bacterial pellet was mixed. This was then centrifuged again, and the process repeated. From this inoculum, 20 uL was placed in 1980 uL sterile PBS to gain a final inoculum (~1 x 10⁻⁷).

To prepare humidity chambers for experiments filter paper was placed inside a sterile 90 mm petri dish, wetted with 2 mL PBS. Two toothpicks were placed parallel to each other on top of the wetted filter paper, of which a microscope

slide was placed on top, perpendicular to the toothpicks. Antimicrobial endotracheal tube material samples were placed on the microscope slides, and 50 uL of inoculum placed on top of each sample. These petri dishes were then either placed in a dark box as a control or in light conditions (white light: 10,000 lux, confirmed by light meter Onecall, mini light meter, resolution 0.1 lux, laser light: Ondine Biomedical Ltd MRSAid Fibre Optic laser model MW3000, 655-675 nm, at 2cm distance from sample, output is 14 mW/cm2). Three biological repeats were conducted for all microbiological testing.

4.2.5 SARS-COV-2 ASSAY

This work was performed by Dr Maximillian Woodall at the Clinical Centre for Microbiology, as this requires biosafety level 3 training to test against SARS-CoV-2. Microbiology: SARS-CoV-2 Plaque Assay standard operating procedure MM12 Version - A, derived from Public Health England methods was used.

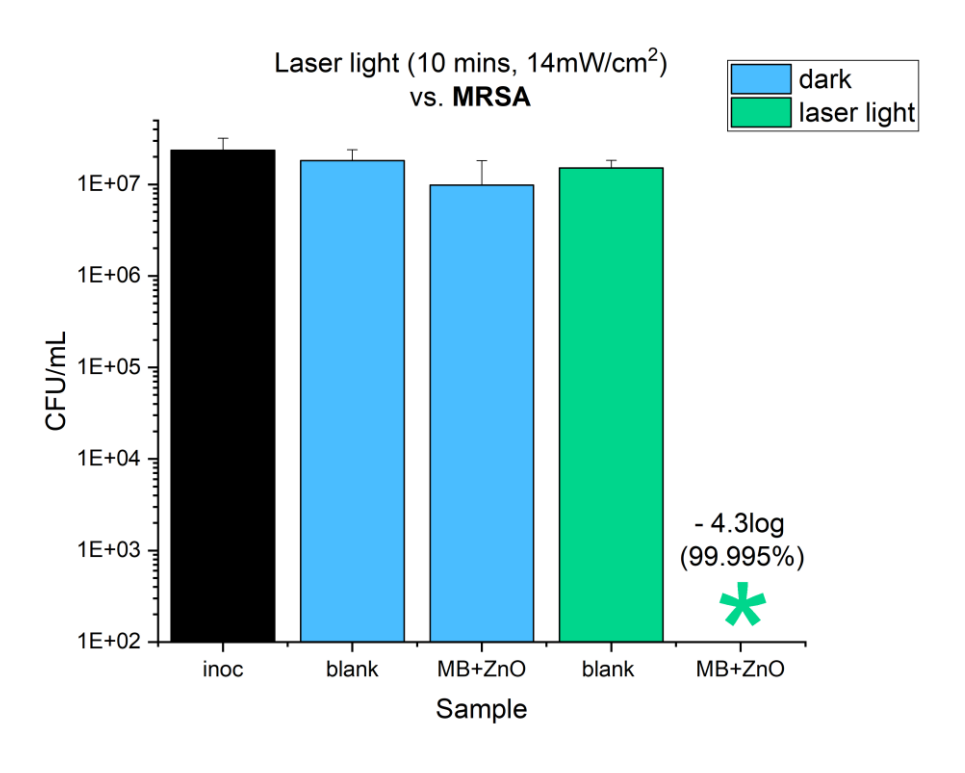
4.3 RESULTS & DISCUSSION

4.3.1 PRINTED MEDICAL DEVICES MICROBIOLOGICAL ACTIVITY

It is important to note hard polymers as used in the experiments described here (Formfutura, clear LCD resin, methacrylate oligomer-based photopolymer) were readily available and as such were used. The idea is this would be transferrable to different types of 3D printing including flexible biocompatible polymers required for tracheostomy/endotracheal tubes. Sections of the tube were then broken off for microbiology analysis to ensure this 3D printing was transferrable from 1x1cm squares to functional shapes.

Laser Activation Microbiological Results

One question is how this would work in clinic practice where half of the endotracheal tube is in a dark environment inside the trachea, and without currently knowing how long the activity from white light lasts, an alternative solution may be required. Ondine Biomedical currently treat nasal pathogens by a fibre optic laser treatment (655-675 nm), which activates MB solution resulting in significant bacterial kill. This laser could be fed through an endotracheal tube to provide additional activation as an alternative boost to dark or white light activation. From the initial scanning results above, it was decided to continue further testing using the MB/ZnO mix using Ondine Biomedical fibre optic laser treatment as the light source. The next experiment comprised a comparison of the MB/ZnO mix against drug resistant Gram-positive and -negative bacteria using laser light to activate.



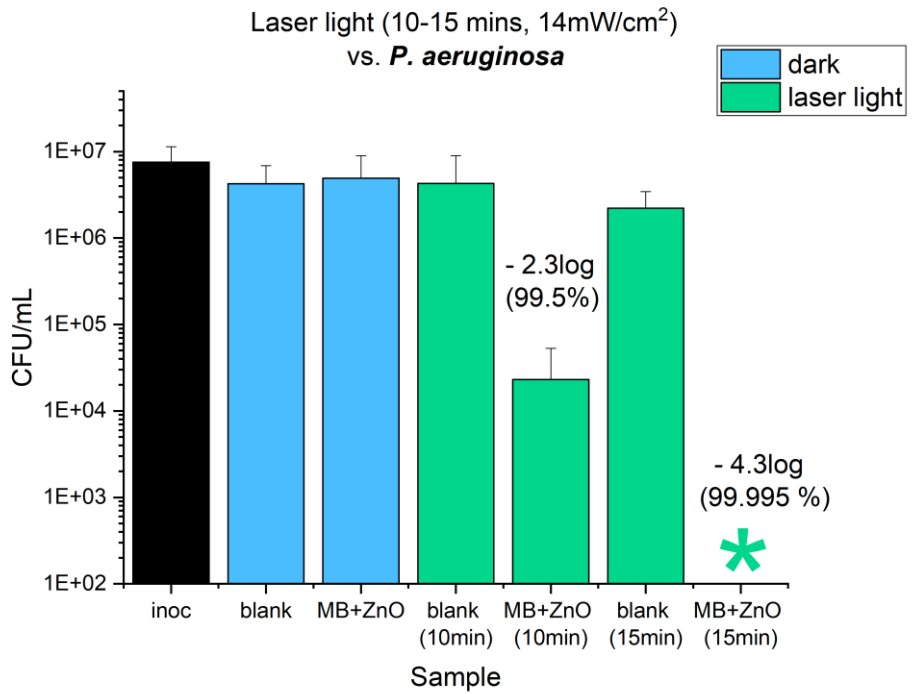


Figure 40. Graph showing the activity of 3D printed methylene blue and zinc oxide materials against drug resistant isolates of gram-positive and -negative bacteria (MRSA US137 and *P. aeruginosa* RS080) within 15 minutes of laser activation. Two biological replicates.

Within 15 minutes of laser activation, kills to below detection levels (100 CFU/mL) were seen for both *P. aeruginosa* and MRSA on 3D printed samples. *P. aeruginosa* required 15 minutes of activation to reach >99.99% kill whereas MRSA only took 10 minutes to reach >99.99% kill. This is a significant finding as both are recent clinical isolates, and the *P. aeruginosa* isolate is multi-drug resistant (Dr Vicky Enne, personal communication,).

These sections of the 3D printed tube are much thinner than the squares used in previous testing and an interesting observation was made whilst carrying out the laser experiments. So far, visible photobleaching has not been noted as a result of white light or laser light in these 3D printed square samples. However, in this case where the tested material was a broken off piece of 3D printed tracheostomy tube (significantly thinner), a lighter circle of visible photobleaching around where the inoculum droplet was placed on the sample was observed (figure 42). However, the level of kill was not compromised, therefore suggesting either activation from MB further into the photocured product, or migration to the surface to then activate occurred, or that the product was so concentrated that there was enough to continue killing even at reduced concentration. Therefore, mechanism of action testing should be done

at a later stage to further understand the interaction between the MB, ZnO and resin interacts once photocured to produce an antimicrobial effect.

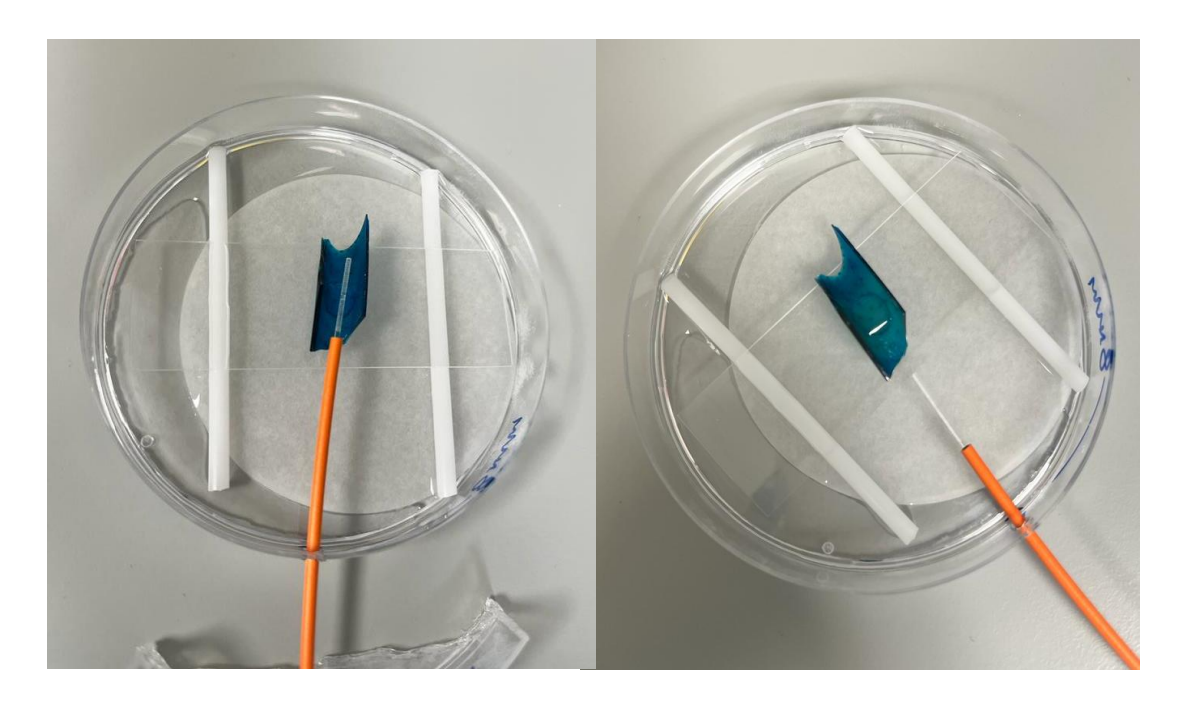
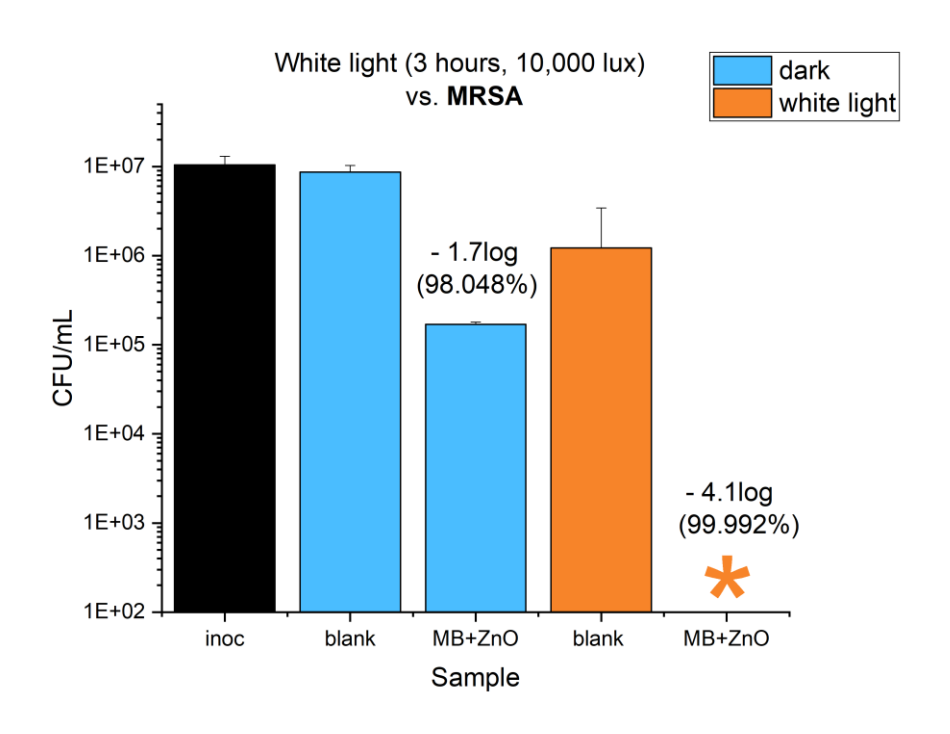


Figure 41. Side by side image of pieces of endotracheal tube broken off for testing, the left-hand side is before laser activation and the right-hand side is after laser activation.

White Light Activation Microbiological Results

When exposed to white light, both *P. aeruginosa* and MRSA reached >99.99% kill within 3 hours of white light activation. Significant kill was also seen for control samples kept in the dark (within 3 hours) in the case of MRSA at 98.05%.



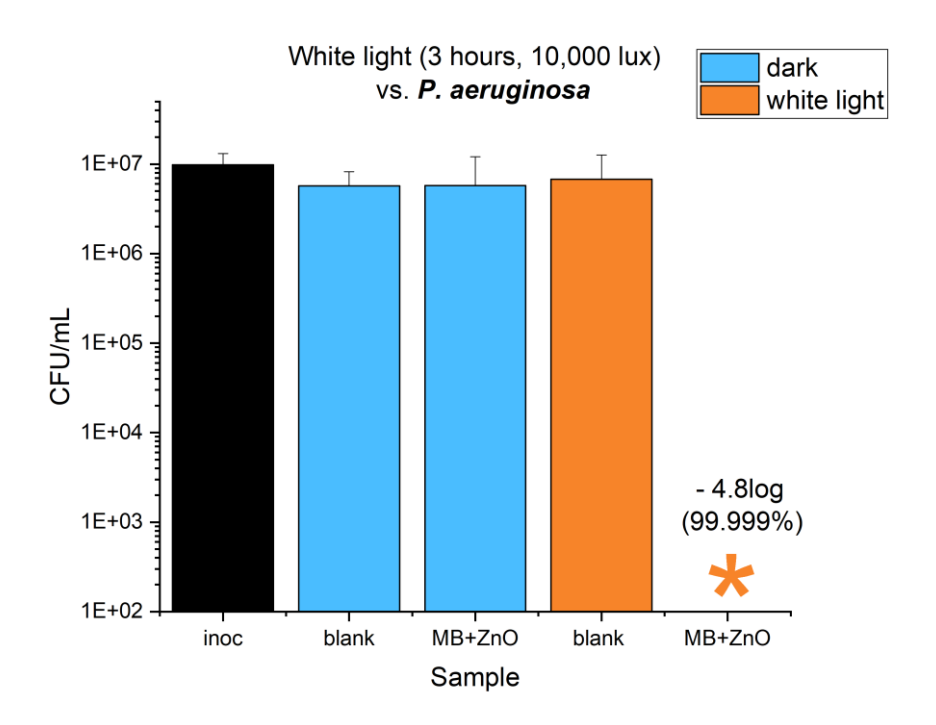


Figure 42. Graph showing the activity of 3D printed methylene blue and zinc oxide materials against drug resistant isolates of gram-positive and -negative bacteria (MRSA US137 and *P. aeruginosa* RS080) within 3 hours of white light exposure. Two biological replicates.

This research suggests ZnO nanoparticles encapsulated in 3D printed materials alone may be enough to significantly hinder biofilm growth by Grampositive bacteria like MRSA and Gram-negative *E coli*, as 98% and *91-92%* kill is observed (respectively) in the dark. However, for *P. aeruginosa* frequently seen as colonizers of endotracheal tubes, 68, 92, 93 the combination of photosensitizer dye and ZnO with light activation is required for significant kill.

4.3.2 MATERIALS CHARACTERISATION

The addition of ZnO and MB can be visually confirmed by the presence of a cloudy white 3D print for ZnO and a blue 3D print for MB. Materials were characterized by SEM, which showed little change from the addition of MB and ZnO on the surface morphology. The only notable difference being small holes scattered irregularly over the surface of the MB+ZnO samples (~50-100µm). These are small and irregular enough that the overall material is not compromised; and is possibly evidence of MBs ability to inhibit polymerization reactions as noted in previous literature. 94, 95 This would suggest the MB cation appears not to interact with the polymerizable resin matrix during 3D printing, which would be assumed to be the case for other polymer matrices as well. Alternatively, it is possible polymerization is triggered by MB-mediated free radical formation resulting in a chain reaction, as opposed to direct UV initiated photopolymerization in standard resin 3D printing. Very high concentrations of ZnO and MB were incorporated into these 3D prints for proof of concept, which may be reduced in future once a minimum effective concentration has been established, and hence reduce the potential frequency of holes.

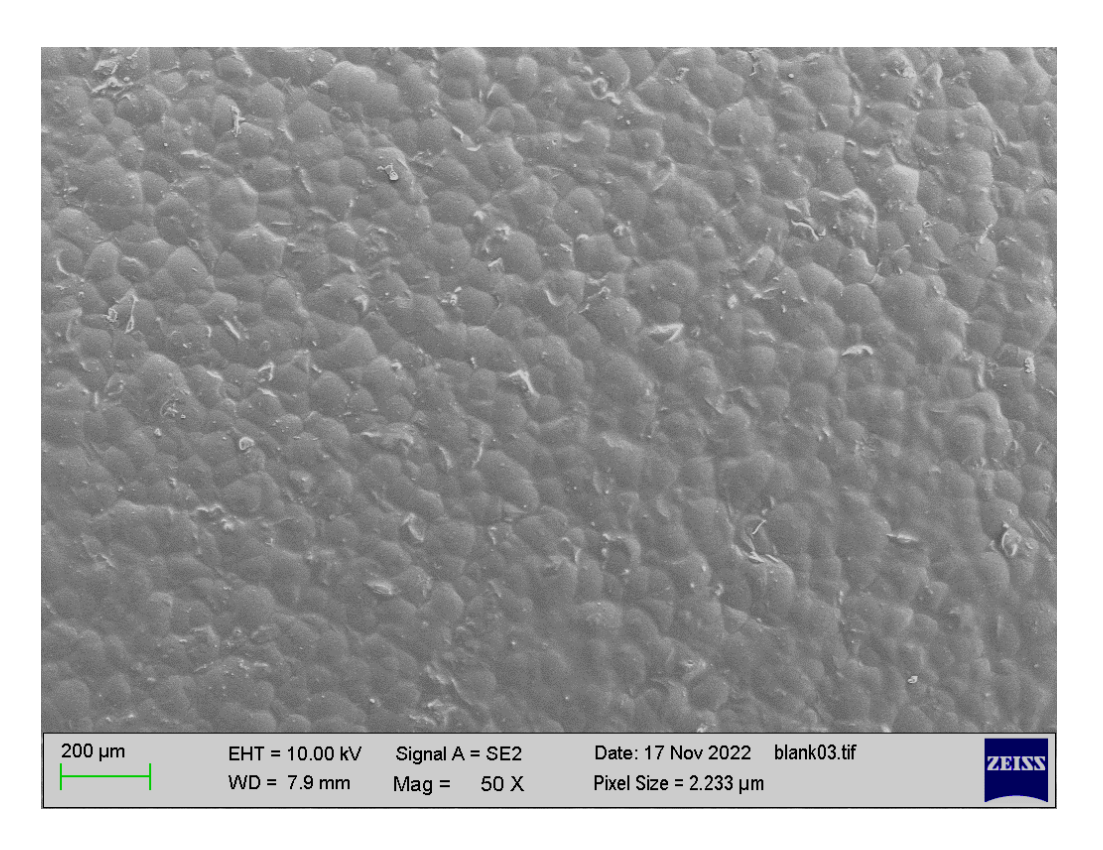


Figure 43. Scanning electron microscope image of the blank 3D printed control square.

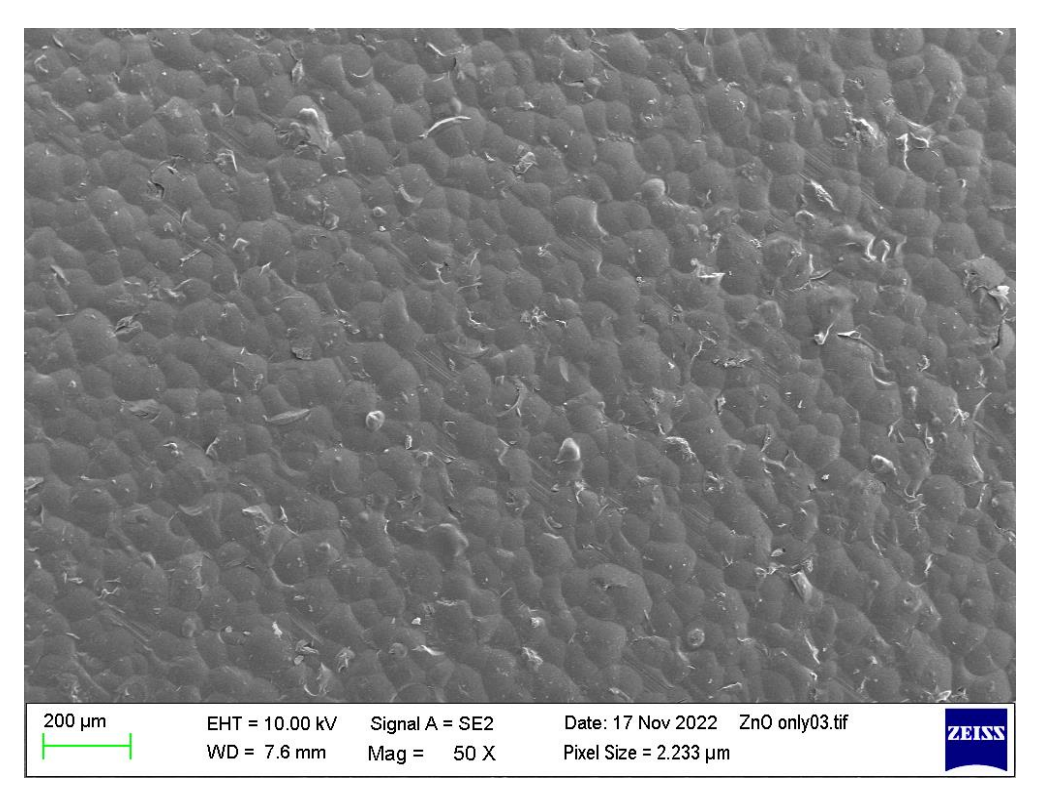


Figure 45. Scanning electron microscope image of the zinc oxide 3D printed control square.

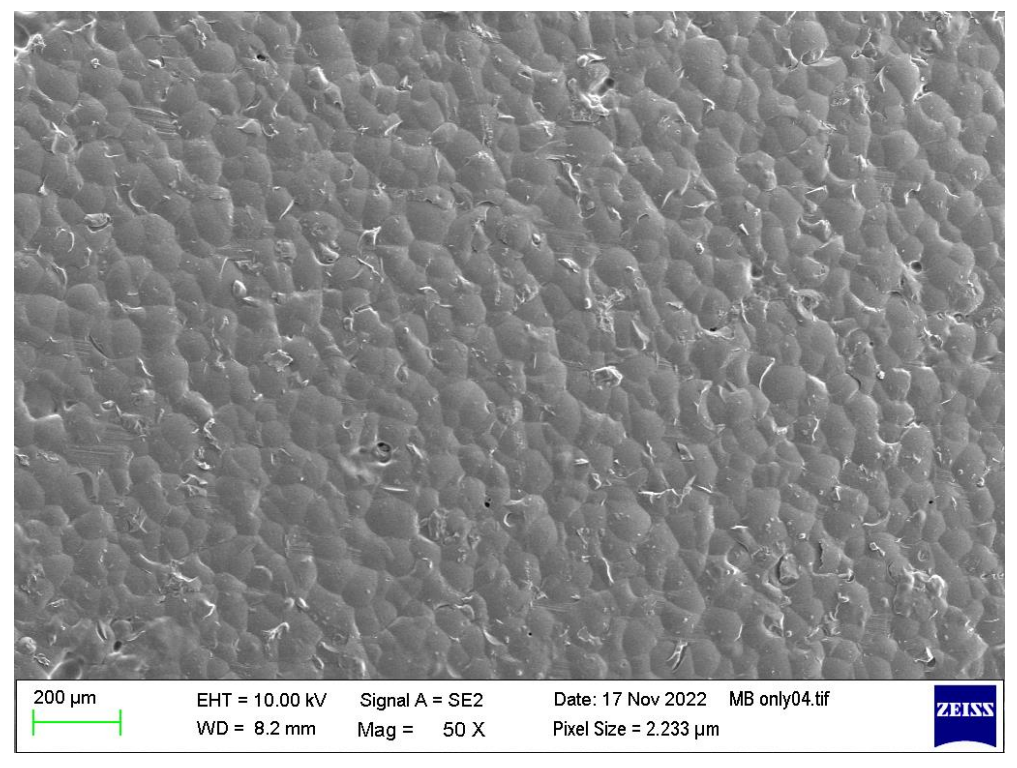


Figure 44. Scanning electron microscope image of the methylene blue 3D printed control square.

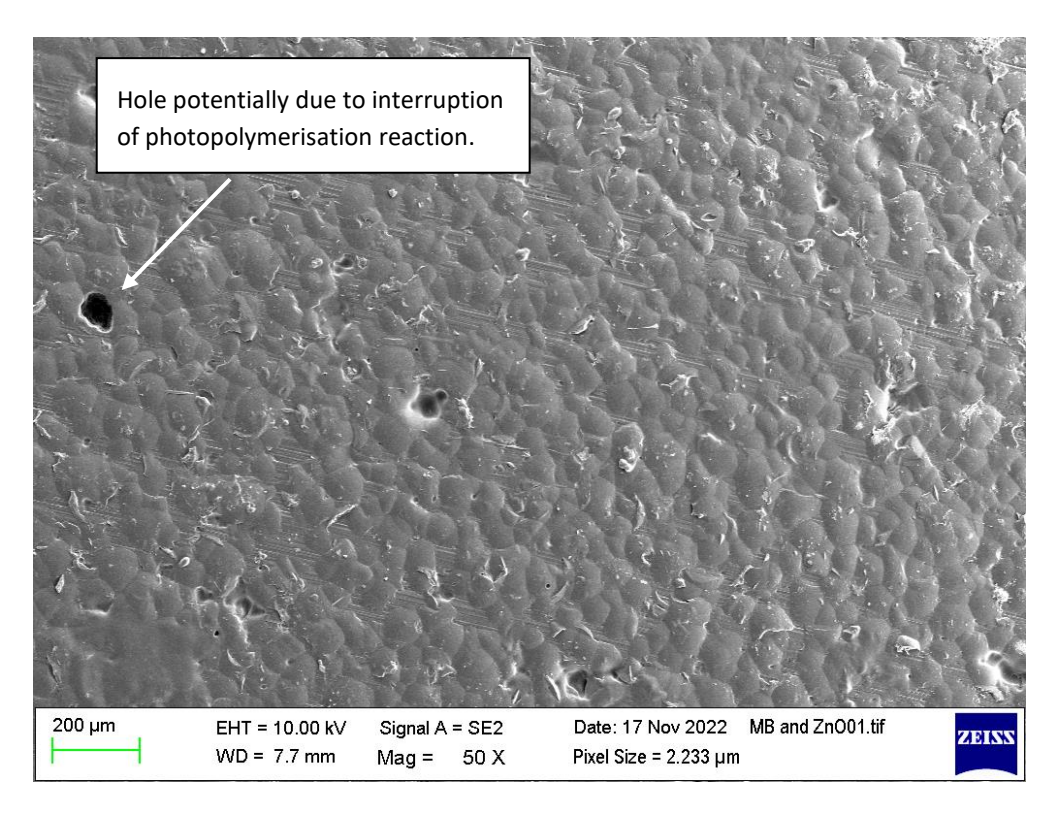


Figure 46. Scanning electron microscope image of the antimicrobial 3D printed sample containing methylene blue and zinc oxide. Hole illustrated by arrow and note.

What we learnt from these images is that small holes do appear throughout the SEM images on the addition of ZnO and MB, however a significant amount of ZnO and MB was used in these samples and no disruption to photopolymerization was noticeable by eye. These holes may be due to the amount of ZnO and MB added and its therefore recommended this SEM analysis is repeated after optimization experiments have been conducted.

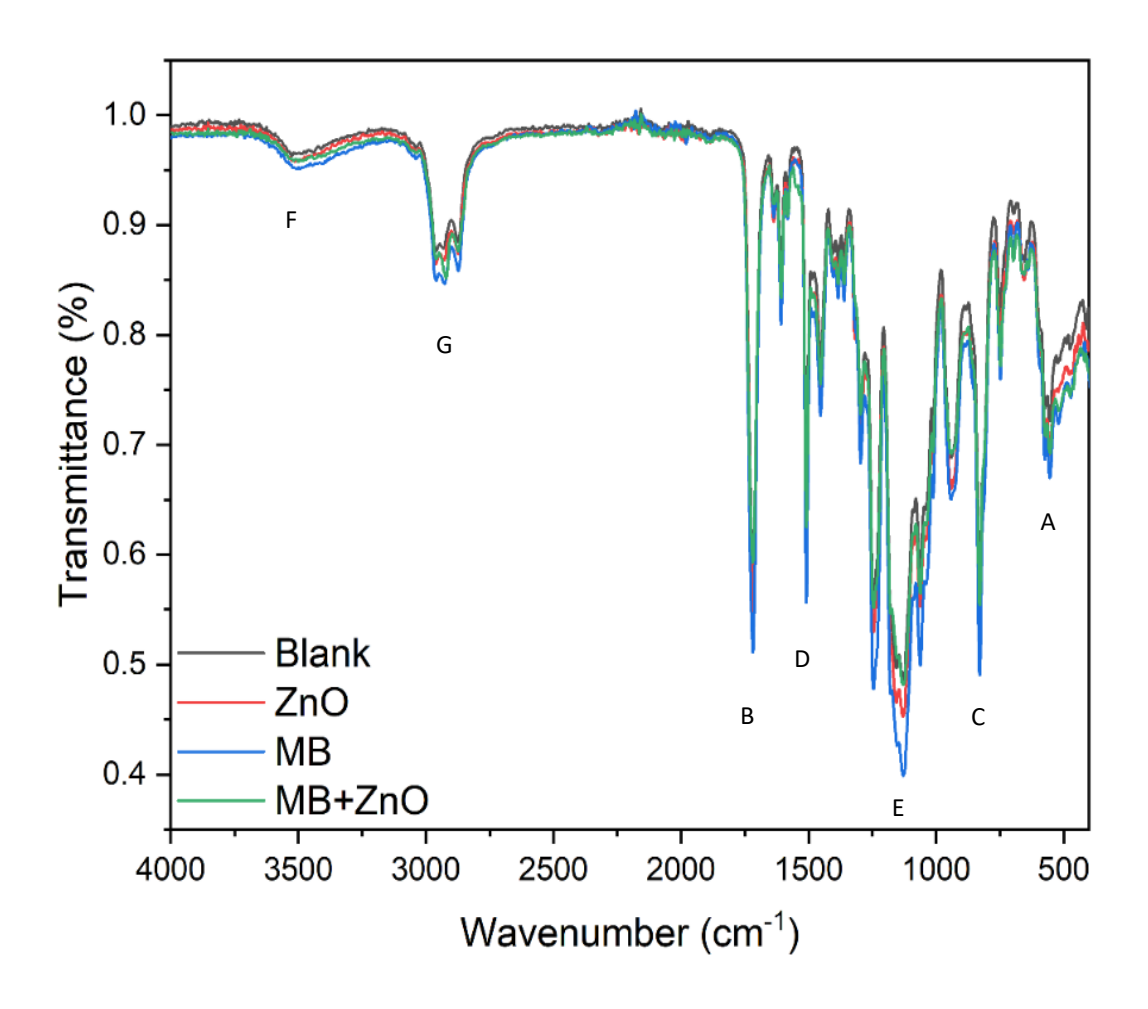


Figure 47. Infrared spectrum of 3D printed antimicrobial sample containing methylene blue and zinc oxide (green), methylene blue control (blue), zinc oxide control (red), and blank control (black).

Table 6. Table summarising assignments for peaks of IR spectra between 3D printed antimicrobial samples.

Assignment	Group	Absorption (cm ⁻¹)	
A	ZnO band	~500	
В	C-H (aromatic)	2000 - 1650	
С	C-H (bending)	700 - 800	
D	C-C (aromatic)	1600 - 1585 and 1500 - 1400	
Е	C-N (aromatic amine)	1342 - 1266	

F	N-H (amine)	3000 - 2840
G	C-H (stretching alkane)	3000 - 2800

Figure 48. Chemical structure of methylene blue with IR assignments.

IR confirmed the presence of MB and ZnO, but no structural differences between the materials.

Water contact angle measurements revealed a decrease in hydrophilicity from 77.28° (blank) to 85.05° (MB+ZnO), the largest change was bought about by the addition of ZnO (+4.86°) compared to the addition of MB (+3.40°).

Table 7. Summary of the mean contact angle (CA) measurements of water and diiodo-methane in air and total surface free energy (SFE).

Sample	Water in air (mean CA°)	Diiodo- methane in air (mean CA°)	Surface free energy (total)
Blank	77.3 (±3.0)	37.8 (±4.5)	44.9 ±3.3 mN/m
Methylene blue	80.7 (±5.3)	40.9 (±3.7)	42.5 ±3.6 mN/m
Zinc oxide	82.1 (±6.6)	36.4 (±4.6)	43.9 ±4.1 mN/m
Methylene blue + 85.1 (±2.0) zinc oxide		37.8 (±4.7)	42.6 ±2.9 mN/m

4.3.3 SCREENING STUDY MICROBIOLOGICAL ACTIVITY

Using 3D printing allows for the first time to have a true set of control samples containing only nanoparticle or dye, rather than the combination. This is not possible with swell encapsulation, as the synergy between the dye and nanoparticle aids in the swell encapsulation process, so trying to swell encapsulate solely nanoparticle or dye, does not yield the same results [visually for example the MB samples are significantly lighter than the MB and Au₂₅(Cys)₁₈ samples] even where the swell encapsulation solution is the same concentration. For this reason, these controls are not included in swell encapsulation. However, in this case, as each component is mixed with resin and directly printed, the exact amount of each component in the samples can be quantified. Combinations of rose Bengal (RB), methylene blue (MB) with zinc oxide (ZnO) were tested using the 3D printing method.

From previous research noted in Chapter 1, a Zinc (II) dioctylphosphinate/MB mix was attempted using the swell encapsulation method, in combination with the MB/ Au₂₅(Cys)₁₈ mix. However, this was found to be detrimental to the antimicrobial action in the light, and therefore was abandoned at this point. A mix whereby the nanoparticle brings antimicrobial action in the dark, and the photosensitiser brings antimicrobial action in the light, would be very beneficial to the current light-activated-only based antimicrobial materials. As well, an alternative to swell encapsulation as this method is wasteful would also be very beneficial. This led me to 3D printing. In this case, the addition of commercially available ZnO nanopowder (Sigma Aldrich, CAS: 1314-13-2) of <50 nm particle size was used instead of synthesising Zinc (II) dioctylphosphinate

(which was only required as it had to be soluble in solvents for swell encapsulation).

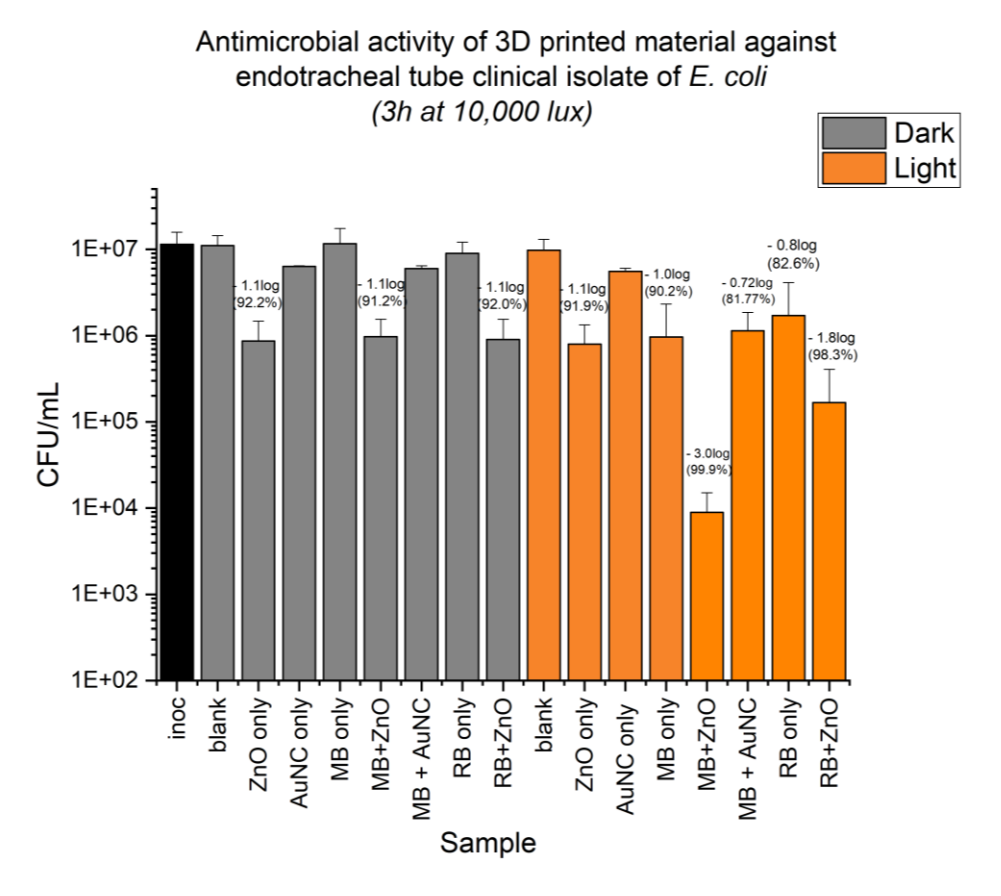


Figure 49. Antimicrobial activity of 3D printed materials using mixes of rose Bengal, methylene blue with zinc oxide or gold nanoclusters, against clinical isolate of *E. coli* using white light exposure (3h at 10,000 lux). Two biological replicates.

In the dark samples containing photosensitizer dye only did not cause any reduction in bacteria numbers as expected, and it has also confirmed that Au₂₅(Cys)₁₈ has no antimicrobial activity on its own in the dark against Gramnegative bacteria as suspected in previous work described in Chapter 1. The mixes containing ZnO showed some activity in the dark in each sample (ZnO only, MB mix and RB mix) ranging from 91.2 - 92.2%. A similar reduction

(91.9%) was observed for the ZnO only sample in the light, confirming the ZnO mode of action for microbial kill is not light dependant. As well, as previously theorised in Chapter 1, when used combined with photosensitiser dye should increase the materials activity in the dark, which was a drawback of the MB/Au₂₅(Cys)₁₈ swell encapsulated material. In the light conditions, increased activity was achieved for the MB-ZnO and RB-ZnO mixes with 3-log (99.9%) and 1.8-log (98.3%) reductions in bacteria numbers respectively after 3h of white light exposure (10,000 lux).

From our previous swell encapsulation experiments it was expected that the MB/Au₂₅(Cys)₁₈ would have the best activity and a complete kill to below the detection level, however the Au₂₅(Cys)₁₈ used were dried previously a month before use, and they appeared to be hygroscopic which was a new finding for the group. Therefore, when the Au₂₅(Cys)₁₈ powder was mixed with the resin, as the powder had partially clumped the resulting mix was not as thorough resulting in a surface with poorly dispersed Au₂₅(Cys)₁₈. As some antimicrobial activity is shown, if the clusters could be synthesised and dried down successfully into a powder and kept dry, potentially this may have been as successful as the ZnO mixes. However, ZnO is widely already commercially available, is inexpensive and is well known within healthcare such as its use in sunscreens and so on. Due to the lengthy drying step for the Au₂₅(Cys)₁₈ clusters and the ease of using ZnO, combined with its antimicrobial results, it was decided to continue printing ZnO mixes. Though RB and MB both showed antimicrobial activity, the MB/ZnO mix had overall the best antimicrobial activity and so MB was chosen for printing other shapes. MB is also already

used in healthcare with a well-known toxicology profile and should therefore be easier to commercialise.

4.3.4 ACTIVITY AGAINST SARS-COV-2

There is evidence to suggest patients who develop bacterial and viral coinfections or superinfections, are at an increased risk for longer hospital stays,
and were more likely to suffer complications and death. 14, 96, 97 Researchers
have investigated how SARS-CoV-2 may induce secondary bacterial
infections, which is thought to be due to the damage caused to the respiratory
epithelium by viruses, which encourages subsequent bacterial colonization
and adherence. 11, 12 Another study noted increased levels of infection related
biomarkers and inflammatory cytokines in patients with SARS-CoV-2, which
provides evidence that viral infections like SARS-CoV-2 induce secondary
bacterial infections by dysregulating the immune system. 13 Therefore, it's
important to test this material against SARS-CoV-2 and determine how this
might affect co-infected or superinfected patients, potentially stopping infection
at the root cause if viral infections are a common predisposition for bacterial
infections in the respiratory tract.

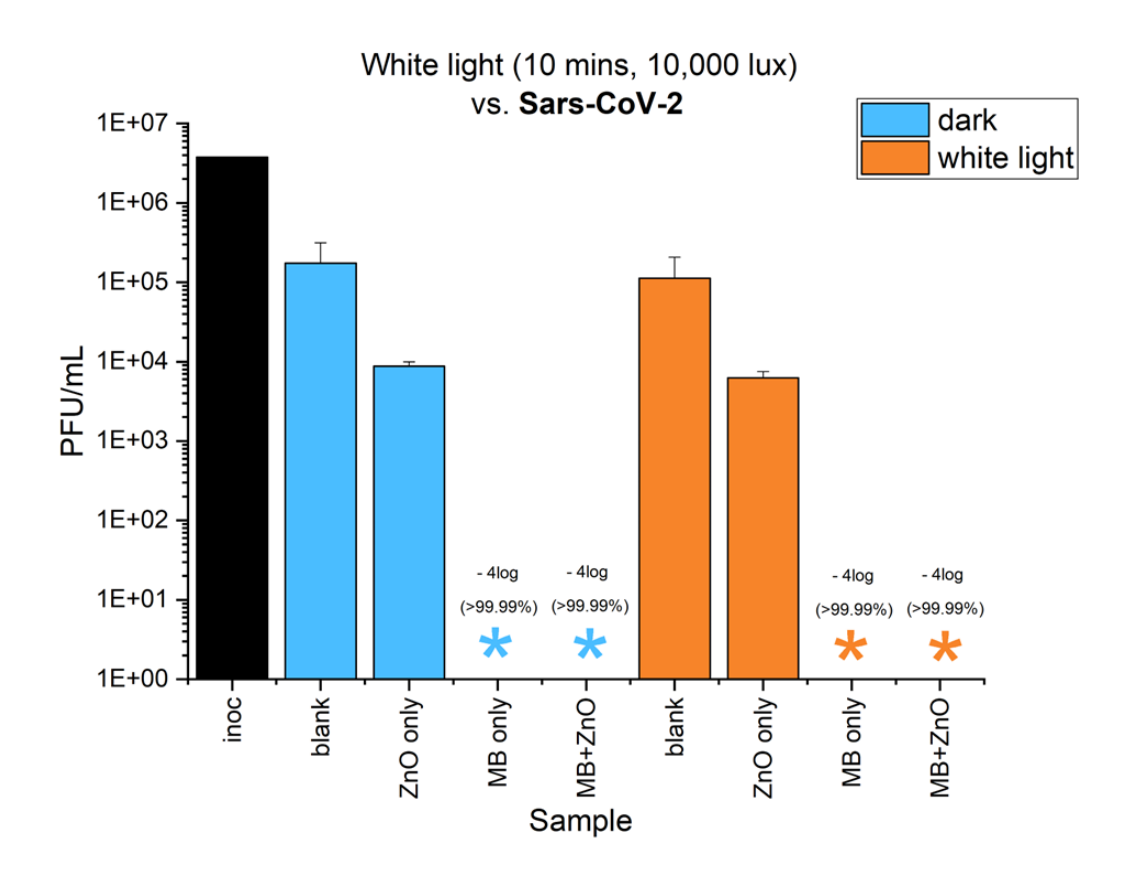


Figure 50. Results showing the activity of 3D printed antimicrobial material using MB and ZnO mixes against SARS-CoV-2 within just 10 minutes in the dark and exposed to white light. Three biological replicates. * = below detection level (25 PFU).

Results of MB+ZnO antimicrobial material against SARS-CoV-2 in the dark and light. Within just 10 minutes, without requiring any light activation, a 4-log reduction (>99.99%) to below detection levels was achieved; showing SARS-CoV-2 was far more susceptible to these surfaces when compared to bacteria, and the level of kill achieved is significant.

The kill against SARS-CoV-2 seen using 3D printed antimicrobial materials is the fastest observed from the literature exceeding semiconductor photocatalysts, ⁹⁸ functionalized polymers, ⁹⁹ and copper-based surfaces. ^{100, 101}

In one example, copper oxide nanoparticles are bound into a thin film with polyurethane to develop an antimicrobial coating applicable to many materials. This coating showed overall a 3-log reduction in SARS-CoV-2 viability in 1 hour. 100 As well, a polydopamine coating with copper to the surface also reports a 3-log reduction in SARS-CoV-2 in 1 hour. 101 In another, conjugated polymers and oligomers were shown to be highly effective in the light, with their best oligomer yielding a 5-log reduction in near-UV light within 10 minutes. However, none of the polymers or oligomers showed activity in the dark. 99 More recently, a flexible thin plastic film, UV pre-conditioned for 144 hours with 30 wt% tin dioxide has also been developed. Log reductions of ~5-log* and ~3-log* in 3 hours were noted in the white light and dark respectively (*values estimated from graphs). 98

As a direct comparison, in the dark, the 3D printed antimicrobial material presented here using MB and ZnO showed a > 4-log reduction (99.99%) to below detection levels in just 10 minutes. MB alone yields the same log reduction (4-log). As samples are not kept in the dark prior to testing (exposed to normal room lighting) and are only in complete darkness for the testing time, it's thought this reduction is caused by residual activation from being in the light previously. Though the ZnO alone also provides reduction (94.97% and 94.44% in the dark and light respectively) it is clear the MB is the primary antimicrobial source in the case of inactivation of SARS-CoV-2.

To account for any reduction caused by heat from the lamp, reduction calculations use the 'blank' exposed sample as the original number, as opposed to inoculum count. For both bacterial and viral experiments, triplicates

were performed as a minimum. The European Medicines Agency (EMA) considers virucidal activity a reduction of 4 logs or more, ¹⁰² and though there is no equivalent guidance for bacteria, usually a reduction of 3-5 logs bactericidal activity is considered significant according to the European standard EN1276. ¹⁰³ Therefore, as this 3D printed material achieves 4 logs or more reductions across both multi-drug resistant Gram-positive and -negative bacteria in the light, as well as 4 log reductions against SARS-CoV-2 even in the dark, this is a significant finding.

It's important to note other differences between this 3D printed material and other technology described above, considering the desired application in medical devices. The material developed is not limited by the finite release of a compound for activity as with some silver and styrylbenzene based antimicrobials, 104, 105 nor reliant on coating an existing material (which may be subject to wear and tear), 106, 107 and takes just 5 minutes of preparation time before printing any almost any shape imaginable. Both MB and ZnO are already well known in medical settings, MB solution is used as an injectable treatment for methemoglobinemia and more recently in the treatment of ifosfamide neurotoxicity and refractory vasoplegic shock, 64 and is also used in Ondine Biomedical Ltd Steriwave photodisinfection treatments for nasal decolonization. 108 ZnO nanoparticles are commonly used in sunscreens worldwide, 109 with safety data showing ZnO nanoparticles do not penetrate the skin. 110 Therefore, as well researched compounds, with well-known safety and toxicology profiles, these are ideal for use in the development of novel antimicrobial medical devices.

4.3.5 BROADER APPLICATIONS OF 3D PRINTING

The applications of 3D printing due to the nature of printing are almost limitless, only limited by what you are able to design on the computer. The resin type can be changed and modified to print different types of polymers with different mechanical properties, and therefore endotracheal tubes may not potentially be the best use of this technology. 3D printed antimicrobial materials may be better suited to personalized medicine such as implants for example, where these need to be printed to suit each persons need and are not produced on a large scale, which is a potential barrier of the 3D printing technology regarding commercialisation potential.

5 CHAPTER 5 – CLINICAL STUDY

5.1 INTRODUCTION

At the point of beginning this research VAP was not very well understood in terms of very conflicting reports of what the potential causative pathogens were. Hence, I decided alongside my research into the development of an antimicrobial endotracheal tube that it would be useful to learn more about the types of bacteria growing on endotracheal tubes at UCLH by conducting a clinical study to investigate this. The protocol, application, ethical approval and experimental work was all designed, developed and conducted by me. Health Research Authority (HRA) and Health and Care Research Wales (HCRW) approval issued 18th August 2022. IRAS project ID 274984, REC reference 21/LO/0909. This type of clinical study design could be extended to other

populations such as paediatric, where it would be interesting to note any differences or similarities in the types of bacteria found on extubated endotracheal tubes where there is notable biofilm growth, and how this affects mortality or morbidity outcomes.

The original aim of the clinical study was primarily to understand what the causative organisms are for VAP patients at UCLH, culture more bacteria to use in antimicrobial materials testing, and also to investigate a potential rapid diagnostic technique. This study is still ongoing and so initial results collected from the first 10 tubes will be discussed here.

Recently more literature has become available regarding VAP as a result of the pandemic, due to its nature in being heavily related to mechanical ventilated patients and therefore involving cases of VAP. Researchers in France found the primary bacterium to be *S. aureus* ⁷⁴, which contradicts the associated accepted norm of *E. coli* ⁵⁴. Therefore, the clinical study will not exclude Covid-19 patients, but whether or not a diagnosis has been made will be recorded and considered in the analysis of the endotracheal tubes, to determine any differences between patients with and without Covid-19.

The other major aim was to look at developing a rapid diagnostic technique for VAP, which is inherently difficult due to symptom similarities with sepsis ¹¹¹ and Covid-19 pneumonia ¹¹². A hugely problematic knock-on effect of this is that because delays in treating sepsis for example significantly increases mortality, HCPs are hesitant to discontinue antibiotics in patients presenting with symptoms until confirmation test results are received. The most problematic of these tests is microbial culture, where cultures need to be grown

and plates read, therefore taking a matter of days to receive results back. In the meantime, broad spectrum antibiotics will be administered, and if the diagnostic turns out to be negative then antimicrobial resistance is being promoted needlessly. In turn, creating even more dangerous resistant superbugs, which are harder to kill and treat. As such, an accurate, rapid, diagnostic technique to aid or replace microbial culture would help to slow down the rate of growth of antimicrobial resistant organisms.

Hence here it is proposed biofilm found on the endotracheal tubes would be analysed by NMR by a sort of metabolomics style analysis, where hopefully signature peaks or 'fingerprints' for certain bacterium can be identified. This would eventually result in a ~30 min testing time (plus sample prep which is yet to be optimised) compared to ~2-3 days. NMR Metabolomics has already proved a powerful tool in biological sample analysis, going as far as being sensitive enough to distinguish between different developmental stages of a biological sample ¹¹³, and so isn't too far of a jump to suggest NMR could have the potential to indicate the onset of VAP before the infection has the chance to fully develop.

5.2 METHODS

5.2.1 STUDY OUTLINE

Study title: Analysis of endotracheal tube biofilm (including type of bacteria, biofilm architecture and structural components) in patients who have been intubated for 5 or more days.

The primary objective was to analyse the bacterial biofilm found on endotracheal tubes extubated from patients who have been intubated for 5 or more days, to learn more about the type of bacteria and physical and chemical structure of biofilms causing ventilator associated pneumonia. This would then be used to guide smart design of antimicrobial materials for endotracheal tube applications. The secondary objective is that together with patient data on ventilator associated pneumonia diagnosis, by utilizing NMR analysis it is hoped that patterns may emerge and provide 'fingerprints' for particular biofilms or bacterial strains, which could potentially provide a very significant diagnostic tool for the infection, as microbial cultures to determine the causative bacteria takes days (whereas NMR could provide results in minutes). Additionally, provide insight into the EPS structure of biofilms of this nature, to guide future research into antimicrobial materials and how best to target these biofilms. As well, a bank of cultured strains directly from this study will be kept for future testing against antimicrobial materials, therefore providing a wider range of bacteria to test against and thus increasing the confidence in the material.

5.2.2 STUDY DESIGN

- Single centre, cohort observational
- Inclusion criteria is adult who has been intubated ≥ 5 days, other no population/group exclusion criteria.
- Total study population >30
- Approximate duration of enrolment 2 hours (30 min consent, 60 min review of patient notes, 30 min extubation). No follow up requiring contacting the patient, only routine outcome data will be recorded.
- First of its kind investigational study, therefore no statistics were used in deriving the number for sample size.

Inclusion criteria: any adult patient (aged 18 and above) due to be extubated, who has been intubated 5 ≥ days. Exclusion criteria: extubated endotracheal tubes < 5 days, extubated endotracheal tubes with no visible biofilm present, extubated endotracheal tubes from children (under 18).

5.2.3 STUDY SCHEDULE

Patients were identified as those expected to be extubated, who had been intubated for 5 or more days. These patients were identified by the direct care team. The study proposed the research sample is taken after routine extubation has been completed, where otherwise the research sample (endotracheal tube) would usually be disposed of. The clinical team would then alert a delegated member of the research team (embedded within the direct care team), who approached the patient, or the consultee, for participation in the study. Patient records were viewed by the direct care

team and a sample number allocated to the research sample so that it is anonymised.

Patients would be screened in all environments using electronic and paper based medical records. Screened patients were be noted on a screening log. However, any data recorded, or samples taken would be identified through a unique study identification number (pseudonymised data). Clinical outcome data will be reviewed in all enrolled patients. The data requested to accompany the endotracheal tubes for each tube are as follows: age, sex, diagnosis requiring intubation, days of intubation, days of current endotracheal tube, antibiotics given, if yes name of antibiotics/antifungals, and positive culture in the last 5 days (site/organism).

Patients were followed up during their stay by the direct care team (however long that may be) and routine outcome data will be recorded.

Consultees were be updated on the study and had the opportunity to withdraw agreement at any point. Patients are to be withdrawn at either the patients request, the consultees request, or request of the treating clinical team. A contact phone number was provided in the information sheet should anyone want to contact the research team.

The study will end once 30 endotracheal tubes with sufficient enough biofilm on to be successfully analysed have been collected, the study will end.

5.2.4 MICROBIAL CULTURE

The extubated tube was removed from the sterile bag and placed in a biosafety cabinet. The tubes brand name, size and whether or not visible biofilm could be seen was recorded. The tube is placed on a sterile chopping board. The tube was then separated into three sections carefully using a scalpel and cut as follows: 1) top (open end) 2) middle and 3) bottom (distal end inside the patient). Each section cutting was guided by the endotracheal tube markings 'ID' and depth markers '24-26'.

For each section, biofilm material was swabbed and plated onto Blood, MacConkey and Mannitol Salt agars and incubated in 5% CO2 for 48-36 h at 37 °C.

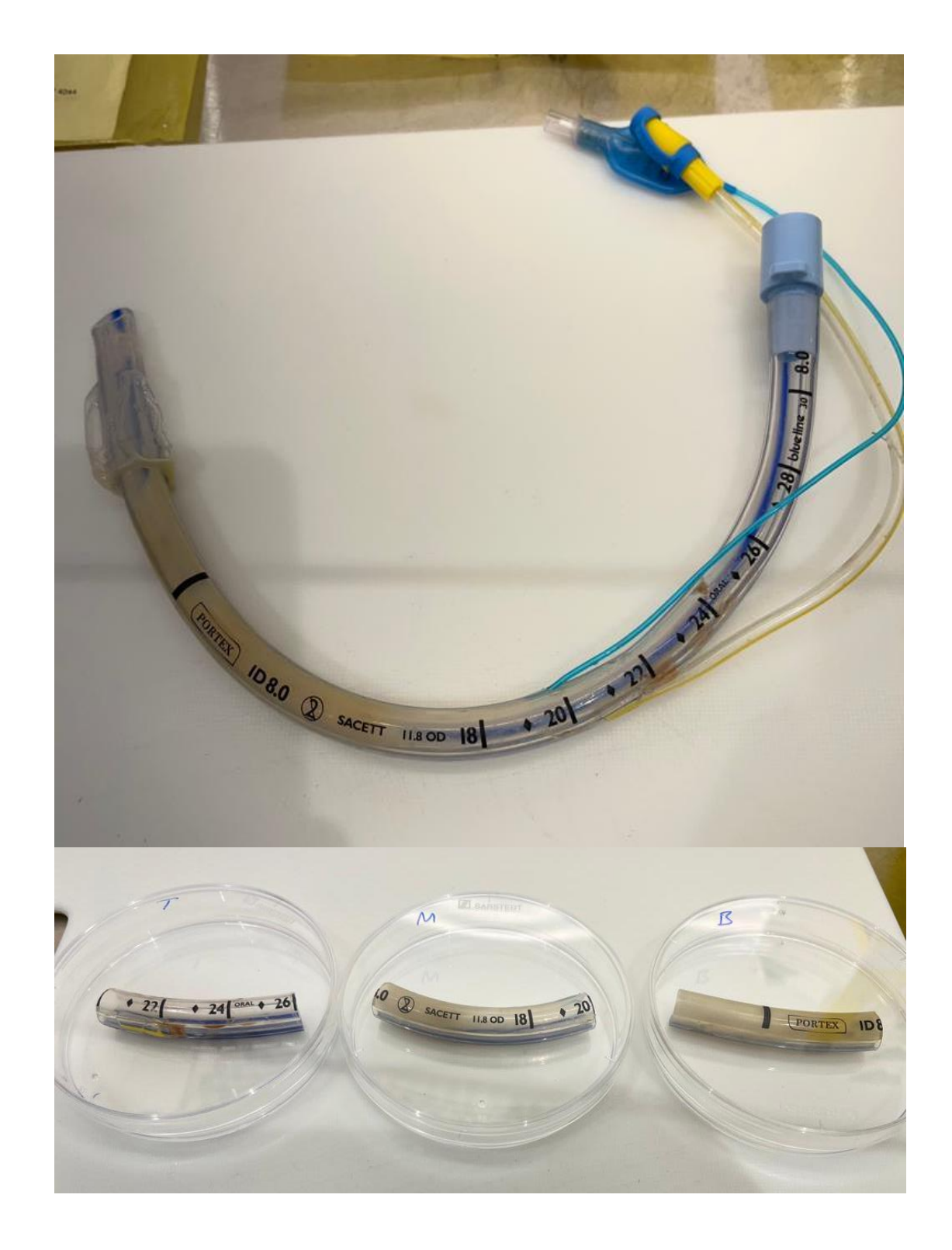


Figure 51. Images of the endotracheal tube after it has been removed from its sealed bag, intact. Below this is a comparative image of the prepared sections (top, middle, bottom = T, M, B) for analysis.

5.2.5 SEM ANALYSIS

For each section above (top, middle, bottom), small ~1cm long sections were cut and placed into a well (12 well plates used) to be fixed for SEM analysis. The fixature solution (4% paraformaldehyde, 1% glutaraldehyde) was prepared by adding 0.80 g sodium phosphate monobasic (NaH₂PO₄, Sigma Aldrich) and 2.73 g disodium hydrogen phosphate (Na₂HPO₄, Sigma Aldrich) to DIW which was made up to 250 mL and pH adjusted to 7.4. The solution was transported to a fume hood, where 10 g paraformaldehyde powder (Sigma Aldrich, 95%) was added, and the mixture heated whilst stirring to 60 °C. Once reached, 1-2 drops of 1 N NaOH was added to aid dissolving. Once dissolved, the solution was taken off heat and 5 mL glutaraldehyde were added to the solution (Sigma Aldrich, grade I, 50% aqueous solution).

The fixative solution was carefully added so that the solution just covered the sample. Excess fixing solution was removed by glass pipette and was replaced with crescent volumes of increasing ethanol concentration (35%, 50%, 75%, 95%, and 100%). Once 100% was reached, this was repeated a further x2 times. Finally, samples were considered dry. Samples were then submerged in hexamethyldisilazane (HMDS, Sigma Aldrich, reagent grade ≥ 99%) for 2 minutes, before placing on filter paper to remove residual HMDS. Samples were then gold sputtered (Agar Scientific, sputter coater) for 10 secs at 0.08 mbar, and analysed using the Zeiss Field Emission Scanning Electron Microscope, FESEM Sigma 300VP.

5.2.6 NMR ANALYSIS

Due to the numbers of samples for NMR analysis and the time intensity of doing so, it was decided only the distal end inside the patient would be analysed by NMR (bottom sections). A small section (2-3cm long) of the endotracheal tube was cut off and placed in a 50mL centrifuge tube for recovery of (i) water-soluble and (ii) NaOH-soluble material. Water soluble biofilm material was collected by adding 3mL of sterile water (Molecular Biology Reagent, Sigma Aldrich, W4502) to the tube and vortexing to solubilise. The tube section was carefully removed using sterile disposable tweezers and placed into a second centrifuge tube containing 3 mL NaOH (0.1 M) and again vortexed to solubilise. The tube section was carefully removed using disposable plastic tweezers. Both tubes (water soluble phase and NaOH soluble phase) were then centrifuged for 5 minutes at room temperature at 5,000 rpm to remove insoluble material. The recovered supernatant was poured into new sterile tubes for freezing at -80 °C. Once frozen (~18h) the tubes were transferred to the freeze drier and until completely dry. The dried material was dissolved in 1 mL D2O (Sigma Aldrich, 99.9% atom D) and analysis carried out on the Bruker Avance Neo 700MHz instrument.

5.3 RESULTS & DISCUSSION

The first 5 tubes will be detailed here. The clinical study collection of tubes has finished with a total of 17 tubes collected due to time restraints. The following results are therefore preliminary findings from the first 5 tubes, strains will all be confirmed later by either 16S rRNA gene sequencing or matrix-assisted laser desorption/ionization-time of flight (MALDI-TOF) analysis. The clinical study in full will form a separate report for publishing after ID data is gathered.

5.3.1 MICROBIAL CULTURE

Below is a table summarising the first 5 tubes brand, size and whether there was visual biofilm present, as well as proposed identification.

Table 8. Summary of the suspected organisms growing on the endotracheal tubes from samples 1-5 based off colony morphology, gram stain and selective agar plate growth.

Sample	Brand	Size	Biofilm	Suggested ID
ET001	Portex	7.5	Y	Isolate 1: Staphylococcus epidermis.
				Isolate 2: Pseudomonas aeruginosa.
ET002	Portex	8	Y	Isolate 1: Staphylococcus aureus.
				Isolate 2: Streptococcus pneumoniae.
ET003	Portex	8	Υ	Isolate 1: Staphylococcus aureus.
				Isolate 2: Streptococcus pneumoniae.
ET004	Portex	8	Υ	Isolate 1: Streptococcus pneumoniae.
				Isolate 2: Staphylococcus aureus.
ET005	Shiley	7.5	N	Isolate 1: Streptococcus agalactiae.
				Isolate 2: Candida glabrata.

The full analysis of the first 5 endotracheal tubes including colony morphological descriptions, the gram stain observations and further selective agar cultures can be seen in the appendix. As an example, for ET001-1, two types of colonies were noted on blood agar. One type grew on MacConkey and one type grew on Mannitol Salt. For the organism growing on Mannitol Salt (isolate 1), the gram stain showed purple cocci shaped clusters. Cocci clusters suggest a *Staphylococcus* strain. This combined with the fact the colonies were pink with pink coloured media and therefore non-Mannitol

fermenters. It has therefore been suggested that isolate 1 was likely to be Staphylococcus epidermis.

For the organism growing on MacConkey (isolate 2), these colonies were filamentous flat yellow colonies and therefore non-lactose fermenting, with beta-haemolysis around colonies on blood. Gram stain revealed red bacilli shaped bacteria. Therefore, it was suggested isolate 2 is likely to be *Pseudomonas aeruginosa*.

A similar pattern to this was followed to suggest identifications for the remaining endotracheal tube isolates, combining colony morphology, results from selective plates and gram staining to form a suggestion. Where the gram stain showed unusual results, such as large bulbous shapes suspected to be yeast, a further test on CHROMagar Candida Medium was conducted to confirm (as in the case of ET005). It is currently planned to complete the clinical trial analysis of results using either 16S or MALDI-TOF mass spectrometry to accurately confirm identifications and use this in conjunction with observations noted.

From visual observation of the plates together, it appears that in some cases the concentrations of different bacteria changes throughout the tube. In this image below, a clear decrease in concentration going from 'top' to 'bottom' can be seen. Once IDs have been confirmed by either 16S MALDI-TOF the bacteria associated with VAP and/or increased mortality can be determined, and if these tend to lie towards the bottom or top end of the tube which may lead to suggestions of infection source (environment/body). From this, it may

be revealed if the source for VAP-causing bacteria comes mostly from the environment (like reservoirs such as hospital sinks) or from the body.

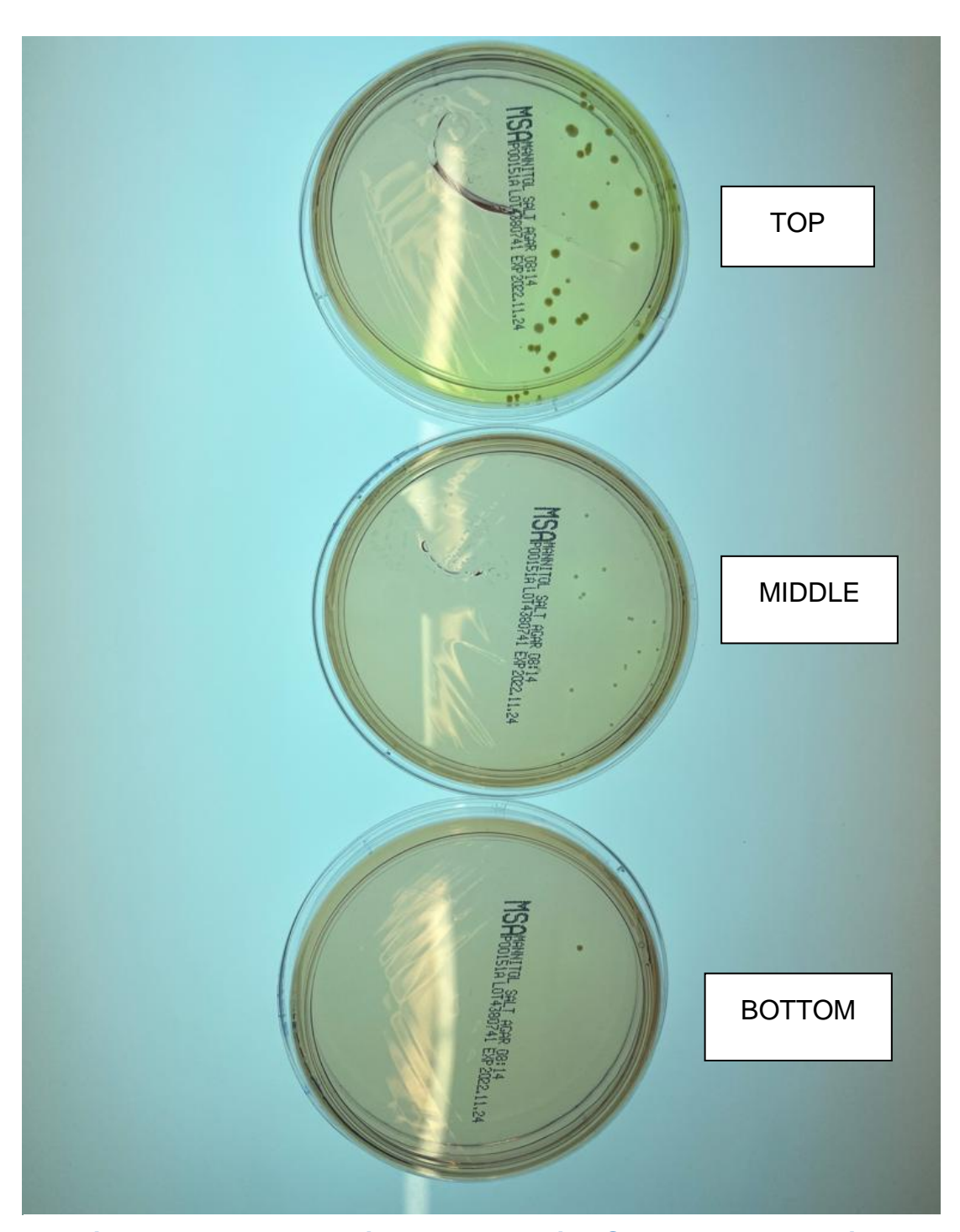


Figure 52. Image showing three Mannitol Salt agar plates which illustrate the difference in concentration of certain bacteria throughout the tube. In this case suspected *S. aureus* is in high concentration at the top of the tube and low concentration at the bottom of the tube.

In total, preliminary findings shows the following organisms present on endotracheal tubes: *Staphylococcus aureus* (3/5), *Streptococcus pneumoniae* (3/5), *Pseudomonas aeruginosa* (1/5), *Streptococcus agalactiae* (1/5) and *Candida glabrata* (1/5). From this, it appears gram-positive bacteria are the most common colonizers so far and that *S. aureus* and *S. pneumoniae* appear together. This is unsurprising as these are two of the most commonly known bacteria to cause bacterial pneumonia and have been shown to form stable biofilms *in-vitro*.¹¹⁴ However, these identifications are yet to be confirmed, so concrete conclusions cannot be made at such an early stage with such few samples.

5.3.2 PATIENT DATA

Below is a summary of the anonymised data collected for tubes 1-5.

Table 9. Table summarising the primary anonymised data collected from patients from tubes ET001-ET005.

#	Days	Diagnosis	Positive cultures	Suggested ID
	Intubated			
ET001	17.89	Drop in	Clostridium difficile	S. epidermis/P.
		GCS/seizures	(faecal)	aeruginosa
ET002	17.25	Hospital acquired	Candida albicans	S. aureus/ S.
		pneumonia	(urine)	pneumonia.
ET003	18.31	Dermatomyositis	Blastocystis hominis	S. aureus/ S.
			(faecal) / E. coli (urine)	pneumoniae.
ET004	5.02	Acute respiratory	BDG positive (fungal	S. aureus/ S.
		distress syndrome	disease)	pneumoniae
ET005	6.41	Respiratory	Staphylococcus	S. agalactiae/ C.
		arrest/COVID-19	haemolyticus (blood) /	glabrata
			Candida glabrata (urine)	

For ET001 it's possible the suggestion of P. aeruginosa could actually be C. difficile. C. difficile are gram-positive bacteria, however they can decolourise easily and appear gram-negative. They also present as bacilli and form large colonies (4-6 mm) grey and white irregular shaped raised colonies, which aligns with the descriptions from blood plates (full details of morphology analysis included in Appendix: 8.2). This highlights the need for accurate IDs to make any conclusive statements about the results in this clinical study.

However, it is for example promising to see overlaps such as in ET005 where Candida glabrata was found both from urine culture and on the tube as a result from the analysis performed in this study. So though not able to confirm identifications, it does provide an indication for some initial preliminary analyses.

For every single patient included in this study, antibiotics and/or antifungals were administered. In ET001 a total of 5 were given: erythromycin, fluconazole, gentamycin, meropenem and teicoplanin. In ET002 just ceftazidime was given. In ET003 meropenem and voriconazole were given. In ET004 meropenem, acyclovir and septrin were given. In ET005 clindamycin was given. Carbapenems such as meropenem (given to 3/5 patients) are used to treat serious nosocomial and mixed bacterial infections. 115 However, carbapenem-resistant P. aeruginosa (CRPA) is becoming increasingly prevalent worldwide. 116 In this study they found that carbapenemase producing CRPAs were more likely to have high-level meropenem resistance and were also associated therefore with increased mortality rates compared to their noncarbapenemase-producing counterparts (22% vs 12% respectively). This also varied globally, for example they found only 2% of CRPA isolates in the USA had carbapenemase, as much as 69% of CRPA isolates found in south and central America had carbapenemase. 116 However, it is important to note carbapenemase is not the only cause for carbapenem resistance in P. aeruginosa, and the low prevalence of these in America does not necessarily relate to less CRPAs but could highlight the difference in available antibiotics

in different regions, and hence resulting in different selective pressures on CRPAs in different regions.

5.3.3 SEM ANALYSIS OF BIOFILM

SEM analysis has been utilised for a long time regarding microbiologic analysis of biofilms, primarily for confirmation of bacterial species and observation of EPS structures formed by different biofilms. There has been an investigation into biofilms on endotracheal tubes in relation to VAP using this technique ⁹², where over a 7-month period, patients from the ICU who required mechanical ventilation for > 24 h were included in the study, and VAP status recorded. However, the sample ETT processing included scraping the biofilm from the inner surface of the ETT and subsequent homogenizing using vortexing, prior to chemical fixing ⁹².

Hence, as a result of this additional step, it is not known what features of the biofilm architecture were lost. Instead, this thesis details a simple preparation step where a section of the tube was cut off and fixed immediately after collection (within 24 hours of extubation). After drying, a section of the endotracheal tube was then cut for SEM imaging, so the original biofilm architecture should be preserved as if it were still inside the body including any mixed biofilms present. Below is an image of a sterile Portex tube analysed immediately after opening from packaging.

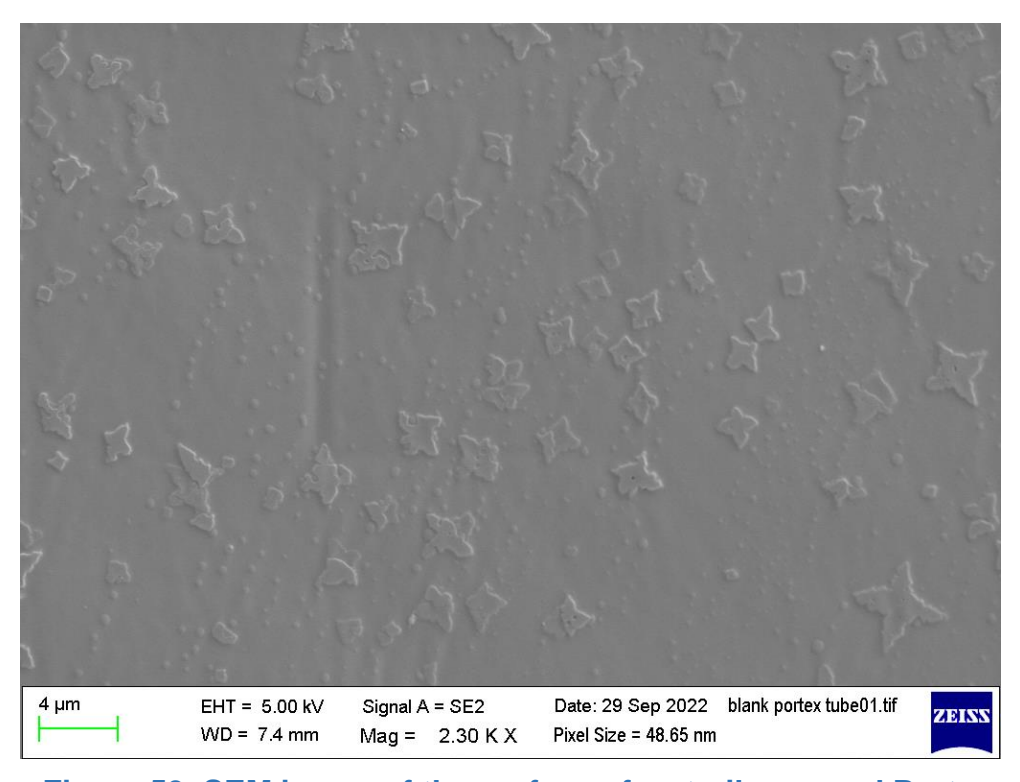


Figure 53. SEM image of the surface of a sterile unused Portex endotracheal tube (inner lumen).

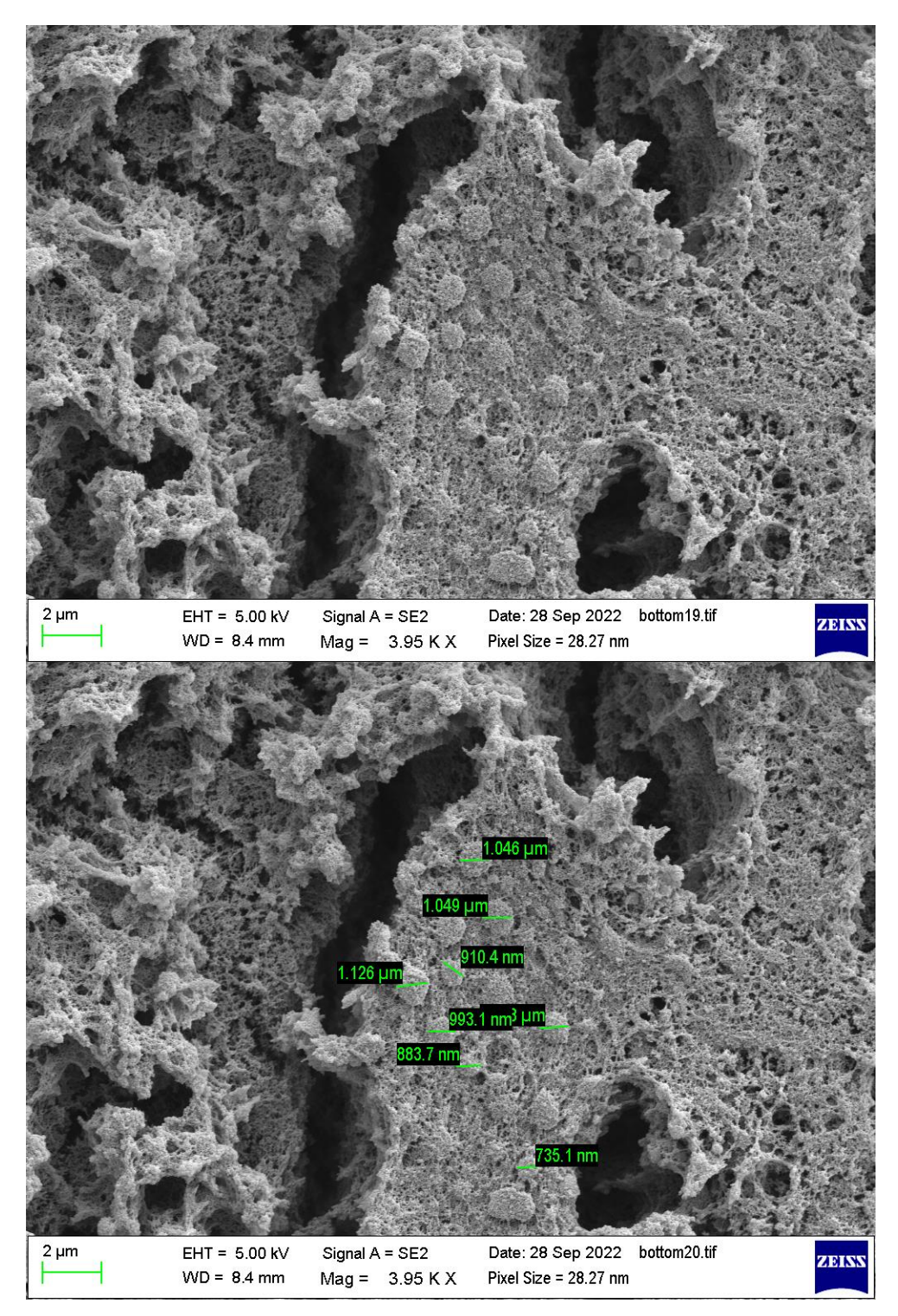


Figure 54. SEM images of ET001, suspected *S. epidermis* due to cocci shaped bacteria of the right size (0.5-1.5µm).

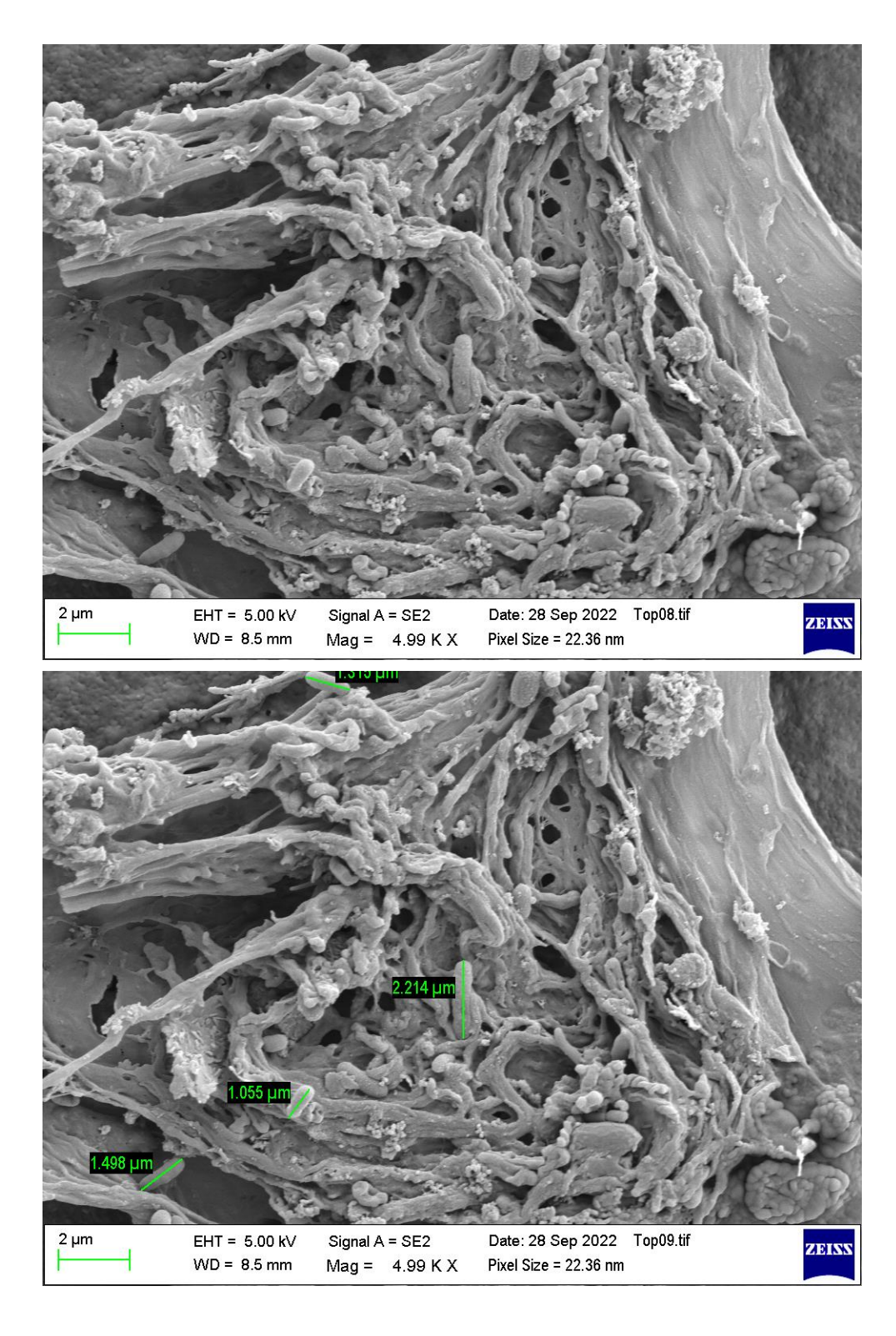


Figure 55. SEM images of ET001, suspected *P. aeruginosa* or *C. difficile*, due to rod-shaped bacteria of the right size for both (1-5 μ m).

ET002 – S. aureus and S. pneumoniae.

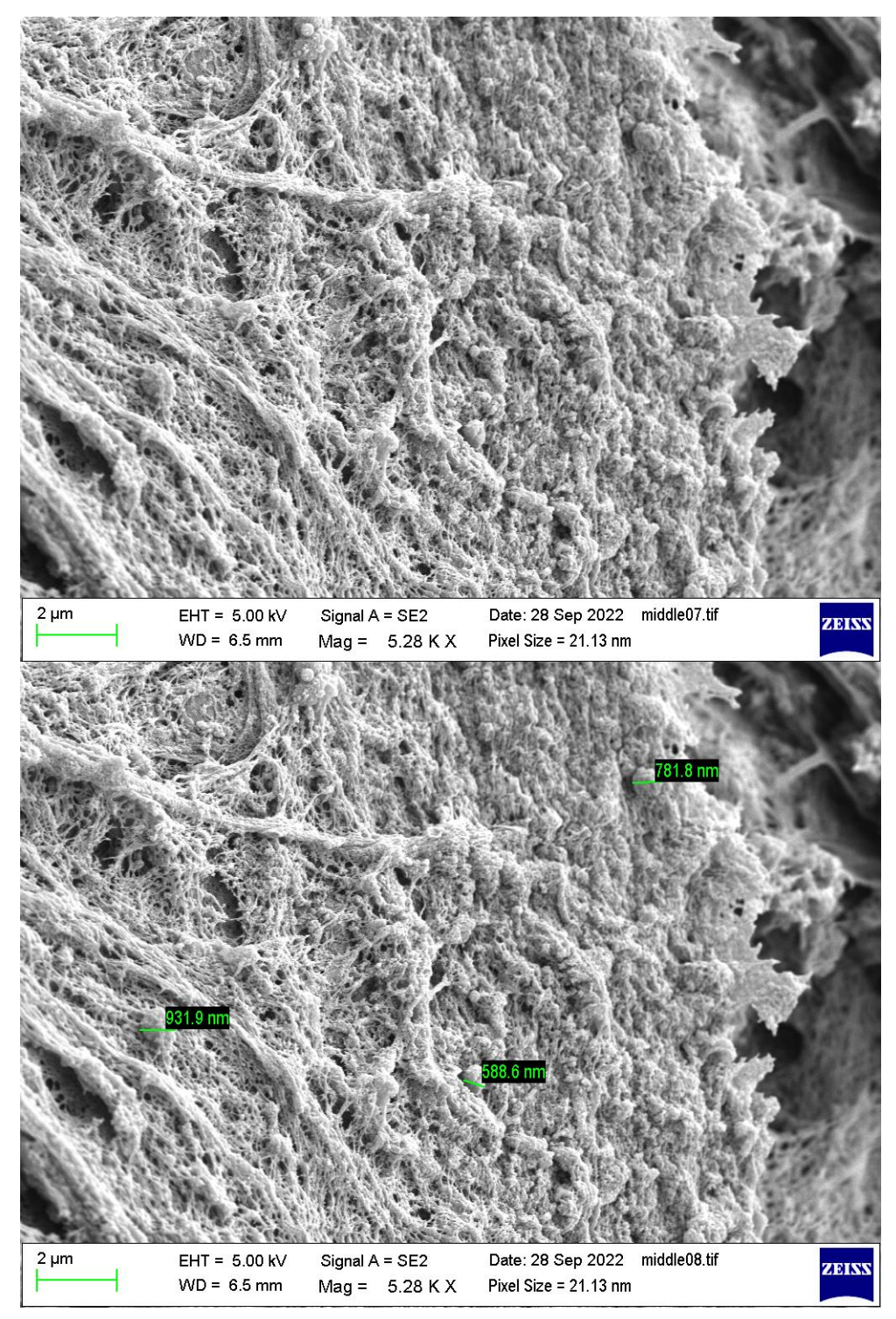


Figure 56. SEM images of ET002, either *S. aureus* and/or *S. pneumoniae* due to both having cocci shaped bacteria of the right size (0.5-1.25µm).

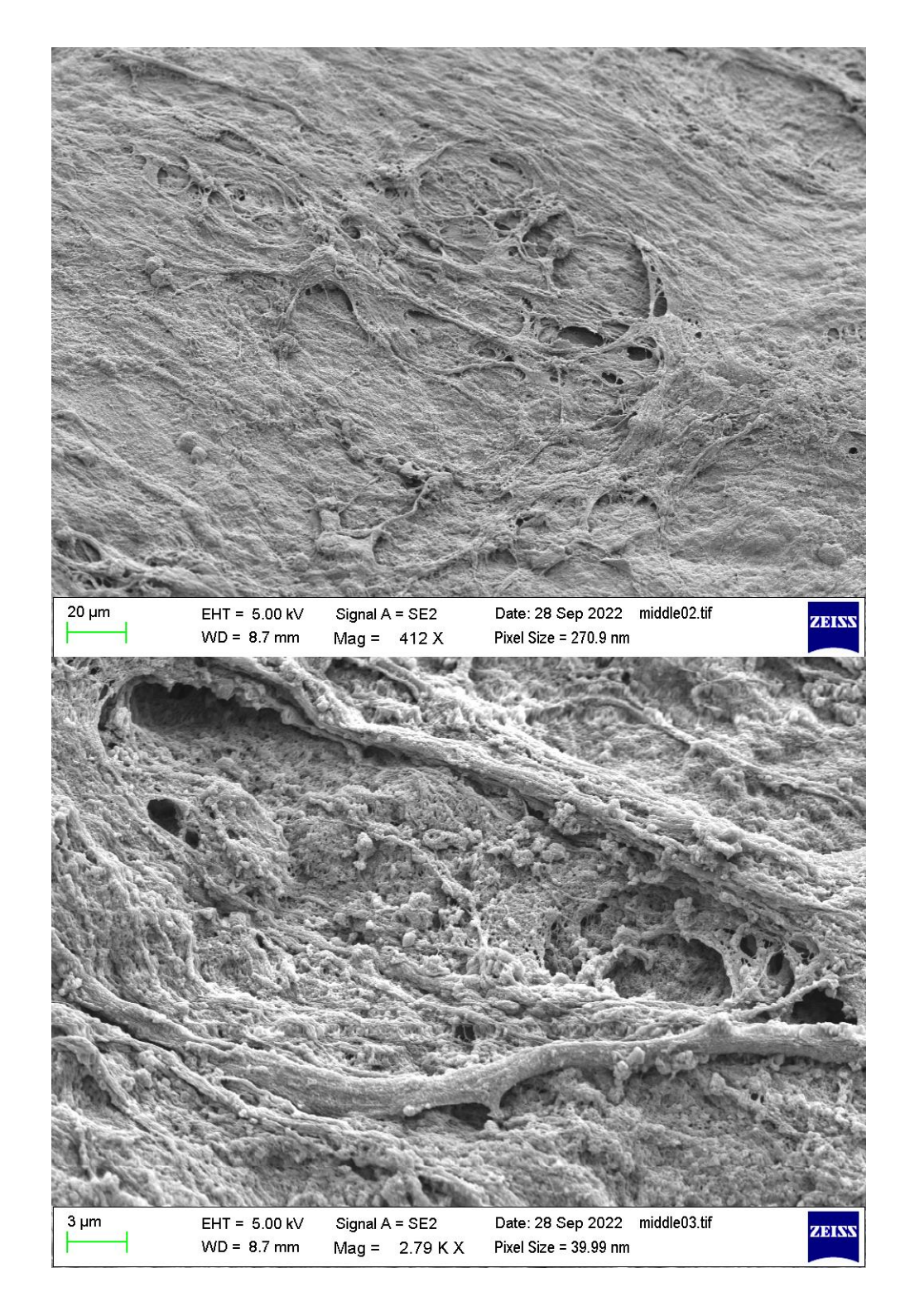


Figure 57. SEM images of ET002 at lower magnifications to see overarching biofilm extracellular polymeric substance architecture.

ET003 – S. aureus and S. pneumoniae.

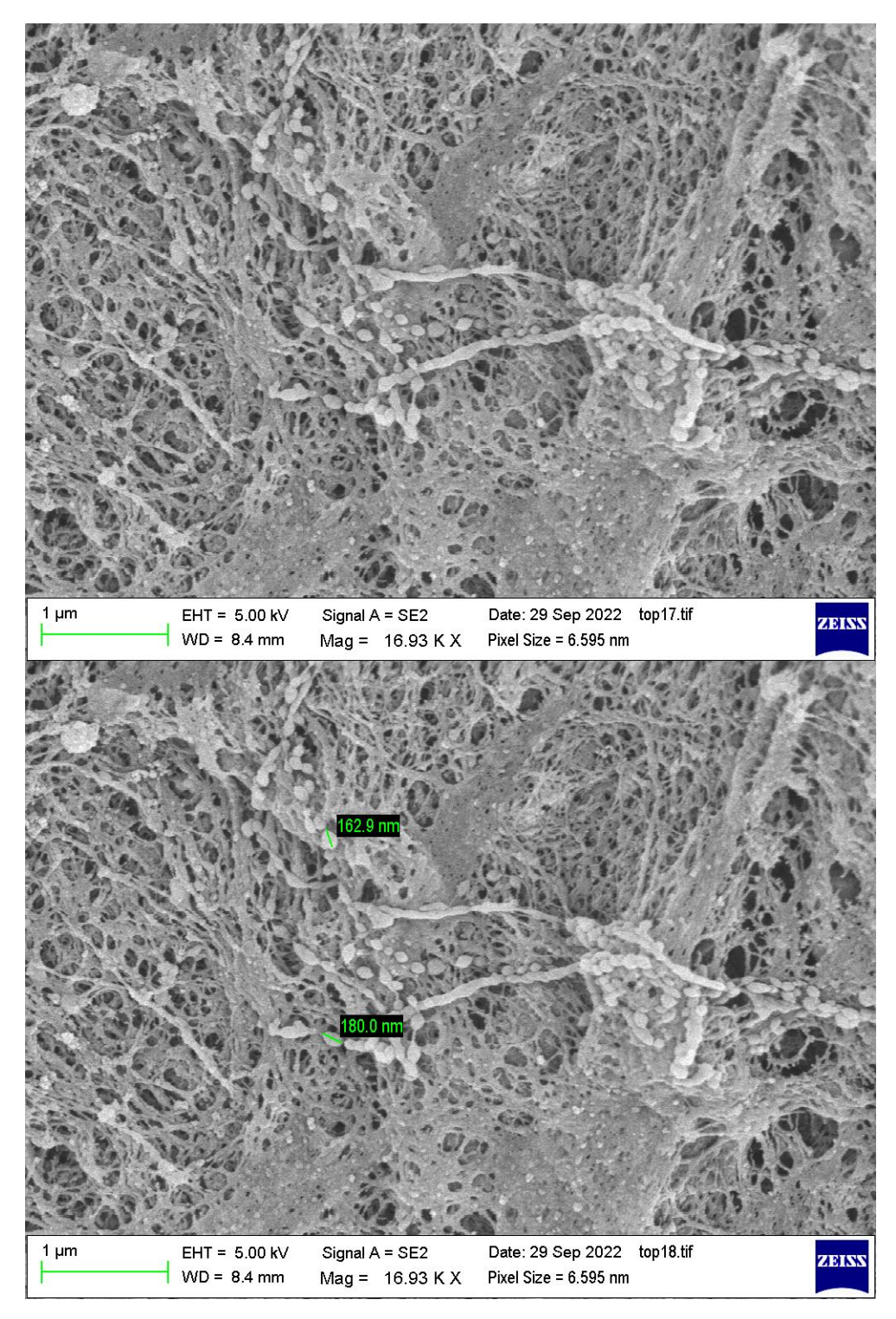


Figure 58. SEM image of ET003, suspected *S. pneumoniae* due to the smaller cocci shaped bacteria in singular chains.

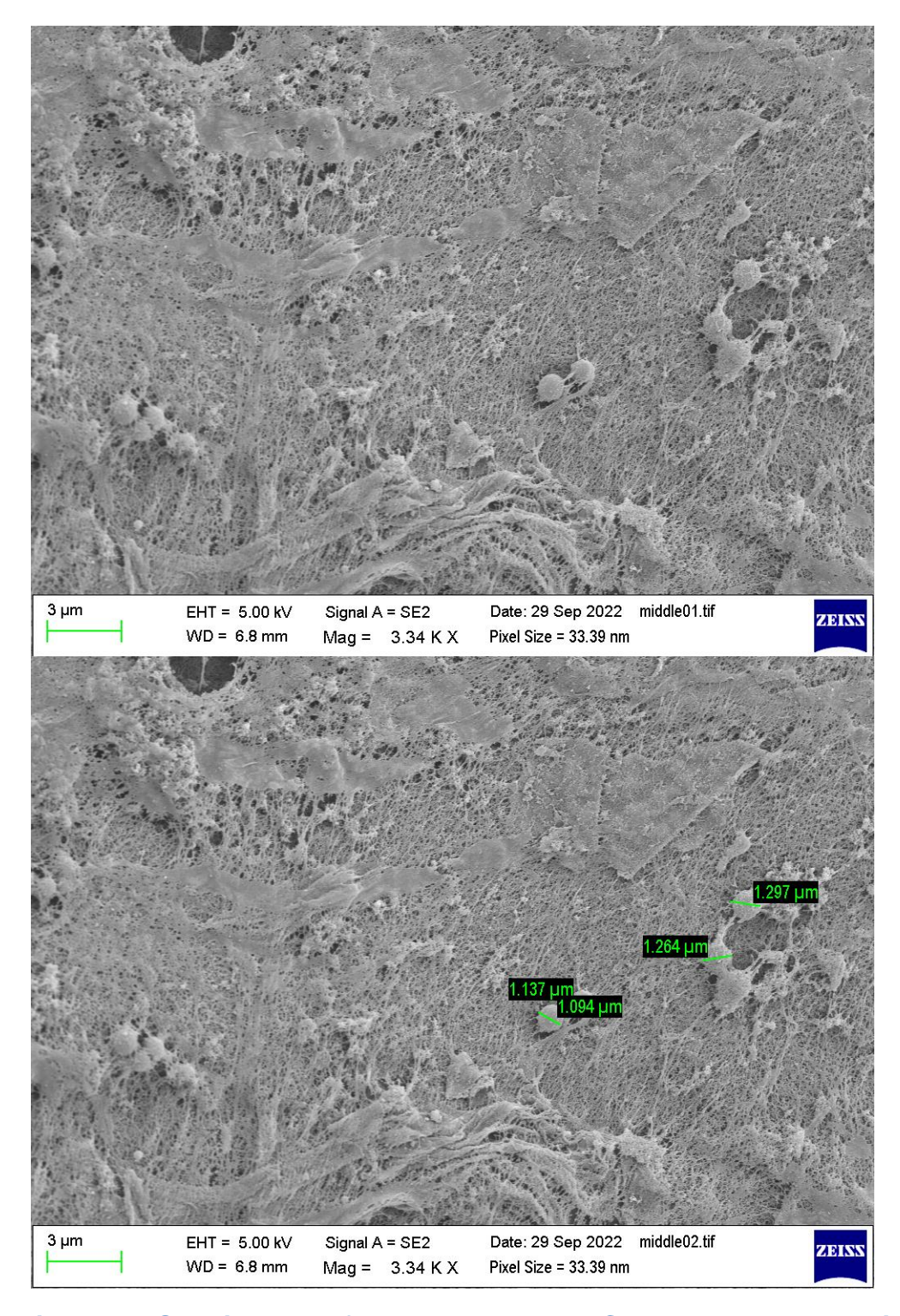


Figure 59. SEM images of ET003, suspected *S. aureus* due to cocci shaped bacteria of the right size slightly larger than the above (0.5- $1.5\mu m$).

ET004 – S. pneumoniae and S. aureus.

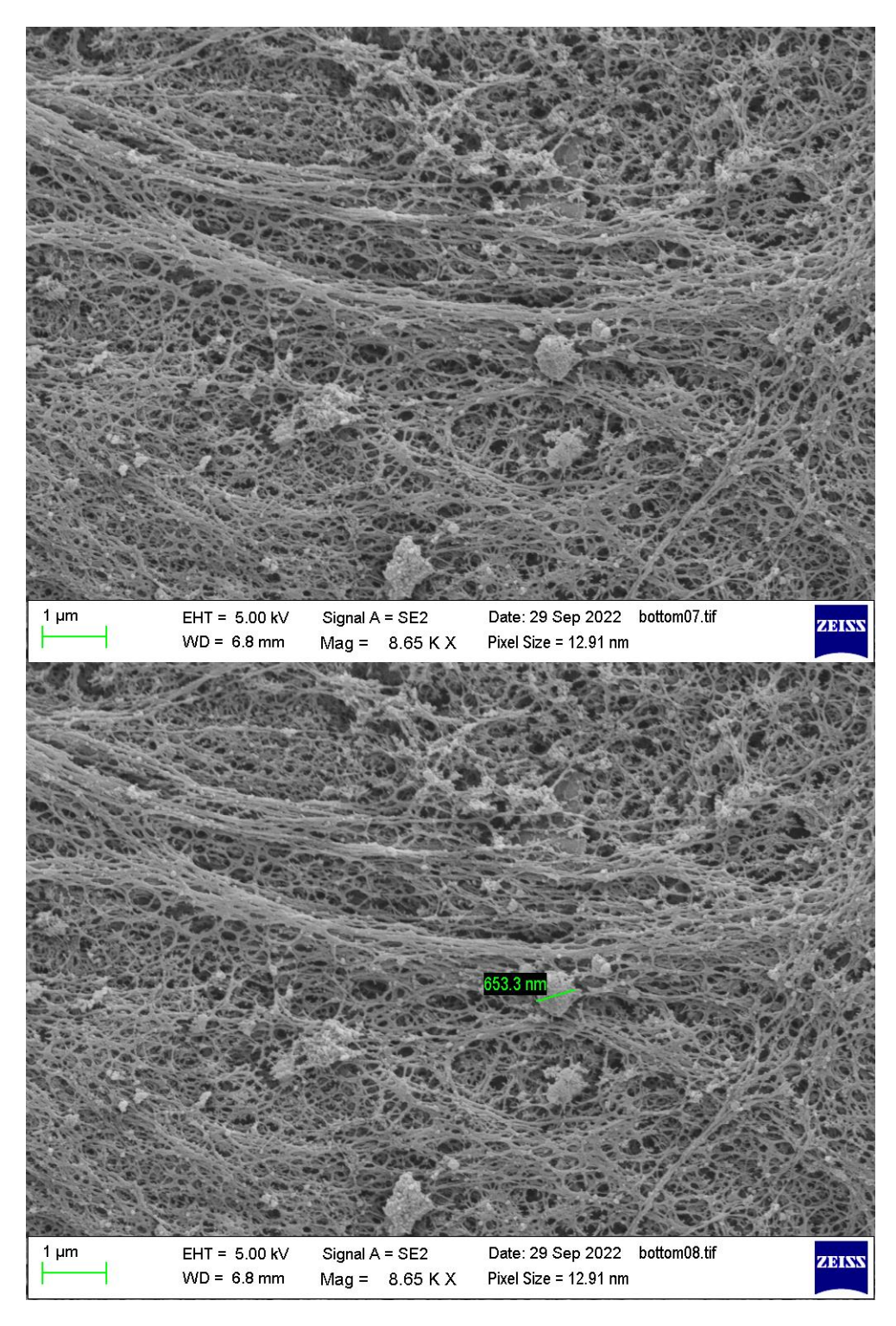


Figure 60. SEM image of ET004, either *S. aureus* and/or *S. pneumoniae* due to both having cocci shaped bacteria of the right size (0.5-1.25µm).

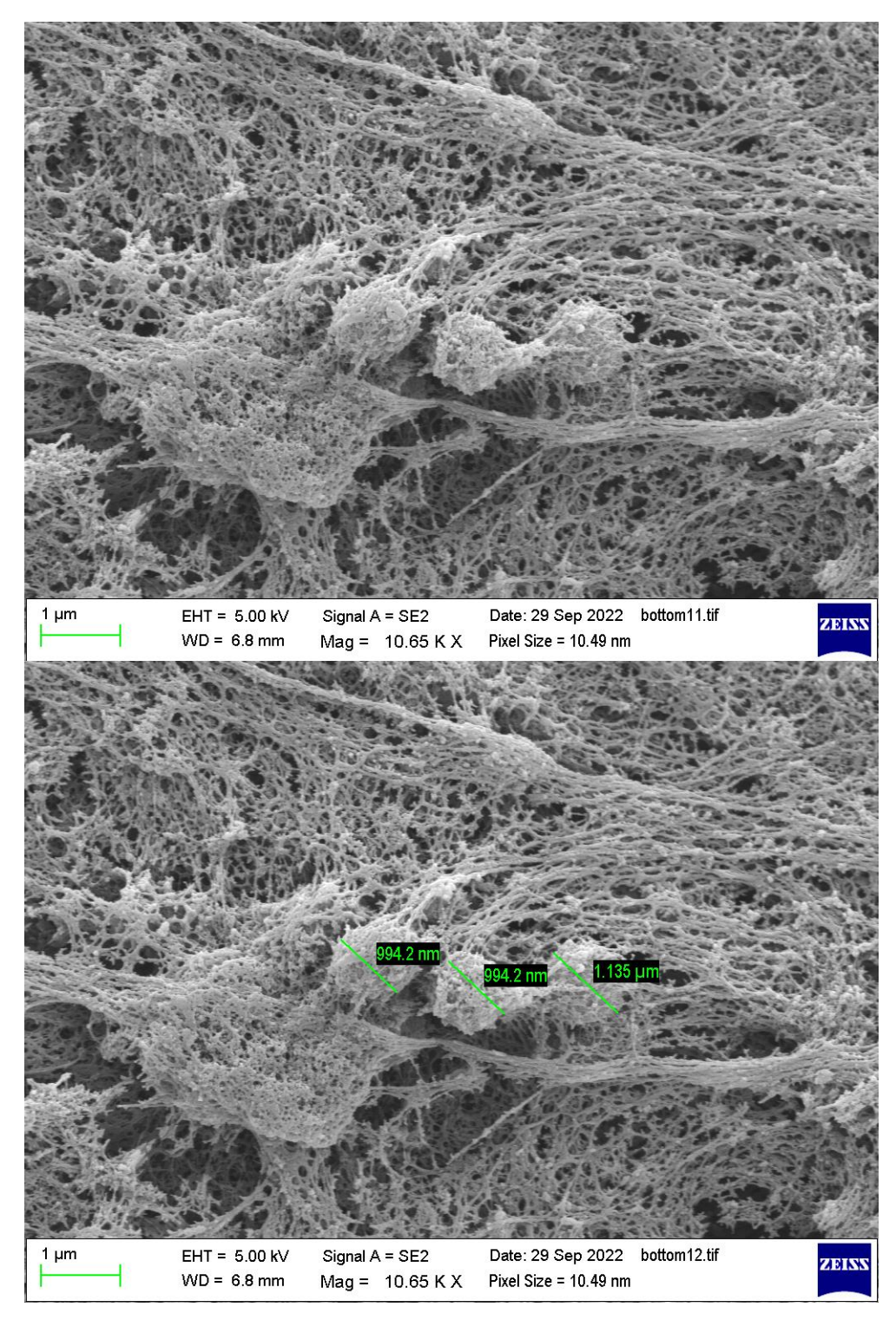


Figure 61. SEM image of ET004, either *S. aureus* and/or *S. pneumoniae* due to both having cocci shaped bacteria of the right size (0.5-1.25µm).

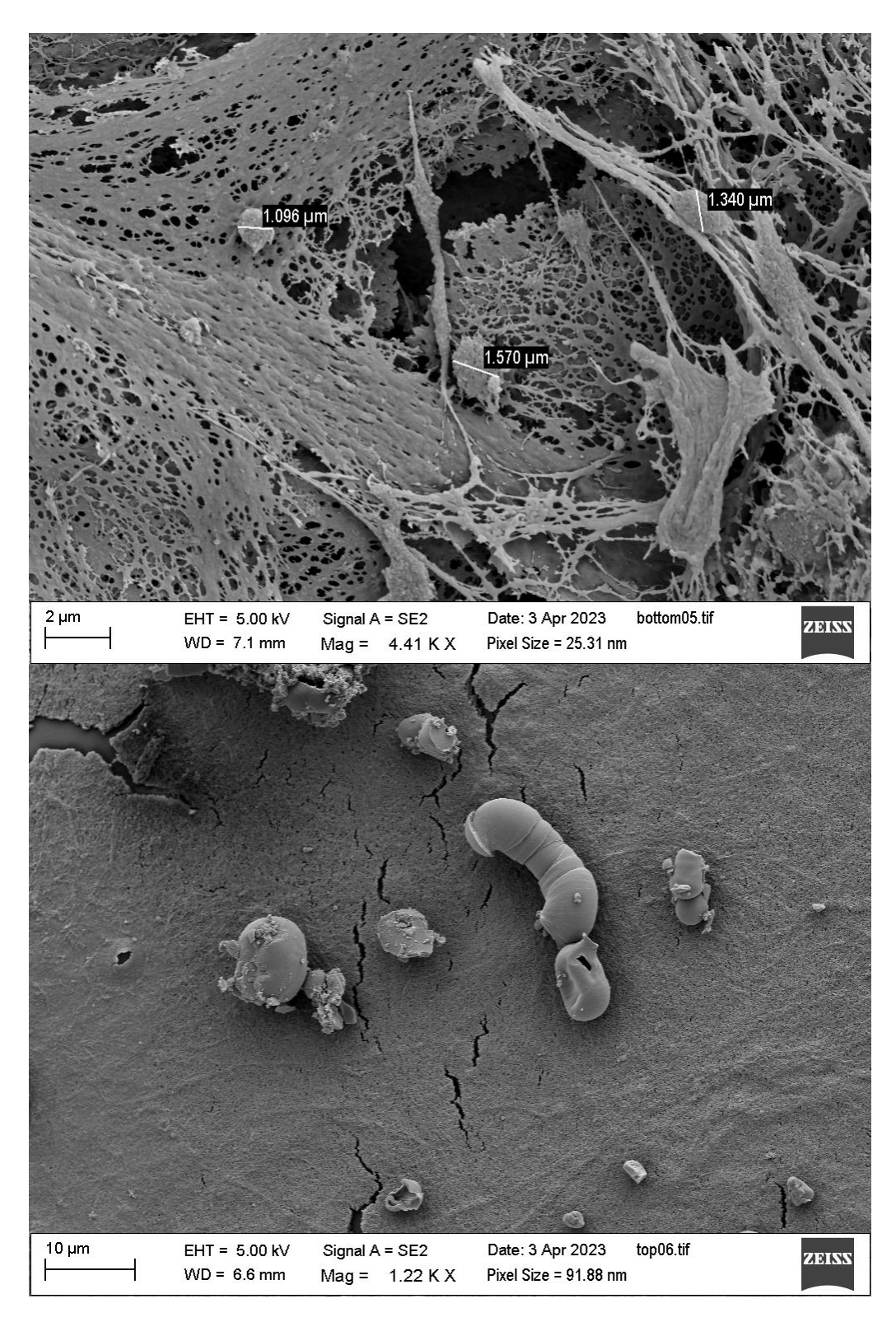


Figure 62. SEM image of ET005. Top image suspected *C. glabrata* due to the singular spherical shapes. Bottom image suspected *S. agalactiae* due to appearance of a chain, though size is slightly too large.

Also interesting from these SEM images is the overarching polymeric matrix structures surrounding the bacteria. Some appear more spider-web like (such as ET002/3/4) and some appear thicker and more like a blanket covering the surface (ET001). On the full analysis of all tubes with confirmed IDs, these observations can be further elucidated to form more conclusions about whether different types of bacteria tend to produce different types of biofilm structures, and how this information could potentially be used to target specific biofilm types in future antimicrobial materials development.

5.3.4 NMR ANALYSIS OF BIOFILM

NMR analysis of biofilm taken directly from a patient ETT is understood to be a completely novel idea. Based on previous studies the solvents water and NaOH were chosen as the solvents likely to recover substantial portions of the biofilm. The method used was kept as simple as possible to not alter the biofilm from its original state, whilst trying to solubilise as much of the biofilm as possible. It is noted that in some cases it is likely that not all the biofilm was solubilised and therefore recovered, so this is not a full analysis of the biofilms but rather hopefully an indication as to whether NMR could be used as a diagnostic technique for bacterial biofilms. This could be significant, as currently, though MALDI-TOF is used in hospitals to ID bacteria and is accurate and fast, but the preparation still requires culturing bacteria on plates for >48h and then preparing for MALDI-TOF analysis. The proposed NMR technique here in this case uses a small cut section of the endotracheal tube (~ 1cm off the end) which could be transferred to scraping off a section of biofilm in clinical practice, solubilising in both water and NaOH in two parts,

freeze drying and then re-dissolving in deuterated water (D2O) for NMR analysis. The freeze-drying step currently involves leaving the solution in the -80 °C freezer overnight before drying under vacuum, however this step did not have a predetermined length and no optimisation of this step was performed. However, with the right equipment and optimisation this whole procedure could potentially be completed in > 24h, faster than MALDI-TOF including preparation steps and any potential delays as a result of contamination issues when plating.

Without the confirmed identifications it is hard to make any concrete conclusions about the NMR data. However, it is hoped this preliminary analysis will provide a sense of proof of concept that using this method bacterial biofilms can be analysed by NMR to form clearly resolved peaks, which was unexpected considering the complexity of biofilms. However, sediment has not been visually noted in the tube after the final centrifugation step (post-NaOH), suggesting that for the most biofilms seen in this study, water followed by NaOH solubilises the majority of biofilms. If this were to be repeated a third step could be investigated to ensure the full picture of biofilms growing on endotracheal tubes was being captured in the NMR analysis. Multiplet analysis was completed using MNova analysis tools.

First, a blank of the D2O used for all the analysis was run, as well as sterile tubing exposed to both water and NaOH, were also run.

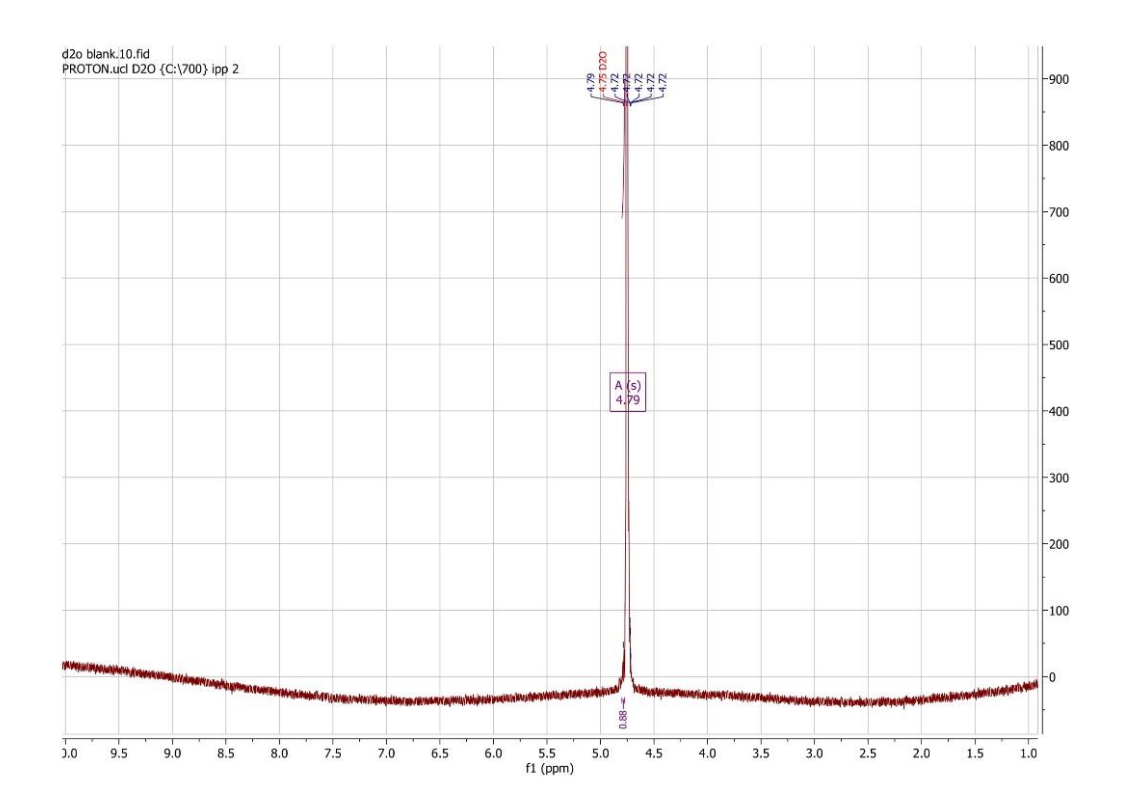


Figure 63. NMR spectra of D2O used to dissolve the powdered biofilm after drying. 1H NMR (700 MHz, D₂O) δ 4.79 (s, 1H).

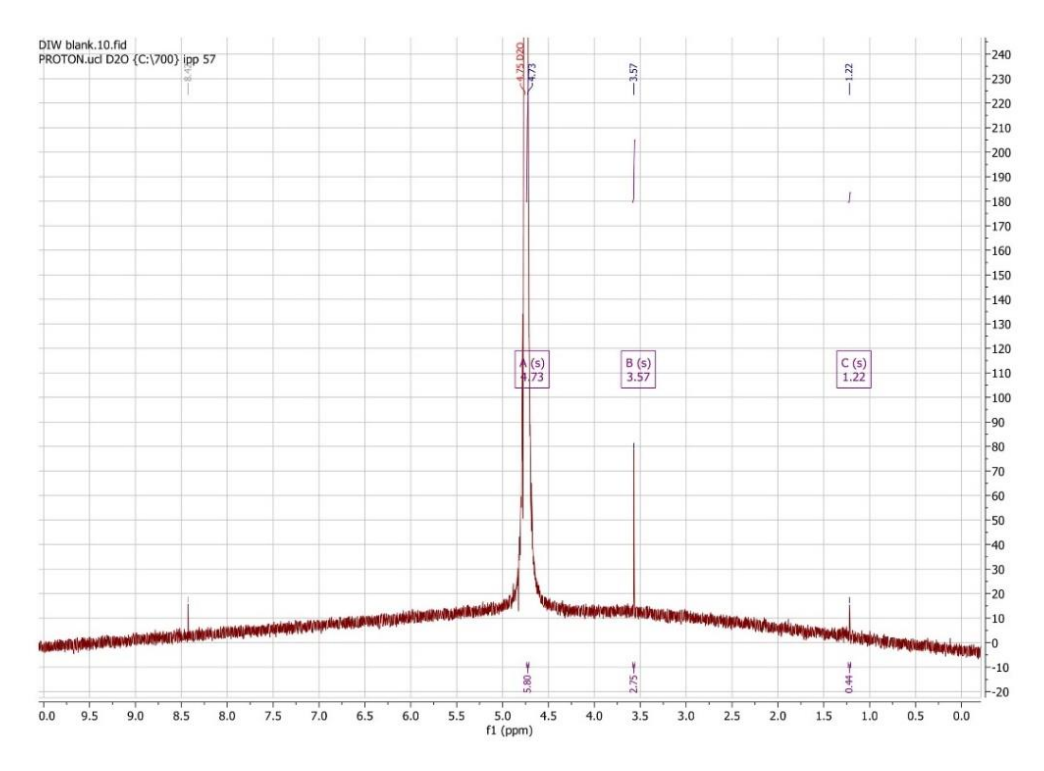


Figure 64. NMR spectra of clean tube material exposed to the pure water used in step 1 of biofilm processing. ^{1}H NMR (700 MHz, $D_{2}O$) δ 4.73 (s, 6H), 3.57 (s, 3H), 1.22 (s, 0H).

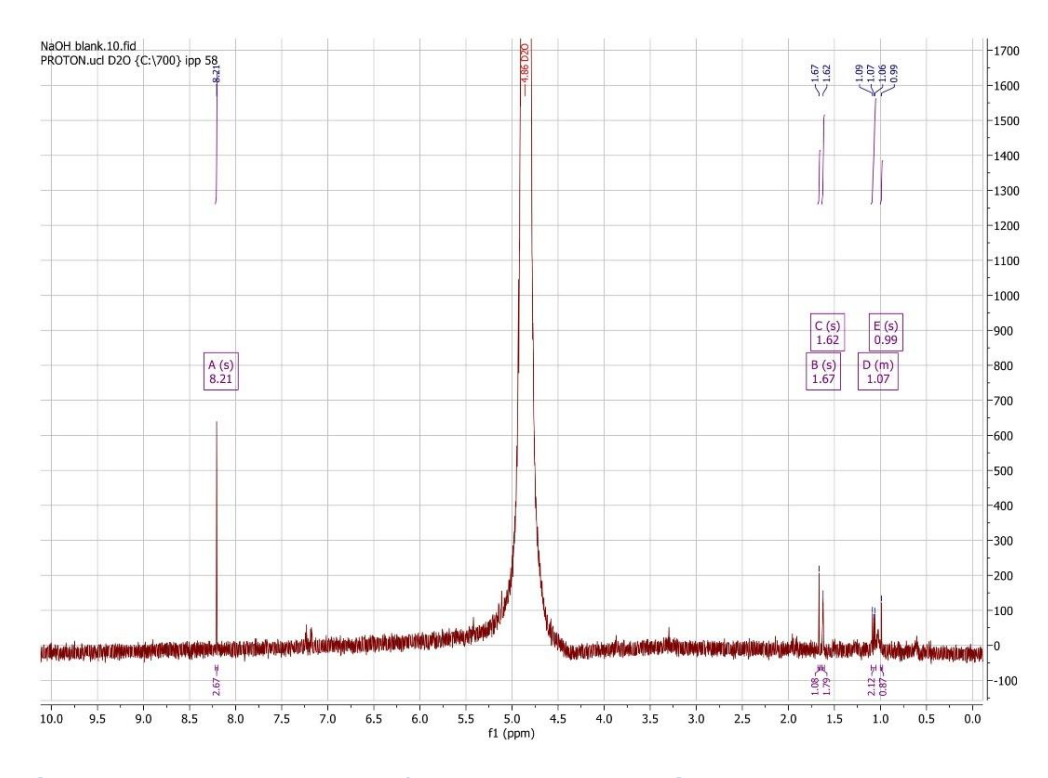


Figure 65. NMR spectra of clean tube material exposed to the NaOH used in step 2 of biofilm processing. 1H NMR (700 MHz, D₂O) δ 8.21 (s, 3H), 1.67 (s, 1H), 1.62 (s, 2H), 1.10 – 1.05 (m, 2H), 0.99 (s, 1H).

The single peak at 4.79 ppm for D2O is as expected. For the peaks seen at ~4 ppm suggests a chlorinated compound which ties in with the endotracheal tube being polyvinylchloride (PVC) based, and ~1 ppm for those hydrogens on the alkyl chain. These are suggested knowing what the tube is made from, however there could be many other possibilities. The one sharp peak at 8.2 ppm suggests an aromatic or amide compound, potentially caused by the NaOH or contamination.

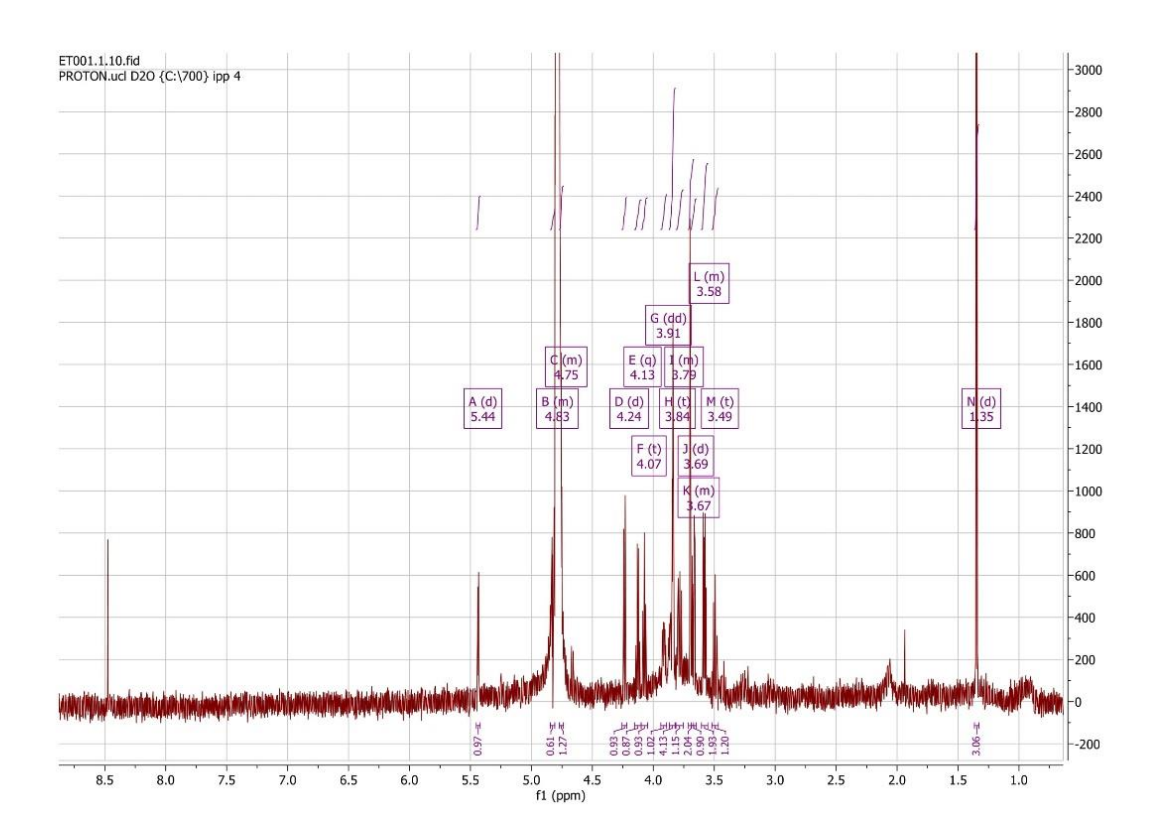


Figure 66. NMR spectra of the water-soluble parts of ET001.

¹H NMR (700 MHz, D₂O) δ 5.44 (d, J = 3.9 Hz, 1H), 4.84 – 4.81 (m, 1H), 4.77 – 4.74 (m, 1H), 4.24 (d, J = 8.8 Hz, 1H), 4.13 (q, J = 6.9 Hz, 1H), 4.07 (t, J = 8.6 Hz, 1H), 3.91 (dd, J = 9.3, 5.4 Hz, 1H), 3.84 (t, J = 3.5 Hz, 4H), 3.81 – 3.76 (m, 1H), 3.69 (d, J = 12.0 Hz, 2H), 3.69 – 3.65 (m, 1H), 3.61 – 3.55 (m, 2H), 3.49 (t, J = 9.6 Hz, 1H), 1.35 (d, J = 7.0 Hz, 3H).

A cluster of peaks around 5.5 - 3.5 ppm are likely to be from alcohols whereas the peaks 3.5 – 1.3 ppm are likely to be from amino acids. Proline for example appears to be the preferred amino acid used in the metabolic pathway for Clostridial species, recently elucidated by Bouillaut et al.¹¹⁸ From the human metabolome database (HMDB) the ¹H NMR spectrum for proline shows multiplets from 4.12 ppm to 1.99 ppm. Regarding *S. epidermis* a commonly

noted metabolite is acetoin, ¹¹⁹ which has multiplets at 4.4 ppm, 2.2 ppm and 1.36 ppm (HMDB). These two metabolites associated with *C. difficile* and *S. epidermis* appear to fit within the range of multiplets seen in this spectrum.

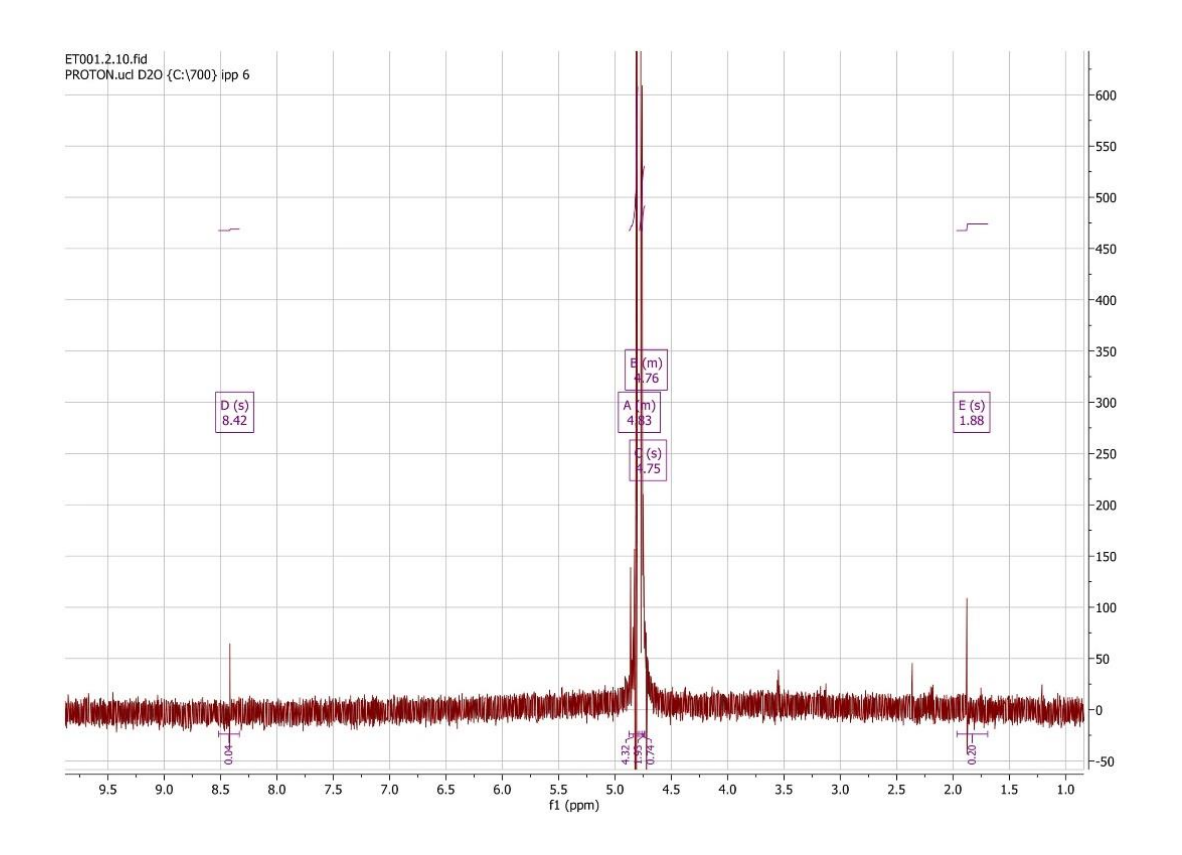


Figure 67. NMR spectra of the NaOH-soluble parts of ET001.

1H NMR (700 MHz, D2O) δ 8.42 (s, 0H), 4.87 - 4.80 (m, 4H), 4.78 - 4.74 (m, 2H), 4.75 (s, 1H), 1.88 (s, 0H).

As peaks around 1 ppm and 8 ppm were seen in the NaOH blank performed (figure 61) it's assumed the biofilm in this case was primarily water soluble and captured in the first steps' resulting NMR spectrum.

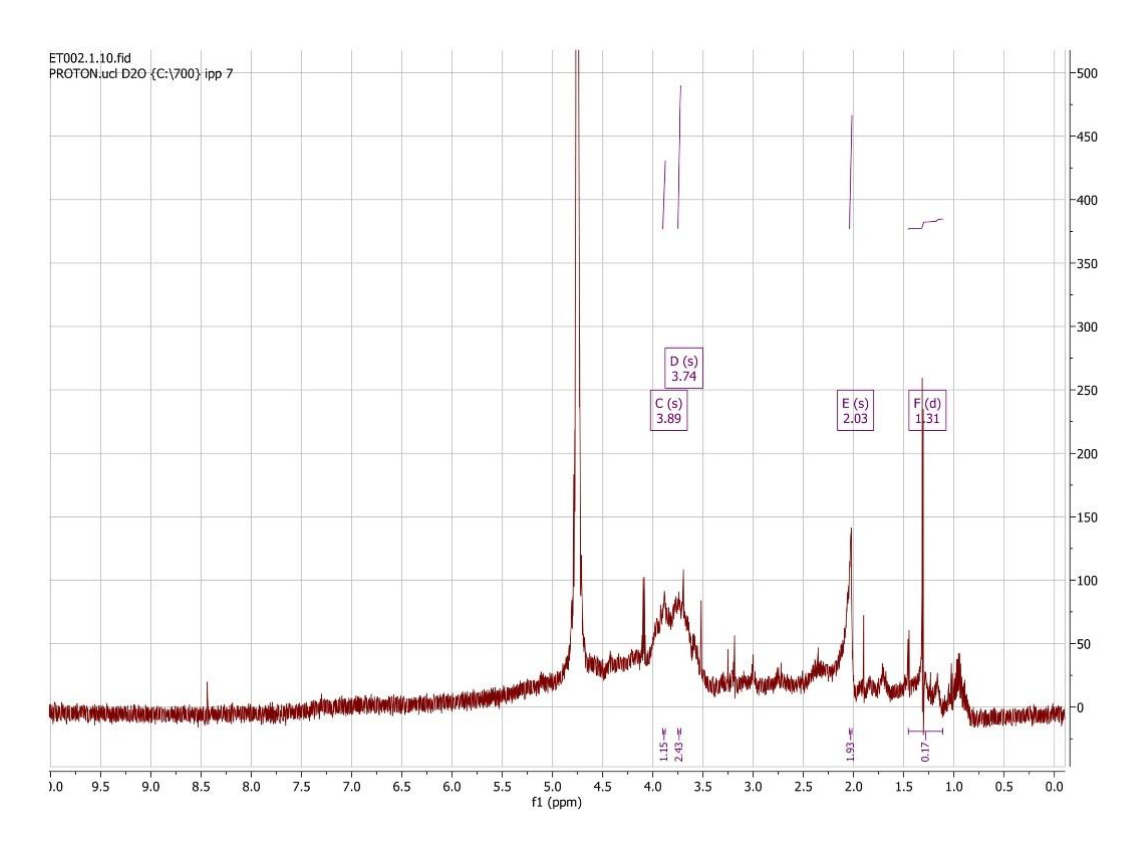


Figure 68. NMR spectra of the water-soluble parts of ET002.

1H NMR (700 MHz, D2O) δ 4.75 (s, 3H), 3.89 (s, 1H), 3.74 (s, 2H), 2.03 (s, 2H), 1.31 (d, J = 6.8 Hz, 0H).

There are clusters of peaks from 4.5 - 1.3 ppm. Peaks around 4.5 – 3.5 ppm are broad which suggests a hydroxyl group and again 3.5 – 1.3 ppm amino acids. For ET002/03/04 the suggested IDs are all both *S. aureus* and *S. pneumoniae*. The metabolites that were found to most significantly differentiate *S. aureus* from other bacteria are isobutyrate, isovalerate and succinate. 120 Isobutyrate shows a doublet at 1.18 ppm, multiplet at 2.6 ppm and a single peak at 3.6 ppm. This doesn't appear to match the spectrum above. Isovalerate similarly has multiplets starting at 0.9 ppm so doesn't appear to match the spectrum above. Succinates conjugate acid (succinic acid) is a

dicarboxylic acid and has one large multiplet around 2.4 ppm according to the HMDB. Peaks in this spectrum from \sim 4 – 2 ppm appear broad, which could be as a result of the effects of hydroxyl groups on alcohols and carboxylic acids.

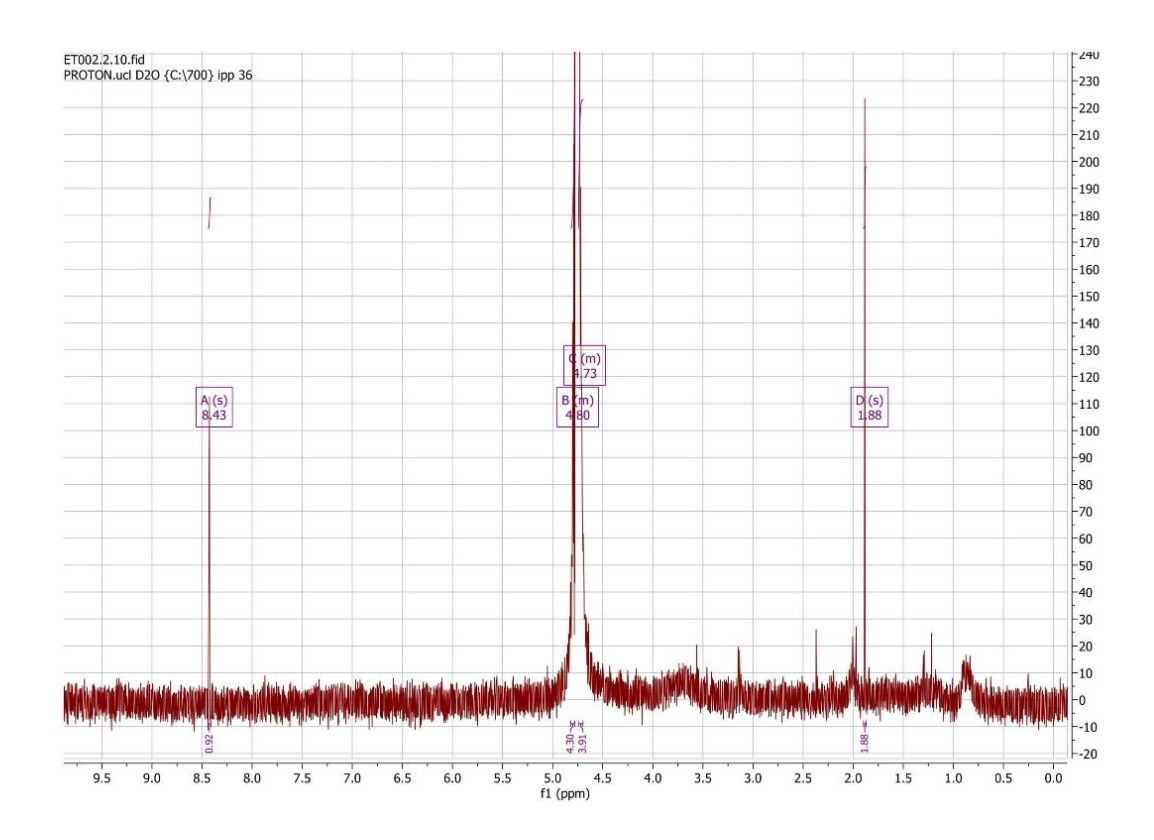


Figure 69. NMR spectra of the NaOH-soluble parts of ET002.

1H NMR (700 MHz, D2O) δ 8.43 (s, 1H), 4.82 – 4.78 (m, 4H), 4.74 – 4.70 (m, 4H), 1.88 (s, 2H).

As peaks around 1 ppm and 8 ppm were seen in the NaOH blank performed (figure 61) it's assumed the biofilm in this case was primarily water soluble and captured in the first steps' resulting NMR spectrum.

ET003 – S. aureus and S. pneumoniae.

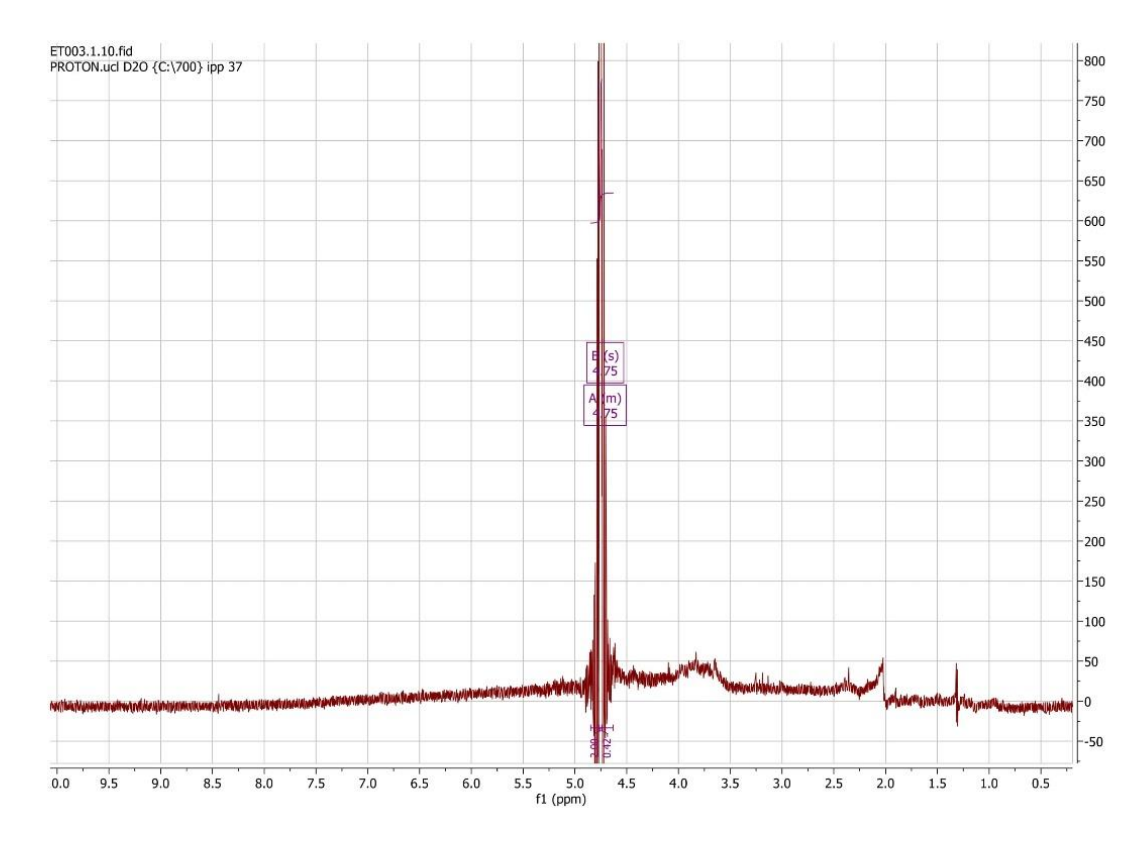


Figure 70. NMR spectra of the water-soluble parts of ET003.

1H NMR (700 MHz, D2O) δ 4.75 (s, 1H).

Alternatively, to ET001/2, ET003 did not pick up any significant peaks in the water step. This does might mean the suggested IDs are not accurate, as ET002 and ET003 were suggested to both have *S. aureus* and *S. pneumoniae* present and therefore expecting similar peaks. However, UCH found ET002 to have *C. albicans* and ET003 to have *Blastocystis hominis* and *E. coli*. So ET002 may show fungus, and ET003 a parasite and gram-negative bacteria. Putting the suggested IDs to one side and focusing just on the cultures UCH

found, this could suggest gram positive bacteria and fungus tend to be water soluble whereas gram negative bacteria and parasites are non-water soluble.

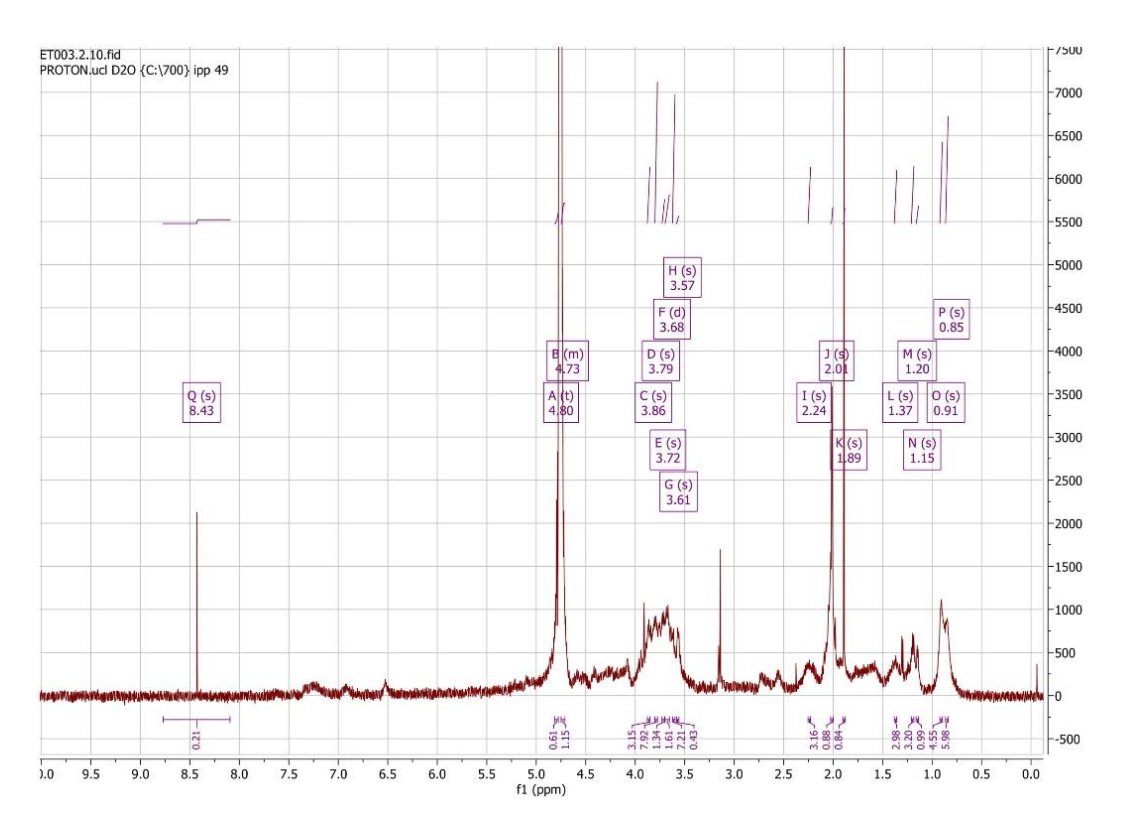


Figure 71. NMR spectra of the NaOH-soluble parts of ET003.

1H NMR (700 MHz, D2O) δ 8.43 (s, 0H), 4.80 (t, J = 4.5 Hz, 1H), 4.75 – 4.71 (m, 1H), 3.86 (s, 3H), 3.79 (s, 8H), 3.72 (s, 1H), 3.68 (d, J = 13.1 Hz, 2H), 3.61 (s, 7H), 3.57 (s, 0H), 2.24 (s, 3H), 2.01 (s, 1H), 1.89 (s, 1H), 1.37 (s, 3H), 1.20 (s, 3H), 1.15 (s, 1H), 0.91 (s, 5H), 0.85 (s, 6H).

The metabolites found in the highest concentration for *B. hominis* are arabinitol and formate.¹²¹ From the HMDB, arabinitol has multiplets from ~3.95 – 3.55 ppm which is in keeping with the large cluster of peaks seen here between the same values. Formate has a single peak at 8.44 ppm, but due to the presence of a single peak in this region in the blank runs, formate is unlikely to be the cause of this peak in this instance. Interestingly *B. hominis* has also been found

to boost the growth of E. coli, ¹²² which was also found by UCH cultures of this patient. Urine samples which have been processed for NMR analysis in a study to determine biomarkers for UTI diagnosis from *E. coli* found that acetate and trimethylamine were the optimal biomarkers for their analysis. ¹²³ This may be different for VAP diagnosis, however using this gives an indication of metabolites of *E. coli* that can be elucidated from NMR. Acetate according to the HMDB has a quartet ~4.1 ppm, a singlet at 2 ppm and a triplet at ~1.2 ppm, and trimethylamine also has a singlet peak at ~2 ppm. This spectrum shows a cluster of broad multiplet ats ~3.75 ppm, ~2 ppm and ~0.8 ppm, though there is some overlap this is also within the range for amino acids which are also likely to be present, therefore once confirmed IDs have been achieved spectrum like this will be able to be further examined with more certainty.

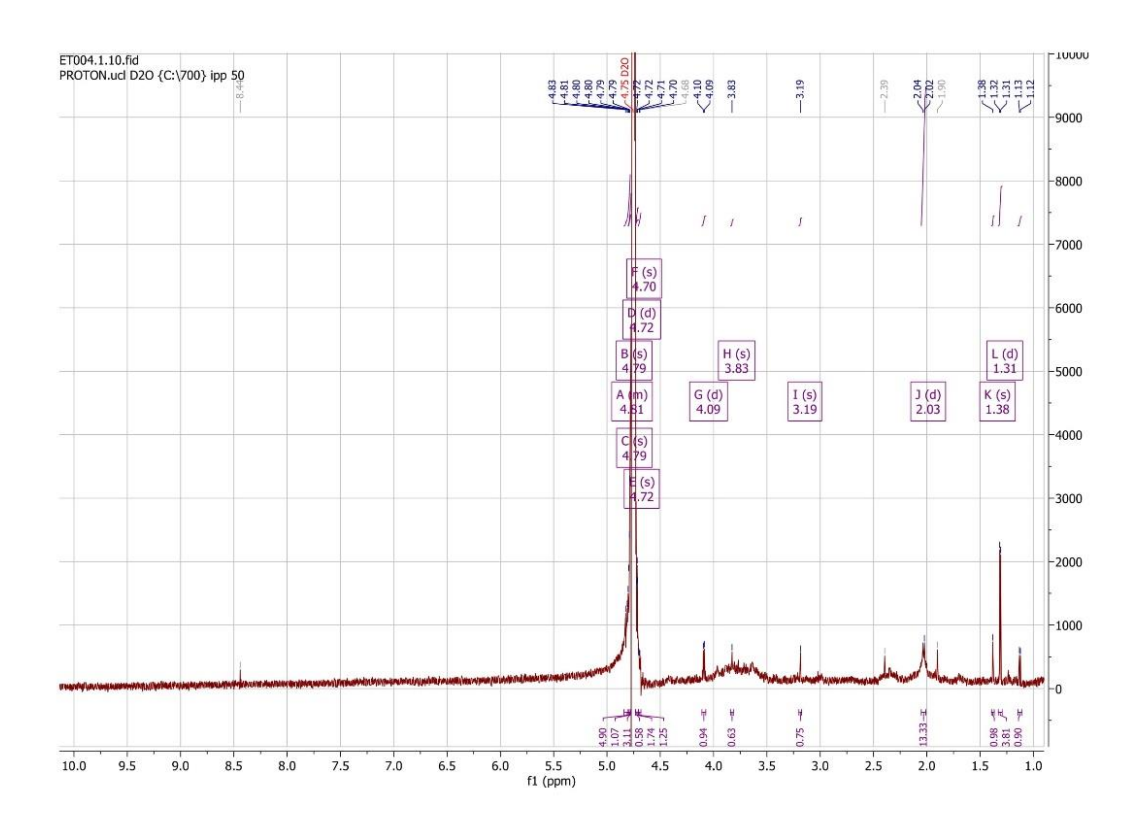


Figure 72. NMR spectra of the water-soluble parts of ET004.

1H NMR (700 MHz, D2O) δ 4.84 - 4.78 (m, 5H), 4.79 (s, 1H), 4.79 (s, 3H), 4.72 (d, J = 3.9 Hz, 1H), 4.72 (s, 2H), 4.70 (s, 1H), 4.09 (d, J = 6.9 Hz, 1H), 3.83 (s, 1H), 3.19 (s, 1H), 2.03 (d, J = 11.5 Hz, 13H), 1.38 (s, 1H), 1.31 (d, J = 6.9 Hz, 4H), 1.13 (d, J = 6.4 Hz, 1H).

Continuing with the pattern observed above and potential theory that gram positive bacteria and fungus are water-soluble, and Gram-negative bacteria and parasites are not water-soluble (a large assumption considering the current sample size), UCH found a 'fungal disease' from a β -d-Glucan test and my own morphology analysis from cultures gave a suggested ID of *S. aureus* and *S. pneumoniae*. Additionally, nothing grew on MacConkey from swabs of the endotracheal tube, which suggests fungus and gram-positive bacteria only

are present. However, in this case, a number of peaks are seen for both the water soluble and not water-soluble parts in these NMR spectra. Therefore, this contradicts the earlier theory or alternatively there is a gram-negative bacteria or parasite that has been missed by my analysis. Again, once IDs are confirmed, more will be known with certainty about the types of organisms growing on these endotracheal tubes, however there is no guarantee that organisms will still have been missed due to the different growth requirements for different organisms. Blood, Mannitol Salt and MacConkey were chosen to cover as many organisms as possible but is not completely exhaustive.

In this spectrum, peaks cluster around ~3.8 ppm, ~2 ppm, and ~1.3 ppm. Due to the lack of certainty about fungus type from the UCH culture nor certainty regarding isolates cultured from the endotracheal tube, it is hard to make any meaningful comments about this spectrum, other than the peaks cluster in the region likely to be amino acids and therefore metabolites of the fungus and bacteria present.

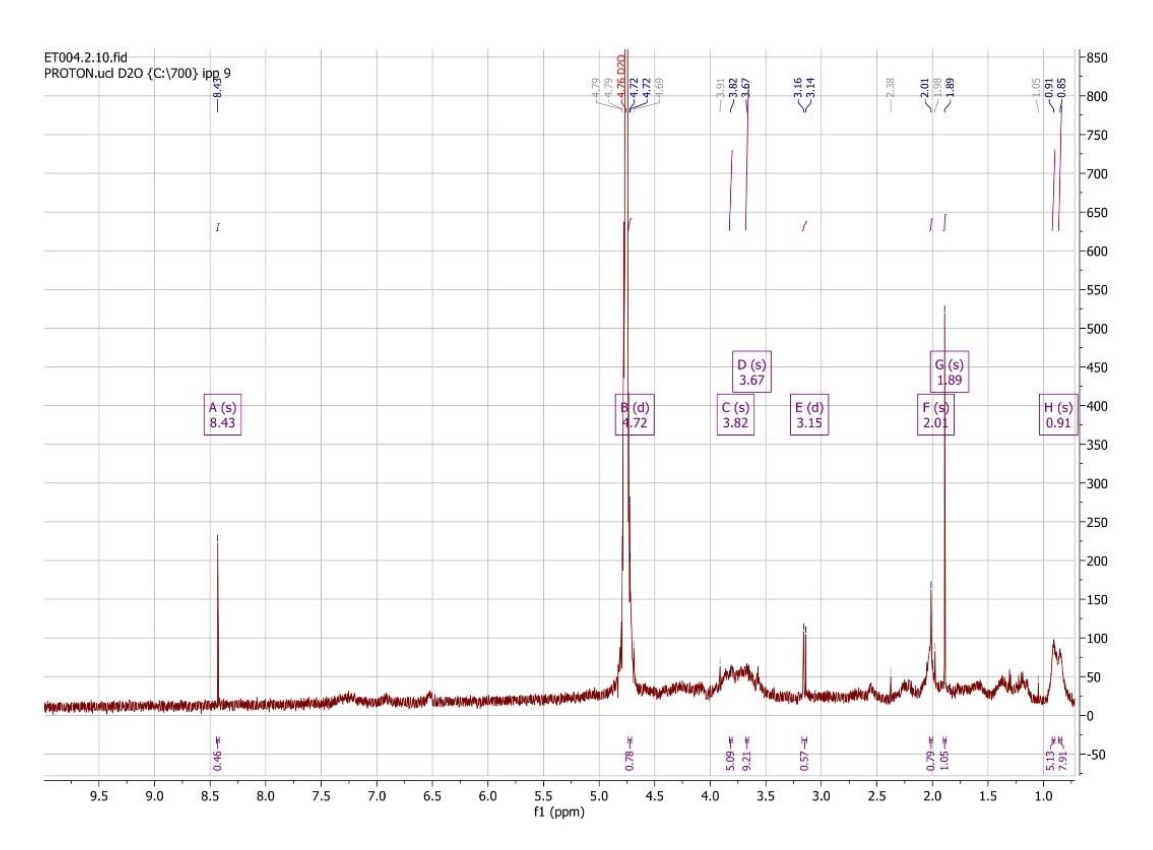


Figure 73. NMR spectra of the NaOH-soluble parts of ET004

1H NMR (700 MHz, D2O) δ 8.43 (s, 0H), 4.72 (d, J = 2.9 Hz, 1H), 3.82 (s, 5H), 3.67 (s, 9H), 3.15 (d, J = 12.7 Hz, 1H), 2.01 (s, 1H), 1.89 (s, 1H), 0.91 (s, 5H), 0.85 (s, 8H).

Similarly, to above, it is hard to make any meaningful comments about this spectrum due to the uncertainty around the types of organisms present. But the spectrum in general follows the pattern of clusters of peaks around the region for amino acids.

ET005 - S. agalactiae and C. glabrata.

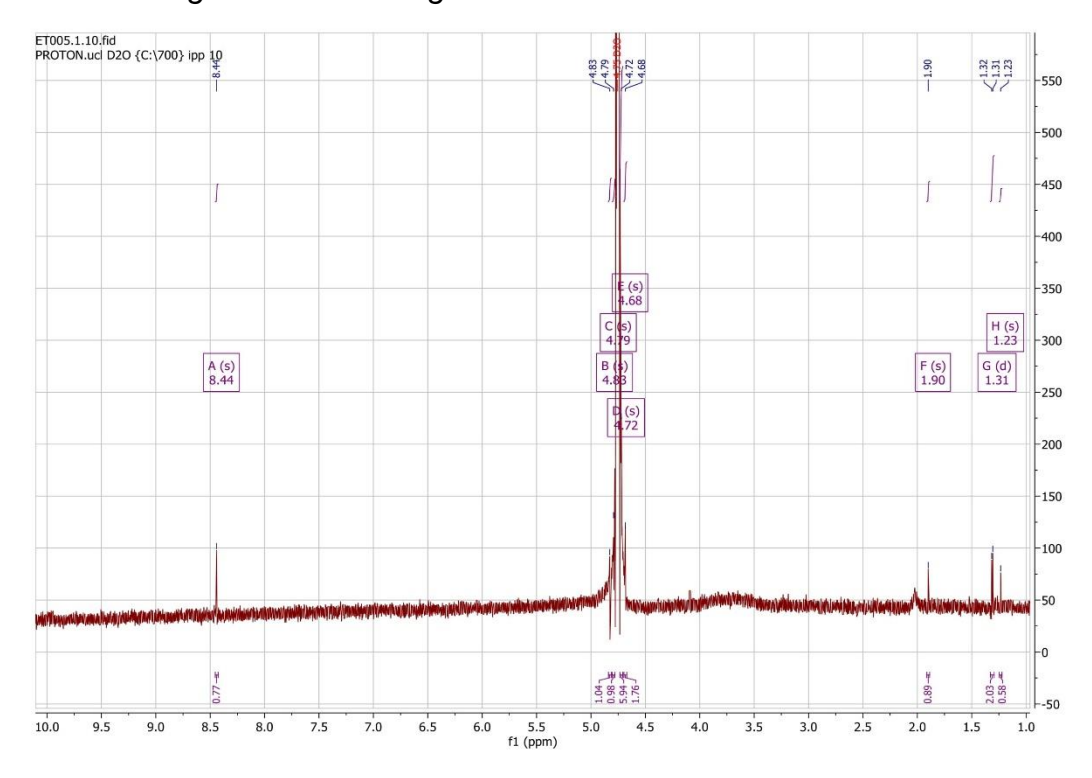


Figure 75. NMR spectra of the water-soluble parts of ET005.

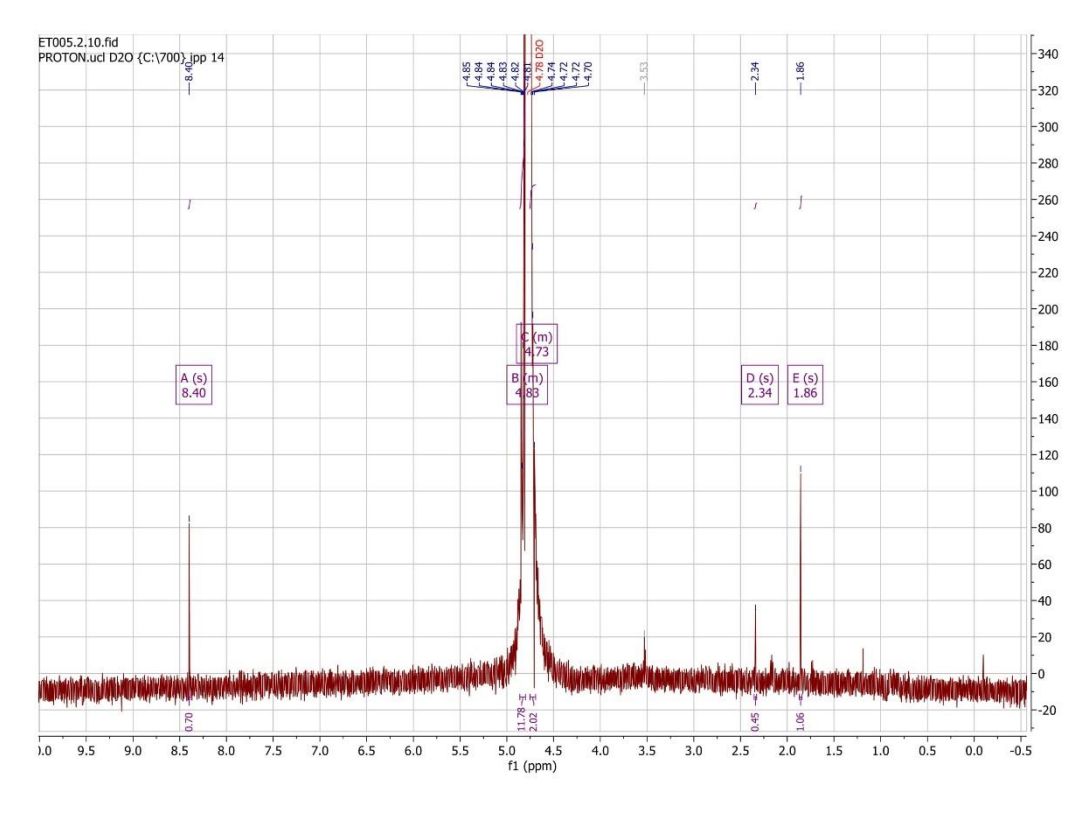


Figure 74. NMR spectra of the NaOH-soluble parts of ET005.

Figure 71: ¹H NMR (700 MHz, D₂O) δ 8.44 (s, 1H), 4.83 (s, 1H), 4.79 (s, 1H), 4.72 (s, 6H), 4.68 (s, 2H), 1.90 (s, 1H), 1.31 (d, J = 6.9 Hz, 2H), 1.23 (s, 1H). Figure 72: ¹H NMR (700 MHz, D₂O) δ 8.40 (s, 1H), 4.86 – 4.80 (m, 12H),

4.75 – 4.69 (m, 2H), 2.34 (s, 0H), 1.86 (s, 1H).

Both UCH and my own culture analysis from the endotracheal tube determined *C. glabrata* was present. A metabolic profiling study found *C. glabrata* isolates contained high concentrations of trehalose and also amino acids glutamine, threonine, glutamate and proline. Trehalose according to the HMDB has clusters of peaks around 3.8 – 3.4 ppm which neither of these spectrum have. Glutamine has multiplets at 3.77 ppm, 2.45 ppm and 2.12 ppm. Threonine has a multiplet at 4.24 ppm, and doublets at 3.58 ppm and 1.32 ppm. Glutamate has multiplets at 3.77 ppm, 2.32 ppm and 2.1 ppm. Proline has multiplets at 4.1 ppm, 3.4 ppm, 2.3 ppm and 2 ppm. Due to the lack of peaks in both spectra aligning with any of these metabolite peaks completely, potentially this fungus was not soluble in either water or NaOH to and therefore was missed by the NMR preparation.

NMR spectra of the suggested compounds found in the above NMR spectra (proline, acetoin, succinate, arabinitol, acetate and trimethylamine) can be found in Appendix 8.3.

5.3.5 CONCLUSIONS

The primary objective of this study was to determine the types of bacteria found on endotracheal tubes and which appear to result in VAP. As well, to determine a rapid diagnostic technique by using NMR analysis. Though we do not have confirmed IDs for bacterial isolates gathered, from purely morphological colony observation there does not appear to be one or two primary species constantly cropping up, each plate appeared quite varied with at least two different isolates growing. The NMR produced are clear and provide well resolved peaks, ideally once combined with IDs and computer technology to do the analysis comparison, fingerprints can be identified for each type of bacteria. Outstanding still is the confirmation of IDs to pull all the puzzle pieces together from this study.

To conclude, analysis of 5 of the collected endotracheal tubes from clinical study is detailed in this thesis. Analysis includes microbiological culture, SEM and NMR. To conclude this work officially IDs of isolates cultured from the inner lumen of the endotracheal tubes is required. It is hard to make any definitive conclusions about the NMR data and it's potential as a diagnostic without full analysis of all 17 collected endotracheal tubes in the full study with the corresponding IDs. However, this does show using a very simple two stage process, samples can easily be prepared for NMR analysis to produce well resolved spectra. It also provides the beginning to insight as to what solvents are best for each type of organism regarding NMR preparation.

As well, both from the culture data supplied by UCH and the suggested IDs from colony morphology/differential plates, so far there does not appear to be

one common type of organism, let alone strain, consistently cropping up in every intubated patient. Again, once IDs have been confirmed, if isolates found on the tube match up with isolates reported by UCH found in faeces, urine, bloods etc, then it is likely to confirm that contamination of the endotracheal tube comes from the patient themselves. Most likely from either the gut and/or oral microbiota, both known to be important in shaping and influencing the immune system of the respiratory tract. As well, this research, upon confirmation of IDs, may bring to light certain pairs of organisms (such as the *B. hominis* and *E. coli*) that tend to grow together in environments like the endotracheal tube. Therefore, if it's likely that the presence of one microorganism encourages another to grow and this is seen frequently, this information can also be used to shorten any potential diagnostic route and may provide valuable insight to clinicians when prescribing antibiotics and antifungals.

SEM provides understanding and a visual to the overarching biofilm structures grown in endotracheal tubes, and how these differ between different organisms. Again, upon confirmation of IDs, the SEMs can be analysed with certainty in depth side by side to compare the types of structures and EPS formed by different types of bacteria. For example, if one type of bacteria produces a much thicker layer of EPS covering all organisms like a blanket, this may be significantly harder for antimicrobial materials to penetrate or take effect against compared to biofilms producing thinner appearing spider-web like biofilms. As well, whether the types of biofilms produced within the same species appear similar or different. So, as well as

providing another method for confirming IDs with the appearance of certain shaped organisms of particular sizes, it may also help with the development of other antimicrobial materials in the future.

6 FINAL REMARKS

Overall, the most significant findings in this thesis are that 1) commercially available endotracheal tubes can be successfully swell encapsulated to produce highly active antimicrobial material against a wide range of organisms including multi-drug resistant bacteria and SARS-CoV-2. 2) Photosensitiser dyes and nanoparticles can successfully be 3D printed by using photocuring resin, to produce any shape, which was a novel finding now patent pending.

3) This clinical study could provide significant findings regarding the pathogenesis of VAP, causative pathogens, in directing future research into antimicrobial materials for this purpose as well as having collected a significant number of relevant isolates to test against in the future. This work on the clinical study could yield incredibly significant results upon ID confirmation.

Swell Encapsulated Antimicrobial Endotracheal Tube

Described in the above work was a static biofilm model using a singular microbe to form the biofilm. Work did begin on developing a polymicrobial biofilm, of which a polymicrobial biofilm was successfully grown once. This however had to be abandoned due to time restraints. This would be a very valuable experiment to get one step closer towards a real-world scenario to test these antimicrobial materials against, as biofilms grow naturally in polymicrobial biofilms in nature (as seen by the clinical study described above).

Once this is done, a flow model should be developed using Ondine's ventilator where a full antimicrobial endotracheal tube could be tested against polymicrobial growing biofilms in a real ventilated situation. This, if successful,

would be a highly significant result and prove the product ready for pre-clinical trials.

Shelf life and stability testing also needs to be done to determine the products life and whether or not this would need to be stored in the dark for example for stability purposes.

3D Printed Antimicrobial Endotracheal Tube

Regarding 3D printed samples, the next stage beyond proof of concept that dyes and nanoparticles can be successfully printed together is the printing of biocompatible flexible polymers with this mix to develop a prototype for testing and see if this carries through into other polymer types.

As well, a series of experiments to determine the true minimum effective concentration of MB and ZnO for commercialisation purposes and the effect the addition of MB and ZnO has on the structural properties of the polymer.

Safety and stability testing with the optimised concentrations should be conducted, such as leaching and shelf life. Additionally, testing the new 3D printed models in the polymicrobial biofilm ventilator model described above would be highly advantageous as a direct comparison against existing technology as well as the swell encapsulated antimicrobial tubes.

Clinical Study

The full set of tubes need to be collected for analysis to give meaningful results, alongside the analysis to confirm isolate IDs. Once identifications have been confirmed, any patterns within the NMR can be further elucidated and matched up to the corresponding organisms. Combined with patient data such as medications given, length of stay, diagnosis, it's hoped that the primary causative agents for VAP, or at least those linked with higher mortality rates, can be determined. As well, finally answer the question of if it is more likely for the source being the human body or environment causing these secondary infections in critical care can be further confirmed.

7 REFERENCES

- (1) Guest, J. F.; Keating, T.; Gould, D.; Wigglesworth, N. Modelling the annual NHS costs and outcomes attributable to healthcare-associated infections in England. *BMJ Open* **2020**, *10* (1), e033367. DOI: 10.1136/bmjopen-2019-033367.
- (2) Amanati, A.; Karimi, A.; Fahimzad, A.; Shamshiri, A. R.; Fallah, F.; Mahdavi, A.; Talebian, M. Incidence of Ventilator-Associated Pneumonia in Critically III Children Undergoing Mechanical Ventilation in Pediatric Intensive Care Unit. *Children (Basel)* **2017**, *4* (7). DOI: 10.3390/children4070056 From NLM.
- (3) O'Horo, J. C.; Thompson, D.; Safdar, N. Is the gram stain useful in the microbiologic diagnosis of VAP? A meta-analysis. *Clin Infect Dis* **2012**, *55* (4), 551-561. DOI: 10.1093/cid/cis512 From NLM.
- (4) England, N. NHS Chief launches new fast track funding so NHS patients get treatment innovations faster. https://www.england.nhs.uk/2016/06/treatment-innovations/, 2016.
- (5) Hunter, J. D. Ventilator associated pneumonia. *BMJ : British Medical Journal* **2012**, *344*, e3325. DOI: 10.1136/bmj.e3325.
- (6) Restrepo, M. I.; Peterson, J.; Fernandez, J. F.; Qin, Z.; Fisher, A. C.; Nicholson, S. C. Comparison of the bacterial etiology of early-onset and late-onset ventilator-associated pneumonia in subjects enrolled in 2 large clinical studies. *Respir Care* **2013**, *58* (7), 1220-1225. DOI: 10.4187/respcare.02173 From NLM.
- (7) Wu, D.; Wu, C.; Zhang, S.; Zhong, Y. Risk Factors of Ventilator-Associated Pneumonia in Critically III Patients. *Front Pharmacol* **2019**, *10*, 482. DOI: 10.3389/fphar.2019.00482 From NLM.
- (8) Tarka, P.; Nitsch-Osuch, A. Evaluating the Virucidal Activity of Disinfectants According to European Union Standards. *Viruses* **2021**, *13* (4). DOI: 10.3390/v13040534 From NLM.
- (9) Bolten, A.; Schmidt, V.; Steinhauer, K. Use of the European standardization framework established by CEN/TC 216 for effective disinfection strategies in human medicine, veterinary medicine, food hygiene, industry, and domestic and institutional use a review. *GMS Hyg Infect Control* **2022**, *17*, Doc14. DOI: 10.3205/dgkh000417 From NLM.
- (10) Maes, M.; Higginson, E.; Pereira-Dias, J.; Curran, M. D.; Parmar, S.; Khokhar, F.; Cuchet-Lourenço, D.; Lux, J.; Sharma-Hajela, S.; Ravenhill, B.; et al. Ventilator-associated pneumonia in critically ill patients with COVID-19. *Critical Care* **2021**, *25* (1), 25. DOI: 10.1186/s13054-021-03460-5.
- (11) Tay, M. Z.; Poh, C. M.; Rénia, L.; MacAry, P. A.; Ng, L. F. P. The trinity of COVID-19: immunity, inflammation and intervention. *Nature Reviews Immunology* **2020**, *20* (6), 363-374. DOI: 10.1038/s41577-020-0311-8.

- (12) Bakaletz, L. O. Viral–bacterial co-infections in the respiratory tract. *Current Opinion in Microbiology* **2017**, *35*, 30-35. DOI: https://doi.org/10.1016/j.mib.2016.11.003.
- (13) Zhang, B.; Liu, S.; Tan, T.; Huang, W.; Dong, Y.; Chen, L.; Chen, Q.; Zhang, L.; Zhong, Q.; Zhang, X.; et al. Treatment With Convalescent Plasma for Critically III Patients With Severe Acute Respiratory Syndrome Coronavirus 2 Infection. *Chest* **2020**, *158* (1), e9-e13. DOI: https://doi.org/10.1016/j.chest.2020.03.039.
- (14) Garcia-Vidal, C.; Sanjuan, G.; Moreno-García, E.; Puerta-Alcalde, P.; Garcia-Pouton, N.; Chumbita, M.; Fernandez-Pittol, M.; Pitart, C.; Inciarte, A.; Bodro, M.; et al. Incidence of co-infections and superinfections in hospitalized patients with COVID-19: a retrospective cohort study. *Clinical Microbiology and Infection* **2021**, *27* (1), 83-88. DOI: https://doi.org/10.1016/j.cmi.2020.07.041.
- (15) Girona-Alarcón, M.; Bobillo-Perez, S.; Solé-Ribalta, A.; Cuadras, D.; Guitart, C.; Balaguer, M.; Cambra, F.-J.; Jordan, I. RISK score for developing ventilator-associated pneumonia in children: The RISVAP study. *Pediatric Pulmonology* **2022**, *57* (7), 1635-1642, https://doi.org/10.1002/ppul.25929. DOI: https://doi.org/10.1002/ppul.25929 (accessed 2022/08/12).
- (16) Gunasekera, P.; Gratrix, A. Ventilator-associated pneumonia. *BJA Education* **2016**, *16* (6), 198-202. DOI: 10.1093/bjaed/mkv046 (accessed 8/26/2022).
- (17) Blot, S. I.; Poelaert, J.; Kollef, M. How to avoid microaspiration? A key element for the prevention of ventilator-associated pneumonia in intubated ICU patients. *BMC Infectious Diseases* **2014**, *14* (1), 119. DOI: 10.1186/1471-2334-14-119.
- (18) Thorarinsdottir, H. R.; Kander, T.; Holmberg, A.; Petronis, S.; Klarin, B. Biofilm formation on three different endotracheal tubes: a prospective clinical trial. *Critical Care* **2020**, *24* (1), 382. DOI: 10.1186/s13054-020-03092-1.
- (19) Evans, C. R.; Sharpe, J. P.; Swanson, J. M.; Wood, G. C.; Fabian, T. C.; Croce, M. A.; Magnotti, L. J. Keeping it simple: impact of a restrictive antibiotic policy for ventilator-associated pneumonia in trauma patients on incidence and sensitivities of causative pathogens. *Surgical Infections* **2018**, *19* (7), 672-678.
- (20) Rhodes, N. J.; Cruce, C. E.; O'Donnell, J. N.; Wunderink, R. G.; Hauser, A. R. Resistance trends and treatment options in gram-negative ventilator-associated pneumonia. *Current infectious disease reports* **2018**, *20* (2), 1-15.
- (21) Nejad, S.; Allegranzi, B.; Syed, S.; Ellis, B.; Didier, P. Health-Care-Associated Infection in Africa: A Systematic Review. *Bulletin of the World Health Organizaton* **2011**, *89*, 757-765.
- (22) Kifle, F.; Boru, Y.; Tamiru, H. D.; Sultan, M.; Walelign, Y.; Demelash, A.; Beane, A.; Haniffa, R.; Gebreyesus, A.; Moore, J. Intensive Care in Sub-Saharan Africa: A National Review of the Service Status in Ethiopia. *Anesthesia & Analgesia* **2022**, *134* (5).

- (23) Liang, Y.; Zhu, C.; Tian, C.; Lin, Q.; Li, Z.; Li, Z.; Ni, D.; Ma, X. Early prediction of ventilator-associated pneumonia in critical care patients: a machine learning model. *BMC Pulmonary Medicine* **2022**, *22* (1), 250. DOI: 10.1186/s12890-022-02031-w.
- (24) Organization, W. H. International organizations unite on critical recommendations to combat drug-resistant infections and prevent staggering number of deaths each year. https://www.who.int/news/item/29-04-2019-new-report-calls-for-urgent-action-to-avert-antimicrobial-resistance-crisis, 2019.
- (25) Kollef, M. H.; Afessa, B.; Anzueto, A.; Veremakis, C.; Kerr, K. M.; Margolis, B. D.; Craven, D. E.; Roberts, P. R.; Arroliga, A. C.; Hubmayr, R. D.; et al. Silver-coated endotracheal tubes and incidence of ventilator-associated pneumonia: the NASCENT randomized trial. *Jama* **2008**, *300* (7), 805-813. DOI: 10.1001/jama.300.7.805 From NLM.
- (26) McNeilly, O.; Mann, R.; Hamidian, M.; Gunawan, C. Emerging Concern for Silver Nanoparticle Resistance in Acinetobacter baumannii and Other Bacteria. *Front Microbiol* **2021**, *12*, 652863. DOI: 10.3389/fmicb.2021.652863 From NLM.
- (27) Organization., W. H. Prioritization of pathogens to guide discovery, research and development of new antibiotics for drug-resistant bacterial infections, including tuberculosis. 2017.
- (28) Hwang, G. B.; Huang, H.; Wu, G.; Shin, J.; Kafizas, A.; Karu, K.; Toit, H. D.; Alotaibi, A. M.; Mohammad-Hadi, L.; Allan, E.; et al. Photobactericidal activity activated by thiolated gold nanoclusters at low flux levels of white light. *Nature Communications* **2020**, *11* (1), 1207. DOI: 10.1038/s41467-020-15004-6.
- (29) Hwang, G. B.; Allan, E.; Parkin, I. P. White Light-Activated Antimicrobial Paint using Crystal Violet. *ACS Appl Mater Interfaces* **2016**, *8* (24), 15033-15039. DOI: 10.1021/acsami.5b06927 From NLM.
- (30) Li, Y.; Zhang, W.; Niu, J.; Chen, Y. Mechanism of Photogenerated Reactive Oxygen Species and Correlation with the Antibacterial Properties of Engineered Metal-Oxide Nanoparticles. *ACS Nano* **2012**, *6* (6), 5164-5173. DOI: 10.1021/nn300934k.
- (31) Ozkan, E.; Allan, E.; Parkin, I. White-Light-Activated Antibacterial Surfaces Generated by Synergy between Zinc Oxide Nanoparticles and Crystal Violet. *ACS Omega* **2018**, *3* (3), 3190-3199. DOI: 10.1021/acsomega.7b01473.
- (32) Kadiyala, U.; Turali-Emre, E. S.; Bahng, J. H.; Kotov, N. A.; VanEpps, J. S. Unexpected insights into antibacterial activity of zinc oxide nanoparticles against methicillin resistant Staphylococcus aureus (MRSA). *Nanoscale* **2018**, *10* (10), 4927-4939, 10.1039/C7NR08499D. DOI: 10.1039/C7NR08499D.
- (33) Painter, K. L.; Strange, E.; Parkhill, J.; Bamford, K. B.; Armstrong-James, D.; Edwards, A. M. Staphylococcus aureus adapts to oxidative stress by producing H2O2-resistant small-colony variants via the SOS response.

- *Infect Immun* **2015**, 83 (5), 1830-1844. DOI: 10.1128/iai.03016-14 From NLM.
- (34) Gambino, M.; Cappitelli, F. Mini-review: Biofilm responses to oxidative stress. *Biofouling* **2016**, *32* (2), 167-178. DOI: 10.1080/08927014.2015.1134515 From NLM.
- (35) von Moos, N.; Slaveykova, V. I. Oxidative stress induced by inorganic nanoparticles in bacteria and aquatic microalgae--state of the art and knowledge gaps. *Nanotoxicology* **2014**, *8* (6), 605-630. DOI: 10.3109/17435390.2013.809810 From NLM.
- (36) Cáp, M.; Váchová, L.; Palková, Z. Reactive oxygen species in the signaling and adaptation of multicellular microbial communities. *Oxid Med Cell Longev* **2012**, *2012*, 976753. DOI: 10.1155/2012/976753 From NLM.
- (37) Li, H.; Zhou, X.; Huang, Y.; Liao, B.; Cheng, L.; Ren, B. Reactive Oxygen Species in Pathogen Clearance: The Killing Mechanisms, the Adaption Response, and the Side Effects. *Front Microbiol* **2020**, *11*, 622534. DOI: 10.3389/fmicb.2020.622534 From NLM.
- (38) Qin, Q. L.; Li, Y.; Zhang, Y. J.; Zhou, Z. M.; Zhang, W. X.; Chen, X. L.; Zhang, X. Y.; Zhou, B. C.; Wang, L.; Zhang, Y. Z. Comparative genomics reveals a deep-sea sediment-adapted life style of Pseudoalteromonas sp. SM9913. *Isme j* **2011**, *5* (2), 274-284. DOI: 10.1038/ismej.2010.103 From NLM.
- (39) Al-Mutairi, R.; Tovmasyan, A.; Batinic-Haberle, I.; Benov, L. Sublethal Photodynamic Treatment Does Not Lead to Development of Resistance. *Front Microbiol* **2018**, *9*, 1699. DOI: 10.3389/fmicb.2018.01699 From NLM.
- (40) Lisa, A. P.; Aaron, J. G.; Robert, J. S.; Cale, N. S. Absence of bacterial resistance following repeat exposure to photodynamic therapy. In *Proc.SPIE*, 2009; Vol. 7380, p 73803H. DOI: 10.1117/12.822834.
- (41) Costa, L.; Tomé, J. P.; Neves, M. G.; Tomé, A. C.; Cavaleiro, J. A.; Faustino, M. A.; Cunha, Â.; Gomes, N. C.; Almeida, A. Evaluation of resistance development and viability recovery by a non-enveloped virus after repeated cycles of aPDT. *Antiviral Res* **2011**, *91* (3), 278-282. DOI: 10.1016/j.antiviral.2011.06.007 From NLM.
- (42) Stark, G. Functional consequences of oxidative membrane damage. *J Membr Biol* **2005**, 205 (1), 1-16. DOI: 10.1007/s00232-005-0753-8 From NLM.
- (43) Olson, M. E.; Harmon, B. G.; Kollef, M. H. Silver-coated endotracheal tubes associated with reduced bacterial burden in the lungs of mechanically ventilated dogs. *Chest* **2002**, *121* (3), 863-870, Article. DOI: 10.1378/chest.121.3.863 Scopus.
- (44) Rello, J.; Kollef, M.; Diaz, E.; Sandiumenge, A.; del Castillo, Y.; Corbella, X.; Zachskorn, R. Reduced burden of bacterial airway colonization with a novel silver-coated endotracheal tube in a randomized multiple-center feasibility study. *Crit Care Med* **2006**, *34* (11), 2766-2772. DOI: 10.1097/01.ccm.0000242154.49632.b0 From NLM.

- (45) Greulich, C.; Braun, D.; Peetsch, A.; Diendorf, J.; Siebers, B.; Epple, M.; Köller, M. The toxic effect of silver ions and silver nanoparticles towards bacteria and human cells occurs in the same concentration range. *RSC Advances* **2012**, *2* (17), 6981-6987, 10.1039/C2RA20684F. DOI: 10.1039/C2RA20684F.
- (46) Infection Prevention Endotracheal Tube BIP Bactiguard. 2015. (accessed 19th August 2022).
- (47) Bjorling, G.; Johansson, D.; Bergstrom, L.; Jalal, S.; Kohn, I.; Frostell, C.; Kalman, S. Tolerability and performance of BIP endotracheal tubes with noble metal alloy coating--a randomized clinical evaluation study. *BMC Anesthesiol* **2015**, *15*, 174. DOI: 10.1186/s12871-015-0156-z From NLM.
- (48) Damas, P.; Legrain, C.; Lambermont, B.; Dardenne, N.; Guntz, J.; Kisoka, G.; Demaret, P.; Rousseau, A.-F.; Jadot, L.; Piret, S.; et al. Prevention of ventilator-associated pneumonia by noble metal coating of endotracheal tubes: a multi-center, randomized, double-blind study. *Annals of Intensive Care* **2022**, *12* (1), 1. DOI: 10.1186/s13613-021-00961-y.
- (49) Hashemi, M. M.; Rovig, J.; Bateman, J.; Holden, B. S.; Modelzelewski, T.; Gueorguieva, I.; von Dyck, M.; Bracken, R.; Genberg, C.; Deng, S.; et al. Preclinical testing of a broad-spectrum antimicrobial endotracheal tube coated with an innate immune synthetic mimic. *J Antimicrob Chemother* **2018**, 73 (1), 143-150. DOI: 10.1093/jac/dkx347 From NLM.
- (50) Danin, P.-E.; Girou, E.; Legrand, P.; Louis, B.; Fodil, R.; Christov, C.; Devaquet, J.; Isabey, D.; Brochard, L. Description and Microbiology of Endotracheal Tube Biofilm in Mechanically Ventilated Subjects. *Respiratory Care* **2015**, *60* (1), 21. DOI: 10.4187/respcare.02722.
- (51) Health Canada Grants Emergency Use Authorization for N8 Medical CeraShield™ Endotracheal Tubes in Mechanically Ventilated COVID-19 Patients. Cision PR Newswire, 2020.
- (52) Mann, E. E.; Magin, C. M.; Mettetal, M. R.; May, R. M.; Henry, M. M.; DeLoid, H.; Prater, J.; Sullivan, L.; Thomas, J. G.; Twite, M. D.; et al. Micropatterned Endotracheal Tubes Reduce Secretion-Related Lumen Occlusion. *Ann Biomed Eng* **2016**, *44* (12), 3645-3654. DOI: 10.1007/s10439-016-1698-z From NLM.
- (53) May, R. M.; Hoffman, M. G.; Sogo, M. J.; Parker, A. E.; O'Toole, G. A.; Brennan, A. B.; Reddy, S. T. Micro-patterned surfaces reduce bacterial colonization and biofilm formation in vitro: Potential for enhancing endotracheal tube designs. *Clin Transl Med* **2014**, *3*, 8. DOI: 10.1186/2001-1326-3-8 From NLM.
- (54) Pilmis, B.; Zahar, J.-R. Ventilator-associated pneumonia related to ESBL-producing gram negative bacilli. *Annals of translational medicine* **2018**, 6 (21), 424-424. DOI: 10.21037/atm.2018.09.34 PubMed.
- (55) Ondine Biomedical Website. Technology. (accessed 2019 19th August).
- (56) Friedman, R. Coronavirus cure, or at least preventative? Canadian firm Ondine having success with new treatment at Edmonton nursing home. https://www.showbiz411.com/2020/03/25/coronavirus-cure-or-at-least-

- <u>preventative-canadian-firm-ondine-having-success-with-new-treatment-at-edmonton-nursing-home</u>, 2020.
- (57) Loebel, N.; Cross, C.; Meller, D.; Hickok, J.; Anderson, R. Antimicrobial Photodisinfection Therapy: Essential Technology for Infection Control. https://ondinebio.com/wp-content/uploads/2020/03/Antimicrobial-Photodisinfection-Therapy-White-Paper_02.28.2020.pdf, 2020.
- (58) Biel, M. A.; Sievert, C.; Usacheva, M.; Teichert, M.; Wedell, E.; Loebel, N.; Rose, A.; Zimmermann, R. Reduction of endotracheal tube biofilms using antimicrobial photodynamic therapy. *Lasers in Surgery and Medicine* **2011**, 43 (7), 586-590. DOI: 10.1002/lsm.21103 (acccessed 2019/02/05).
- (59) Biel, M. A.; Sievert, C.; Usacheva, M.; Teichert, M.; Wedell, E.; Loebel, N.; Rose, A.; Zimmermann, R. Reduction of Endotracheal Tube Biofilms Using Antimicrobial Photodynamic Therapy. *Lasers Surg Med* **2011**, *43* (7), 586-590. DOI: 10.1002/lsm.21103 From NLM.
- (60) Little, A. Executive Summary of Safety and Toxicity Information Testing Status of Methylene blue trihydrate M90016; 1990.
- (61) Jori, G.; Fabris, C.; Soncin, M.; Ferro, S.; Coppellotti, O.; Dei, D.; Fantetti, L.; Chiti, G.; Roncucci, G. Photodynamic therapy in the treatment of microbial infections: basic principles and perspective applications. *Lasers Surg Med* **2006**, *38* (5), 468-481. DOI: 10.1002/lsm.20361 From NLM.
- (62) Hwang, G. B.; Wu, G.; Shin, J.; Panariello, L.; Sebastian, V.; Karu, K.; Allan, E.; Gavriilidis, A.; Parkin, I. P. Continuous Single-Phase Synthesis of [Au25(Cys)18] Nanoclusters and their Photobactericidal Enhancement. *ACS Applied Materials & Interfaces* **2020**, *12* (43), 49021-49029. DOI: 10.1021/acsami.0c07691.
- (63) Ginimuge, P. R.; Jyothi, S. D. Methylene blue: revisited. *J Anaesthesiol Clin Pharmacol* **2010**, *26* (4), 517-520. From NLM.
- (64) Pushparajah Mak, R. S.; Liebelt, E. L. Methylene Blue: An Antidote for Methemoglobinemia and Beyond. *Pediatric Emergency Care* **2021**, *37* (9).
- (65) Gillman, P. K. Methylene blue implicated in potentially fatal serotonin toxicity. In *Anaesthesia*, Vol. 61; 2006; pp 1013-1014.
- (66) Dewachter, P.; Mouton-Faivre, C.; Tréchot, P.; Lleu, J. C.; Mertes, P. M. Severe anaphylactic shock with methylene blue instillation. *Anesth Analg* **2005**, *101* (1), 149-150, table of contents. DOI: 10.1213/01.ane.0000153497.60047.80 From NLM.
- (67) Rodrigues, M. E.; Lopes, S. P.; Pereira, C. R.; Azevedo, N. F.; Lourenço, A.; Henriques, M.; Pereira, M. O. Polymicrobial Ventilator-Associated Pneumonia: Fighting In Vitro Candida albicans-Pseudomonas aeruginosa Biofilms with Antifungal-Antibacterial Combination Therapy. *PLOS ONE* **2017**, *12* (1), e0170433. DOI: 10.1371/journal.pone.0170433.
- (68) Hotterbeekx, A.; Xavier, B. B.; Bielen, K.; Lammens, C.; Moons, P.; Schepens, T.; leven, M.; Jorens, P. G.; Goossens, H.; Kumar-Singh, S.; et al. The endotracheal tube microbiome associated with Pseudomonas aeruginosa or Staphylococcus epidermidis. *Scientific Reports* **2016**, *6* (1), 36507. DOI: 10.1038/srep36507.

- (69) Chastre, J.; Fagon, J. Y. Ventilator-associated pneumonia. *Am J Respir Crit Care Med* **2002**, *165* (7), 867-903. DOI: 10.1164/ajrccm.165.7.2105078 From NLM.
- (70) Ammann, C. G.; Nagl, M.; Nogler, M.; Coraça-Huber, D. C. Pseudomonas aeruginosa outcompetes other bacteria in the manifestation and maintenance of a biofilm in polyvinylchloride tubing as used in dental devices. *Arch Microbiol* **2016**, *198* (4), 389-391. DOI: 10.1007/s00203-016-1208-6 From NLM.
- (71) Phan, J.; Ranjbar, S.; Kagawa, M.; Gargus, M.; Hochbaum, A. I.; Whiteson, K. L. Thriving Under Stress: Pseudomonas aeruginosa Outcompetes the Background Polymicrobial Community Under Treatment Conditions in a Novel Chronic Wound Model. *Front Cell Infect Microbiol* **2020**, *10*, 569685. DOI: 10.3389/fcimb.2020.569685 From NLM.
- (72) Limoli, D. H.; Whitfield, G. B.; Kitao, T.; Ivey, M. L.; Davis, M. R., Jr.; Grahl, N.; Hogan, D. A.; Rahme, L. G.; Howell, P. L.; O'Toole, G. A.; et al. Pseudomonas aeruginosa Alginate Overproduction Promotes Coexistence with Staphylococcus aureus in a Model of Cystic Fibrosis Respiratory Infection. *mBio* **2017**, *8* (2). DOI: 10.1128/mBio.00186-17 From NLM.
- (73) Póvoa, H. C. C.; Chianca, G. C.; Iorio, N. L. P. P. COVID-19: An Alert to Ventilator-Associated Bacterial Pneumonia. *Infectious diseases and therapy* **2020**, *9* (3), 417-420. DOI: 10.1007/s40121-020-00306-5 PubMed.
- (74) d'Humières, C.; Patrier, J.; Lortat-Jacob, B.; Tran-dinh, A.; Chemali, L.; Maataoui, N.; Rondinaud, E.; Ruppé, E.; Burdet, C.; Ruckly, S.; et al. Two original observations concerning bacterial infections in COVID-19 patients hospitalized in intensive care units during the first wave of the epidemic in France. *PLOS ONE* **2021**, *16* (4), e0250728. DOI: 10.1371/journal.pone.0250728.
- (75) Bell, J. Five key pieces of medical equipment being manufactured with 3D printing. https://www.nsmedicaldevices.com/analysis/3d-printing-medical-equipment/, 2020.
- (76) Hospital, G. O. S. Second set of rare conjoined twins separated at Great Ormond Street Hospital in less than 12 months. https://www.gosh.nhs.uk/news/second-set-rare-conjoined-twins-separated-great-ormond-street-hospital-less-12-months/, 2020.
- (77) Ventola, C. L. Medical Applications for 3D Printing: Current and Projected Uses. *P* & *T* : a peer-reviewed journal for formulary management **2014**, 39 (10), 704-711. PubMed.
- (78) Grass, G.; Rensing, C.; Solioz, M. Metallic copper as an antimicrobial surface. *Applied and environmental microbiology* **2011**, *77* (5), 1541-1547. DOI: 10.1128/AEM.02766-10 PubMed.
- (79) Meghana, S.; Kabra, P.; Chakraborty, S.; Padmavathy, N. Understanding the pathway of antibacterial activity of copper oxide nanoparticles. *RSC Advances* **2015**, *5* (16), 12293-12299, 10.1039/C4RA12163E. DOI: 10.1039/C4RA12163E.

- (80) Salah, I.; Parkin, I. P.; Allan, E. Copper as an antimicrobial agent: recent advances. *RSC Advances* **2021**, *11* (30), 18179-18186, 10.1039/D1RA02149D. DOI: 10.1039/D1RA02149D.
- (81) Dollwet, H.; Sorenson, J. Historic uses of copper compounds in medicine. *Trace elements in medicine* **1985**, *2*, 80-87.
- (82) Raffi, M.; Mehrwan, S.; Bhatti, T. M.; Akhter, J. I.; Hameed, A.; Yawar, W.; ul Hasan, M. M. Investigations into the antibacterial behavior of copper nanoparticles against Escherichia coli. *Annals of Microbiology* **2010**, *60* (1), 75-80. DOI: 10.1007/s13213-010-0015-6.
- (83) Chatterjee, A. K.; Chakraborty, R.; Basu, T. Mechanism of antibacterial activity of copper nanoparticles. *Nanotechnology* **2014**, *25* (13), 135101. DOI: 10.1088/0957-4484/25/13/135101 From NLM.
- (84) Gyawali, R.; Ibrahim, S. A.; Abu Hasfa, S. H.; Smqadri, S. Q.; Haik, Y. Antimicrobial Activity of Copper Alone and in Combination with Lactic Acid against Escherichia coli O157:H7 in Laboratory Medium and on the Surface of Lettuce and Tomatoes. *J Pathog* **2011**, *2011*, 650968. DOI: 10.4061/2011/650968 From NLM.
- (85) Karlsson, H. L.; Cronholm, P.; Gustafsson, J.; Möller, L. Copper oxide nanoparticles are highly toxic: a comparison between metal oxide nanoparticles and carbon nanotubes. *Chem Res Toxicol* **2008**, *21* (9), 1726-1732. DOI: 10.1021/tx800064j From NLM.
- (86) Naz, S.; Gul, A.; Zia, M. Toxicity of copper oxide nanoparticles: a review study. *IET Nanobiotechnology* **2020**, *14* (1), 1-13, https://doi.org/10.1049/iet-nbt.2019.0176 (acccessed 2021/07/29).
- (87) Noimark, S.; Allan, E.; Parkin, I. P. Light-activated antimicrobial surfaces with enhanced efficacy induced by a dark-activated mechanism. *Chemical Science* **2014**, *5* (6), 2216-2223, 10.1039/C3SC53186D. DOI: 10.1039/C3SC53186D.
- (88) Noimark, S.; Dunnill, C. W.; Kay, C. W. M.; Perni, S.; Prokopovich, P.; Ismail, S.; Wilson, M.; Parkin, I. P. Incorporation of methylene blue and nanogold into polyvinyl chloride catheters; a new approach for light-activated disinfection of surfaces. *Journal of Materials Chemistry* **2012**, *22* (30), 15388-15396, 10.1039/C2JM31987J. DOI: 10.1039/C2JM31987J.
- (89) Ozkan, E.; Allan, E.; Parkin, I. P. White-Light-Activated Antibacterial Surfaces Generated by Synergy between Zinc Oxide Nanoparticles and Crystal Violet. *ACS Omega* **2018**, *3* (3), 3190-3199. DOI: 10.1021/acsomega.7b01473 From NLM.
- (90) Sehmi, S. K.; Noimark, S.; Pike, S. D.; Bear, J. C.; Peveler, W. J.; Williams, C. K.; Shaffer, M. S. P.; Allan, E.; Parkin, I. P.; MacRobert, A. J. Enhancing the Antibacterial Activity of Light-Activated Surfaces Containing Crystal Violet and ZnO Nanoparticles: Investigation of Nanoparticle Size, Capping Ligand, and Dopants. *ACS Omega* **2016**, *1* (3), 334-343, Article. DOI: 10.1021/acsomega.6b00017 Scopus.

- (91) Sehmi, S. K.; Noimark, S.; Bear, J. C.; Peveler, W. J.; Bovis, M.; Allan, E.; MacRobert, A. J.; Parkin, I. P. Y. Lethal photosensitisation of Staphylococcus aureus and Escherichia coli using crystal violet and zinc oxide-encapsulated polyurethane. *Journal of Materials Chemistry B* **2015**, (31), 6490. DOI: 10.1039/c5tb00971e m3 10.1039/c5tb00971e.
- (92) Gil-Perotin, S.; Ramirez, P.; Marti, V.; Sahuquillo, J. M.; Gonzalez, E.; Calleja, I.; Menendez, R.; Bonastre, J. Implications of endotracheal tube biofilm in ventilator-associated pneumonia response: a state of concept. *Critical care (London, England)* **2012**, *16* (3), R93-R93. DOI: 10.1186/cc11357 PubMed.
- (93) Vallés, J.; Mariscal, D.; Cortés, P.; Coll, P.; Villagrá, A.; Díaz, E.; Artigas, A.; Rello, J. Patterns of colonization by Pseudomonas aeruginosa in intubated patients: a 3-year prospective study of 1,607 isolates using pulsed-field gel electrophoresis with implications for prevention of ventilator-associated pneumonia. *Intensive Care Medicine* **2004**, *30* (9), 1768-1775. DOI: 10.1007/s00134-004-2382-6.
- (94) Das, N. K.; Mandal, B. M. Methylene blue as a retarder of free radical polymerization: 1. Polymerization of acrylonitrile, methyl methacrylate and styrene. *Polymer* **1982**, 23 (11), 1653-1658. DOI: https://doi.org/10.1016/0032-3861(82)90188-4.
- (95) Molenberg, A. Use of methylene blue as polymerization inhibitor. 2005.
- (96) Alqahtani, A.; Alamer, E.; Mir, M.; Alasmari, A.; Alshahrani, M. M.; Asiri, M.; Ahmad, I.; Alhazmi, A.; Algaissi, A. Bacterial Coinfections Increase Mortality of Severely III COVID-19 Patients in Saudi Arabia. *Int J Environ Res Public Health* **2022**, *19* (4). DOI: 10.3390/ijerph19042424 From NLM.
- (97) Feldman, C.; Anderson, R. The role of co-infections and secondary infections in patients with COVID-19. *Pneumonia* **2021**, *13* (1), 5. DOI: 10.1186/s41479-021-00083-w.
- (98) Han, R.; Coey, J. D.; O'Rourke, C.; Bamford, C. G. G.; Mills, A. Flexible, disposable photocatalytic plastic films for the destruction of viruses. *Journal of Photochemistry and Photobiology B: Biology* **2022**, *235*, 112551. DOI: https://doi.org/10.1016/j.jphotobiol.2022.112551.
- (99) Monge, F. A.; Jagadesan, P.; Bondu, V.; Donabedian, P. L.; Ista, L.; Chi, E. Y.; Schanze, K. S.; Whitten, D. G.; Kell, A. M. Highly Effective Inactivation of SARS-CoV-2 by Conjugated Polymers and Oligomers. *ACS Applied Materials & Interfaces* **2020**, *12* (50), 55688-55695. DOI: 10.1021/acsami.0c17445.
- (100) Behzadinasab, S.; Chin, A.; Hosseini, M.; Poon, L.; Ducker, W. A. A Surface Coating that Rapidly Inactivates SARS-CoV-2. *ACS Applied Materials & Interfaces* **2020**, *12* (31), 34723-34727. DOI: 10.1021/acsami.0c11425.
- (101) Behzadinasab, S.; Williams, M. D.; Hosseini, M.; Poon, L. L. M.; Chin, A. W. H.; Falkinham, J. O., III; Ducker, W. A. Transparent and Sprayable Surface Coatings that Kill Drug-Resistant Bacteria Within Minutes and

- Inactivate SARS-CoV-2 Virus. *ACS Applied Materials & Interfaces* **2021**, *13* (46), 54706-54714. DOI: 10.1021/acsami.1c15505.
- (102) ICH Guideline Q5A(R2) on viral safety evaluation of
- biotechnology products derived from cell lines of human
- or animal origin. Products, C. f. H. M., Ed.; European Medicines Agency, 2022.
- (103) SIST EN 1276:2019 Chemical disinfectants and antiseptics Quantitative suspension test for the evaluation of bactericidal activity of chemical disinfectants and antiseptics used in food, industrial, domestic and institutional areas Test method and requirements (phase 2, step 1). enstandard.eu, 2019.
- (104) Ozcelik, B.; Pasic, P.; Sangwan, P.; Be, C. L.; Glattauer, V.; Thissen, H.; Boulos, R. A. Evaluation of the Novel Antimicrobial BCP3 in a Coating for Endotracheal Tubes. *ACS Omega* **2020**, *5* (18), 10288-10296. DOI: 10.1021/acsomega.9b04178.
- (105) Leuck, A. M.; Johnson, J. R.; Hunt, M. A.; Dhody, K.; Kazempour, K.; Ferrieri, P.; Kline, S. Safety and efficacy of a novel silver-impregnated urinary catheter system for preventing catheter-associated bacteriuria: a pilot randomized clinical trial. *Am J Infect Control* **2015**, *43* (3), 260-265. DOI: 10.1016/j.ajic.2014.11.021 From NLM.
- (106) Srisang, S.; Nasongkla, N. Layer-by-layer dip coating of Foley urinary catheters by chlorhexidine-loaded micelles. *Journal of Drug Delivery Science and Technology* **2019**, *49*, 235-242, Article. DOI: 10.1016/j.jddst.2018.11.019 Scopus.
- (107) Mandakhalikar, K. D.; Wang, R.; Rahmat, J. N.; Chiong, E.; Neoh, K. G.; Tambyah, P. A. Restriction of in vivo infection by antifouling coating on urinary catheter with controllable and sustained silver release: A proof of concept study. *BMC Infectious Diseases* **2018**, *18* (1), Article. DOI: 10.1186/s12879-018-3296-1 Scopus.
- (108) Centre., S. H. S. Methylene Blue-mediated Photodisinfection for SARS-CoV-2 in the Upper Respiratory Tract. In *Identifier: NCT04615936*, ClinicalTrials.gov, 2021.
- (109) Evaluation., T. S. O. o. S. Literature review on the safety of titanium dioxide and zinc oxide nanoparticles in sunscreens. Administration, T. G., Ed.: Australian Government: 2017.
- (110) Mohammed, Y. H.; Holmes, A.; Haridass, I. N.; Sanchez, W. Y.; Studier, H.; Grice, J. E.; Benson, H. A. E.; Roberts, M. S. Support for the Safe Use of Zinc Oxide Nanoparticle Sunscreens: Lack of Skin Penetration or Cellular Toxicity after Repeated Application in Volunteers. *Journal of Investigative Dermatology* **2019**, *139* (2), 308-315. DOI: https://doi.org/10.1016/j.jid.2018.08.024.
- (111) Koenig, S. M.; Truwit, J. D. Ventilator-associated pneumonia: diagnosis, treatment, and prevention. *Clin Microbiol Rev* **2006**, *19* (4), 637-657. DOI: 10.1128/cmr.00051-05 From NLM.

- (112) François, B.; Laterre, P.-F.; Luyt, C.-E.; Chastre, J. The challenge of ventilator-associated pneumonia diagnosis in COVID-19 patients. *Critical Care* **2020**, *24* (1), 289. DOI: 10.1186/s13054-020-03013-2.
- (113) Kruger, N. J.; Troncoso-Ponce, M. A.; Ratcliffe, R. G. 1H NMR metabolite fingerprinting and metabolomic analysis of perchloric acid extracts from plant tissues. *Nat Protoc* **2008**, *3* (6), 1001-1012. DOI: 10.1038/nprot.2008.64 From NLM.
- (114) Reddinger, R. M.; Luke-Marshall, N. R.; Sauberan, S. L.; Hakansson, A. P.; Campagnari, A. A. Streptococcus pneumoniae Modulates Staphylococcus aureus Biofilm Dispersion and the Transition from Colonization to Invasive Disease. *mBio* **2018**, *9* (1). DOI: 10.1128/mBio.02089-17 From NLM.
- (115) Laboratory Detection of Imipenem or Meropenem Resistance in Gramnegative Organisms. Prevention, C. f. D. C. a., Ed.; https://www.cdc.gov/hai/settings/lab/lab_imipenem.html, 2023.
- (116) Reyes, J.; Komarow, L.; Chen, L.; Ge, L.; Hanson, B. M.; Cober, E.; Herc, E.; Alenazi, T.; Kaye, K. S.; Garcia-Diaz, J.; et al. Global epidemiology and clinical outcomes of carbapenem-resistant Pseudomonas aeruginosa and associated carbapenemases (POP): a prospective cohort study. *The Lancet Microbe* **2023**, *4* (3), e159-e170. DOI: 10.1016/S2666-5247(22)00329-9 (acccessed 2023/04/12).
- (117) Salama, Y.; Chennaoui, M.; Sylla, A.; Mountadar, M.; Rihani, M.; Assobhei, O. Characterization, structure, and function of extracellular polymeric substances (EPS) of microbial biofilm in biological wastewater treatment systems: a review. *Desalination and Water Treatment* **2016**, *57* (35), 16220-16237. DOI: 10.1080/19443994.2015.1077739.
- (118) Bouillaut, L.; Self, W. T.; Sonenshein, A. L. Proline-dependent regulation of Clostridium difficile Stickland metabolism. *J Bacteriol* **2013**, *195* (4), 844-854. DOI: 10.1128/jb.01492-12 From NLM.
- (119) Parisi, J. T. Coagulase-negative staphylococci and the epidemiological typing of Staphylococcus epidermidis. *Microbiological Reviews* **1985**, *49* (2), 126-139. DOI: 10.1128/mr.49.2.126-139.1985 (accessed 2023/04/12).
- (120) Sun, J. L.; Zhang, S. K.; Chen, J. Y.; Han, B. Z. Metabolic profiling of Staphylococcus aureus cultivated under aerobic and anaerobic conditions with (1)H NMR-based nontargeted analysis. *Can J Microbiol* **2012**, *58* (6), 709-718. DOI: 10.1139/w2012-046 From NLM.
- (121) Newton, J. M.; Betts, E. L.; Yiangou, L.; Ortega Roldan, J.; Tsaousis, A. D.; Thompson, G. S. Establishing a Metabolite Extraction Method to Study the Metabolome of Blastocystis Using NMR. *Molecules* **2021**, *26* (11). DOI: 10.3390/molecules26113285 From NLM.
- (122) Yason, J. A.; Liang, Y. R.; Png, C. W.; Zhang, Y.; Tan, K. A.-O. X. Interactions between a pathogenic Blastocystis subtype and gut microbiota: in vitro and in vivo studies. (2049-2618 (Electronic)). From 2019 Mar 11.
- (123) Lussu, M.; Camboni, T.; Piras, C.; Serra, C.; Del Carratore, F.; Griffin, J.; Atzori, L.; Manzin, A. 1H NMR spectroscopy-based metabolomics analysis

- for the diagnosis of symptomatic E. coli-associated urinary tract infection (UTI). *BMC Microbiology* **2017**, *17* (1), 201. DOI: 10.1186/s12866-017-1108-1
- (124) Oliver, J. C.; Laghi, L.; Parolin, C.; Foschi, C.; Marangoni, A.; Liberatore, A.; Dias, A. L. T.; Cricca, M.; Vitali, B. Metabolic profiling of Candida clinical isolates of different species and infection sources. *Sci Rep* **2020**, *10* (1), 16716. From NLM.
- (125) Narendrakumar, L.; Ray, A. Chapter Four Respiratory tract microbiome and pneumonia. In *Progress in Molecular Biology and Translational Science*, Das, B., Singh, V. Eds.; Vol. 192; Academic Press, 2022; pp 97-124.

8 APPENDIX

8.1 SPIRAL PLATER AND THE AUTOMATIC COLONY COUNTER

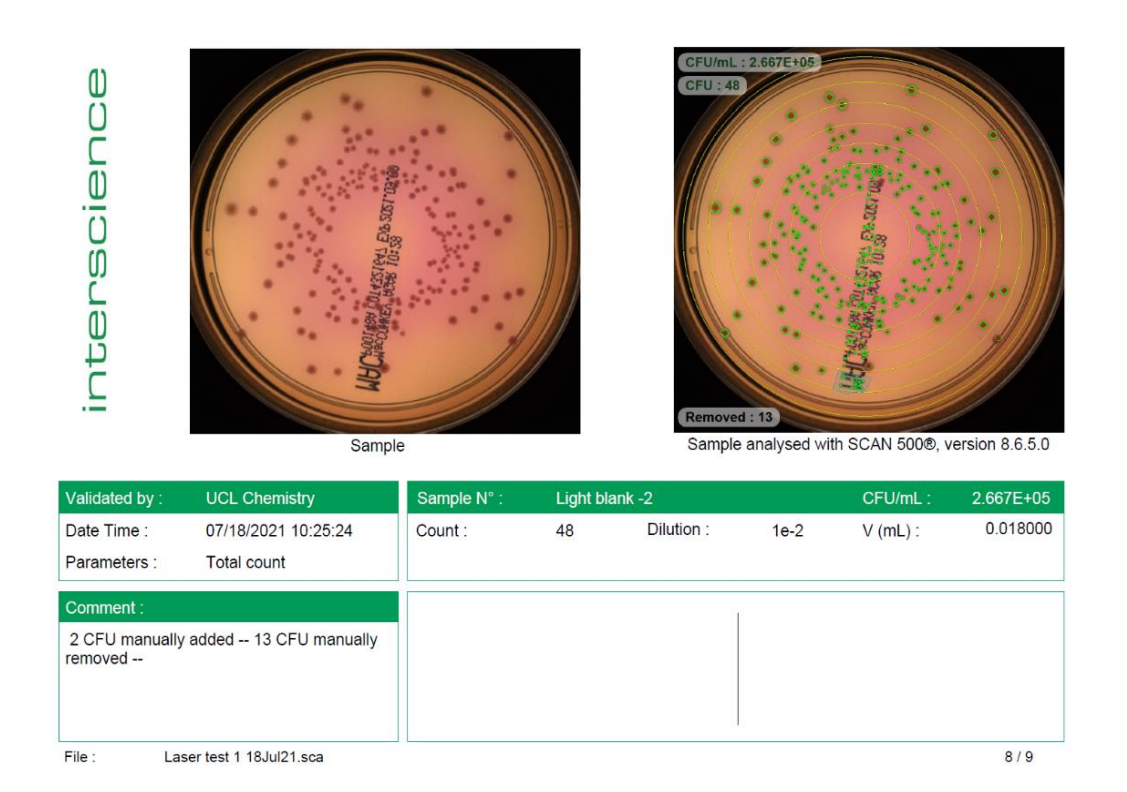


Figure 76. An example of one of the pages from the PDF export from the automatic spiral plate colony counter.

Each sample will result in a screen like this where the colonies are automatically counted by Interscience Scan 500 colony counter and the result validated. Any manual changes made for instance where a colony is counted by mistake or needs to be added, is recorded under the comments for traceability. The data can also be exported to excel format which has then been used to create graphs.

The addition of the spiral plating method has reduced contamination risk significantly, and there have been no issues with contamination since using it. It also has reduced user differences within the group when performing the

same experiment. As well, it has significantly reduced the amount of disposable plastic waste required as 5 dilutions can be plated on one agar plate. This technology has allowed for faster, more accurate, less wasteful experiments and has been hugely helpful in completing this work.

This spiral plater was used side by side against manual methods described in 1.2.7 to validate before use.

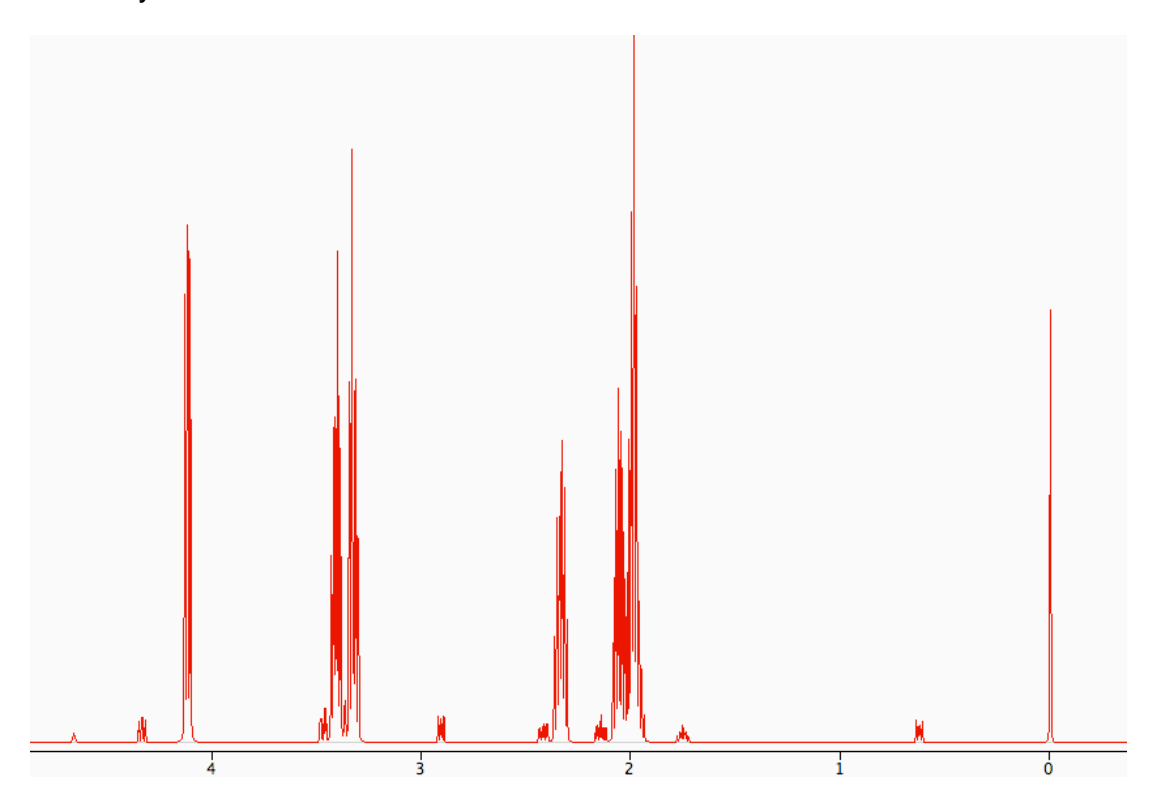
8.2 COLONY MORPHOLOGY ANALYSIS FOR CLINICAL STUDY

	CULTURE OBSERVATIONS		GRAM STAIN RESULTS ID suggestion from colonies/slide		
		Plate type		Gram Stain	ID Suggestion
	Blood	MacConkey	Mannitol Salt		
T001 T	Form = irregular Size = 7mm Bevation = flat Colour = grey Hemolysis = beta (clear zone?)**	Form = circular filamentous, some spreading Size = 3mm Elevation = flat Colour =yellow Lactose fermenter = colourless (N)	n/a		
T001 M	Form = x2 types, irregular and ciruclar Size = Lom and 2mm Blevation = flat and raised Colour = grey and white Hemolysis = beta and gamma	Form = filamentous, some spreading Size = 3mm Elevation = raised Colour = yellow Lactose fermenter = N	Form = circular Size = 1mm Elevation = flat Colour = pink Mannitol fermenter = N (stays pink)		
T001 B	Form = x2 types, irregular and circular Size = 1cm and 2mm Elevation = flat and raised Colour = grey and white Hemolysis = beta and beta	Form = filamentous, some spreading (2) Size = Smm Elevation = Flat Colour = yellow Lactose fermenter = N	Form = circular (1) Size = Imm Elevation = flat Colour = white/pink Mannitol fermenter = N	1 = cocci, dustered 2 = bacili	1 = cocci + diustered = staph, non MSA fermenter = staphylococcus epidermis. 2 = bazili, beta hemolysis, filamentous, non MAC fermenting pseudomonas aeruginosa.
T002 T	Form = x2 types, both dircular Size = 4mm and 2mm Blevation = flat and flat Colour = white and grey Hemolysis = beta (clear) and alpha (green outside)	n/a	Form = x2 types, circular Size = 3mm and 0.3mm Elevation = flat and raised Colour = white pink (both) Mannitol Fermenter = N		
T002 M	Form = x2 types, both circular Size = 2mm and 1mm Elevation = raised (both) Colour = grey (both) Hemolysis = alpha and gamma	n/a	Form = x2 types, circular Size = 3mm and 0.3mm Elevation = flat and raised Colour = white/pink (both) Mannitol fermenter = N		
Т002 В	Form = x2 types, both circular Size = Zmm (both) Blevation = raised and convex Colour = white and grey Hemolysis = beta and alpha (1 and 2)	n/a	Form = x2 types, circular Size = 3mm and 0.3mm (1.AND 2) Elevation = flat and raised Colour = white/pink (both) Mannitol fermenter = N	1 = cocci, clustered 2 = cocci, chain	1 = cocci, dustered = staph, non MSA fermenter, beta hemol flat = staphyloroccus aureus. 2 = cocci, chain = strep, non MSA fermenter, alpha hemolysis raised gey small colonies = group B = streptococcus pneumoniae.
	Form = circular		Form = circular		
T003 T	Size = 4mm Elevation = flat Colour = grey Hemolysis = alpha	n/a	Size = 2mm Elevation = flat Colour = white/pink Mannitol fermenter = N		
ET003 M	Form = circular Size = 3mm Blevation = flat Colour = grey Hemolysis = alpha	n/a	Form = circular Size = 2mm Elevation = flat Colour = white/pink Mannitol fermenter = N		
ET003 B	Form = x2 types, circular Size = 3mm (both) Elevation = flat (both) Colour = grey (both) Hemolysis = beta and alpha	n/a	Form = x2 types, circular Size = 2mm (both) Elevation = raised (both) Colour = yellow and pink (1 AND 2) Mannitol fermenter = Y and N	1 = cocci, clustered 2 = cocci, chains	1 = cocci, dustered = staph, MSA fermenter and yellow, beta hemolysis = staphylococcus sureus. 2 = cocci, chains = strep, non MSA fermenter, alpha hemolysi = group B = streptococcus pneumoniae.
	Form = x2 types, circular	1	Form = circular		
T004 T	Size = 3mm and 4mm Elevation = flat (both) Colour = grey (both) Hemolysis = alpha and beta	n/a	Size = 3mm Elevation = raised Colour = white/pink (1 - PINK) Mannitol fermenter = N		
ET004 M	Form = circular Size = Smm Blevation = flat Colour = grey Hemolysis = beta	n/a	Form = x2 types, circular Size = 2mm and 4mm Elevation = flat and raised Colour = pink and yellow Mannitol fermenter = N and Y		
T004 B	Form = x2 types, circular Size = 3mm and 4mm Elevation = flat (both) Colour = grey (both) Hemolysis = alpha and beta	n/a	Form = x2 types, circular Size = Zmm and 3mm Elevation = flat and raised Colour = pink and yellow (2 - YELLOW) Mannitol fermenter = N and Y	1 = cocci, some chains but spread equally 2 = cocci, clustered	1 = cocci, chalins = strep, pink, non MSA fermenter, alpha hemolysis = streptococcus pneumoniae. 2 = cocci, dustered = staph, MSA fermenter, beta hemolysis staphylococcus aureus.
T005 T	Form = x2 types, circular Size = 5mm and Imm (1 AND 2) Elevation = flat and convex/raised Colour = grey (both) Hemolysis = beta and gamma	n/a	Form = x1 type, circular/irregular Size = 3mm Elevation = flat Colour = pink Mannitol fermenter = N	1 = cocci, chains 2 = large bulbs, yeast, candida?	1 = cocci, chains = streptococcus, non MSA fermenter, beta hemolysis = group A, = streptococcus agalactiae. 2 = large bulb shaped, purple gram stain, candida agar identification lilac = candida glabrata
T005 M	Form = x2 types Size = 6mm and Imm Elevation = flat and convex/raised Colour = grey (both) Hemolysis = beta and gamma	n/a	Form = x1 type, irregular Size = 3mm Elevation = flat Colour = pink Mannitol fermenter = N		
т005 В	Form = x2 types, circular (more of the bigger colonies): Size = 3mm and <1mm Blevation = flat and convex/raised Colour = grey (both) Hemolysis = alpha/beta?	n/a	Form = circular/irregular Size = Elevation = 3mm and 1mm Colour = pink Mannitol fermenter = N		

Figure 77. Summary table of the observations from cultures on blood, MacConkey and Mannitol Salt plates and gram staining.

8.3 NMR SPECTRA AND CHEMICAL STRUCTURE FOR SUGGESTED COMPOUNDS IN CLINICAL STUDY

All NMR spectra are taken from the Human Metabolome Database. Trimethylamine was unavailable to download.



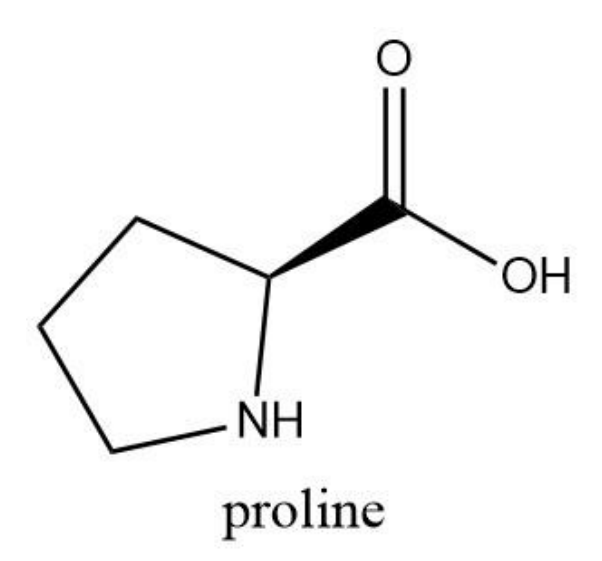
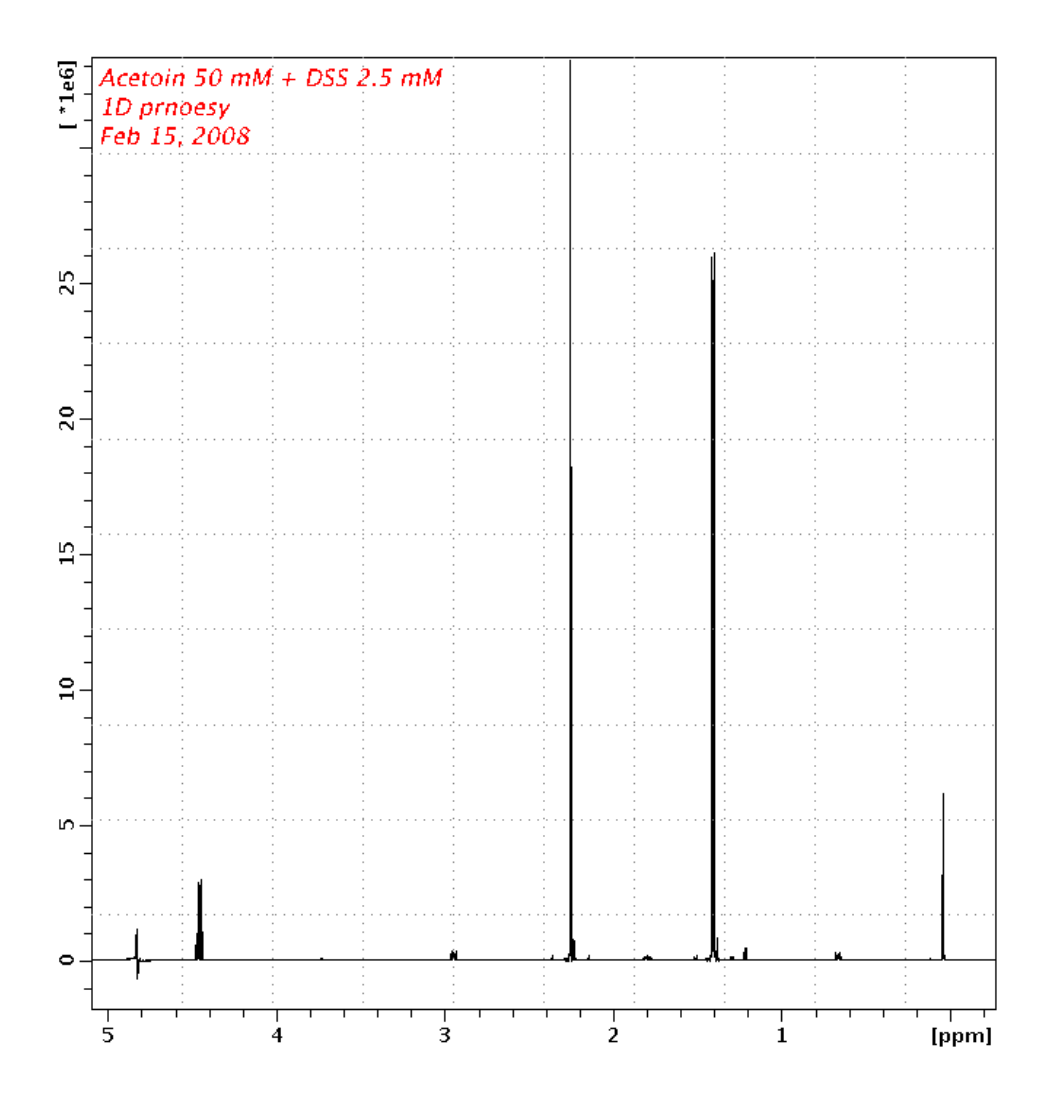


Figure 78. ¹H NMR spectrum and chemical structure for proline available on the Human Metabolome Database.



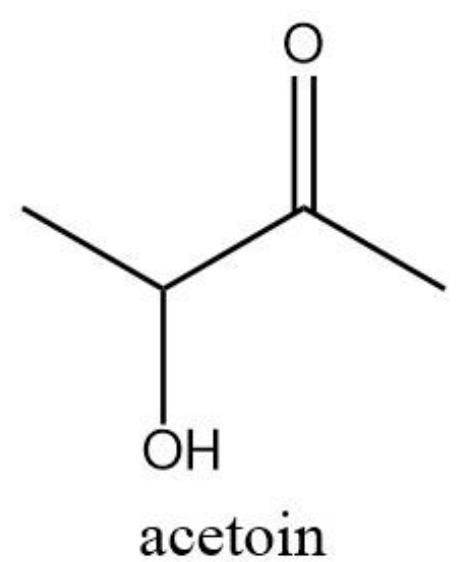
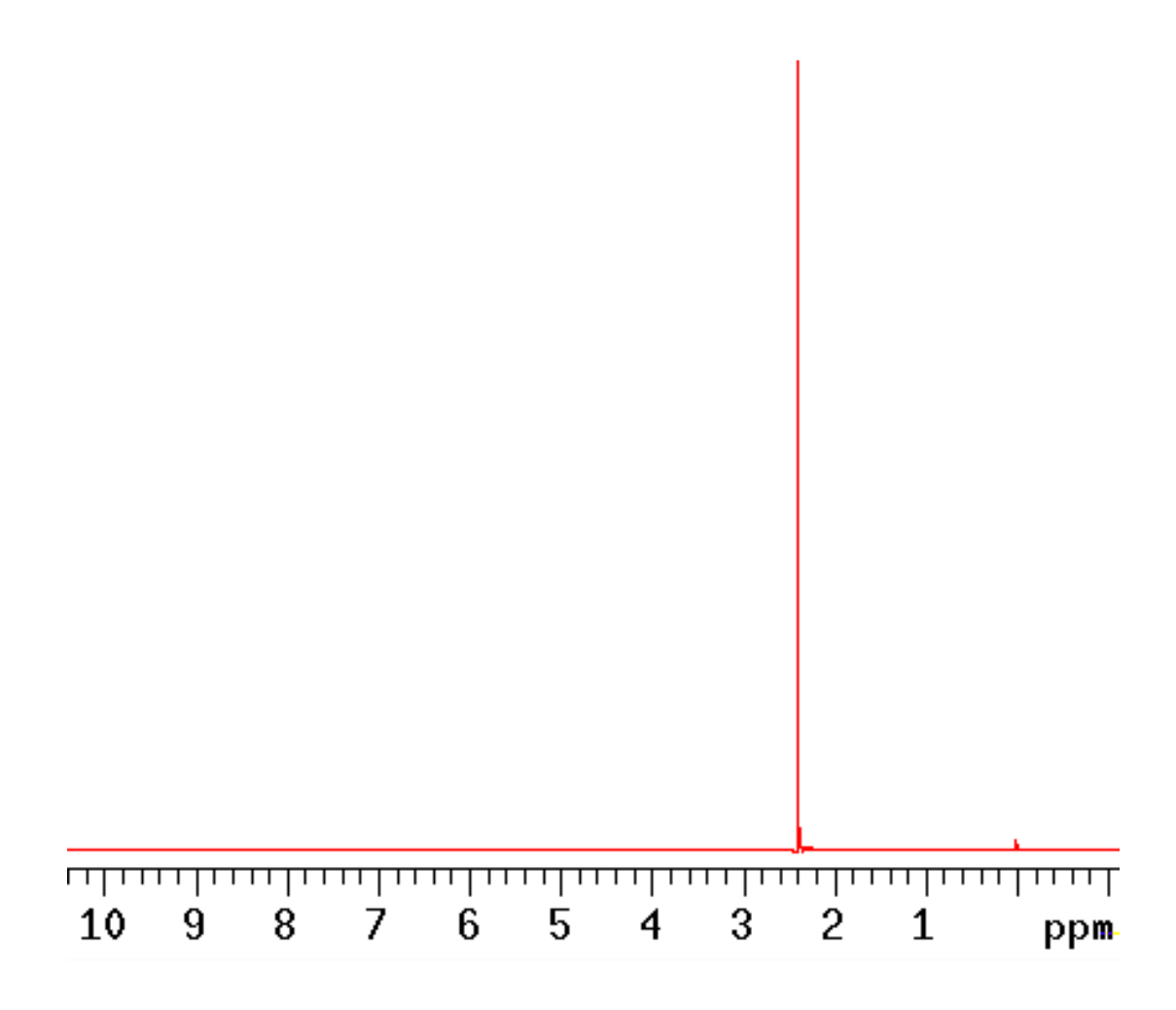
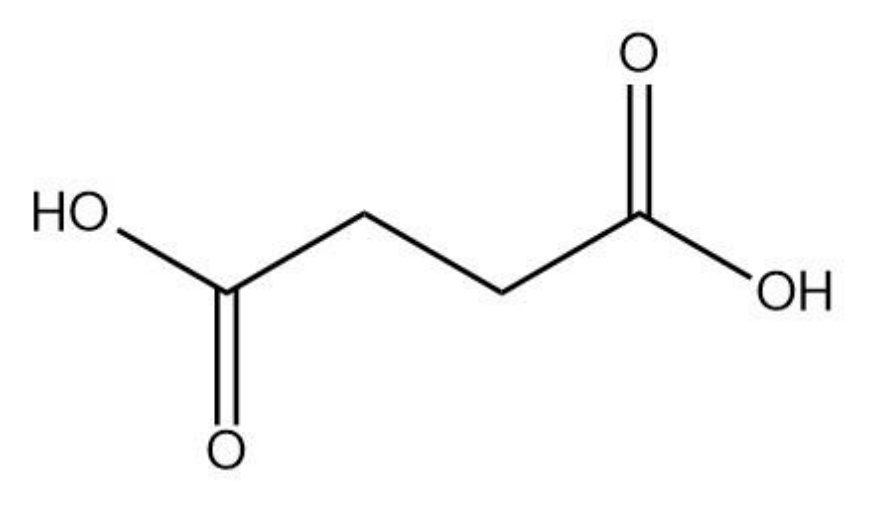


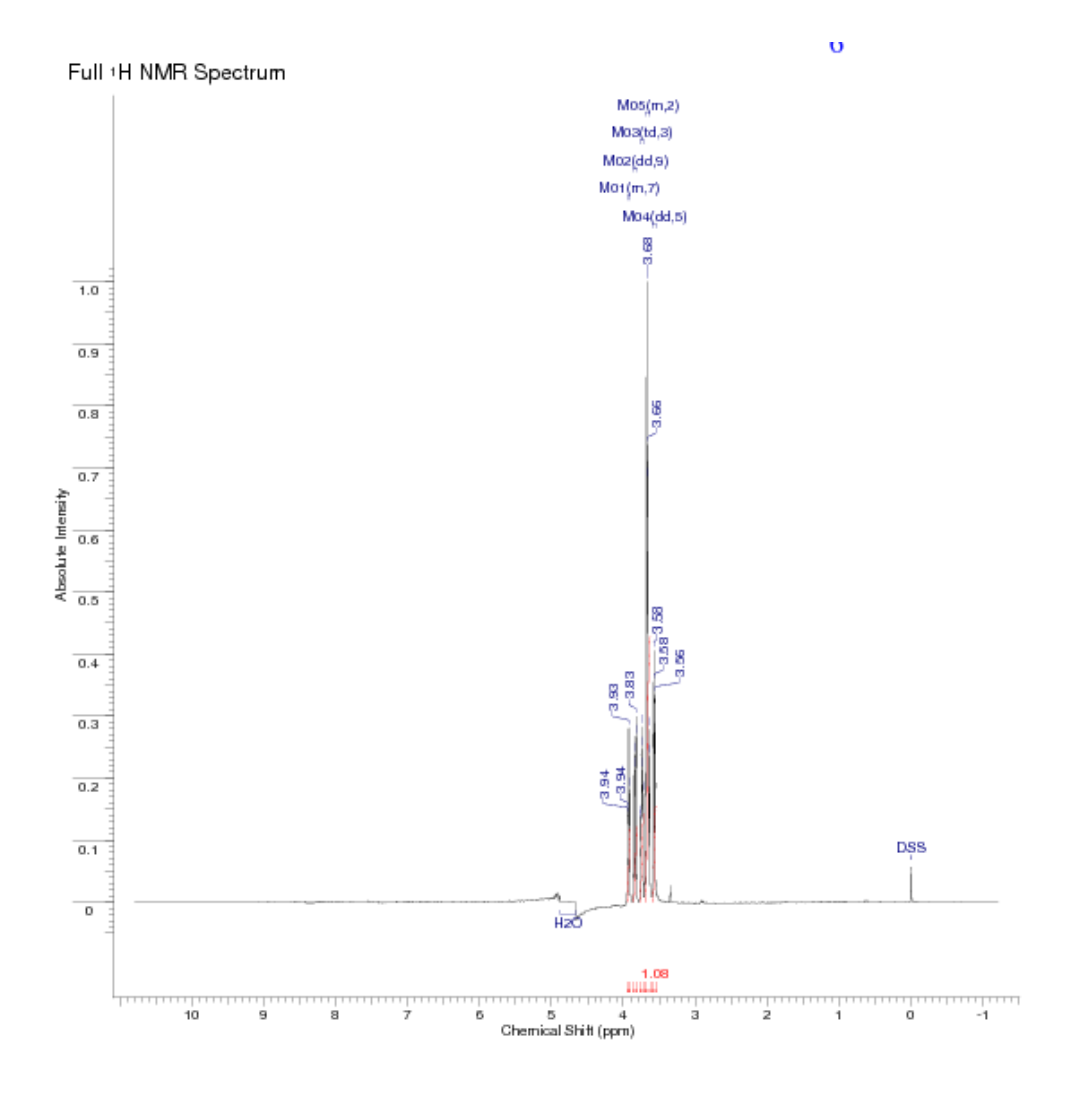
Figure 79. ¹H NMR spectrum for acetoin available on the Human Metabolome Database.





succinic acid

Figure 80. ¹H NMR spectrum for succinate available on the Human Metabolome Database.



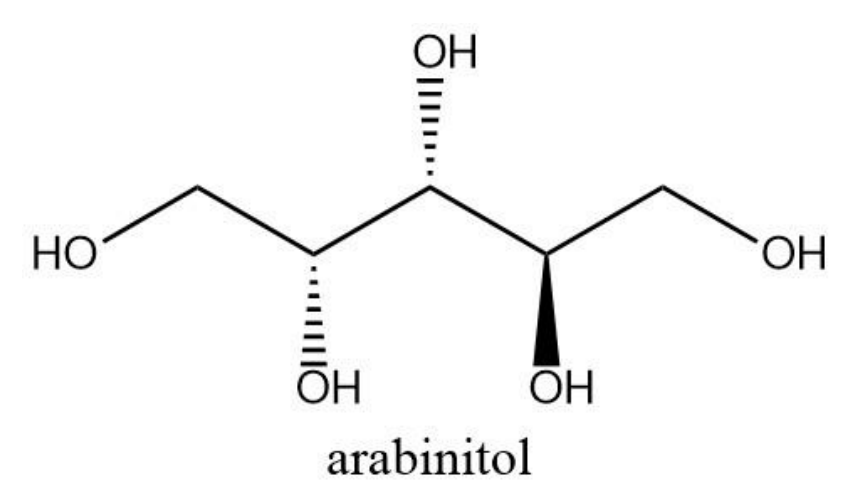
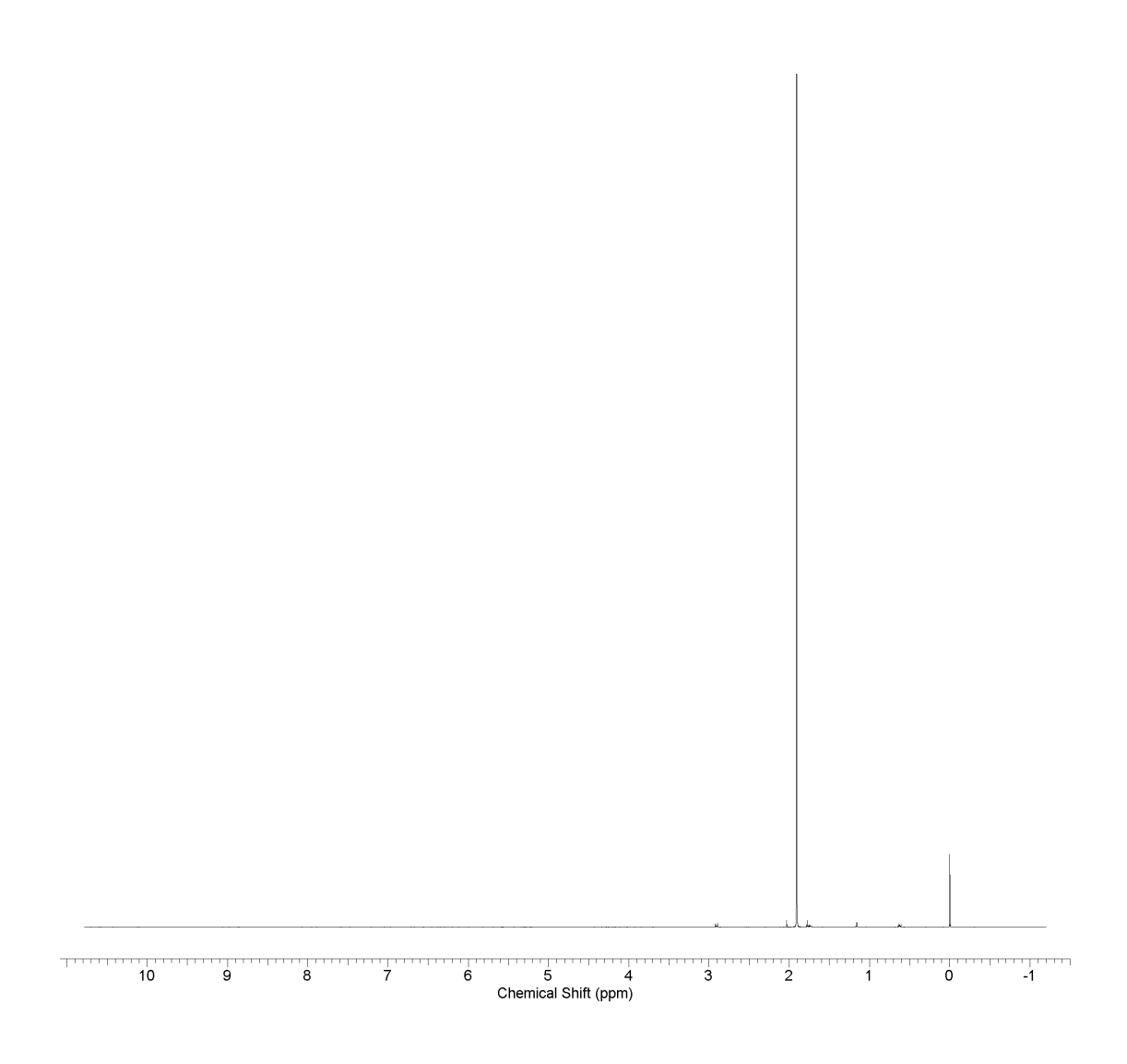
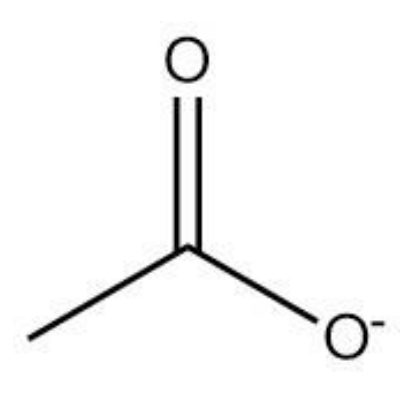


Figure 81. ¹H NMR spectrum for arabinitol available on the Human Metabolome Database.





acetate

Figure 82. ¹H NMR spectrum for acetate available on the Human Metabolome Database.

8.4 SETTING UP A NEW LABORATORY DURING COVID-19 PANDEMIC

A large portion of this work was not conducted at UCL, due to a badly timed proposed move of the Eastman Dental Institute coinciding with the Covid-19 pandemic. I decided I needed to do something to carry on my work as the research was potentially helpful and sought funding to rent a lab privately for 12 months to continue my work. I was successful in being awarded UCL's EPSRC IAA Discovery to Use funding of £93,455. This was a project I managed which included budgeting, equipment and consumables purchasing, hiring of a post-doctoral researcher for SARS-CoV-2 testing and liaising with UCH to start the clinical study. Below are images of the new laboratory I set up and worked in from January 2021 - January 2022.

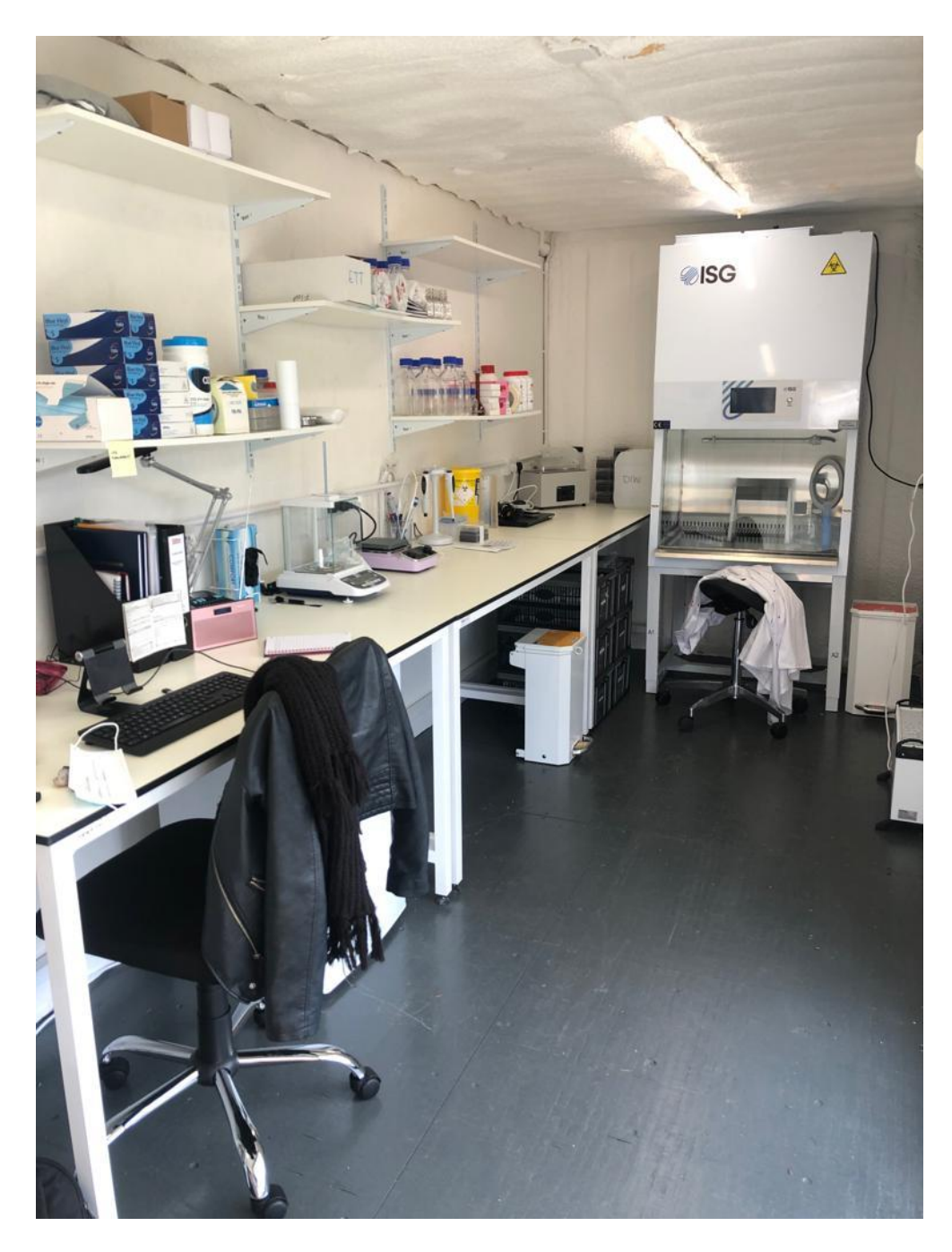


Figure 83. Image of the shipping container turned lab, everything was set up by me and the help of a 'bubble' friend during the Covid-19 pandemic.

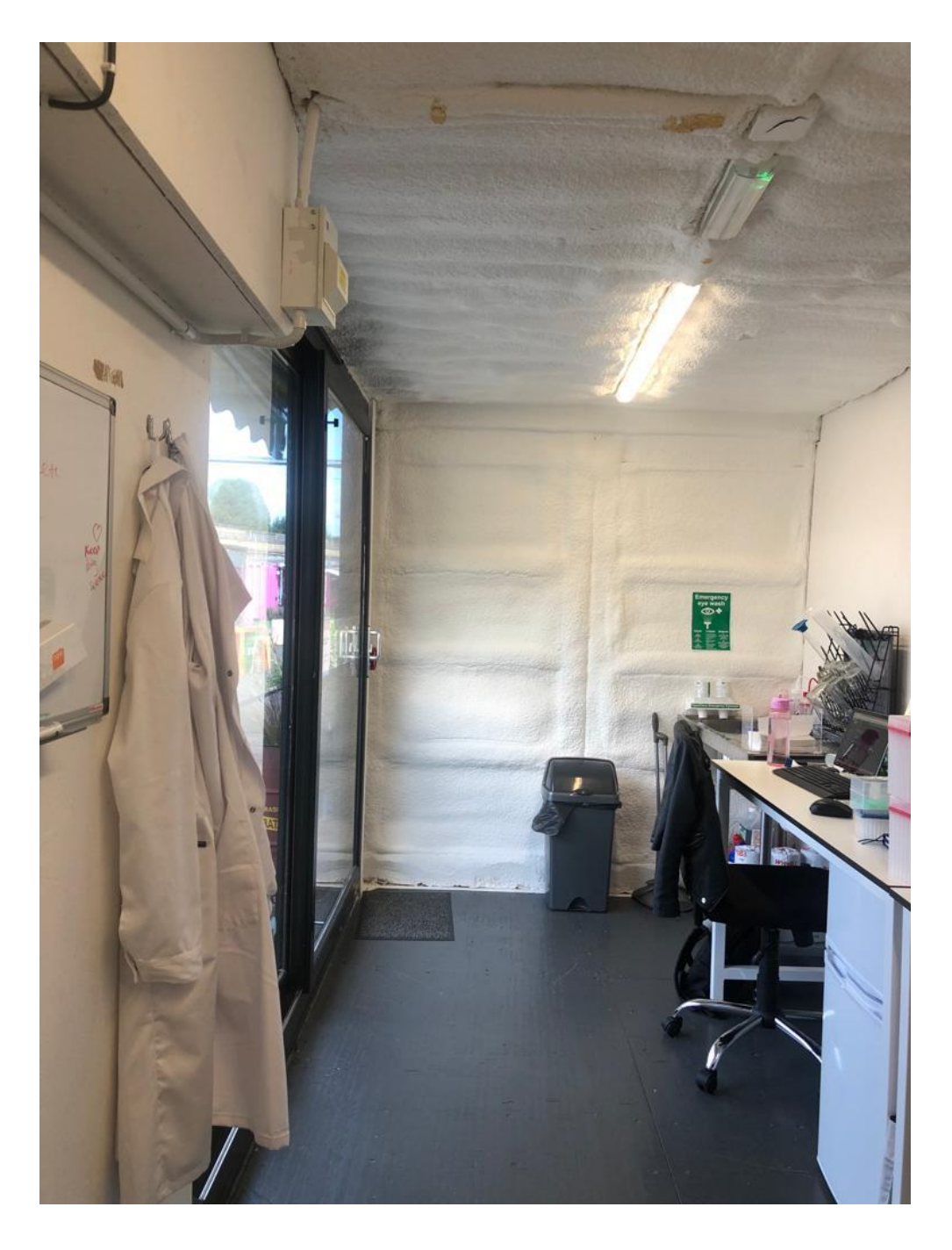


Figure 84. Alternative view of the shipping container lab.



Figure 85. Image of the shipping container lab from the outside.